Chemistry–A European Journal

Supporting Information

Protein-Templated Hit Identification through an Ugi Four-Component Reaction**

Federica Mancini[+],[a, b] M. Yagiz Unver[+],[a, c] Walid A. M. Elgaher,[a] Varsha R. Jumde,[a] Alaa Alhayek,[a, b] Peer Lukat,[d] Jennifer Herrmann,[e] Martin D. Witte,[c] Matthias Köck,[e] Wulf Blankenfeldt,[d, f] Rolf Müller,[b, e] and Anna K. H. Hirsch*[a, b, c]

Table of Contents

Experimental

General procedures for Ugi-4CR-based KTGS using endothiapepsin

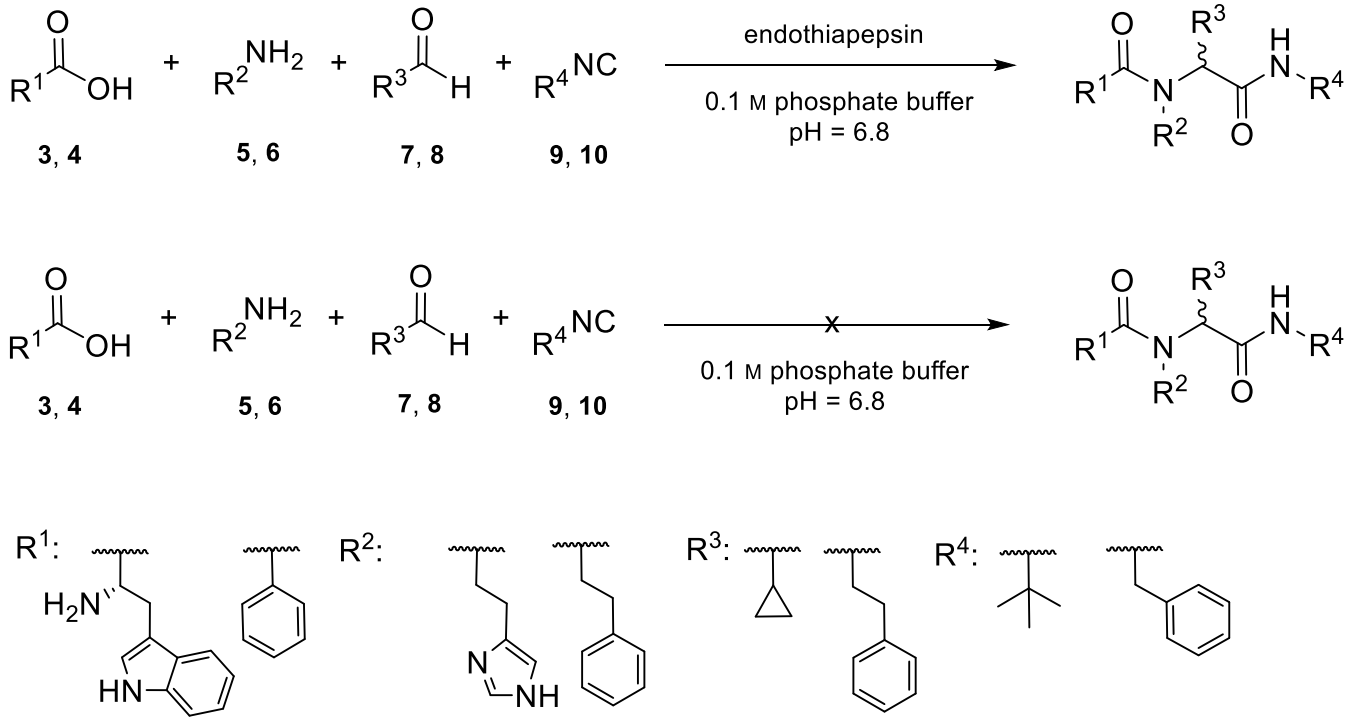

Scheme S1. From top to bottom: *in situ* Ugi reaction, blank reaction.

In situ Ugi 4-component reaction

Endothiapepsin (25 µL, 1.0 mM in phosphate buffer 0.1 M, pH 6.8), the seven building blocks **4**–**10** (1 µL each, 100 mM in DMSO) and L-tryptophan (**3**) (4 µL, 25 mM in DMSO) were added to a mixture of DMSO (89 µL) and phosphate buffer (900 µL, 0.1 M, pH 6.8). The reaction mixture was allowed to rotate on a rotating mixer at room temperature with 10 rpm. After 18 h, the library was analyzed by UPLC-TQD-SIR (electro-spray ionization, (ESI+)) measurement because of its higher sensitivity and greater reliability for product identification.

Blank reaction, negative control:

The 7 building blocks **4**–**10** (1 µL each, 100 mM in DMSO) and L-tryptophan (**3**) (4 µL, 25 mM in DMSO) were added to a mixture of DMSO (89 µL) and phosphate buffer (900 µL, 0.1 M, pH 6.8). The reaction mixture was allowed to rotate on a rotating mixer at room temperature with 10 rpm. After 18 h, the library was analyzed by UPLC-TQD-SIR (electro-spray ionization, (ESI+)) measurement because of its higher sensitivity and greater reliability for product identification.

In situ Ugi experiments using BSA

BSA (25 µL, 1.0 mM in phosphate buffer 0.1 M, pH 6.8), the 7 building blocks **4**–**10** (1 µL each, 100 mM in DMSO) and L-tryptophan (**3**) (4 µL, 25 mM in DMSO) were added to a mixture of DMSO (89 µL) and phosphate buffer (900 µL, 0.1 M, pH 6.8). The reaction mixture was allowed to rotate at room temperature

with 10 rpm. After 18 h, the library was analyzed by UPLC-TQD-SIR (electro-spray ionization, (ESI+)) measurement because of its higher sensitivity and greater reliability for product identification.

In situ Ugi-4CR experiments in the presence of saquinavir

Endothiapepsin (25 µL, 1 mM in phosphate buffer 0.1 M, pH 6.8), the 7 building blocks **4**–**10** (1 µL each, 100 mM in DMSO), L-tryptophan (**3**) (4 µL, 25 mM in DMSO) and saquinavir (1 µL, 100 mM in DMSO) were added to a mixture of DMSO (88 µL) and phosphate buffer (900 µL, 0.1 M, pH 6.8). The reaction mixture was allowed to rotate on a rotating mixer at room temperature with 10 rpm. After 18 h, the library was analyzed by UPLC-TQD-SIR (electro-spray ionization, (ESI+)) measurement because of its higher sensitivity and greater reliability for product identification.

Protein

Endothiapepsin (25 µL, stock solution 1.0 mM in phosphate buffer 0.1 M, pH 6.8) was added to 75 µL of DMSO and 900 µL phosphate buffer 0.1 M, pH 6.8. After 18 h, the enzyme solution was analyzed by UPLC-TQD-SIR (ESI+) measurements and compared with the positive hits identified from in situ Ugi product formation.

UPLC-TQD-SIR method

UPLC-TQD was performed using a Waters Acquity UPLC H-class system coupled to a Waters TQD. All analyses were performed using a reversed-phase UPLC column (ACQUITY HSS T3 Column, 130 Å, 1.8 µm, 2.1 mm x 150 mm). Positive-ion mass spectra were acquired using ES ionization, injecting 10 µL of sample; column temperature 35 °C; flow rate 0.3 mL/min. The eluents, acetonitrile and water contained 0.1% of formic acid. The library components were eluted with a gradient from 95% → 30% over 20 min, then at 5% over 1 min, followed by 5% for 2 min.

The UPLC-TQD-SIR method was used to analyze the formation of Ugi products in in situ and blank reactions. SIR measurements are highly sensitive, where a minute amount of compound can be detected by the mass spectrometer. [M+H]+ were monitored using the full mass range to ensure correct isotope patterns for all possible potential Ugi products both for in situ Ugi and blank reactions. The Ugi products in the protein-templated reaction were identified by comparison of their retention time with those synthesized using conventional methods.

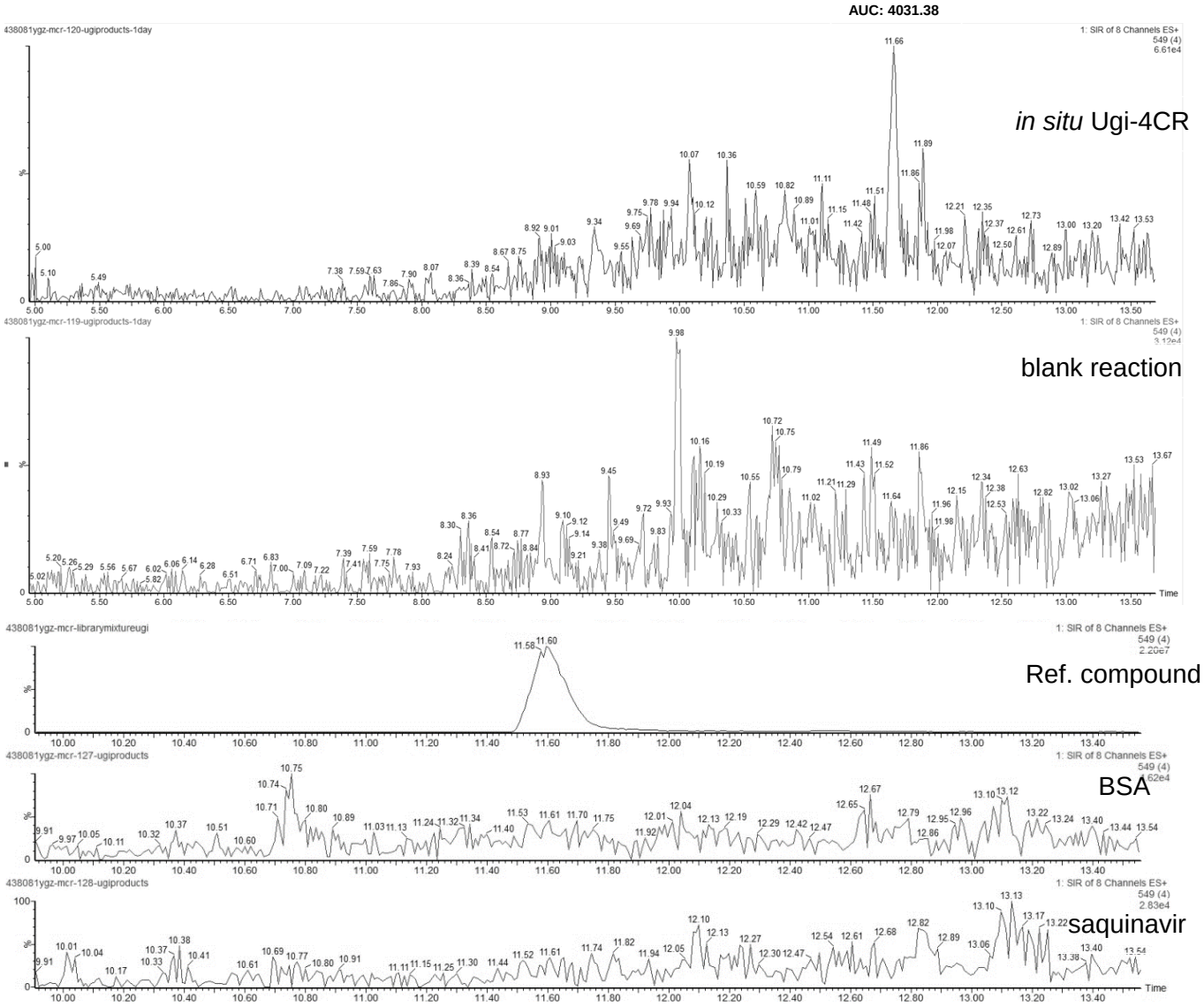

Figure S1. UPLC-TQD-SIR analysis of compound **2** ([*M*+H]$^+$ = 549). Formation of **2** by *in situ* Ugi-4CR was compared with the blank reaction, synthesized compound **2**, BSA and the known inhibitor saquinavir.

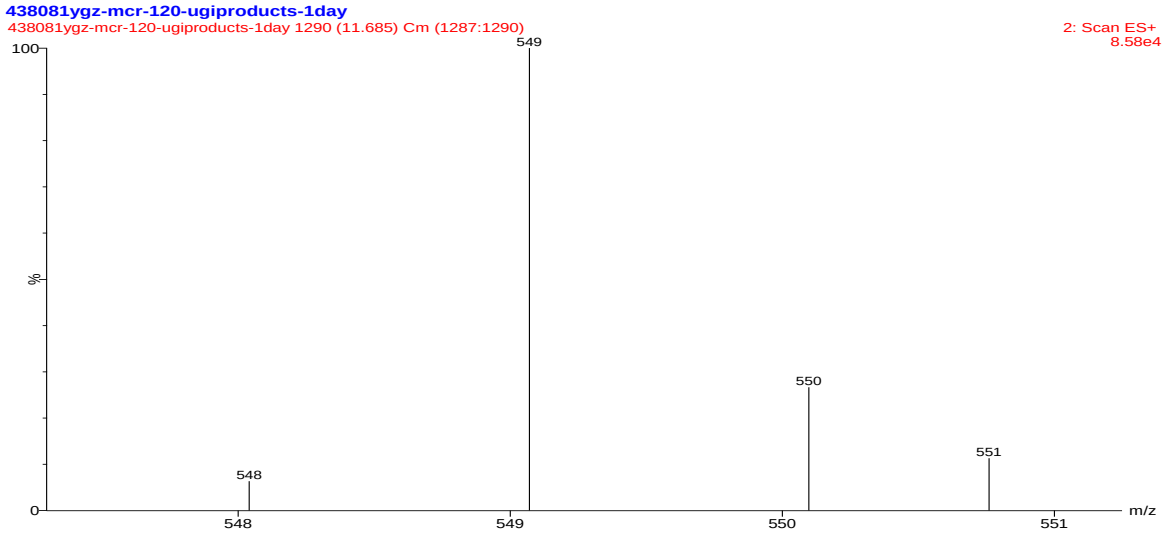

Figure S2. UPLC-TQD-SIR analysis of compound **2** ([M+H]+ = 549), peak at 11.6 min.

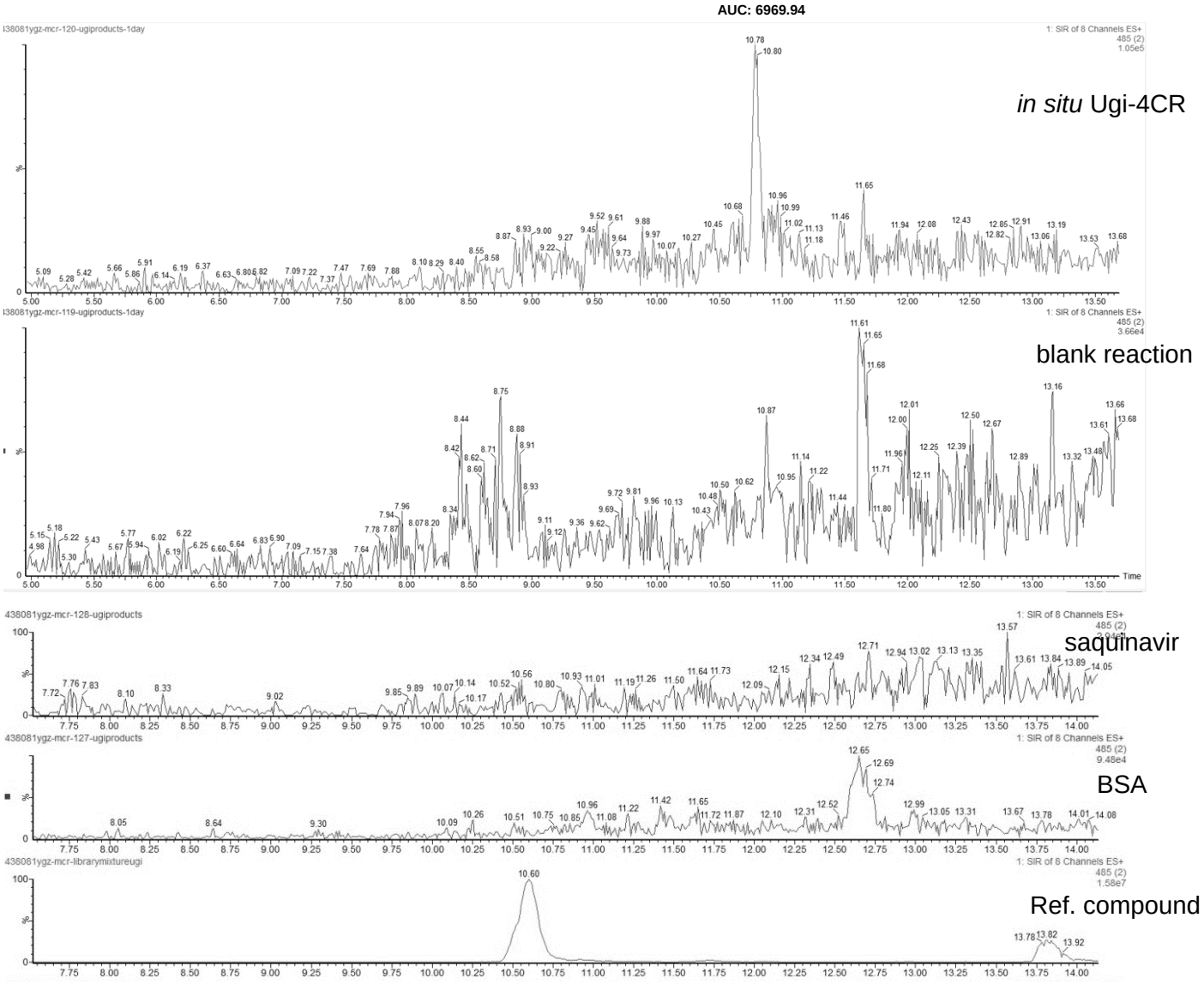

Figure S3. UPLC-TQD-SIR analysis of compound **11** ([M+H]+ = 485). Formation of **11** by in situ Ugi-4CR was compared with the blank reaction, synthesized compound **11**, BSA and the known inhibitor saquinavir.

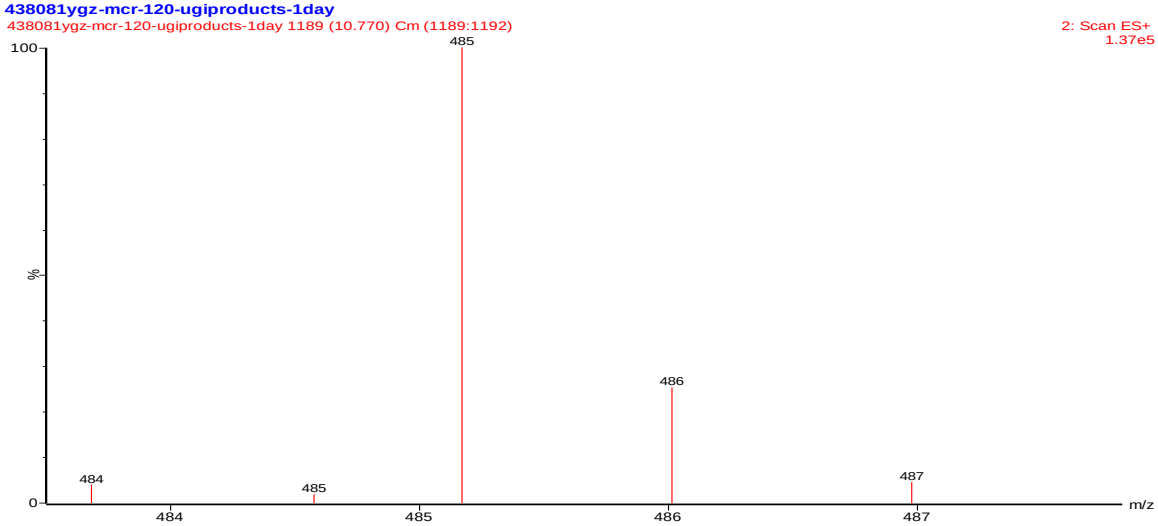

Figure S4. UPLC-TQD-SIR analysis of compound **11** ([M+H]+ = 485), peak at 10.7 min.

General Experimental Details

Starting materials and reagents were purchased from Aldrich or Acros. Yields refer to analytically pure compounds and have not been optimized. All solvents were reagent-grade and if necessary, SPS-grade. Column chromatography was performed on silica gel (Silicycle® SiliaSepTM 40–63 µm 60 Å). TLC was performed with silica gel 60/Kieselguhr F254. Solvents used for column chromatography were pentane, ethyl acetate, dichloromethane and methanol. ^{1}H and ^{13}C spectra were recorded on a Varian AMX400, Bruker Avance Neo 500 MHz with prodigy cryoprobe system or Brucker Ascend(TM) 700 MHz spectrometer (500 or 700 MHz for ^{1}H and 126 or 101 MHz for ^{13}C) at 25 ºC. Chemical shifts (δ) are reported relative to the residual solvent peak. High-resolution mass spectra were recorded with an FTMS orbitrap (Thermo Fisher Scientific) or a Q Exactive Focus (Thermo Scientific) mass spectrometer.

General procedure for Ugi/deprotection reaction

To a 10-mL round-bottomed flask charged with MeOH (4 mL), the corresponding aldehyde **7** or **8** (1 mmol, 1 equiv), amine **5** or **6** (1 mmol, 1 equiv), carboxylic acid **4** or **12** (1 mmol, 1 equiv) and isocyanide **9** or **10** (1 mmol, 1 equiv) were added. The reaction mixture was stirred at room temperature for 24 h. The reaction mixture was concentrated in vacuo and a quick purification over silica gel using EtOAc/pentane (1:1) afforded the corresponding *N*-Boc-protected Ugi product, which was directly used for the following deprotection step. The crude product was dissolved in DCM (4 mL), and HCl/diethyl ether (1 M, 10 mL) was added. After 24 h stirring at r.t., the resulting white precipitate was collected and washed with Et_2O. Complete removal of the solvent afforded the HCl salt of the desired compounds (Scheme S2).

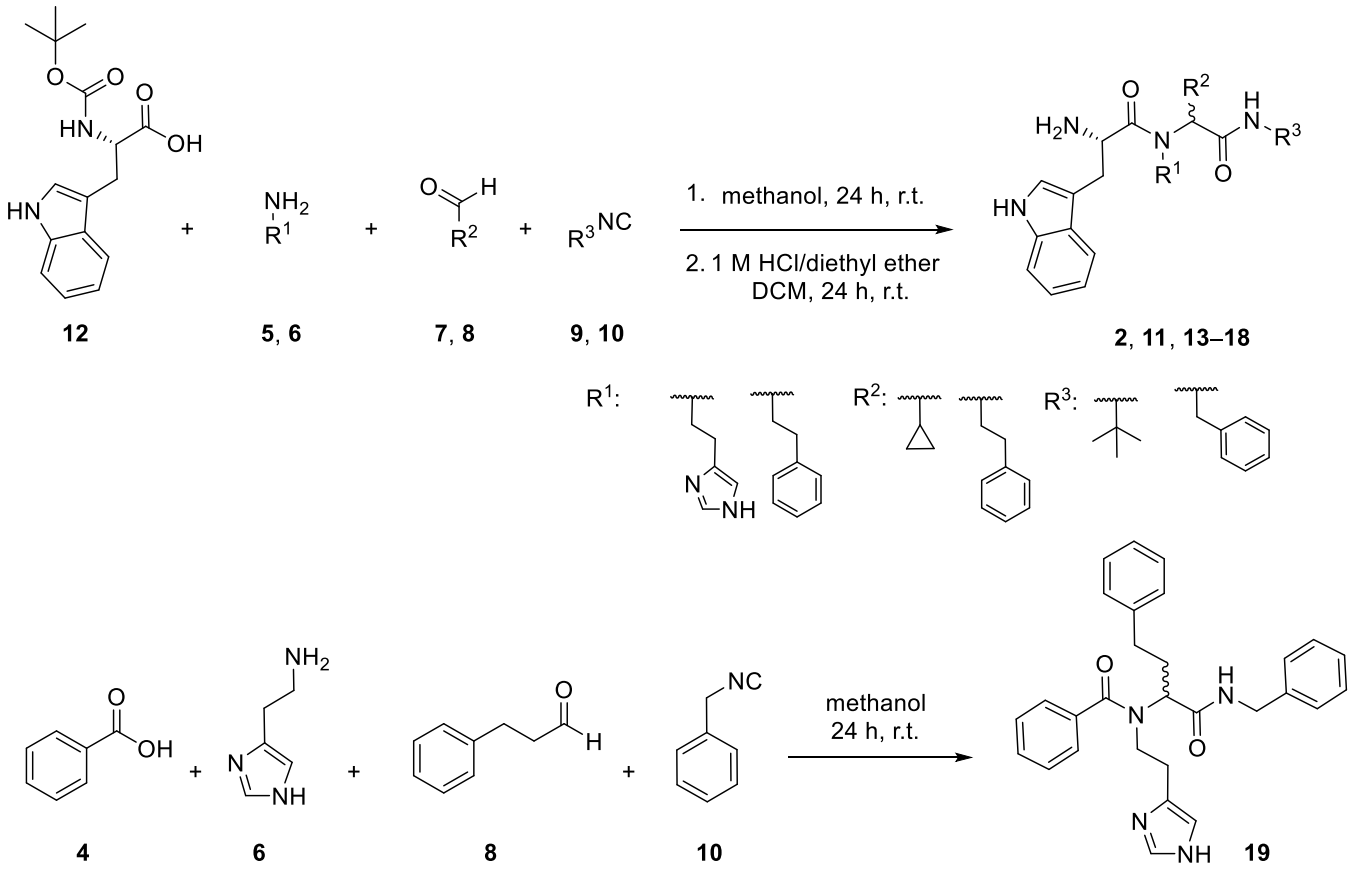

Scheme S2. Synthetic strategy towards compounds **2**, **11**, and **13**–**19**.

2-((*S*)-*N*-(2-(1*H*-Imidazol-4-yl)ethyl)-2-amino-3-(1*H*-indol-3-yl)propanamido)-*N*-benzyl-4-phenyl-butanamide hydrochloride (**2**)

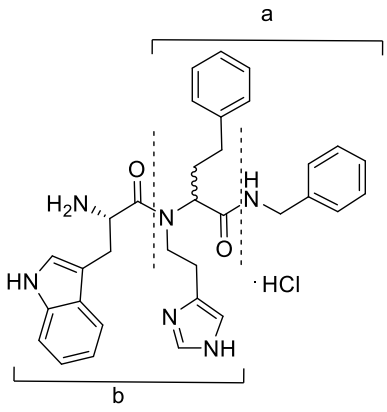

2

General procedure starting from commercially available *N*-Boc-L-Trp (**12**), histamine (**6**) (1 mmol), 3-phenylpropanal (**8**) (1 mmol) and benzyl isocyanide (**10**) (1 mmol) in MeOH (4 mL) afforded the desired product **2** as a white solid as a diastereomeric mixture in 40% yield.

HRMS (ESI) calcd for $C_{33}H_{36}N_6O_2$ $[M+H]^+$: 549.2972, found: 549.2940. calcd for fragment a (m/z): 363.2179, found 363.2161, calcd for fragment b (m/z): 442.2243, found 442.2213.

^{1}H- and ^{13}C-NMR spectra were assigned for the major diastereomers of compound **2** (Table S1). The signals in the aromatic region were not assigned due to severe signal overlap.

Table S1: ^{1}H- and ^{13}C-NMR data of the major diastereomers of compound **2** in methanol-*d*$_4$.[a]

		Diastereomer-1			Diastereomer-2		
Residue	*Position*	δ(^{13}C)	δ(^{1}H)	Mult./*J* [Hz]	δ(^{13}C)	δ(^{1}H)	Mult./*J* [Hz]
Trp	NH_2						
	Cα	52.2	4.73	m	52.4	4.29	m
	CO	171.4			171.0		
	Cβ	29.3	3.43/3.31	m	28.3	3.32/3.16	m
hPhe	N						
	Cα	59.0	4.79	t (7.5)	61.2	4.30	m
	CO	172.1			170.5		
	N-CH_2-CH_2	43.4	3.03/2.97	m	44.6	3.66	m
	N-CH_2-CH_2	25.4	2.77/2.61	m	24.2	2.96/2.86	m
	Cβ	33.3	2.37/2.20	m	32.7	2.65/2.60	m
	Cγ	31.8	1.99/1.36	m	33.4	2.43/2.13	m
C-term. prot.	NH						
	CH_2	44.2	4.40/4.30	d (15.0)	44.3	4.28/4.17	d (14.6)

[a] hPhe: the phenethyl-glycine residue; *C*-term. prot.: the protection group at the *C*-terminus.

(2S)-*N*-(2-(1*H*-Imidazol-4-yl)ethyl)-2-amino-*N*-(2-(benzylamino)-1-cyclopropyl-2 oxoethyl)-3-(1*H*-indol-3-yl)propanamide hydrochloride (11)

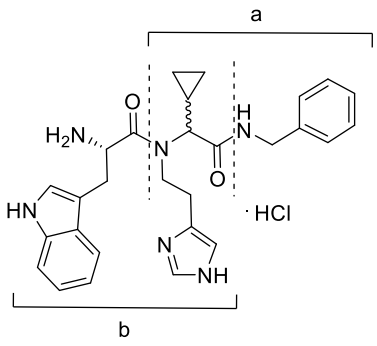

11

General procedure starting from commercially available *N*-Boc-L-Trp (**12**) (1 mmol), histamine (**6**) (1 mmol), cyclopropanecarboxaldehyde (**7**) (1 mmol) and benzyl isocyanide (**10**) (1 mmol) in MeOH (4 mL) afforded the desired product **11** as a white solid as a diastereomeric mixture in 35% yield.

HRMS (ESI) calcd for $C_{28}H_{32}N_6O_2$ [*M*+H]$^+$: 485.2659, found: 485.2640, calcd for fragment a (m/z): 299.1866, found 299.1859, calcd for fragment b (m/z): 378.1925, found 378.1912.

^{1}H- and ^{13}C-NMR spectra were assigned for the major diastereomers of compound **11** (Table S2). The signals in the aromatic region were not assigned due to severe signal overlap.

Table S2: ^{1}H- and ^{13}C-NMR data of the major diastereomers of compound **11** in methanol-d_4.[a]

		Diastereomer-1			Diastereomer-2		
Residue	*Position*	δ(^{13}C)	δ(^{1}H)	Mult./*J* [Hz]	δ(^{13}C)	δ(^{1}H)	Mult./*J* [Hz]
Trp	NH_2						
	Cα	51.8	4.46	dd	52.3	4.59	dd
	CO	170.2			170.9		
	Cβ	29.0	3.37/3.26	m	29.0	3.41/3.26	m
cpGly	N						
	Cα	66.7	3.64	d (10.0)	67.3	3.48	d (10.0)
	CO	173.6			172.6		
	N-CH_2-CH_2	44.0	4.52	m	44.2	4.34	m
	N-CH_2-CH_2	25.8	2.81/2.75	m	24.3	2.77/2.69	m
	Cβ	11.5	1.09	m	11.1	1.59	m
	Cγ1	6.0	0.73/0.62	m	5.8	0.86/0.64	m
	Cγ2	5.1	0.47/-0.26	m	4.7	0.54/0.39	m
C-term. prot.	NH						
	CH_2	43.9	4.43	s	44.3	4.44	s

[a] cpGly: the cyclopropyl-glycine residue; *C*-term. prot.: the protection group at the *C*-terminus.

(2S)-2-Amino-*N*-(2-(tert-butylamino)-1-cyclopropyl-2-oxoethyl)-3-(1*H*-indol-3-yl)-*N*-phenethyl-propanamide hydrochloride (13)

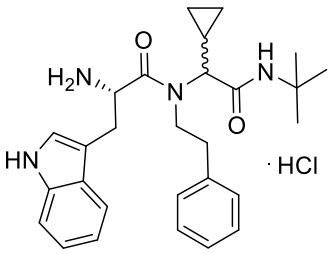

13

General procedure starting from commercially available *N*-Boc-L-Trp (**12**), phenylethylamine (**5**) (1 mmol), cyclopropanecarboxaldehyde (**7**) (1 mmol) and *tert*-butyl isocyanide (**9**) (1 mmol) in MeOH (4 mL) afforded the desired product **13** as a white solid as a diastereomeric mixture in 80% yield.

HRMS (ESI–) calcd for $C_{28}H_{35}N_4O_2$ [*M*–H]$^-$: 459.2754, found: 459.2764.

^{1}H- and ^{13}C-NMR spectra were assigned for the major diastereomers of compound **13** (Table S3). The signals in the aromatic region were not assigned due to severe signal overlap.

Table S3: ^{1}H- and ^{13}C-NMR data of the major diastereomers of compound **13** in methanol-d_4.[a]

		Diastereomer-1			Diastereomer-2		
Residue	*Position*	δ(^{13}C)	δ(^{1}H)	Mult./*J* [Hz]	δ(^{13}C)	δ(^{1}H)	Mult./*J* [Hz]
Trp	NH_2						
	Cα	52.8	4.41	t (7.2)	52.5	4.33	t (7.2)
	CO	170.73			170.32		
	Cβ	29.0	3.34	m	28.9	3.26/3.24	m
cpGly	N						
	Cα	66.5	3.66	d (10.7)	66.8	3.63	d (10.2)
	CO	172.6			171.5		
	N-CH_2-CH_2	46.7	3.26/3.07	m	49.3	3.35/3.20	m
	N-CH_2-CH_2	36.9	2.66/2.58	m	36.9	2.77/2.72	m
	Cβ	11.9	1.06	m	11.8	1.50	m
	Cγ1	5.5	0.68/0.57	m	5.5	0.83/0.72	m
	Cγ2	5.3	0.43/-0.15	m	5.3	0.58/0.43	m
C-term. prot.	NH						
t-Butyl	C	52.0			52.2		
	CH_3	28.7	1.36	s	28.7	1.39	s

[a] cpGly: the cyclopropyl-glycine residue; *C*-term. prot.: the protection group at the *C*-terminus.

2-((S)-2-Amino-3-(1*H*-indol-3-yl)-*N*-phenethylpropanamido)-*N*-(tert-butyl)-4-phenylbutanamide hydrochloride (14)

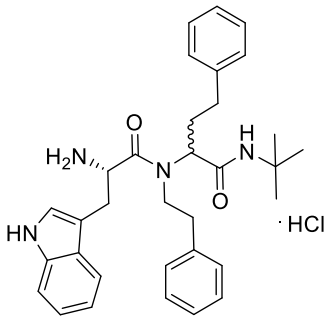

14

General procedure starting from commercially available *N*-Boc-L-Trp (**12**), phenylethylamine (**5**) (1 mmol), 3-phenylpropanal (**8**) (1 mmol) and *tert*-butyl isocyanide (**9**) (1 mmol) in MeOH (4 mL) afforded the desired product **14** as a white solid as a diastereomeric mixture in 60% yield.

HRMS (ESI–) calcd for $C_{33}H_{39}N_4O_2$ [*M*–H]$^-$: 523.3067, found: 523.3079.

^{1}H- and ^{13}C-NMR spectra were assigned for the major diastereomers of compound **14** (Table S4). The signals in the aromatic region were not assigned due to severe signal overlap.

Table S4: ^{1}H- and ^{13}C-NMR data of the major diastereomers of compound **14** in methanol-*d*$_4$.[a]

		Diastereomer-1			Diastereomer-2		
Residue	*Position*	δ(^{13}C)	δ(^{1}H)	Mult./*J* [Hz]	δ(^{13}C)	δ(^{1}H)	Mult./*J* [Hz]
Trp	NH_2						
	Cα	52.7	4.49	dd	52.5	4.42	dd
	CO	171.43			171.16		
	Cβ	29.3	3.36/3.34	m	29.1	3.41/3.30	m
hPhe	N						
	Cα	59.0	4.72	dd	60.7	4.64	dd
	CO	171.39			171.10		
	N-CH_2-CH_2	46.3	3.08	m	48.3	3.29/3.20	m
	N-CH_2-CH_2	36.8	2.63	m	37.1	2.61/2.42	m
	Cβ	32.1	1.99/1.39	m	32.6	2.30/2.01	m
	Cγ	33.2	2.44/2.25	m	33.3	2.61	m
C-term. prot.	NH						
t-Butyl	C	52.7			52.7		
	CH_3	28.6	1.36	s	28.6	1.37	s

[a] hPhe: the phenethyl-glycine residue; *C*-term. prot.: the protection group at the *C*-terminus.

2-((S)-2-Amino-3-(1*H*-indol-3-yl)-*N*-phenethylpropanamido)-*N*-benzyl-4-phenylbutanamide hydrochloride (15)

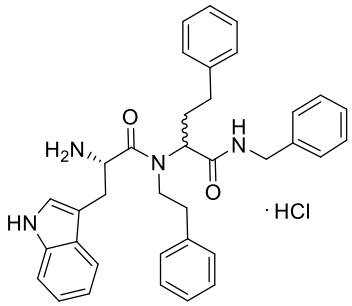

15

General procedure starting from commercially available *N*-Boc-L-Trp (**12**), phenylethylamine (**5**) (1 mmol), 3-phenylpropanal (**8**) (1 mmol) and benzyl isocyanide (**10**) (1 mmol) in MeOH (4 mL) afforded the desired product **15** as a white solid as a diastereomeric mixture in 75% yield.

HRMS (ESI–) calcd for $C_{36}H_{37}N_4O_2$ [*M*–H]$^-$: 557.2911, found: 557.2923.

^{1}H- and ^{13}C-NMR spectra were assigned for the major diastereomers of compound **15** (Table S5). The signals in the aromatic region were not assigned due to severe signal overlap.

Table S5: ^{1}H- and ^{13}C-NMR data of the major diastereomers of compound **15** in methanol-*d*$_4$.[a]

		Diastereomer-1			Diastereomer-2		
Residue	*Position*	δ(^{13}C)	δ(^{1}H)	Mult./*J* [Hz]	δ(^{13}C)	δ(^{1}H)	Mult./*J* [Hz]
Trp	NH_2						
	Cα	52.6	4.45	d	52.4	4.41	dd
	CO	171.5			171.0		
	Cβ	29.1	3.38/3.31	m	29.1	3.34/3.27	m
hPhe	N						
	Cα	59.4	4.81	t (7.5)	61.1	4.57	t (7.4)
	CO	172.2			171.9		
	N-CH_2-CH_2	47.0	3.10	m	49.1	3.13	m
	N-CH_2-CH_2	36.6	2.56/2.50	m	36.8	2.63/2.46	m
	Cβ	32.1	2.12/1.54	m	32.0	2.39/2.08	m
	Cγ	33.3	2.47/2.26	m	33.3	2.60	m
C-term. prot.	NH						
	CH_3	44.1	4.46-4.32	m	44.1	4.46-4.32	m

[a] hPhe: the phenethyl-glycine residue; *C*-term. prot.: the protection group at the *C*-terminus.

(2S)-2-Amino-*N*-(2-(benzylamino)-1-cyclopropyl-2-oxoethyl)-3-(1*H*-indol-3-yl)-*N*-phenethyl-propanamide hydrochloride (16)

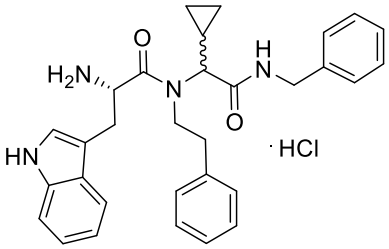

16

General procedure starting from commercially available *N*-Boc-L-Trp (**12**), phenylethylamine (**5**) (1 mmol), cyclopropanecarboxaldehyde (**7**) (1 mmol) and benzyl isocyanide (**10**) (1 mmol) in MeOH (4 mL) afforded the desired product **16** as a white solid as a diastereomeric mixture in 40% yield.

HRMS (ESI–) calcd for $C_{31}H_{33}N_4O_2$ [*M*–H]$^-$: 493.2598, found: 493.2610; ^{1}H- and ^{13}C-NMR spectra were assigned for the major diastereomers of compound **16** (Table S6). The signals in the aromatic region were not assigned due to severe signal overlap.

Table S6: ^{1}H- and ^{13}C-NMR data of the major diastereomers of compound **16** in methanol-*d*$_4$.[a]

		Diastereomer-1			Diastereomer-2		
Residue	*Position*	δ(^{13}C)	δ(^{1}H)	Mult./*J* [Hz]	δ(^{13}C)	δ(^{1}H)	Mult./*J* [Hz]
Trp	NH_2						
	Cα	52.4	4.30	dd	52.8	4.38	dd
	CO	170.6			171.1		
	Cβ	29.3	3.25/3.16	m	29.3	3.34/3.28	m
cpGly	N						
	Cα	66.6	3.74	d (10.0)	67.2	3.66	d (10.0)
	CO	173.7			172.7		
	N-CH_2-CH_2	49.8	3.25/3.17	m	47.3	3.28/3.10	m
	N-CH_2-CH_2	37.2	2.67/2.59	m	37.0	2.76/2.71	m
	Cβ	11.7	1.12	m	11.4	1.58	m
	Cγ1	6.4	0.74/0.60	m	6.2	0.87/0.56	m
	Cγ2	5.5	0.69/0.41	m	5.4	0.47/-0.15	m
C-term. prot.	NH						
	CH_2	44.0	4.43	s	44.0	4.49/4.43	d (15.2)

[a] cpGly: the cyclopropyl-glycine residue; *C*-term. prot.: the protection group at the *C*-terminus.

(2S)-*N*-(2-(1*H*-Imidazol-4-yl)ethyl)-2-amino-*N*-(2-(tert-butylamino)-1-cyclopropyl-2-oxoethyl)-3-(1*H*-indol-3-yl)propanamide hydrochloride (17)

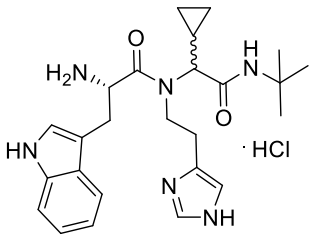

17

General procedure starting from commercially available *N*-Boc-L-Trp (**12**), histamine (**6**) (1 mmol), cyclopropanecarboxaldehyde (**7**) (1 mmol) and *tert*-butyl isocyanide (**9**) (1 mmol) in MeOH (4 mL) afforded the desired product **17** as a white solid as a diastereomeric mixture in 61% yield.

HRMS (ESI–) calcd for $C_{25}H_{33}N_6O_2$ [*M*–H]$^-$: 449.2659, found: 449.2670. ^{1}H- and ^{13}C-NMR spectra were assigned for the major diastereomers of compound **17** (Table S7). The signals in the aromatic region were not assigned due to severe signal overlap.

Table S7: ^{1}H- and ^{13}C-NMR data of the major diastereomers of compound **17** in methanol-d_4.[a]

		Diastereomer-1			Diastereomer-2		
Residue	*Position*	δ(^{13}C)	δ(^{1}H)	Mult./*J* [Hz]	δ(^{13}C)	δ(^{1}H)	Mult./*J* [Hz]
Trp	NH_2						
	Cα	52.3	4.61	t (7.2)	51.8	4.51	t (7.2)
	CO	170.87			170.32		
	Cβ	29.0	3.42/3.26	m	28.9	3.38/3.29	m
cpGly	N						
	Cα	66.5	3.58	d (10.7)	67.0	3.47	d (10.2)
	CO	172.9			171.6		
	N-CH_2-CH_2	43.8	3.67	m	43.8	3.25/3.09	m
	N-CH_2-CH_2	25.8	2.80/2.74	m	24.4	2.82/2.75	m
	Cβ	11.6	1.02	m	11.4	1.47	m
	Cγ1	5.5	0.67/0.60	m	5.2	0.79/0.63	m
	Cγ2	5.2	0.43/-0.25	m	5.2	0.53/0.39	m
C-term. prot.	NH						
t-Butyl	C	52.3			52.3		
	CH_3	28.7	1.34	s	28.7	1.39	s

[a] cpGly: the cyclopropyl-glycine residue; *C*-term. prot.: the protection group at the *C*-terminus.

2-((*S*)-*N*-(2-(1*H*-Imidazol-4-yl)ethyl)-2-amino-3-(1*H*-indol-3-yl)propanamido)-*N*-(tert-butyl)-4-phenylbutanamide hydrochloride (18)

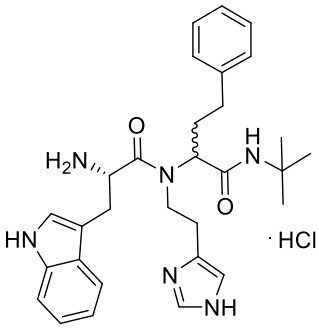

18

General procedure starting from commercially available *N*-Boc-L-Trp (**12**), histamine (**6**) (1 mmol), 3-phenylpropanal (**8**) (1 mmol) and *tert*-butyl isocyanide (**9**) (1 mmol) in MeOH (4 mL) afforded the desired product **18** as a white solid as a diastereomeric mixture in 37% yield.

HRMS (ESI–) calcd for $C_{30}H_{37}N_6O_2$ $[M–H]^-$: 513.2972 found: 513.2985.

^{1}H- and ^{13}C-NMR spectra were assigned for the major diastereomers of compound **18** (Table S8). The signals in the aromatic region were not assigned due to severe signal overlap.

Table S8: ^{1}H- and ^{13}C-NMR data of the major diastereomers of compound **18** in methanol-d_4.[a]

		Diastereomer-1			Diastereomer-2		
Residue	*Position*	δ(^{13}C)	δ(^{1}H)	Mult./*J* [Hz]	δ(^{13}C)	δ(^{1}H)	Mult./*J* [Hz]
Trp	NH_2						
	Cα	52.2	4.76	dd	52.5	4.63	m
	CO	171.43			171.16		
	Cβ	29.2	3.46/3.32	m	27.9	3.37/3.27	m
hPhe	N						
	Cα	59.1	4.70	dd	61.8	4.62	m
	CO	171.39			171.10		
	N-CH_2-CH_2	43.0	3.01/2.94	m	43.7	3.69/3.52	m
	N-CH_2-CH_2	25.5	2.82/2.75	m	24.2	3.09/3.00	m
	Cβ	32.1	1.91/1.20	m	34.6	2.33/2.16	m
	Cγ	33.2	2.35/2.17	m	33.3	2.70/2.57	m
C-term. prot.	NH						
t-Butyl	C	52.4			52.5		
	CH_3	28.6	1.32	s	28.6	1.35	s

[a] hPhe: the phenethyl-glycine residue; *C*-term. prot.: the protection group at the *C*-terminus.

***N*-(2-(1*H*-Imidazol-4-yl)ethyl)-*N*-(1-(benzylamino)-1-oxo-4-phenylbutan-2-yl)benzamide (19)**

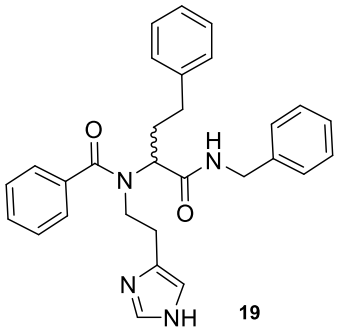

19

General procedure starting from commercially available benzoic acid (**4**), histamine (**6**) (1 mmol), 3-phenylpropanal (**8**) (1 mmol) and benzyl isocyanide (**10**) (1 mmol) in MeOH (4 mL) afforded the desired product **19** as a white solid in 32% yield.

^{1}H NMR (500 MHz, acetone-d_6) δ 11.16 (s, 1H), 9.52 (s, 1H), 7.51 – 6.99 (m, 16H), 6.88 – 6.52 (s, 1H), 4.58 – 4.20 (m, 3H), 3.72 – 3.44 (m, 2H), 3.11 – 2.44 (m, 4H), 2.40 – 2.01 (m, 2H); ^{13}C NMR (126 MHz, DMSO-d_6) δ 171.25, 169.97, 141.68, 140.69, 139.74, 136.97, 134.54, 128.95, 128.38 (2C), 128.28 (2C), 128.20 (4C), 127.28 (2C), 126.66, 126.42, 126.13, 125.93 (2C), 112.57, 58.29, 48.84, 42.43, 32.55, 30.74, 26.84; HRMS (ESI) calcd for $C_{29}H_{31}N_4O_2$ $[M+H]^+$: 467.2442 found: 467.2435.

Modeling and docking

The X-ray crystal structure of the complex of endothiapepsin (PDB code: 4KUP) with compound **1** was used for our modeling studies. The energy of the system was minimized using the MAB force field as implemented in the computer program MOLOC.[1] Taking inspiration from the cocrystal structure of endothiapepsin with compound **1**, as well as from hot-spot analysis[2] of the active site of endothiapepsin, a new Ugi scaffold was designed and subsequent energy minimization (MAB force field) was done using MOLOC. All types of interactions (H-bonding, lipophilic and repulsive interactions) between designed Ugi products and protein were analyzed in MOLOC. Designed compounds were subsequently docked into the active site of endothiapepsin by using the FlexX docking module in the LeadIT suite. During the docking, the binding site in the protein was restricted to 6.5 Å around the cocrystallized ligand **1**, and the 30 top (FlexX)-scored solutions were retained, subsequently post-scored with SEESAR[3], and the best scored pose was selected.

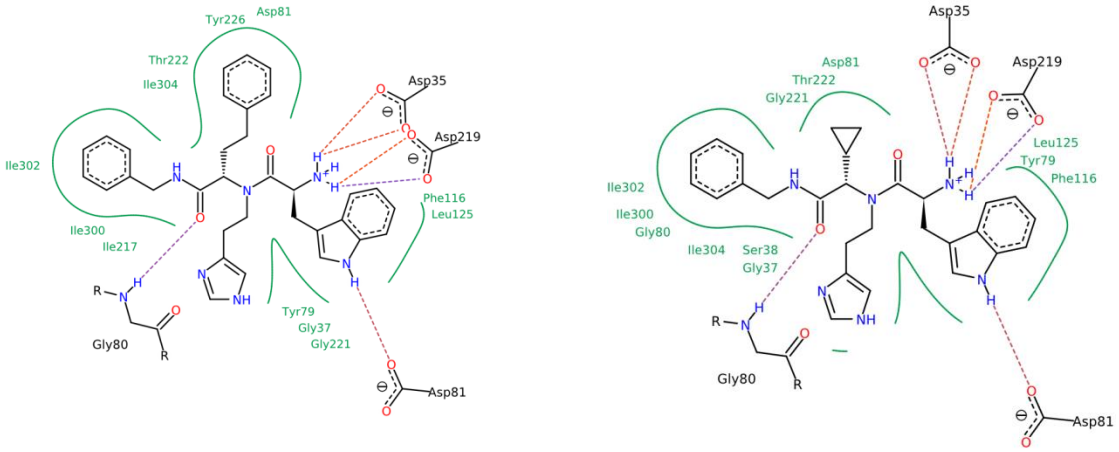

Figure S5. Predicted binding modes of compounds **2** and **11**. These binding modes are the result of a docking run using the FlexX docking module with 30 poses and represent the top-scoring pose after HYDE scoring with SEESAR and careful visual inspection to exclude poses with significant inter- or intra-molecular clash terms or unfavorable conformations. The figures were generated with PoseView as implemented in the LeadIT suite.[3]

^{1}H-STD-NMR binding experiments

All ^{1}H-STD-NMR experiments were performed at 25 °C on a Varian 600 MHz spectrometer. The on-resonance irradiation on endothiapepsin was set to 0 ppm. In each experiment, one ligand (3 mM) and endothiapepsin (10 µM) were present.

All fragments of two Ugi hit compounds **2** and **11**, identified in the protein-templated Ugi reaction, were tested to verify their interaction with the protein by STD-NMR technique.

First, the ^{1}H-NMR spectra of the fragments Trp.HCl (**3**), histamine (**6**), 3-phenylpropanal (**8**), cyclopropanecarboxaldehyde (**7**), benzyl isocyanide (**10**) in NaOAc buffer (100 mM, NaOAc of pD = 4.7 in deuterated water (pH = 4.3)) and 5% DMSO-d_6, except for 3-phenylpropanal (**8**) (10% DMSO-d_6 was used for the solubility reason) in the presence of protein (off-resonance ^{1}H NMR spectra) were recorded. Subsequently, on-resonance ^{1}H-NMR spectra were recorded with minimum 512 scans. ^{1}H-STD-NMR spectra were obtained by subtracting the on-resonance spectrum from the corresponding off-resonance spectrum. ^{1}H-STD-NMR analysis revealed that all five fragments except for the cyclopropanecarboxaldehyde (**7**) bind to the protein with good to moderate interaction realized by the intensity of the peaks in the STD NMR (Figure S6–S10).

^{1}H-STD-NMR competition experiments

First, the ^{1}H-STD-NMR of each fragment (final concentration 3 mM), was recorded as mentioned above. Subsequently, bisacylhydrazone **20** (reported inhibitor, IC_{50} = 54 nM) was added to the same NMR tube in order to have a final concentration of 3 mM. Subsequently a second ^{1}H-STD NMR spectrum was recorded showing the appearance of bisacylhydrazone peaks and disappearance (or reduced intensity) of peaks of some fragments such as Trp.HCl (**3**) and histamine (**6**), indicating that they are displaced by the bisacylhydrazone **20** and bind in the active site of endothiapepsin where bisacylhydrazone is hosted (PDB: 5HCT). This experiment confirms that fragments Trp.HCl (**3**) and histamine (**6**) bind to the same binding pocket of the enzyme (Figure S11–S15).

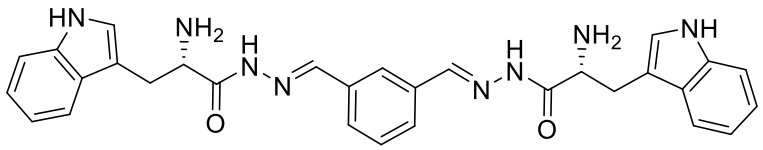

20
Bisacylhydrazone inhibitor

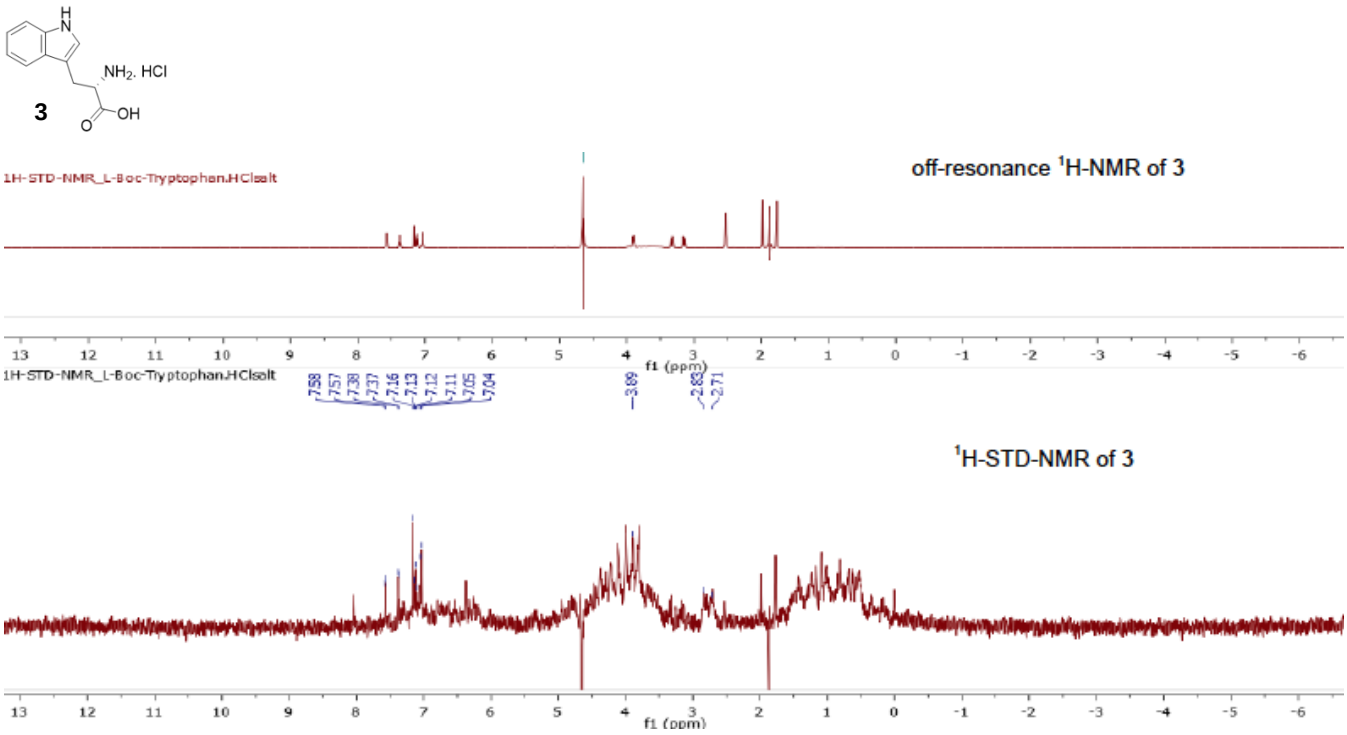

Figure S6. [1]H NMR reference spectrum (off-resonance) and STD spectrum for fragment **3**.

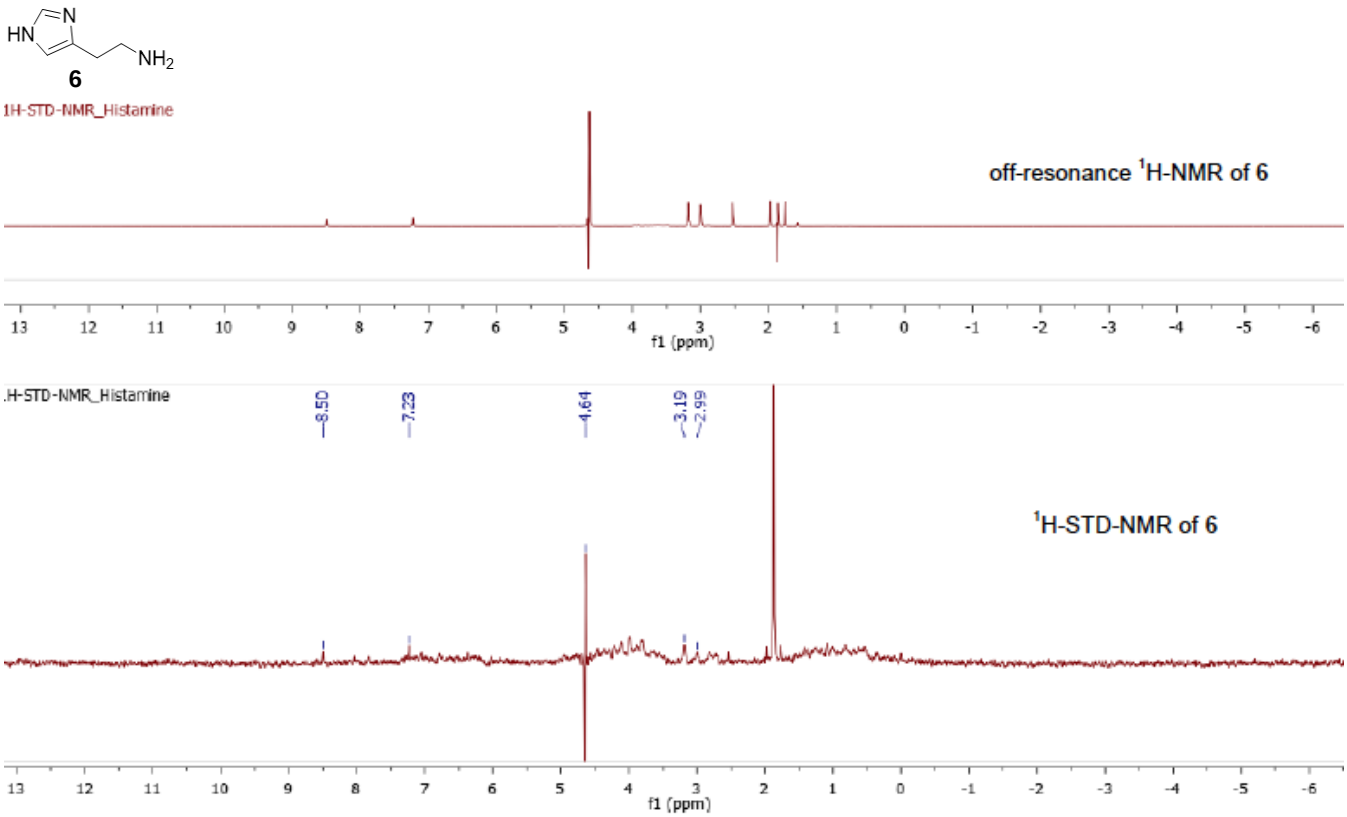

Figure S7. [1]H NMR reference spectrum (off-resonance) and STD spectrum for fragment **6**.

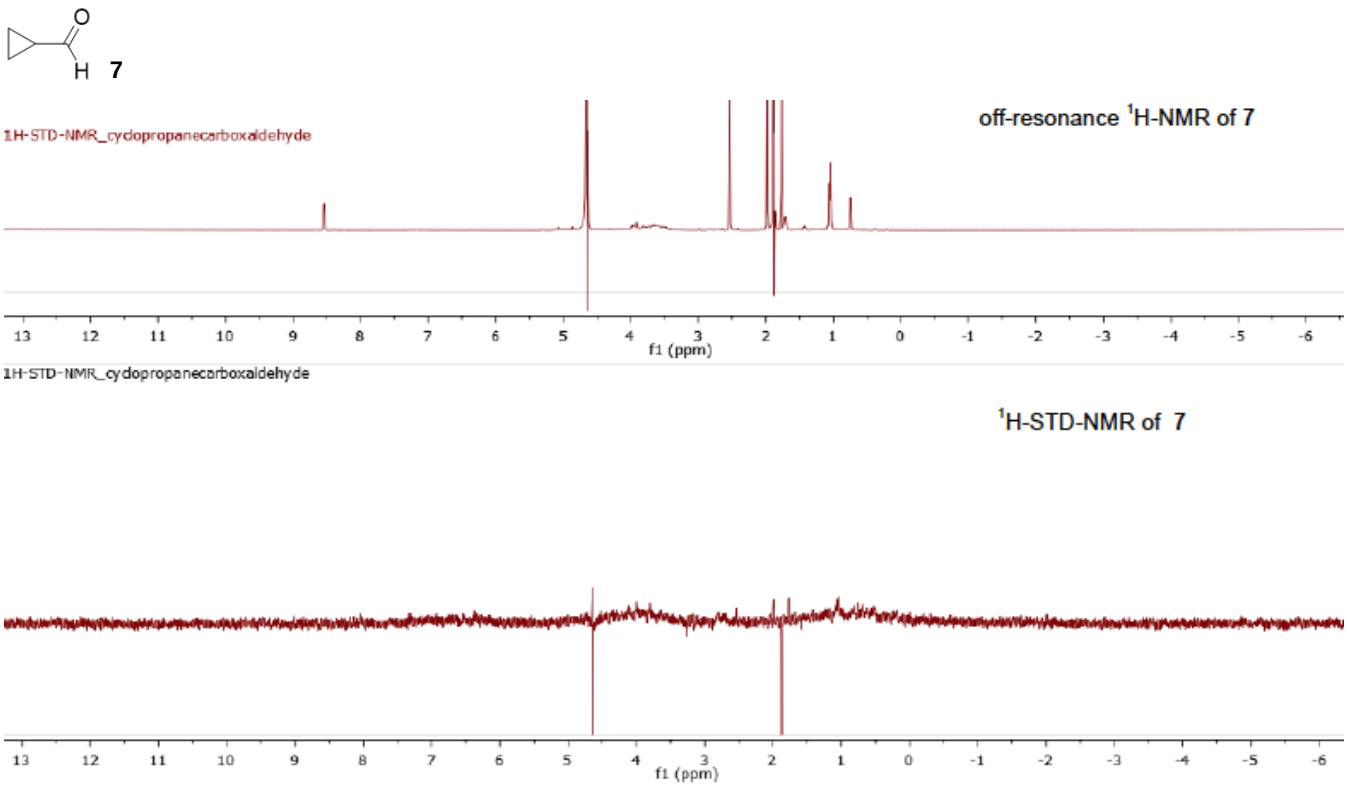

Figure S8. ^{1}H NMR reference spectrum (off-resonance) and STD spectrum for fragment **7**.

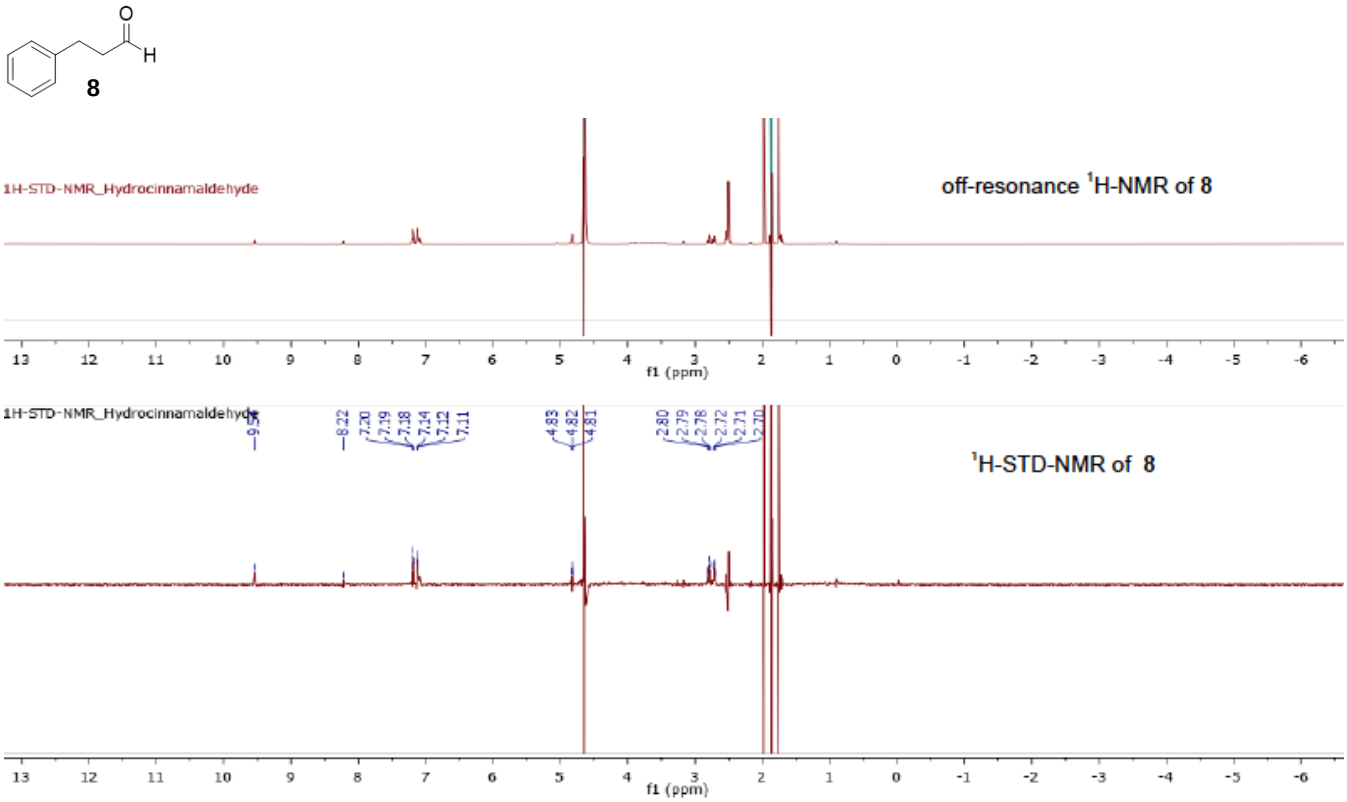

Figure S9. ^{1}H NMR reference spectrum (off-resonance) and STD spectrum for fragment **8.**

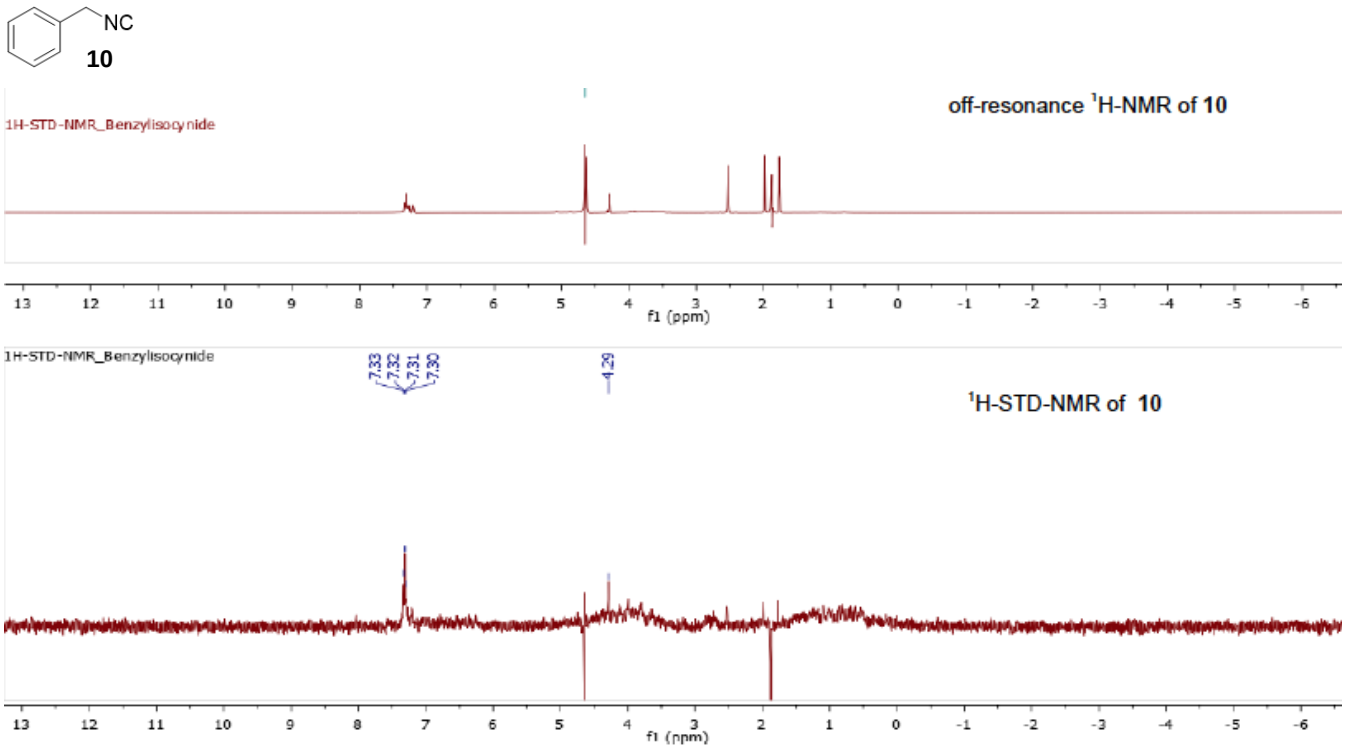

Figure S10. ^{1}H NMR reference spectrum (off-resonance) and STD spectrum for fragment **10**.

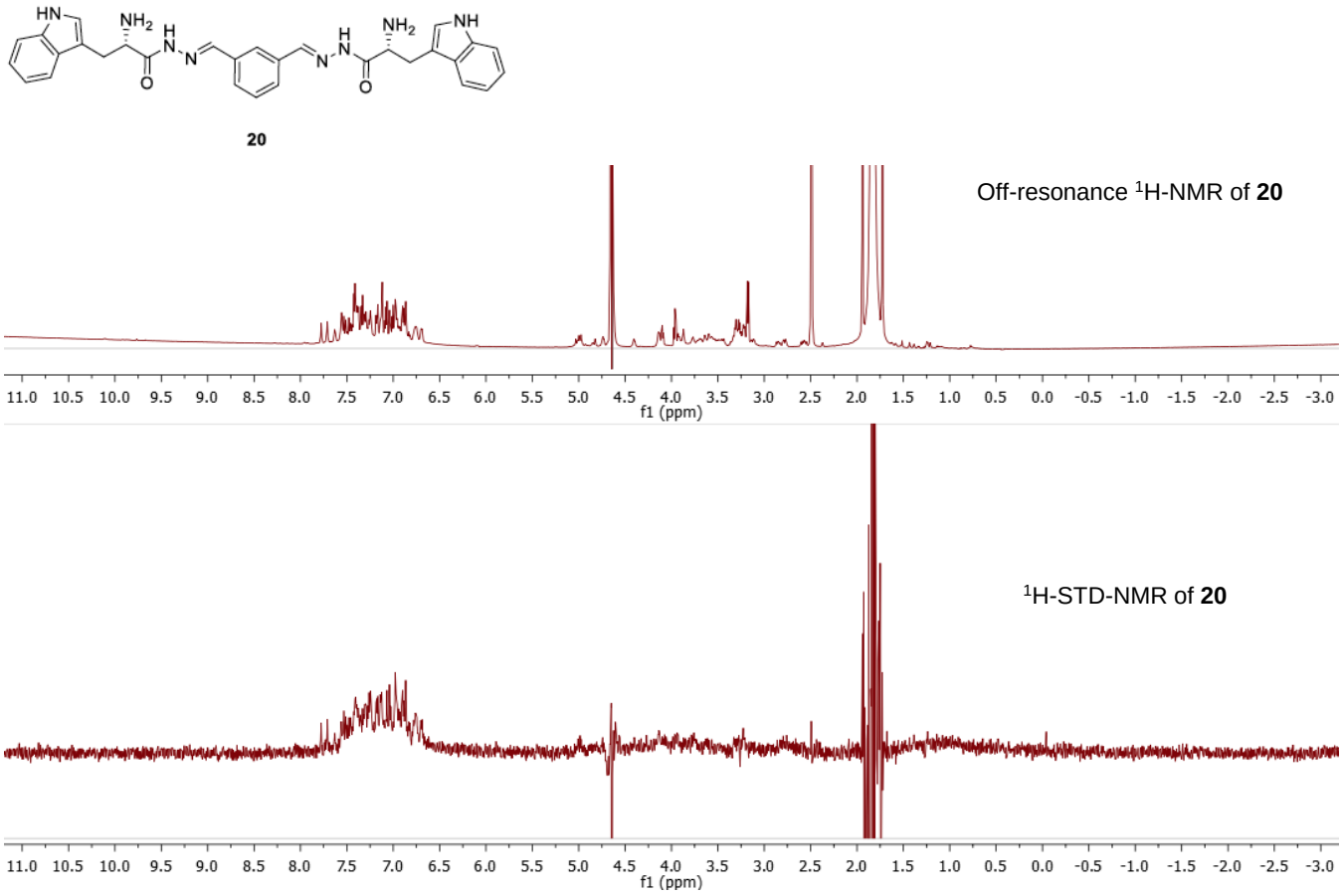

Figure S11. ^{1}H NMR reference spectrum (off-resonance) and STD spectrum for bisacylhydrazone **20.**

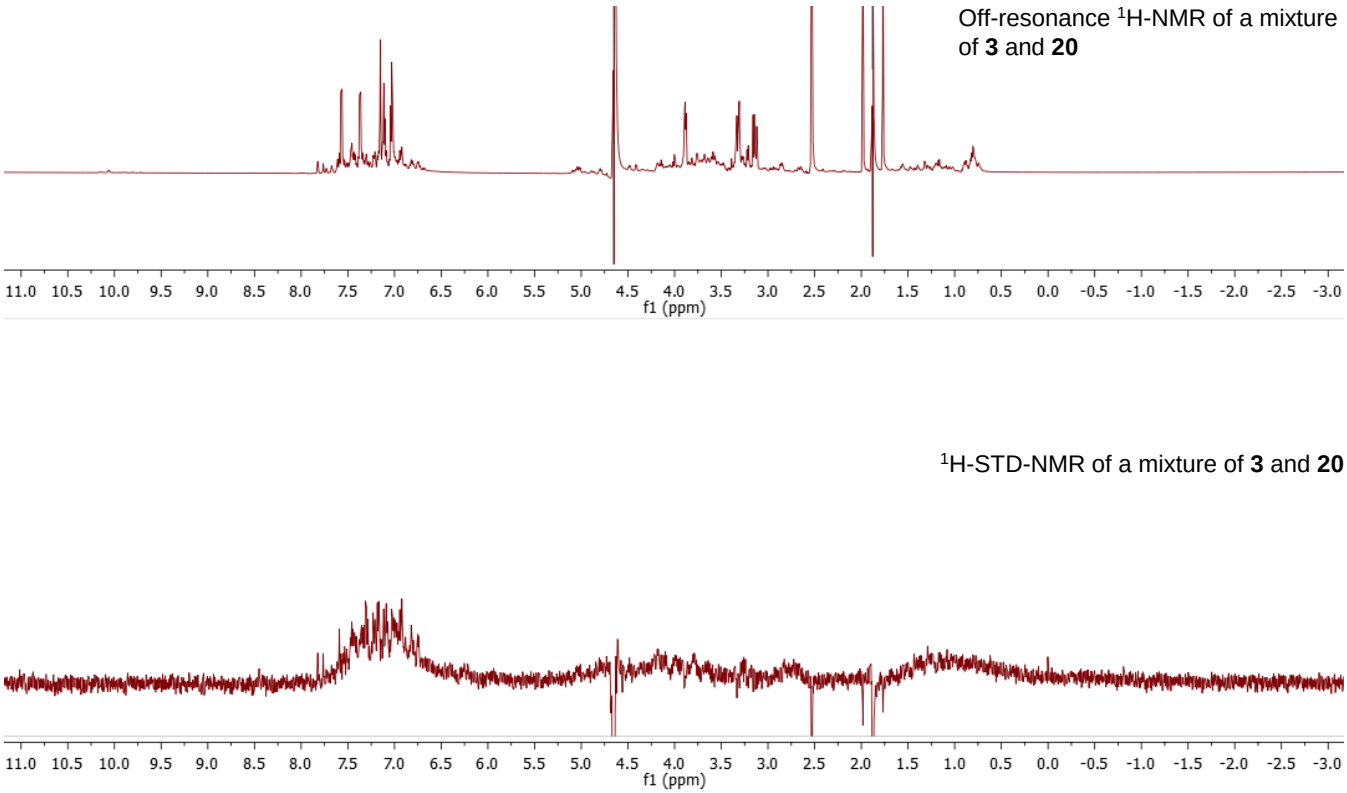

Figure S12. Competition STD-NMR of fragment **3** and bisacylhydrazone **20**, ^{1}H NMR reference spectrum (off-resonance) and STD spectrum.

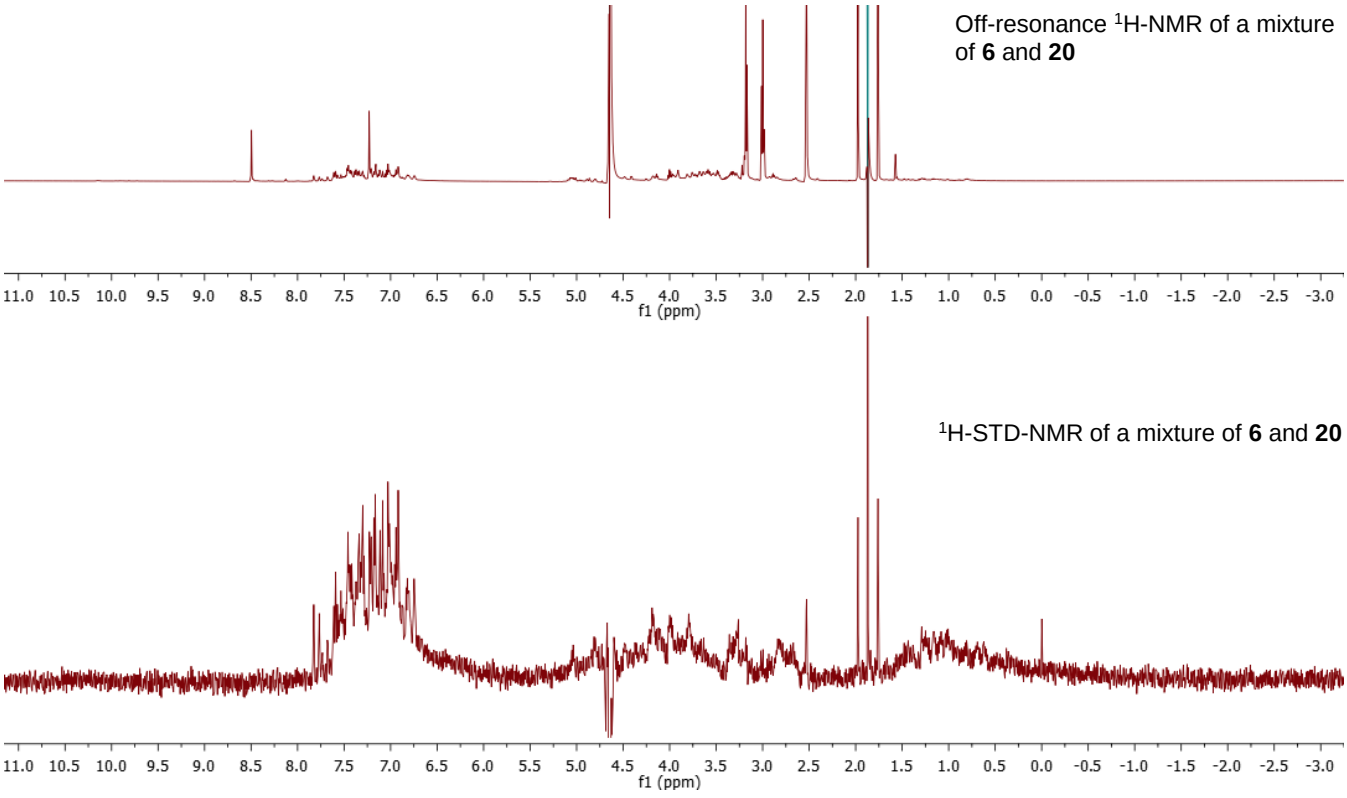

Figure S13. Competition STD-NMR of fragment **6** and bisacylhydrazone **20,** ^{1}H NMR reference spectrum (off-resonance) and STD spectrum.

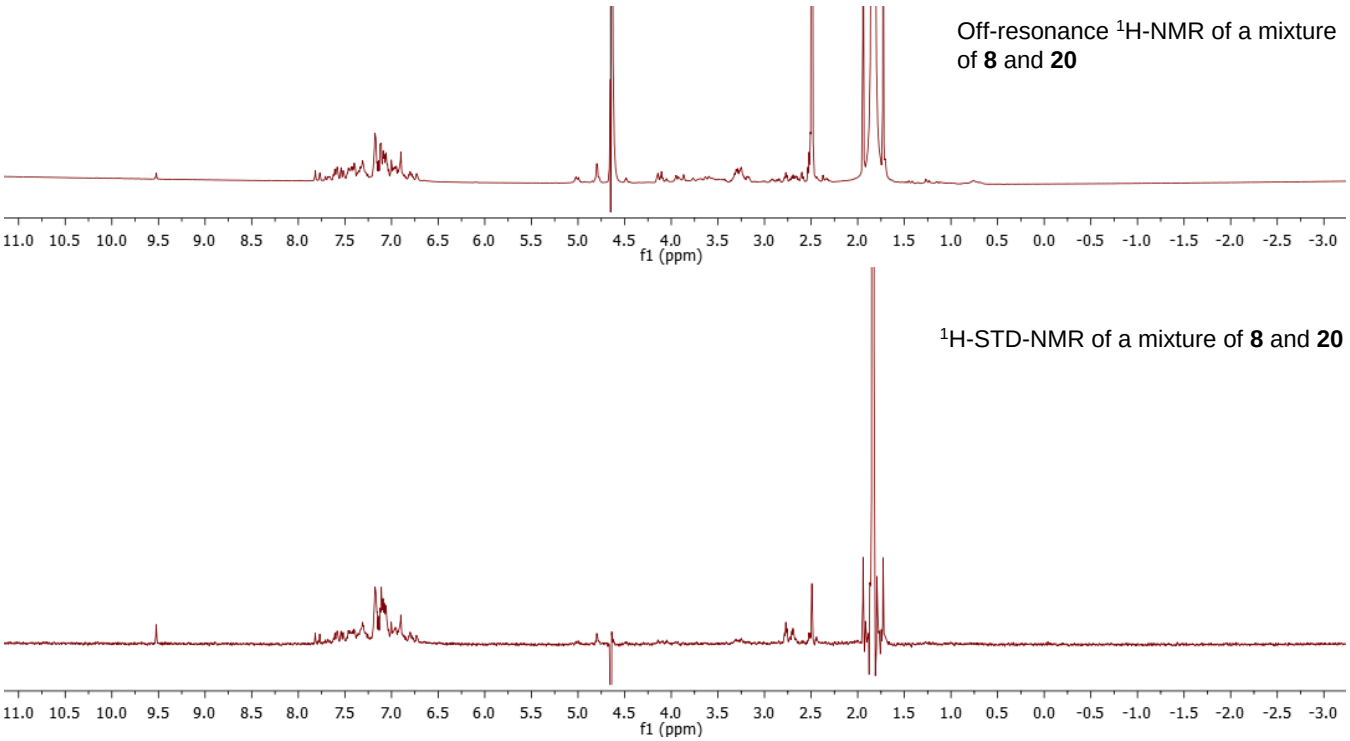

Figure S14. Competition STD-NMR of fragment **8** and bisacylhydrazone **20,** ^{1}H NMR reference spectrum (off-resonance) and STD spectrum.

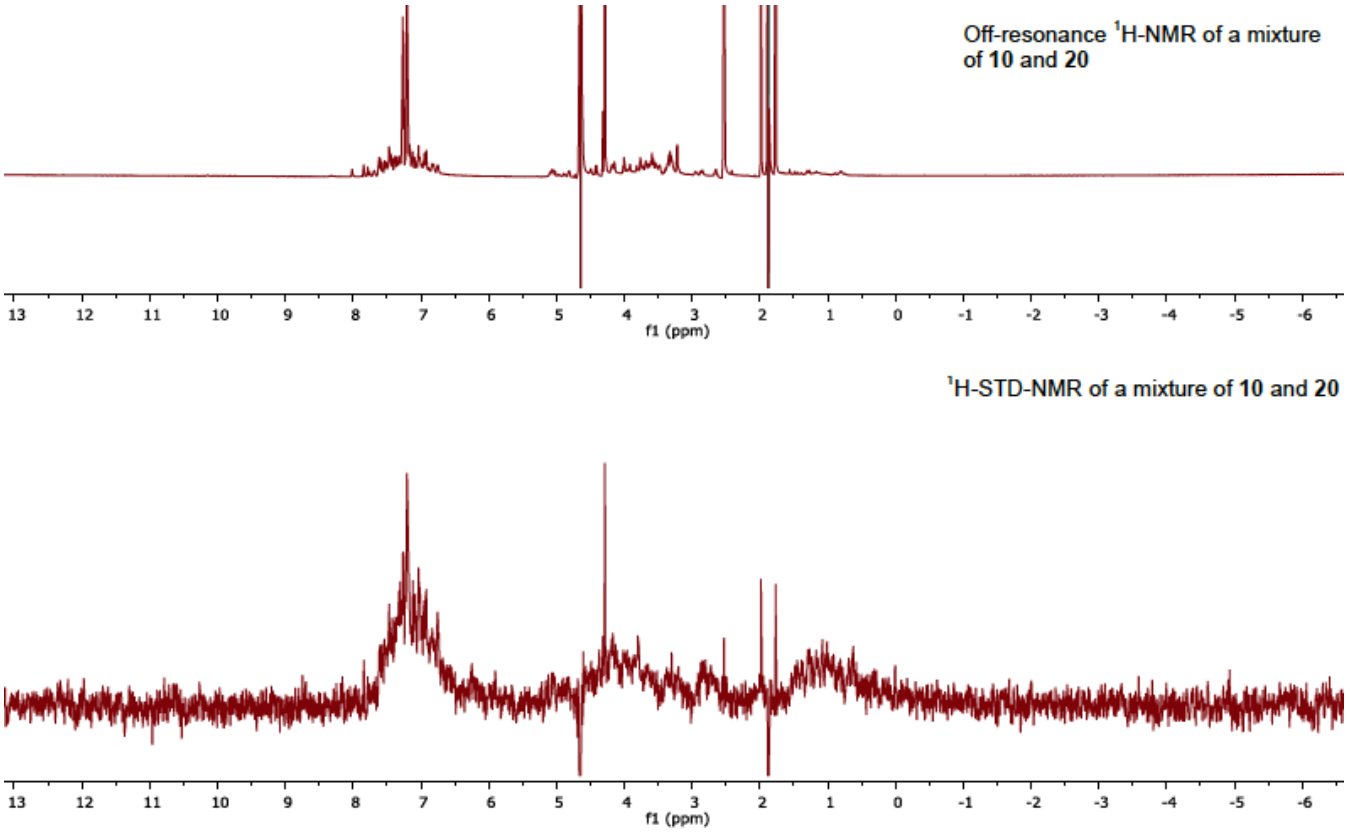

Figure S15. Competition STD-NMR of fragment **10** and bisacylhydrazone **20,** ^{1}H NMR reference spectrum (off-resonance) and STD spectrum.

Fluorescence-based inhibition assay

Endothiapepsin was purified from Suparen® (kindly provided by DSM Food Specialties) by exchanging the buffer to sodium acetate buffer (0.1 M, pH 4.6) using a Vivaspin 500 with a molecular weight cut-off at 10,000 Da. Measurement of the absorption at 280 nm, assuming an extinction coefficient of 1.15 for 1 mg/mL solutions, afforded the protein concentration. Stock solutions (100 mM in DMSO) were prepared for all Ugi compounds. The final reaction volume was 200 µL containing 0.4 nM endothiapepsin, 1.8 µM substrate and 2.1% DMSO. The final concentration of inhibitors was 250 µM in the first well and subsequent half dilution in the next 10 wells. In the same way, blanks were prepared using DMSO instead of the inhibitor stock solutions. As substrate, Abz-Thr-Ile-Nle-*p*-nitro-Phe-Gln-Arg-NH_2 (purchased from Bachem) was used for the fluorescence screening assay. The assay was performed with flat bottom 96-well microplates (purchased from Greiner Bio-One) using a Synergy Mx microplate reader at an excitation wavelength of 337 nm and an emission wavelength of 414 nm. The K_m of the substrate toward endothiapepsin was known, 1.6 µM. The assay buffer (0.1 M sodium acetate buffer, pH 4.6, containing 0.001% Tween 20) was premixed with the substrate and inhibitor; endothiapepsin was added directly before the measurement. As the substrate is a fluorogenic substrate, during measurement the fluorescence increased because of substrate hydrolysis by endothiapepsin. The initial slopes of the fluorescence in the wells containing the Ugi compound were compared to the initial slope of the blanks for data analysis. Each compound was measured in duplicate. The result represents the average of both measurements (Figure S16–S24).

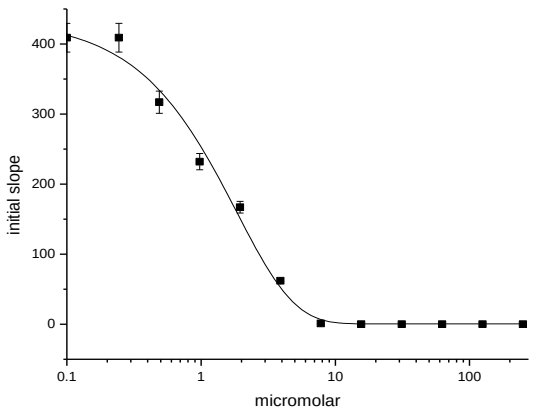

Model	DoseResp		
Equation	y = A1 + (A2-A1)/(1 + 10^((LOGx0-x)*p))		
Reduced Chi-Sqr	254.82007	301.55489	
Adj. R-Square	0.9909	0.98921	
		Value	Standard Error
1ST	A1	0.52394	6.81889
	A2	452944.276	2.52843E8
	LOGx0	-12.75382	1029.77094
	p	-0.23656	0.07746
	span	452943.75207	
	IC50	1.29	
2ND	A1	4.23962	7.27544
	A2	317600.60299	1.32367E8
	LOGx0	-10.35392	661.18149
	p	-0.27558	0.09701
	span	317596.36336	
	IC50	1.24	
FINAL		1.30± 0.03 µM	

Figure S16. IC_{50} inhibition curve of compound **2**.

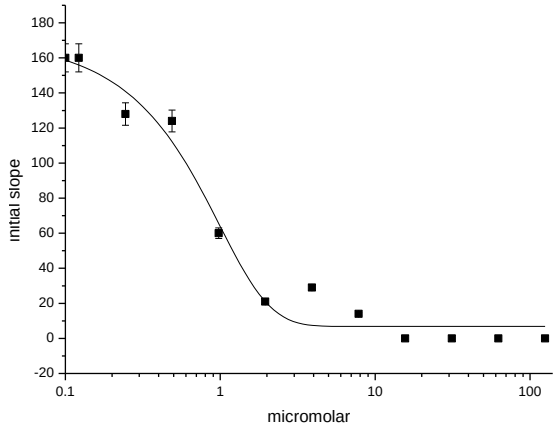

Model	DoseResp		
Equation	y = A1 + (A2-A1)/(1 + 10^((LOGx0-x)*p))		
Reduced Chi-Sqr	132.28946	104.02666	
Adj. R-Square	0.96947	0.97843	
		Value	Standard Error
1ST	A1	6.8363	4.74583
	A2	311.01194	295.64917
	LOGx0	0.09794	1.15793
	p	-0.70656	0.36463
	span	304.17563	
	IC50	0.8	
2ND	A1	3.2442	
	A2	183.10832	
	LOGx0	0.83969	4.14221
	p	-1.02049	33.10057
	span	179.86412	0.2064
	IC50	0.97	
FINAL		0.89 ±0.9 µM	

Figure S17. IC_{50} inhibition curve of single diastereomer of compound **2.**

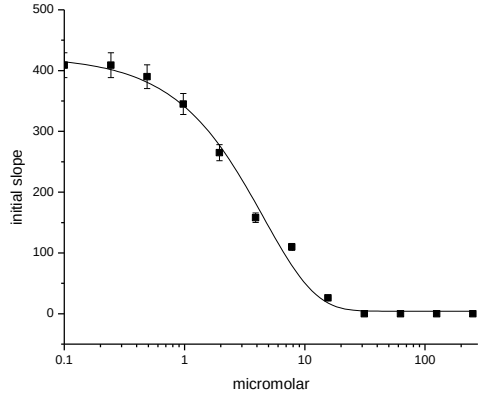

Model	DoseResp		
Equation	y = A1 + (A2-A1)/(1 + 10^((LOGx0-x)*p))		
Reduced Chi-Sqr	245.87784	771.22104	
Adj. R-Square	0.99209	0.97269	
		Value	Standard Error
1ST	A1	4.20673	7.66233
	A2	521409.48568	3.23385E8
	LOGx0	-32.3353	2827.03171
	p	-0.09569	0.03087
	span	521405.27895	
	IC50	3.35	
2ND	A1	20.11986	13.79425
	A2	553684.27857	7.23674E8
	LOGx0	-36.13727	6544.85419
	p	-0.08707	0.05275
	span	553664.15872	
	IC50	3.6	
FINAL		3.5± 0.1 µM	

Figure S18. IC_{50} inhibition curve of compound **11**.

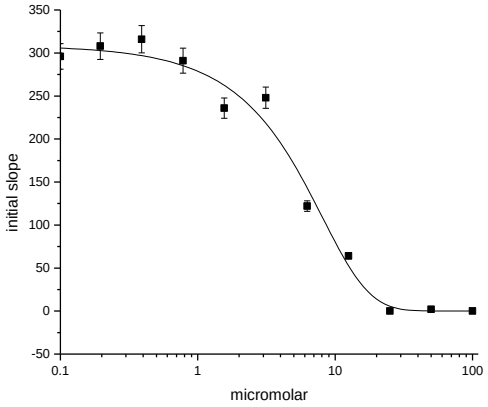

Model	DoseResp		
Equation	y = A1 + (A2-A1)/(1 + 10^((LOGx0-x)*p))		
Reduced Chi-Sqr	350.78997	276.04691	
Adj. R-Square	0.98023	0.98483	
		Value	Standard Error
1ST	A1	0.09664	11.81017
	A2	645.80625	518.00582
	LOGx0	-0.47444	8.17878
	p	-0.08107	0.03384
	span	645.70962	
	IC50	6	
2ND	A1	3.6597	10.18968
	A2	545.25655	260.6572
	LOGx0	1.38083	4.64851
	p	-0.09208	0.03157
	span	541.59684	
	IC50	5.93	
FINAL		6± 0.2 µM	

Figure S19. IC_{50} inhibition curve of compound **13**.

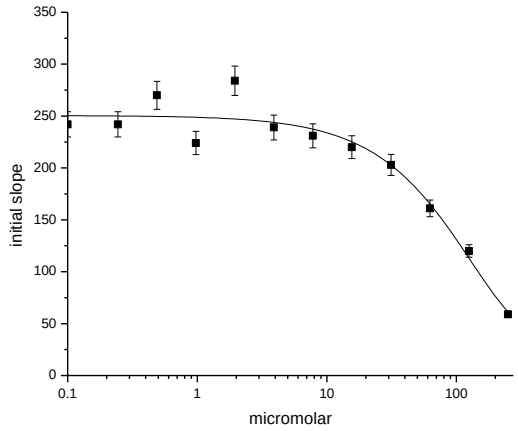

Model	DoseResp		
Equation	y = A1 + (A2-A1)/(1 + 10^((LOGx0-x)*p))		
Reduced Chi-Sqr	335.81307	1387.25489	
Adj. R-Square	0.9197	0.78114	
		Value	Standard Error
1ST	A1	30.35252	131.14288
	A2	39734.60335	2.04314E7
	LOGx0	-660.18555	67679.84449
	p	-0.00341	0.01004
	span	39704.25084	
	IC50	164.4	
2ND	A1	54.33219	38.90085
	A2	384.99411	527.24876
	LOGx0	15.40712	126.67285
	p	-0.0112	0.01525
	span	330.66192	
	IC50	93.8	
FINAL		129 ± 35 µM	

Figure S20. IC_{50} inhibition curve of compound **14***

***** low solubility, 250 µM, 5% DMSO.

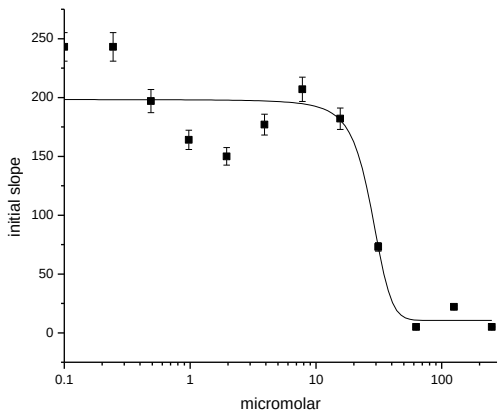

Model	DoseResp		
Equation	y = A1 + (A2-A1)/(1 + 10^((LOGx0-x)*p))		
Reduced Chi-Sqr	1025.56987	1207.91558	
Adj. R-Square	0.87124	0.84698	
		Value	Standard Error
1ST	A1	10.55165	18.566
	A2	199.33929	16.24107
	LOGx0	27.50495	4.72454
	p	-0.08108	0.06696
	span	188.78765	
	IC50	25.2	
2ND	A1	8.69543	24.34623
	A2	256496.69814	7.25721E8
	LOGx0	-145.50061	57823.76694
	p	-0.02135	0.03302
	span	256488.00271	
	IC50	13	
FINAL		19 ± 3 µM	

Figure S21. IC_{50} inhibition curve of compound **15**.

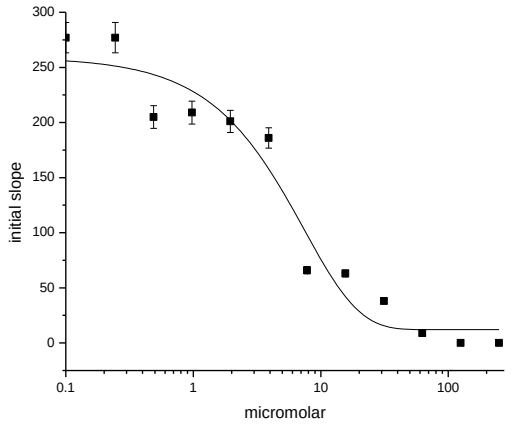

Model	DoseResp		
Equation	y = A1 + (A2-A1)/(1 + 10^((LOGx0-x)*p))		
Reduced Chi-Sqr	754.61969	241.38589	
Adj. R-Square	0.93549	0.97751	
		Value	Standard Error
1ST	A1	12.04224	14.69871
	A2	267065.36988	4.14944E8
	LOGx0	-51.64174	11546.8156
	p	-0.05873	0.056
	span	267053.32764	
	IC50	6.13	
2ND	A1	4.67556	8.31547
	A2	233.72314	16.98913
	LOGx0	15.13701	1.38989
	p	-0.09429	0.03782
	span	229.04758	
	IC50	13.69	
FINAL		10± 4 µM	

Figure S22. IC_{50} inhibition curve of compound **16**.

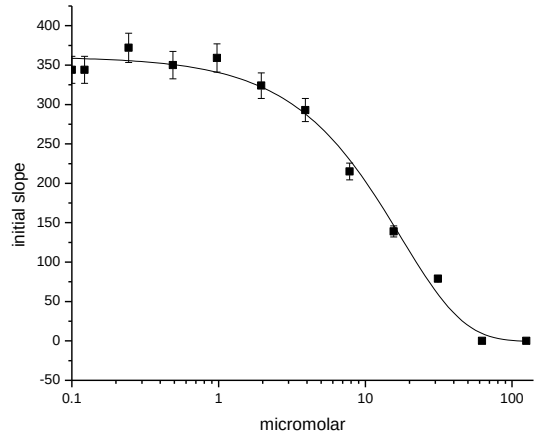

Model	DoseResp		
Equation	y = A1 + (A2-A1)/(1 + 10^((LOGx0-x)*p))		
Reduced Chi-Sqr	223.95513	147.6884	
Adj. R-Square	0.98914	0.99287	
		Value	Standard Error
1ST	A1	-0.51022	13.27949
	A2	141137.12519	3.02223E7
	LOGx0	-103.49733	3763.92819
	p	-0.02503	0.00998
	span	141137.63541	
	IC50	12.8	
2ND	A1	-0.38576	10.24377
	A2	587.07354	145.78275
	LOGx0	6.86374	7.22023
	p	-0.03143	0.00692
	span	587.4593	
	IC50	18.4	
FINAL		16± 3 µM	

Figure S23. IC_{50} inhibition curve of compound **17**.

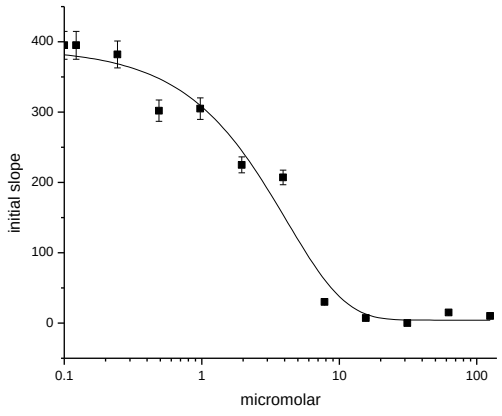

Model	DoseResp		
Equation	y = A1 + (A2-A1)/(1 + 10^((LOGx0-x)*p))		
Reduced Chi-Sqr	893.27644	325.14997	
Adj. R-Square	0.96793	0.98704	
		Value	Standard Error
1ST	A1	4.23	16.33931
	A2	23532.1097	1.42712E6
	LOGx0	-16.66926	261.76337
	p	-0.10662	0.07114
	span	23527.8797	
	IC50	2.85	
2ND	A1	4.41692	9.93995
	A2	1864.41947	4771.98042
	LOGx0	-5.79254	15.22128
	p	-0.10551	0.04147
	span	1860.00255	
	IC50	3.67	
FINAL		3.3± 0.4 µM	

Figure S24. IC_{50} inhibition curve of compound **18**.

Adaptation protocol for protein-modification test experiment

Seven reactions were started in parallel, an in situ Ugi reaction with all library members **3**–1**0** and individual fragments **3**, **6**–**8** and **10** (100 µM) were incubated with endothiapepsin (25 µM) in phosphate buffer (0.1 M, pH 6.8). Finally, pure protein was incubated in the same reaction buffer as a reference. After 18 h, reaction mixtures were diluted to 4 nM and were directly used as protein stock solutions.

Endothiapepsin was purified from Suparen® (kindly provided by DSM Food Specialties) by exchanging the buffer to potassium phosphate buffer (0.1 M, pH 6.8) using a Vivaspin 500 with a molecular weight cut-off at 10,000 Da. Measurement of the absorption at 280 nm, assuming an extinction coefficient of 1.15 for 1 mg/mL solutions, afforded the protein concentration.[4] The final reaction volume was 200 µL containing 0.4 nM endothiapepsin (from each test reaction), 1.8 µM substrate and 2.1% DMSO. As substrate, Abz-Thr-Ile-Nle-*p*-nitro-Phe-Gln-Arg-NH_2 (purchased from Bachem) was used for the fluorescence screening assay. The assay was performed with flat bottom 96-well microplates (purchased from Greiner Bio-One) using a Synergy Mx microplate reader at an excitation wavelength of 337 nm and an emission wavelength of 414 nm. The K_m of the substrate toward endothiapepsin was known, 1.6 µM.[5] The assay buffer (phosphate buffer 0.1 M, pH 6.8), containing 0.001% Tween 20) was premixed with the substrate, endothiapepsin was added directly before the measurement. As the substrate is a fluorogenic substrate, during measurement the fluorescence increased because of substrate hydrolysis by endothiapepsin. The initial slopes of the fluorescence in the wells containing different protein solutions were compared for data analysis. Each compound was measured in duplicate (Figure S25 and S26).

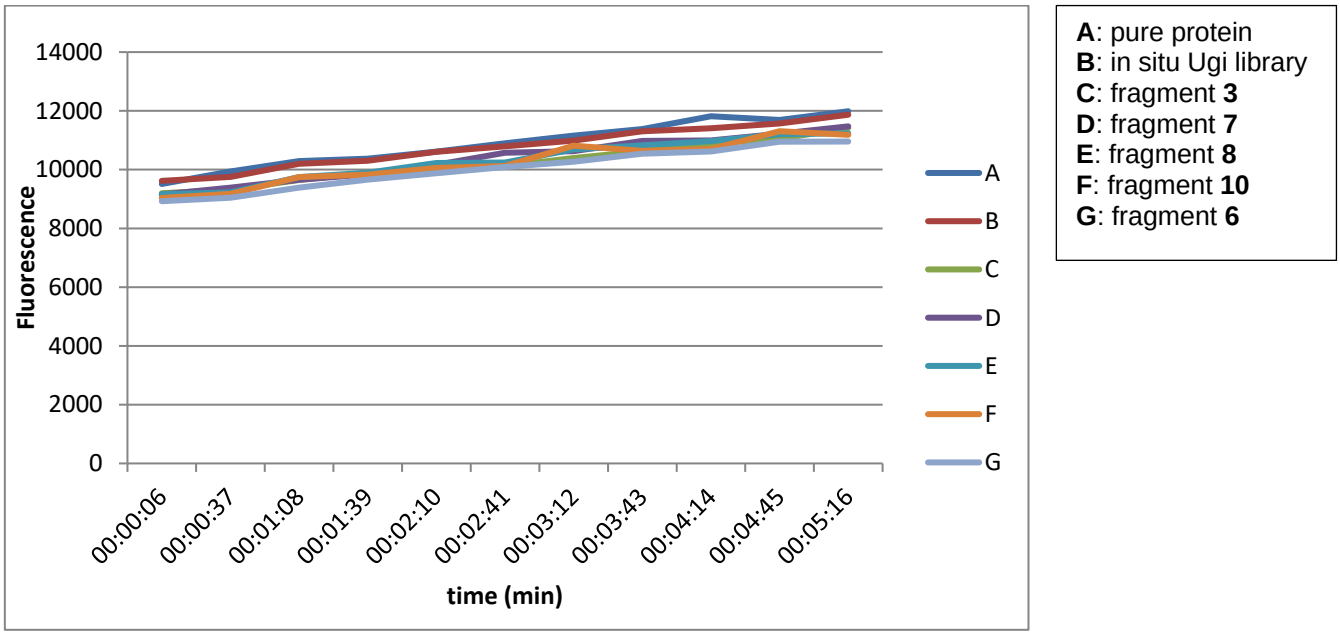

Figure S25. Protein-modification test first measurement.

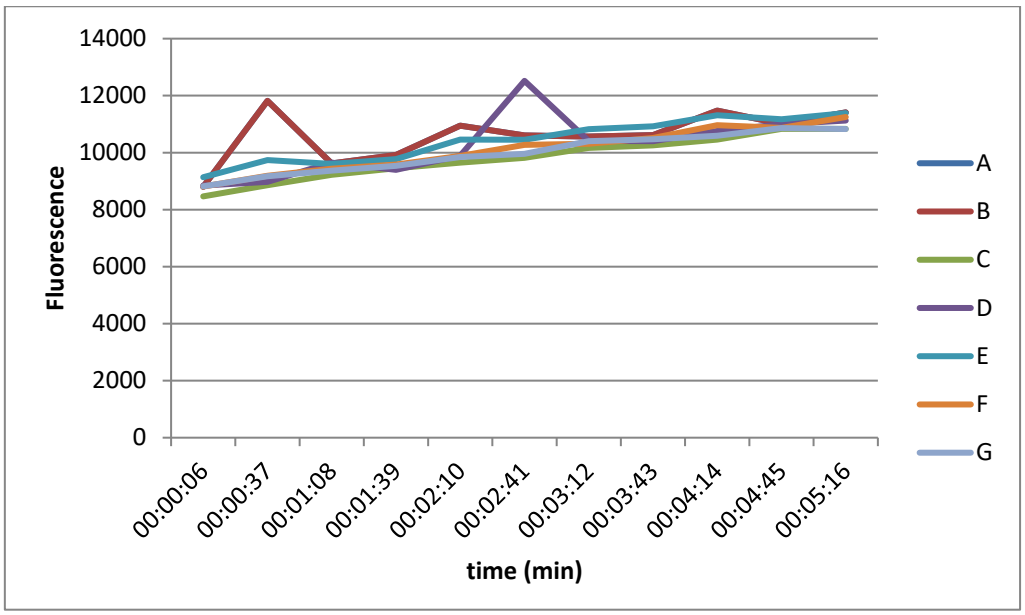

A: pure protein
B: in situ Ugi library
C: fragment **3**
D: fragment **7**
E: fragment **8**
F: fragment **10**
G: fragment **6**

Figure S26. Protein-modification test second measurement.

General procedures for Ugi-4CR-based KTGS using β-sliding clamp DnaN

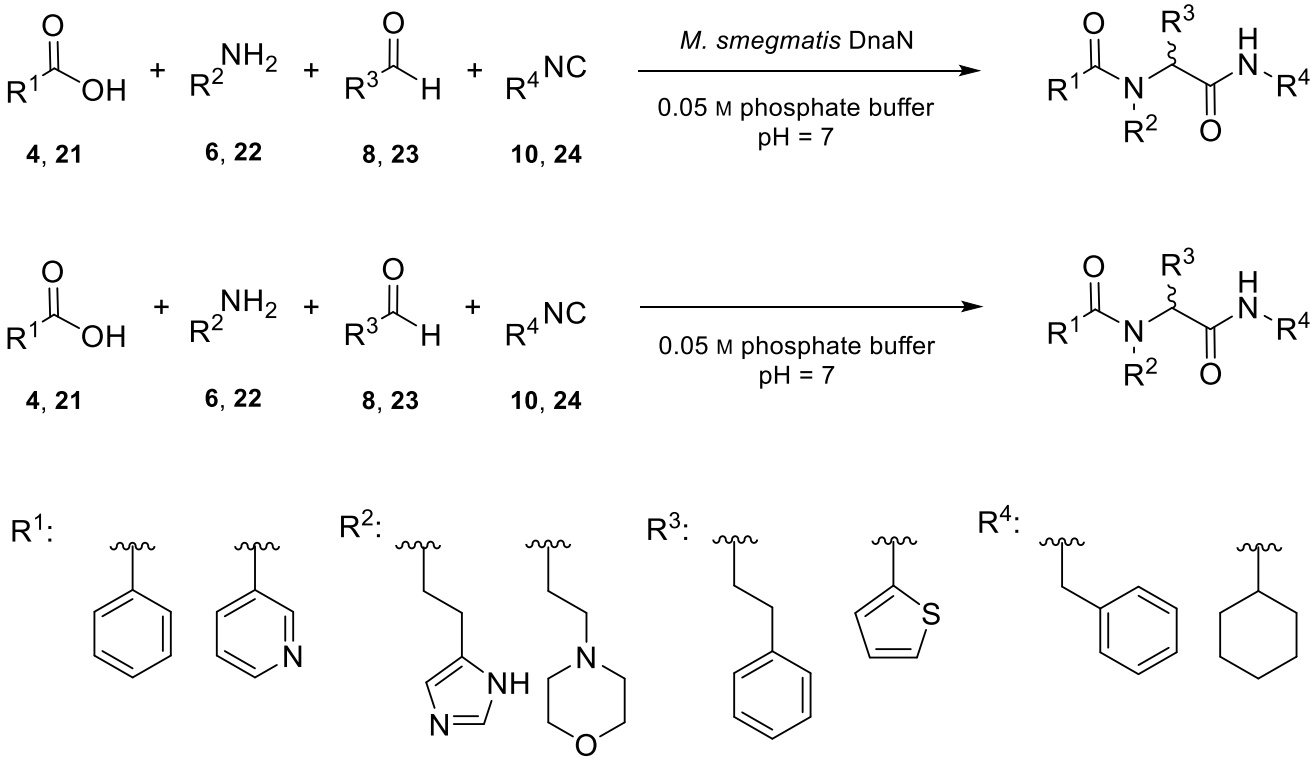

Scheme S3. From top to bottom: *in situ* Ugi reaction, blank reaction.

In situ Ugi 4-component reaction

DnaN (25 µL, 1.0 mM in phosphate buffer 0.05 M, pH 6.95), the 8 building blocks **4**, **6**, **8**, **10**, and **21**–**24** (1 µL each, 50 mM in DMSO) were added to a mixture of DMSO (42 µL) and phosphate buffer (925 µL, 0.05 M, pH 7). The reaction mixture was allowed to rotate on a rotating mixer at room temperature with 10 rpm. After 6 h, acetonitrile (100 µL) was added to a sample (50 µL) and was centrifuged at 9,727 *g* for 2 min and the supernatant was analysed by HPLC-HRMS measurement.

Blank reaction, negative control

The 8 building blocks **4**, **6**, **8**, **10**, and **21**–**24** (1 µL each, 50 mM in DMSO) were added to a mixture of DMSO (42 µL) and phosphate buffer (950 µL, 0.05 M, pH 7). The reaction mixture was allowed to rotate on a rotating mixer at room temperature with 10 rpm. After 6 h, acetonitrile (100 µL) was added to a sample (50 µL) and was centrifuged at 9,727 *g* for 2 min and the supernatant was analysed by HPLC-HRMS measurement.

In situ Ugi Experiments using endothiapepsin

Endothiapepsin (25 µL, 1.0 mM in phosphate buffer 0.05 M, pH 7), the 8 building blocks **4**, **6**, **8**, **10**, and **21**–**24** (1 µL each, 50 mM in DMSO) were added to a mixture of DMSO (42 µL) and phosphate buffer (925 µL, 0.05 M, pH 7). The reaction mixture was allowed to rotate on a rotating mixer at room temperature with 10 rpm. After 6 h, acetonitrile (100 µL) was added to a sample (50 µL) and was centrifuged at 9,727 *g* for 2 min and the supernatant was analysed by HPLC-HRMS measurement.

In situ Ugi-4CR experiments in presence of griselimycin

DnaN (25 µL, 1.0 mM in phosphate buffer 0.05 M, pH 7), the 8 building blocks **4**, **6**, **8**, **10**, and **21**–**24** (1 µL each, 50 mM in DMSO) and griselimycin (25 µL, 1.0 mM in DMSO) were added to a mixture of DMSO (17 µL) and phosphate buffer (850 µL, 0.05 M, pH 7). The reaction mixture was allowed to rotate on a rotating mixer at room temperature with 10 rpm. After 6 h, acetonitrile (100 µL) was added to a sample (50 µL) and was centrifuged at 9,727 *g* for 2 min and the supernatant was analysed by HPLC-HRMS measurement.

HLPC-HRMS method

All analyses were performed using a Thermo Scientific Dionex UltiMate 3000 UHPLC$^+$ focused system with a reversed-phase UPLC column (ACQUITY UPLC BEH C8 Column, 130 Å, 1.7 µm, 2.1 mm x 150 mm) coupled to a Thermo Scientific Q Exactive Focus system. Positive-ion mass spectra were acquired using ES ionization, injecting 4 µL of sample; column temperature 35 °C; flow rate 0.250 mL/min. The eluents, water (A) and acetonitrile (B) contained 0.1% of formic acid. The library components were eluted with a gradient of 90% (A) for 1 min, then from 90% → 5% (A) over 9 min, then at 5% (A) over 2 min, followed by 90% (A) for 1.8 min for column equilibration.

Quantification of Ugi 4CR products using external standard calibration

The detected amounts of compounds **19** and **25** were quantified through calibration curves of the synthetic references. Seventeen concentrations of each compound in acetonitrile/phosphate buffer (2:1) mixture containing DMSO 1.6% (v/v) (similar conditions to the HLPC-HRMS analysis) were prepared starting from 10.0 µM to 152.5879 pM in a serial dilution manner to find the appropriate concentration range covering the detected amounts in KTGS and blank experiments. Concentrations of samples were determined in triplicate by HLPC-HRMS using the same method as mentioned above. Calculation of the area under the curve (AUC) from the total ion current (TIC) chromatogram was performed using Thermo Xcalibur 3.0.63 program. Calibration curves using seven concentrations (9.7656 nM – 152.5879 pM) and the mean of the corresponding AUC for three measurements as well as the linear fitting were calculated by OriginPro 2019b software.

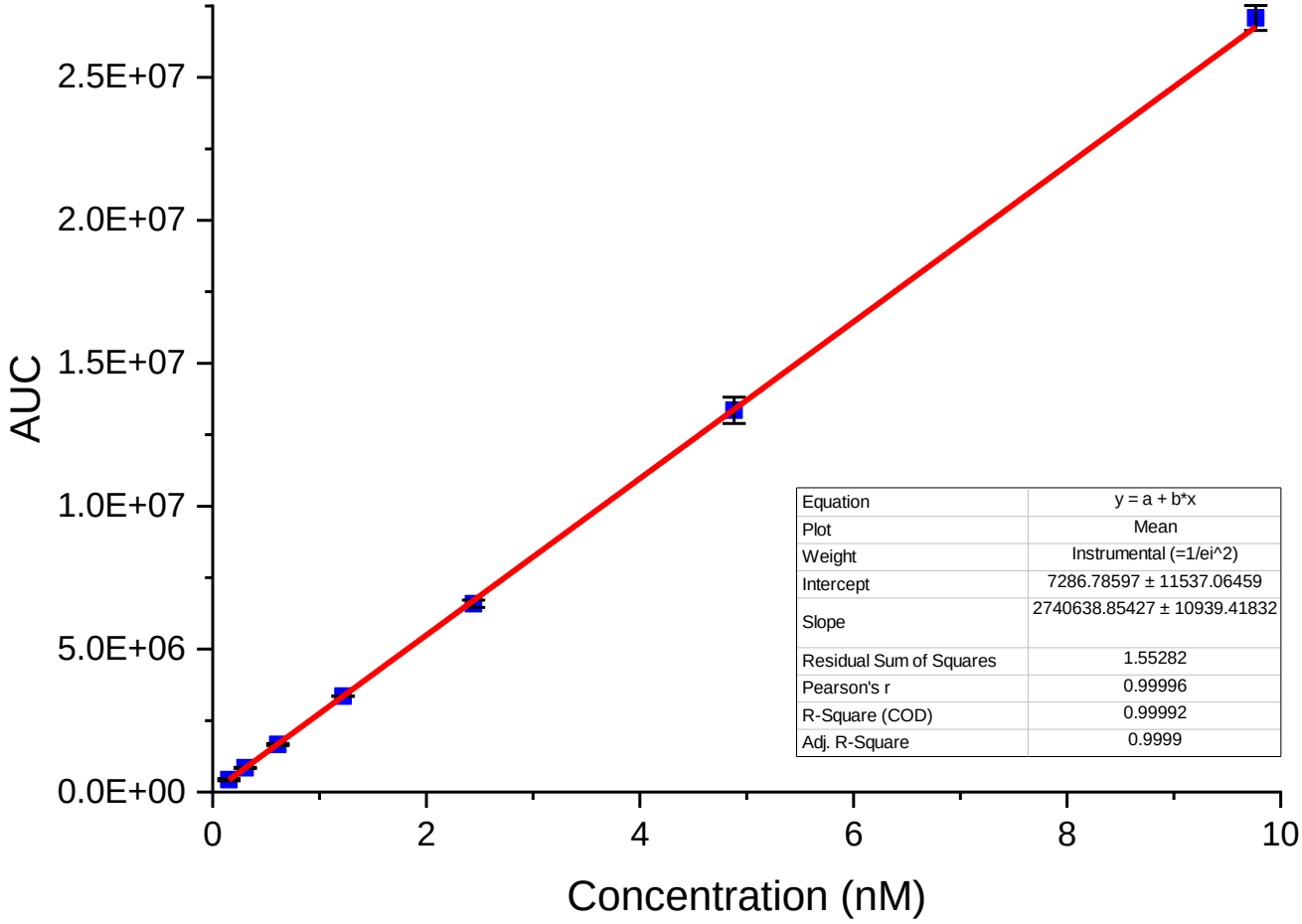

Figure S27. Calibration curve using compound **19** as an external standard at concentrations of 9.7656 nM – 152.5879 pM in a two-fold serial dilution. Error bars indicate the standard deviation for the mean of AUC from three measurements.

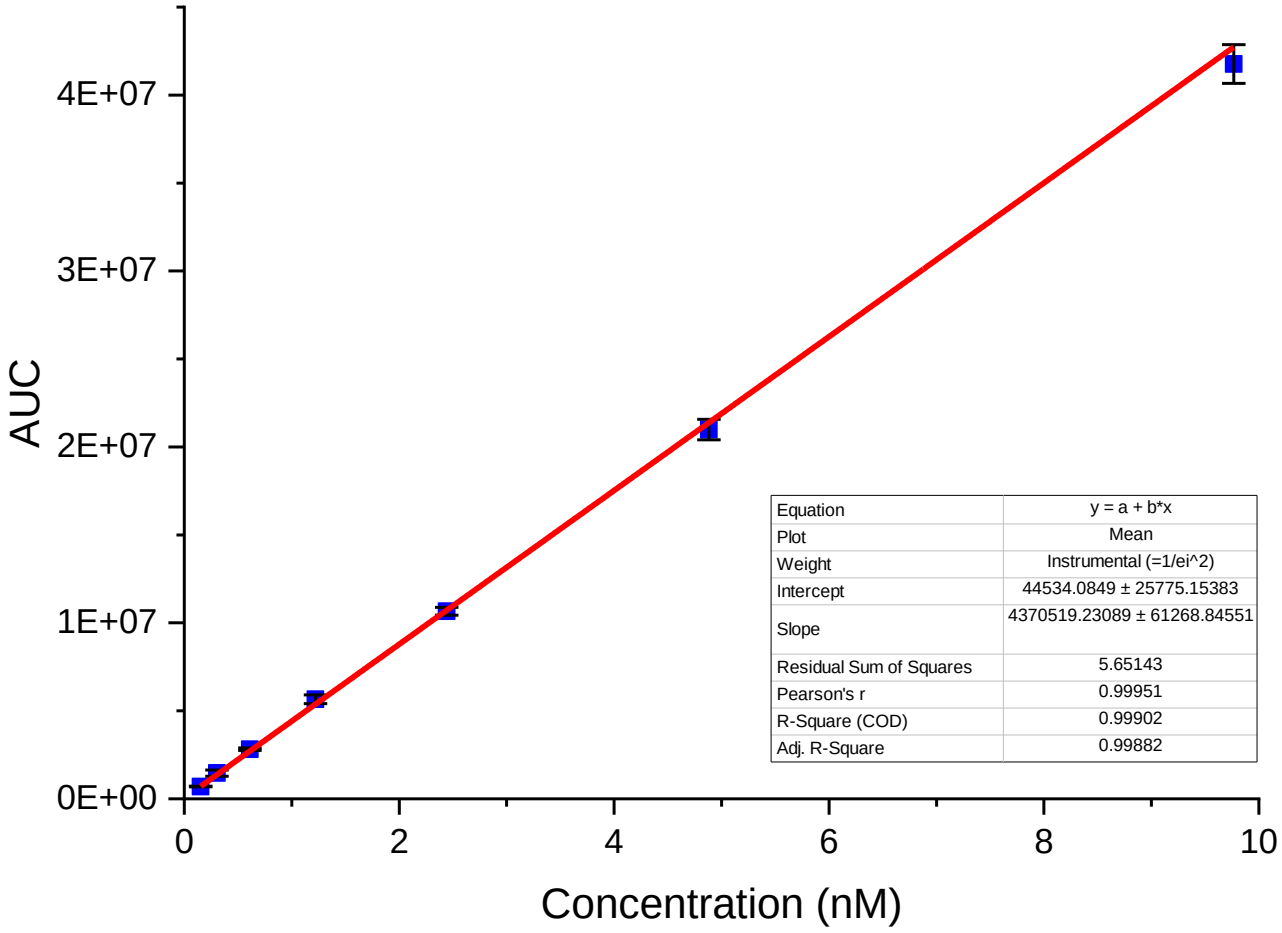

Figure S28. Calibration curve using compound **25** as an external standard at concentrations of 9.7656 nM – 152.5879 pM in a two-fold serial dilution. Error bars indicate the standard deviation for the mean of AUC from three measurements.

HPLC HRMS chromatograms

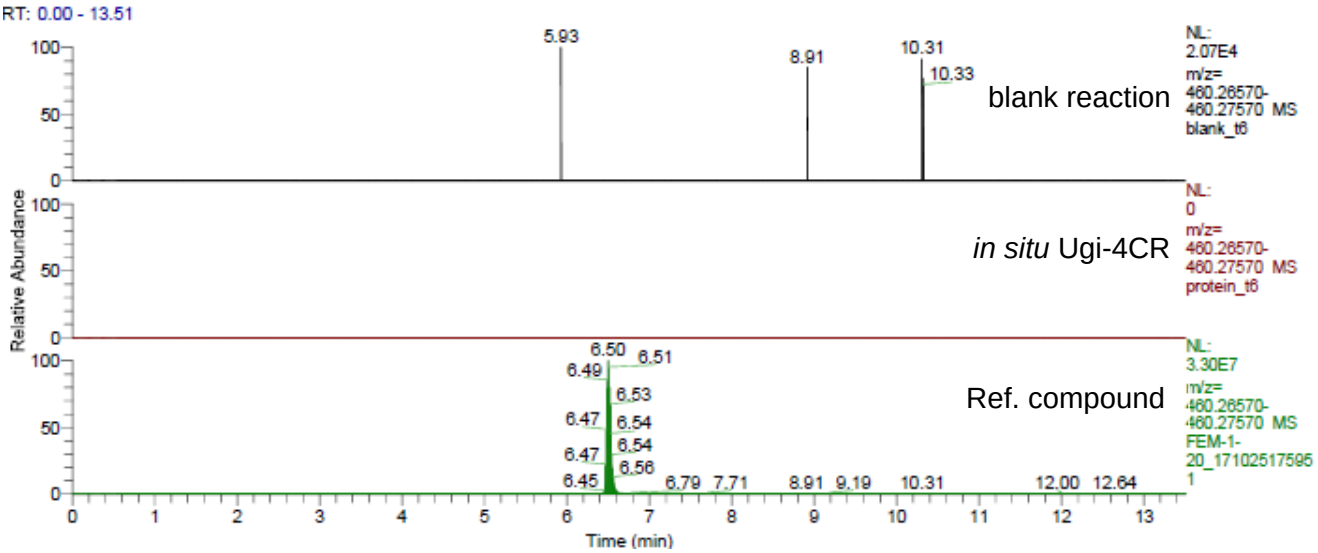

Figure S29. HPLC-HRMS analysis of compound **26** ([*M*+H]$^+$ = 460.27016). *In situ* Ugi-4CR was compared with the blank reaction and the synthesized compound as reference.

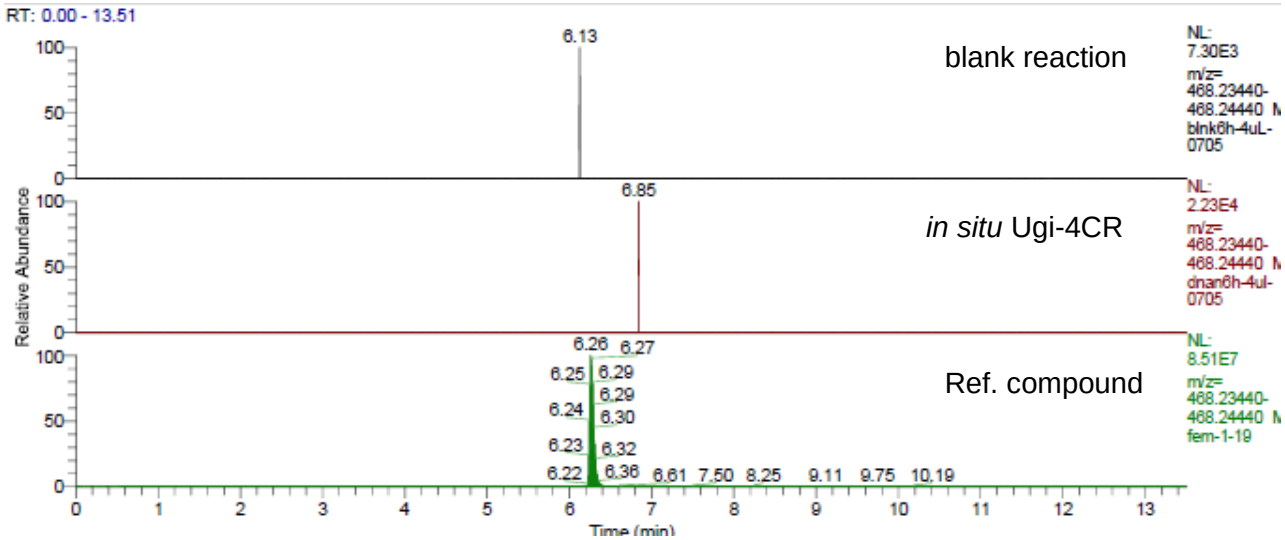

Figure S30. HPLC-HRMS analysis of compound **27** ([*M*+H]$^+$ = 468.23910). *In situ* Ugi-4CR was compared with the blank reaction and the synthesized compound as reference.

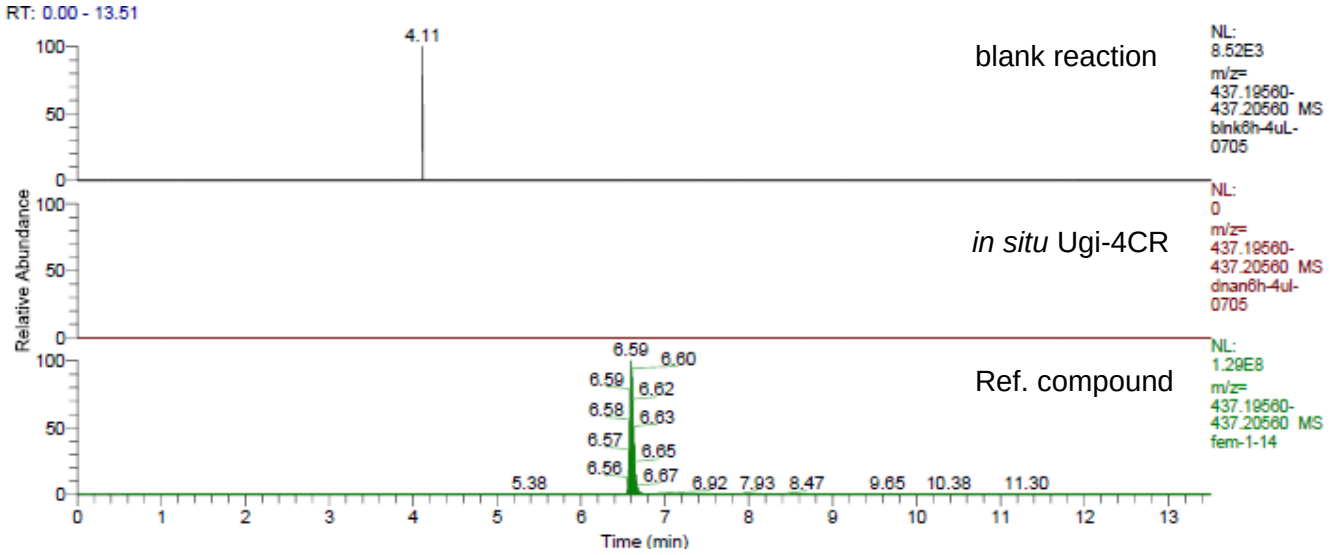

Figure S31. HPLC-HRMS analysis of compound **28** ([*M*+H]$^+$ = 437.2000). *In situ* Ugi-4CR was compared with the blank reaction and the synthesized compound as reference.

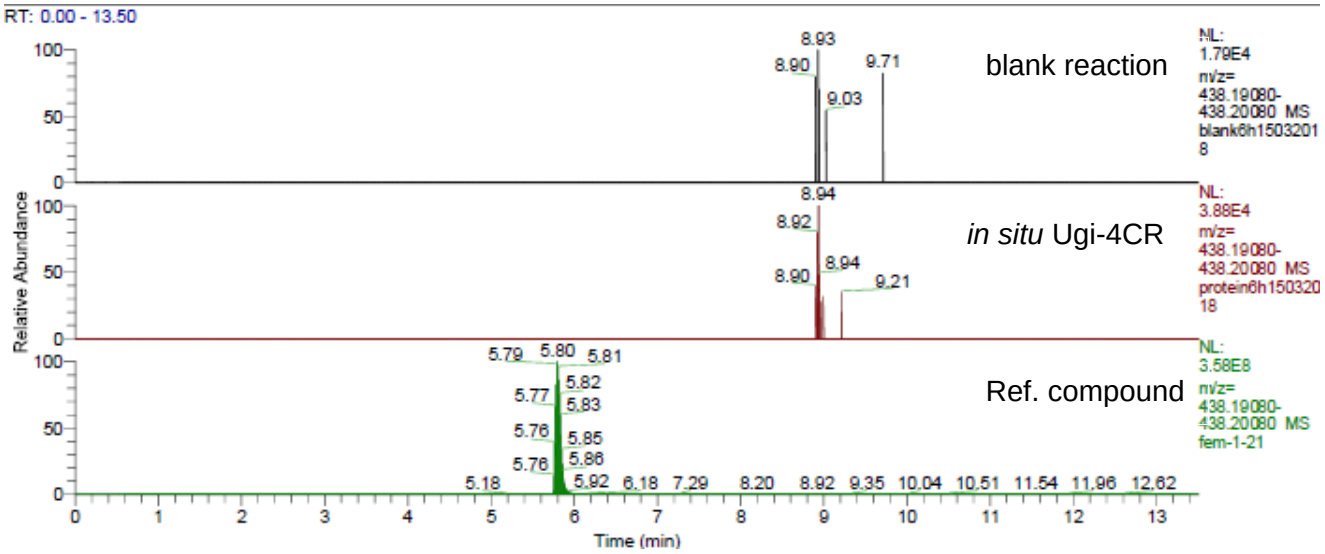

Figure S32. HPLC-HRMS analysis of compound **29** ([*M*+H]$^+$ = 438.19539). *In situ* Ugi-4CR was compared with the blank reaction and the synthesized compound as reference.

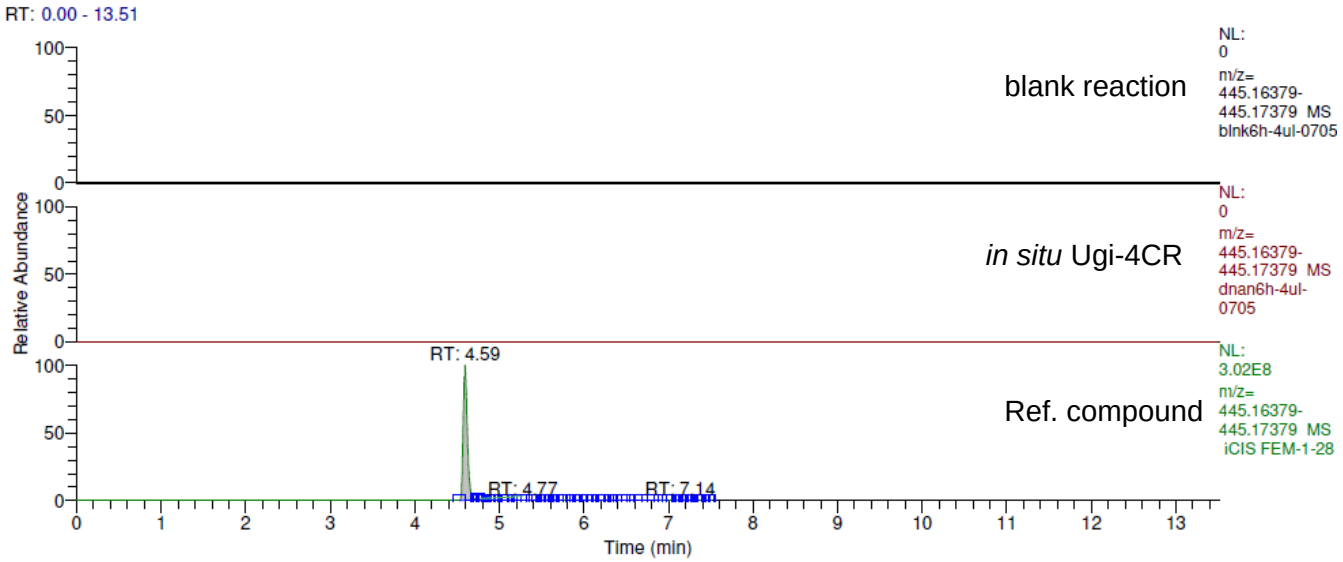

Figure S33. HPLC-HRMS analysis of compound **30** ([*M*+H]$^+$ = 445.16879). *In situ* Ugi-4CR was compared with the blank reaction and the synthesized compound as reference.

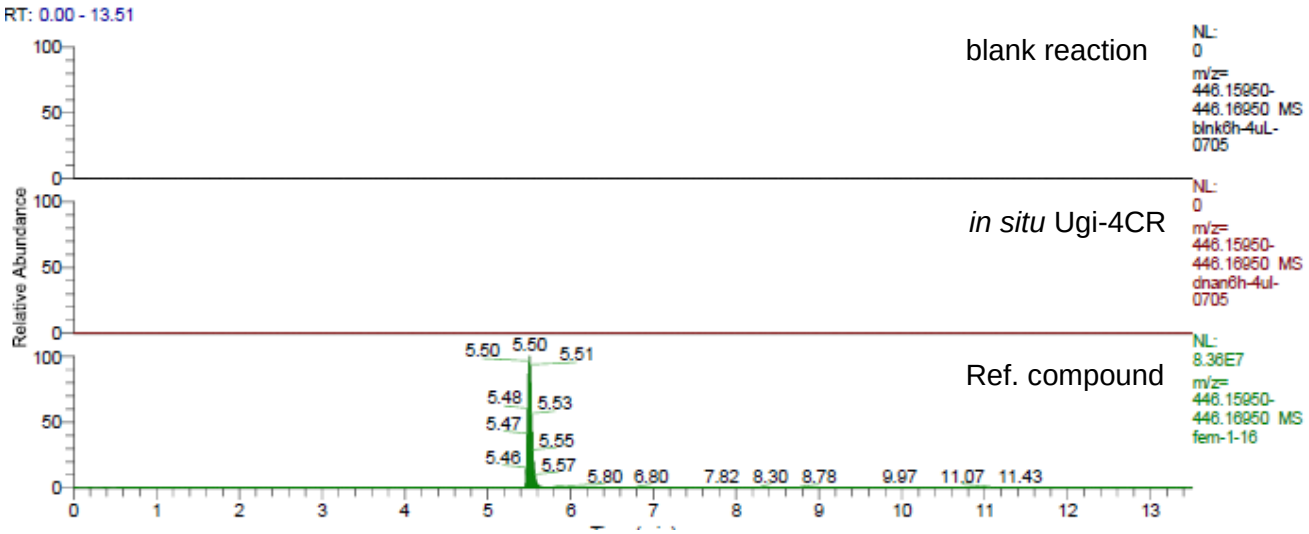

Figure S34. HPLC-HRMS analysis of compound **31** ([*M*+H]$^+$ = 446.16410). *In situ* Ugi-4CR was compared with the blank reaction and the synthesized compound as reference.

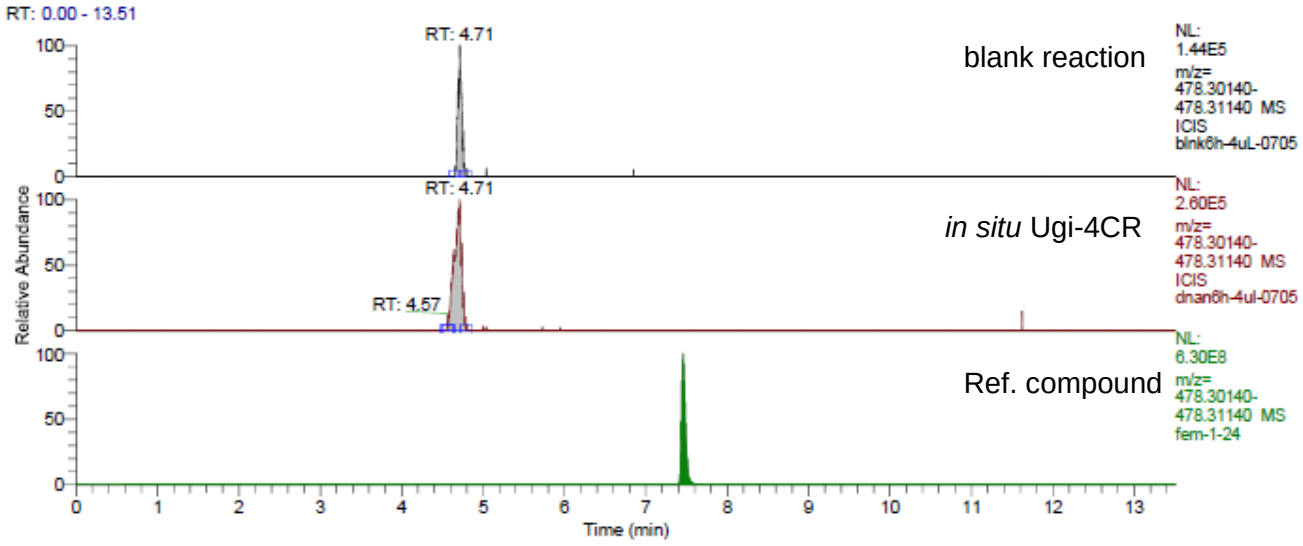

Figure S35. HPLC-HRMS analysis of compound **32** ([*M*+H]$^+$ = 478.30576. *In situ* Ugi-4CR was compared with the blank reaction and the synthesized compound as reference.

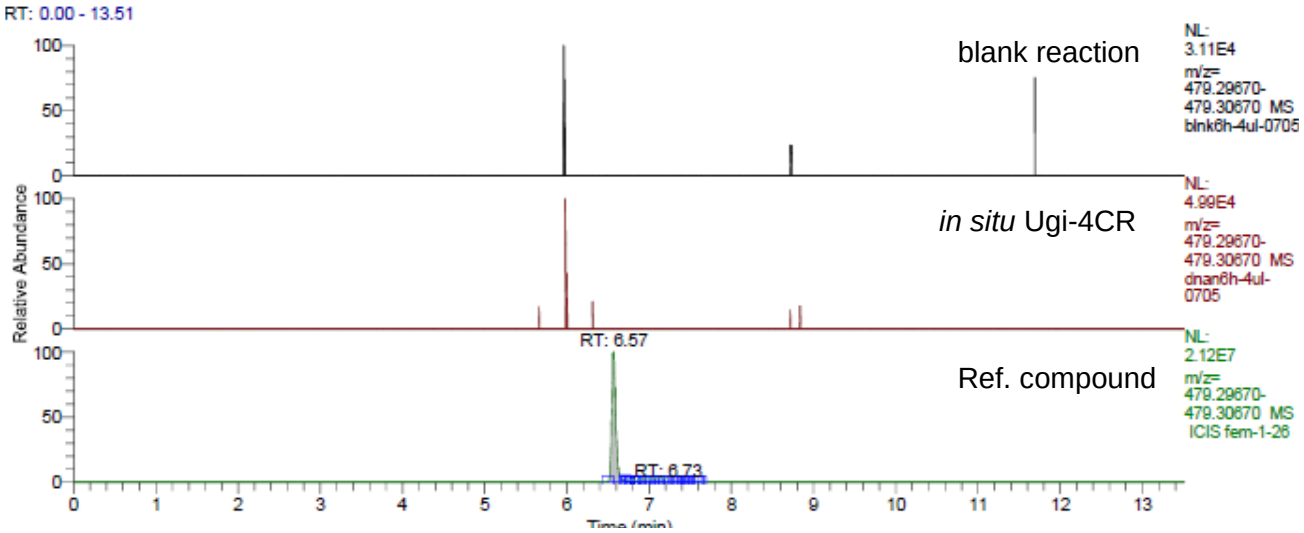

Figure S36. HPLC-HRMS analysis of compound **33** ([*M*+H]$^+$ = 479.30124). *In situ* Ugi-4CR was compared with the blank reaction and the synthesized compound as reference.

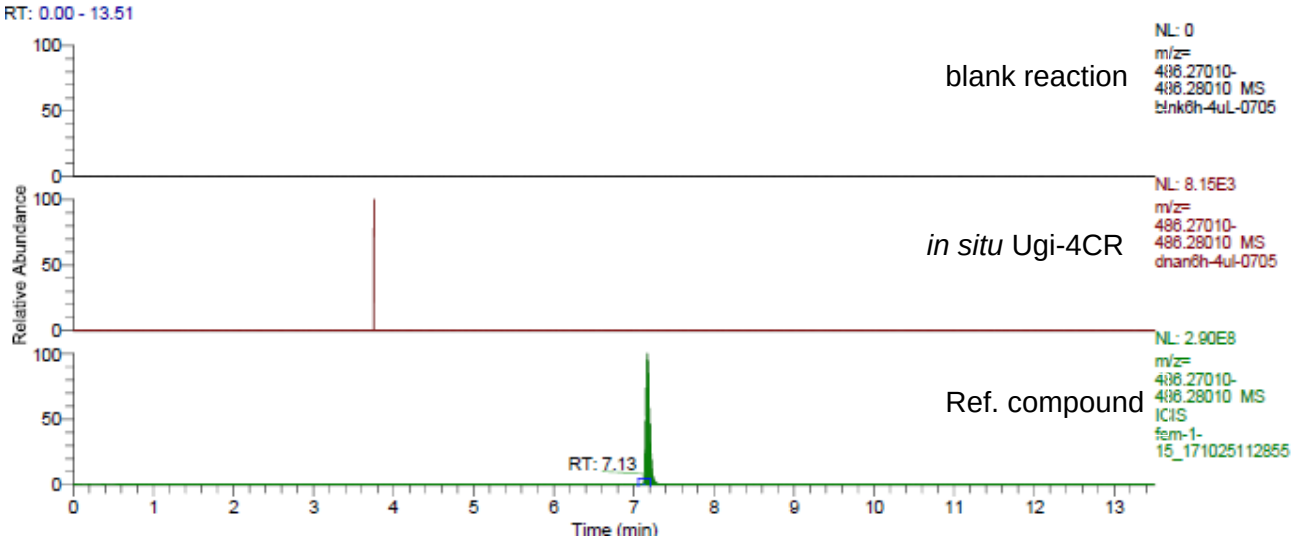

Figure S37. HPLC-HRMS analysis of compound **34** ([*M*+H]$^+$ = 486.27464). *In situ* Ugi-4CR was compared with the blank reaction and the synthesized compound as reference.

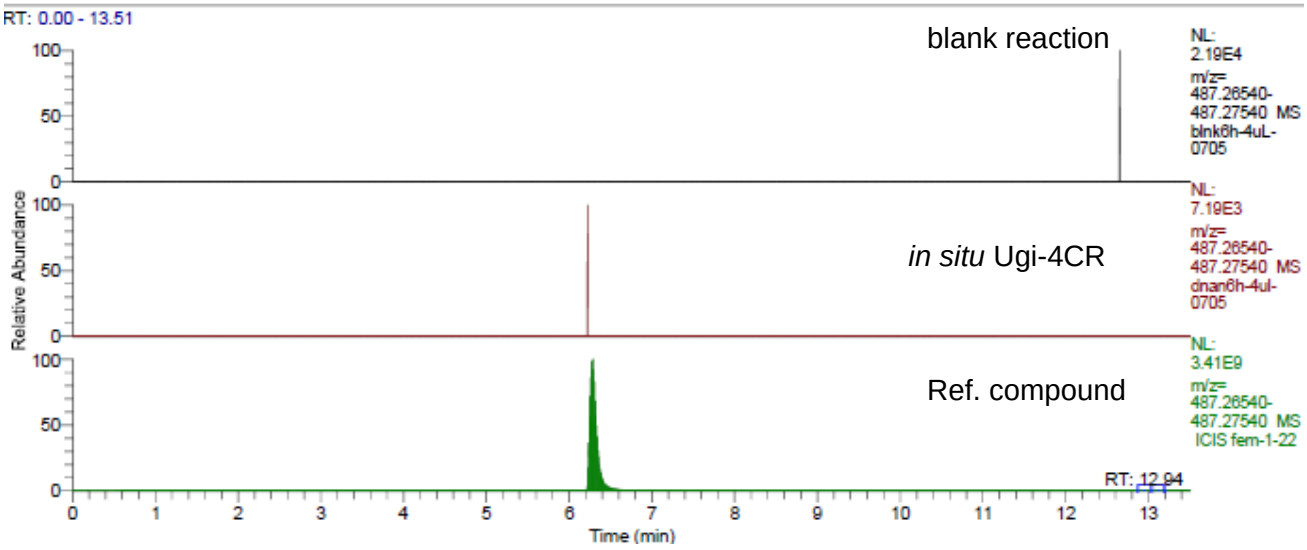

Figure S38. HPLC-HRMS analysis of compound **35** ([*M*+H]$^+$ = 487.26994). *In situ* Ugi-4CR was compared with the blank reaction and the synthesized compound as reference.

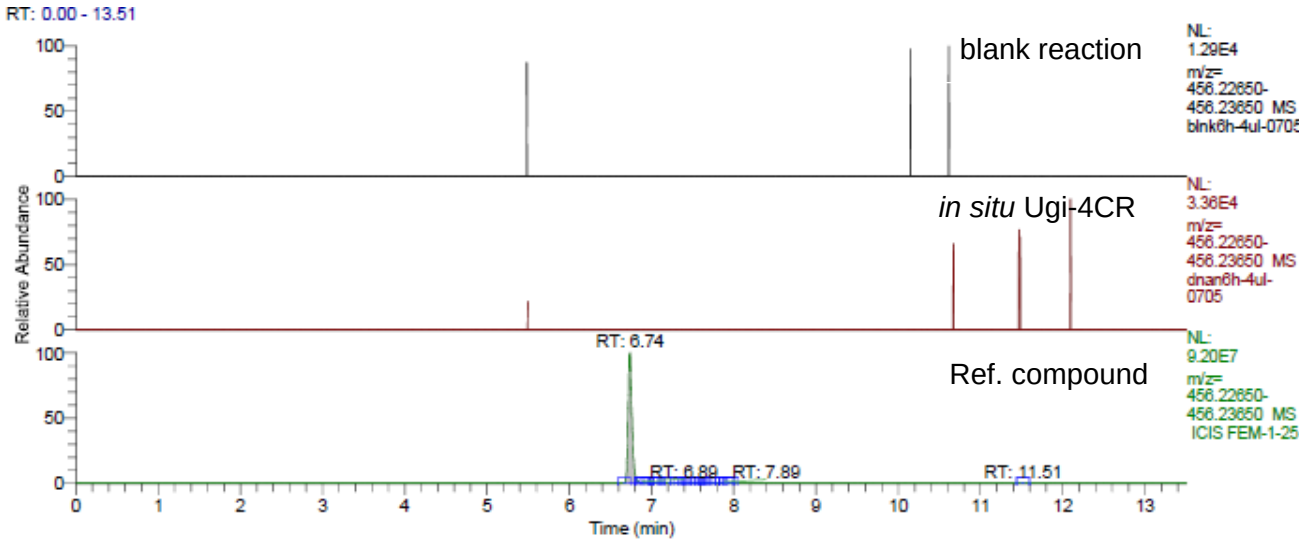

Figure S39. HPLC-HRMS analysis of compound **36** ([*M*+H]$^+$ = 456.23102). *In situ* Ugi-4CR was compared with the blank reaction and the synthesized compound as reference.

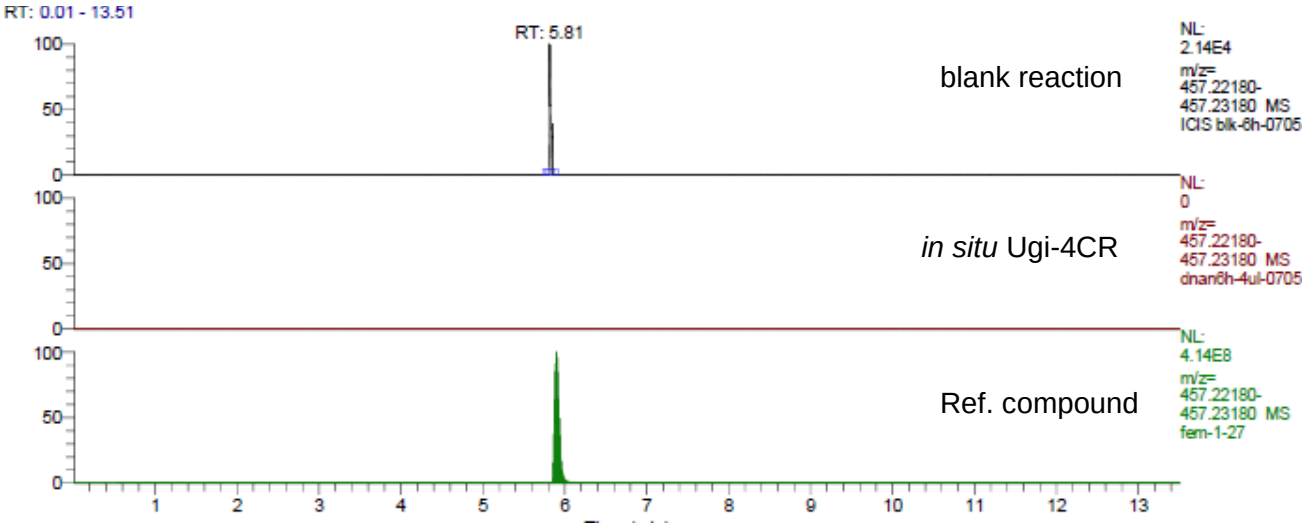

Figure S40. HPLC-HRMS analysis of compound **37** ([*M*+H]$^+$ = 457.22602). *In situ* Ugi-4CR was compared with the blank reaction and the synthesized compound as reference.

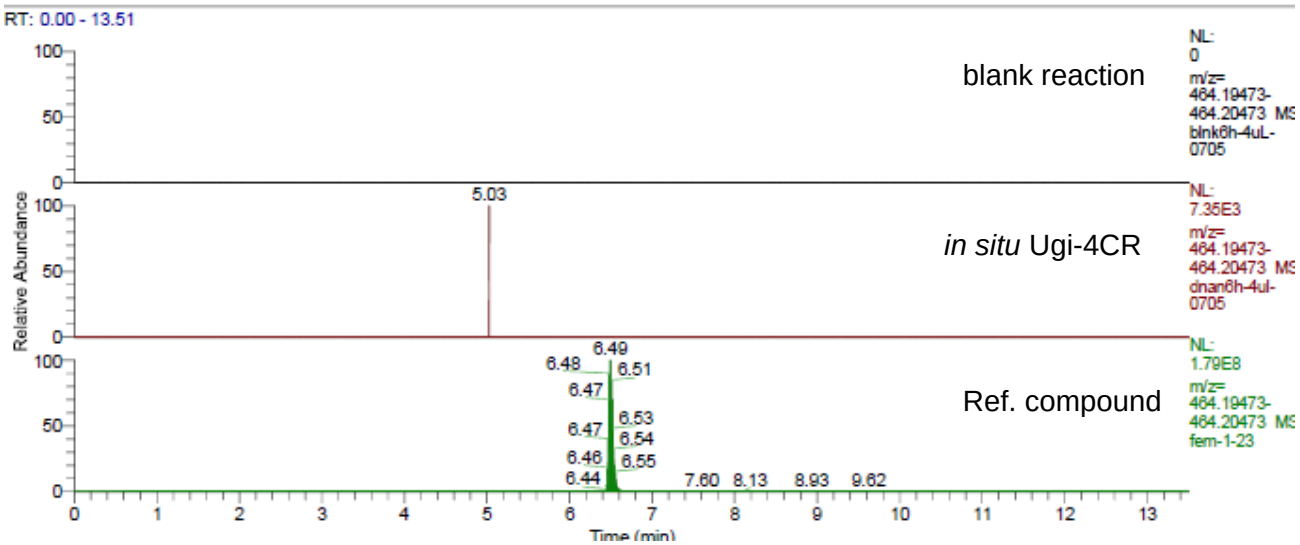

Figure S41. HPLC-HRMS analysis of compound **38** ([*M*+H]$^+$ = 464.2001). *In situ* Ugi-4CR was compared with the blank reaction and the synthesized compound as reference.

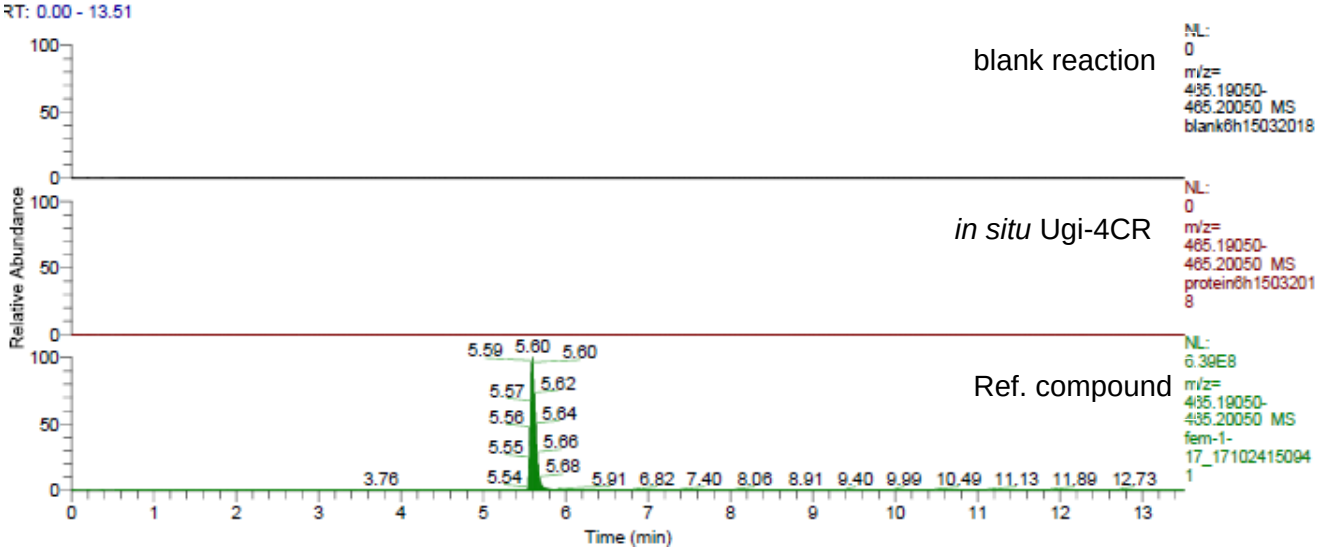

Figure S42. HPLC-HRMS analysis of compound **39** ([*M*+H]$^+$ = 465.19511). *In situ* Ugi-4CR was compared with the blank reaction and the synthesized compound as reference.

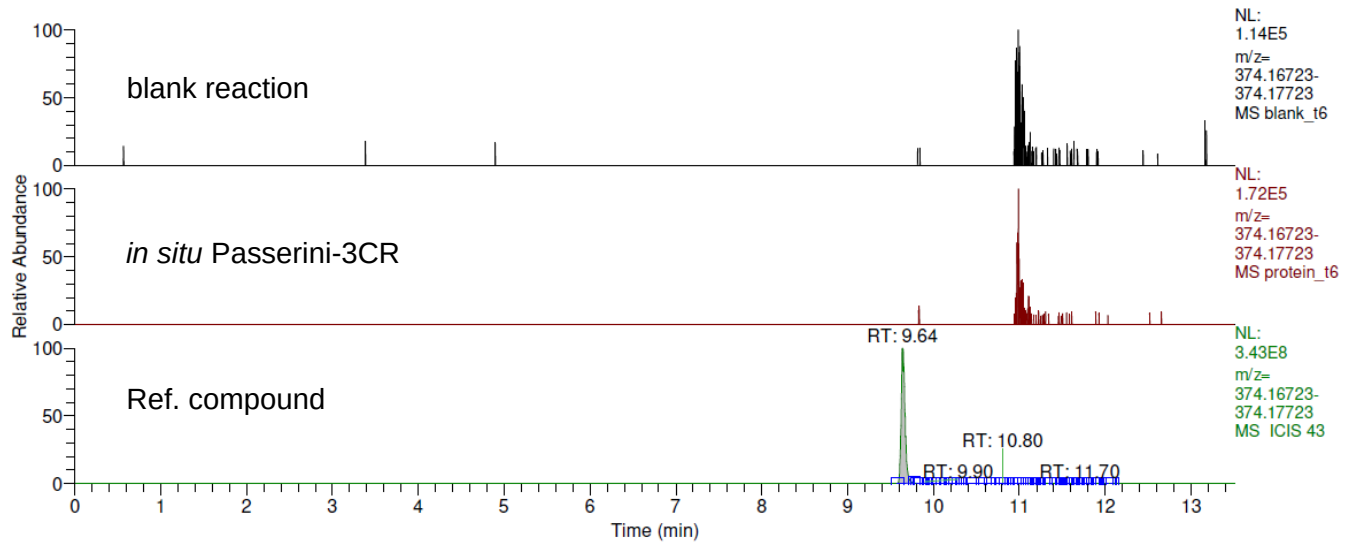

Figure S43. HPLC-HRMS analysis of compound **40** ([*M*+H]$^+$ = 374.17226). *In situ* Passerini-3CR was compared with the blank reaction and the synthesized compound as reference.

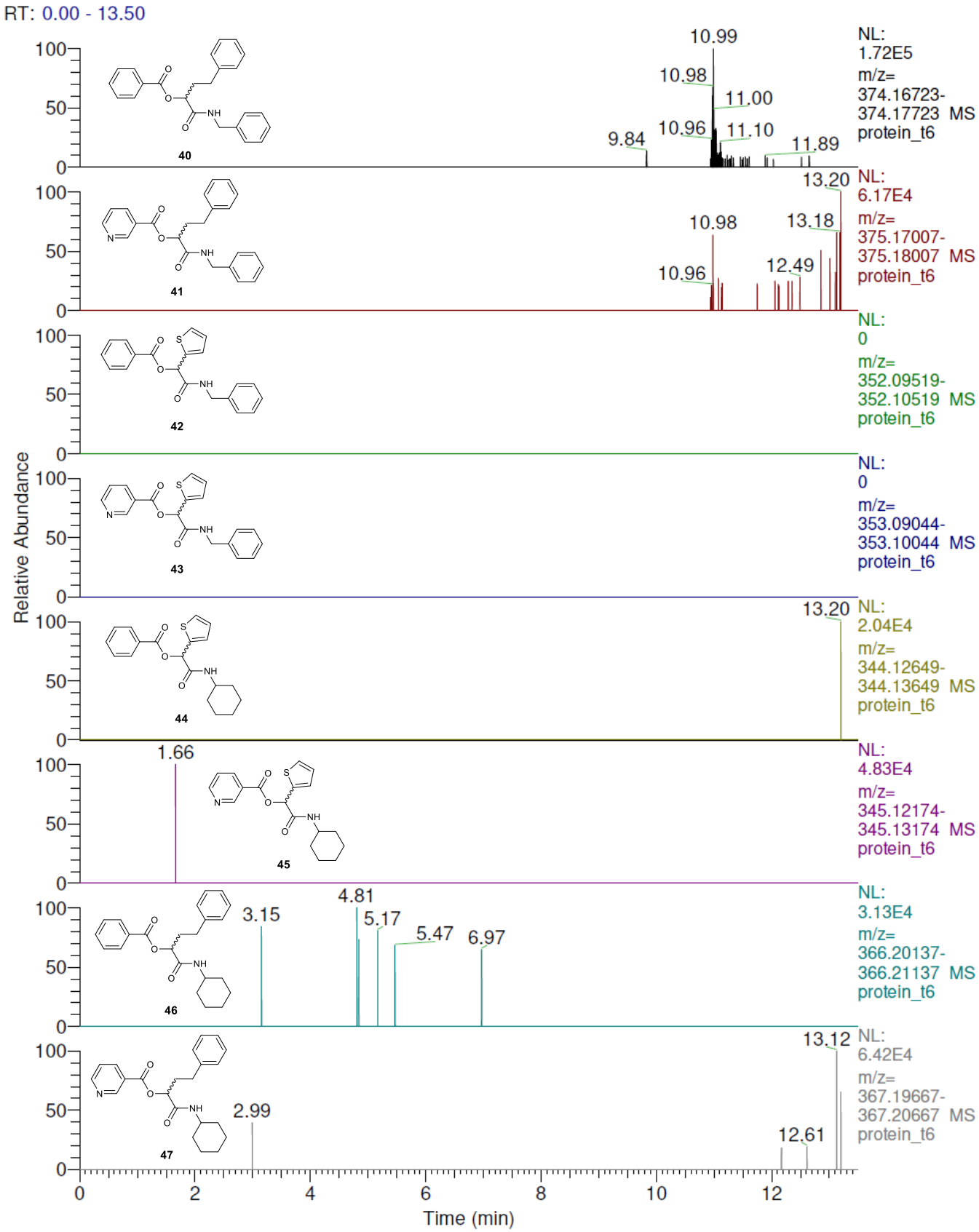

Figure S44. HPLC-HRMS analysis of *in situ* Passerini-3CR derivatives **40**–**47**.

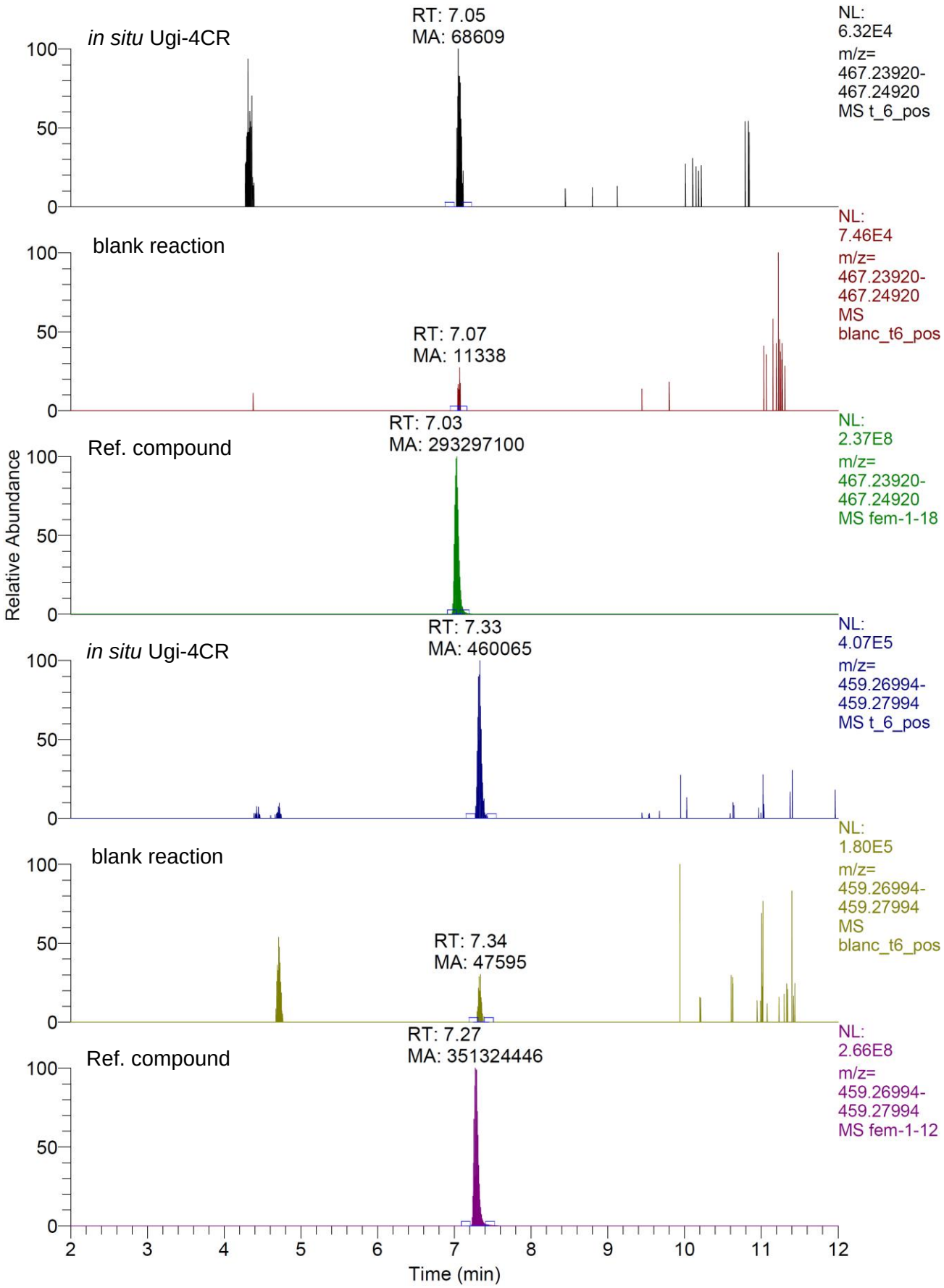

Figure S45. HPLC-HRMS analysis of compound **19** ([*M*+H]$^+$ = 467.24358, t_R 7.03 min) and **25** ([*M*+H]$^+$ = 459.27494, t_R 7.27 min), respectively. Data of the second *in situ* Ugi-4CR experiment was compared with the blank reaction and the synthesized compound as reference.

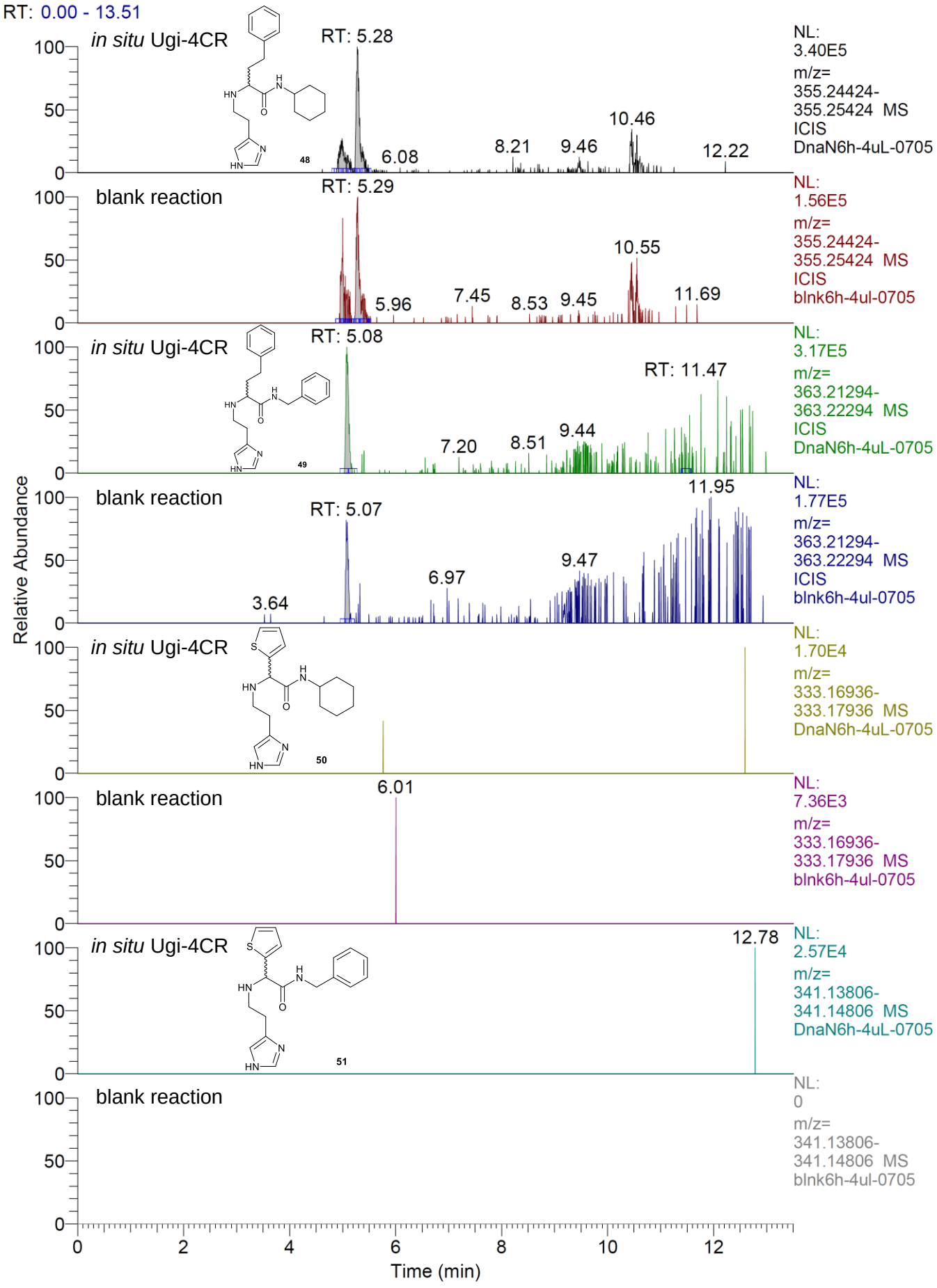

Figure S46. HPLC-HRMS analysis of *in situ* Ugi-4CR products **48**–**51** with water as acid component.

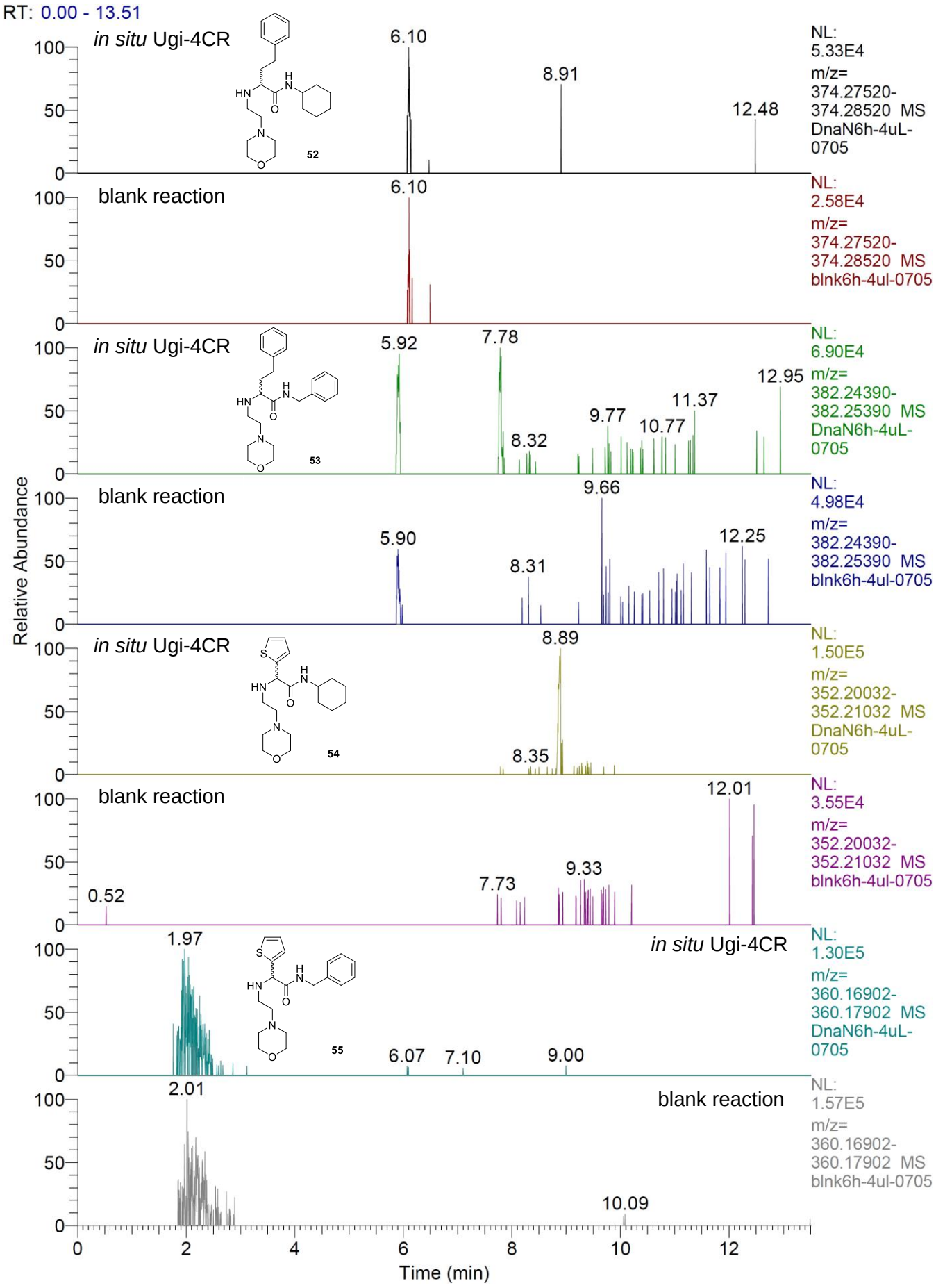

Figure S47. HPLC-HRMS analysis of *in situ* Ugi-4CR products **52**–**55** with water as acid component.

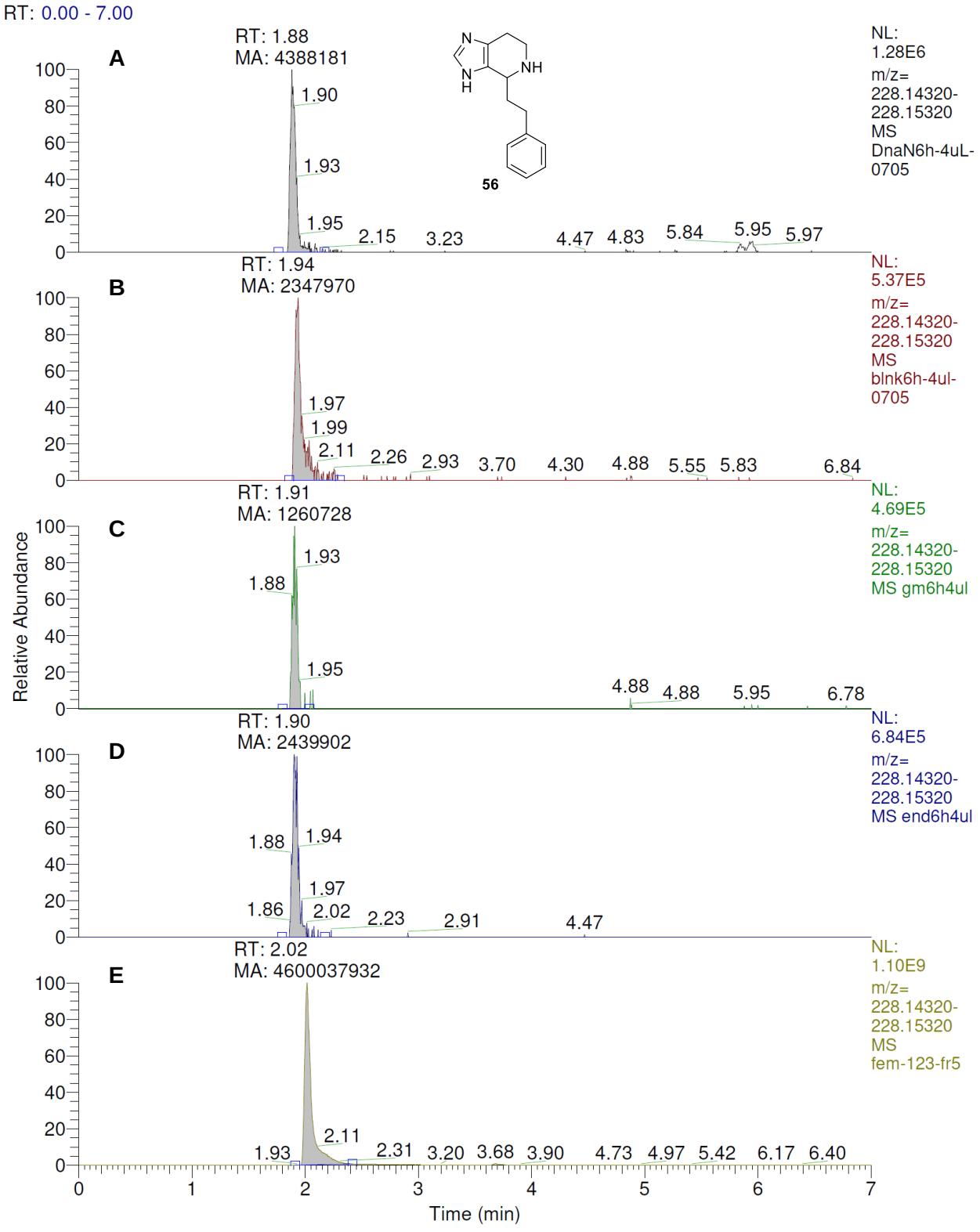

Fig S48. HPLC-HRMS analysis of compound **56** ([*M*+H]$^+$ = 228.14815): (A) Formation of **56** in the presence of *M. smegmatis* DnaN after 6 h of incubation; (B) Formation of **56** in buffer without protein after 6 h of incubation; (C) Formation of **56** in DnaN-templated reaction in the presence of GM; (D) Formation of **56** in the presence of endothiapepsin; (E) Reference compound **56** obtained by synthetic pathway.

General procedure for Ugi-4CR for DnaN library

To a 10-mL round-bottomed flask charged with MeOH (4 mL), the corresponding aldehyde **8** or **23** (1 mmol, 1 equiv), amine **6** or **22** (1 mmol, 1 equiv), carboxylic acid **4** or **21** (1 mmol, 1 equiv) and isocyanide **10** or **24** (1 mmol, 1 equiv) were added. The reaction mixture was stirred at room temperature for 24 h. The reaction mixture was concentrated *in vacuo* and purification by flash chromatography over silica gel using DCM/MeOH (96:4) afforded the corresponding Ugi product (Scheme S4).

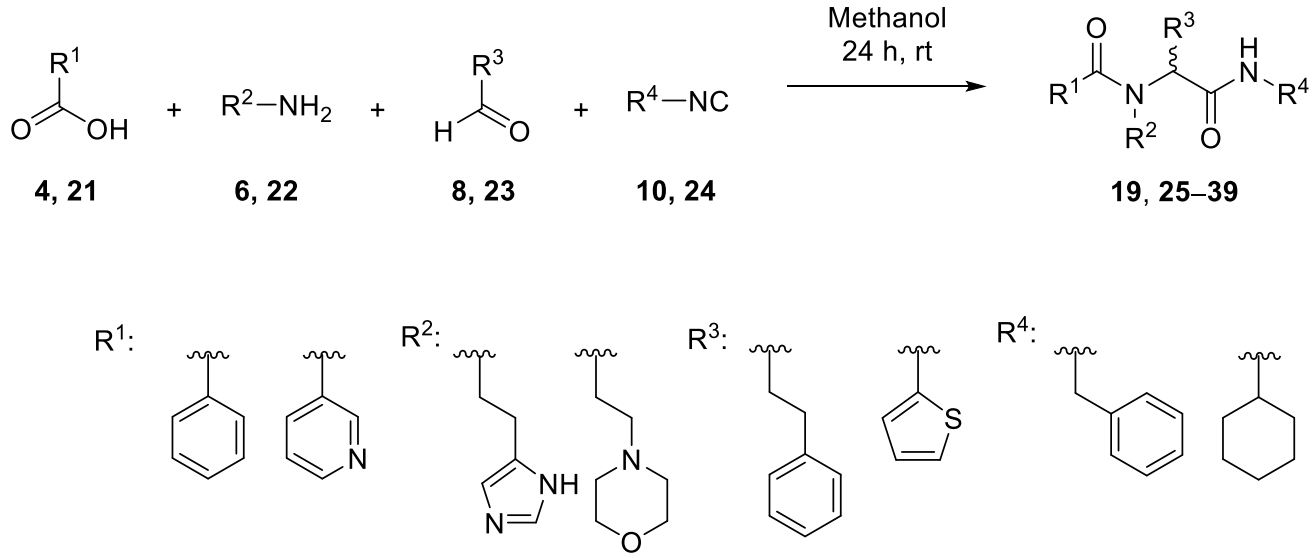

Scheme S4. Synthetic strategy towards compounds **19**, **25**–**39**.

***N*-(2-(1*H*-imidazol-4-yl)ethyl)-*N*-(1-(cyclohexylamino)-1-oxo-4-phenylbutan-2-yl)benzamide (25)**

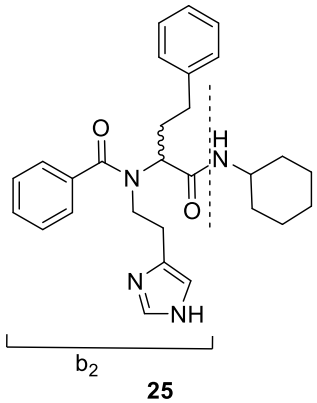

General procedure starting from commercially available benzoic acid (**4**) (1 mmol), histamine (**6**) (1 mmol), 3-phenylpropanal (**8**) (1 mmol) and cyclohexyl isocyanide (**10**) (1 mmol) in MeOH (4 mL). Afterwards purification of crude **25** by preparative HPLC using a gradient of acetonitrile + 0.05% formic acid from 10% to 100% afforded the desired product **25** as a white solid in 26% yield. ^{1}H NMR (500 MHz, methanol-d_4) δ 7.84 – 6.35 (m, 12H), 4.67 – 4.20 (m, 1H), 3.87 – 3.48 (m, 3H), 3.17 – 2.73 (m, 2H), 2.63 – 2.01 (m, 3H), 1.88 – 1.64 (m, 5H), 1.51 – 1.14 (m, 5H); ^{13}C NMR (126 MHz, methanol-d_4) δ 175.36, 171.57, 137.58, 135.99 (2C), 130.86, 129.75 (2C), 129.60 (2C), 129.51, 127.59, 127.24 (2C), 64.22, 60.43, 50.07, 40.41, 33.61 (2C), 32.04, 27.66, 26.60, 26.13 (2C); HRMS (ESI) calcd for $C_{28}H_{35}N_4O_2$ $[M+H]^+$: 459.2755, found: 459.2749, calcd for b_2 fragment (m/z): 360.1729, found: 360.1699.

***N*-(2-(1*H*-imidazol-4-yl)ethyl)-*N*-(1-(cyclohexylamino)-1-oxo-4-phenylbutan-2-yl)nicotinamide (26)**

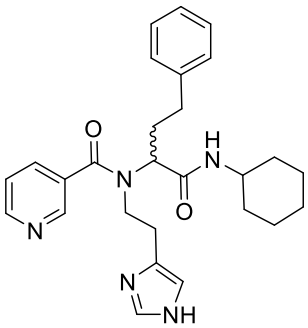

26

General procedure starting from commercially available nicotinic acid (**21**) (1 mmol), histamine (**6**) (1mmol), 3-phenylpropanal (**8**) (1 mmol) and cyclohexyl isocyanide (**24**) (1 mmol) in MeOH (4 mL) afforded the desired product **26** as a white solid in 11% yield.

^{1}H NMR (500 MHz, acetone-d_6) δ 8.54 (s, 1H), 8.33 (s, 1H), 8.16 (s, 1H), 7.83 – 6.91 (m, 9H), 6.70 (s, 1H), 4.34 (m, 1H), 3.97 – 3.40 (m, 3H), 3.18 – 2.57 (m, 4H), 2.50 – 2.10 (m, 2H), 1.95 – 1.55 (m, 5H), 1.27 (d, J = 70.4 Hz, 5H); ^{13}C NMR (126 MHz, acetone-d_6) δ 169.55, 169.17, 149.89, 147.37, 142.08, 135.88, 134.68, 133.97, 133.07, 128.42 (2C), 128.36 (2C), 125.87, 123.01, 115.45, 59.03, 49.37, 48.43, 40.37, 32.65 (2C), 30.62, 26.34, 25.51, 24.98 (2C); HRMS (ESI) calcd for $C_{27}H_{34}N_5O_2$ [M+H]$^+$: 460.2707, found: 460.2702.

***N*-(2-(1*H*-Imidazol-4-yl)ethyl)-*N*-(1-(benzylamino)-1-oxo-4-phenylbutan-2-yl)benzamide (27)**

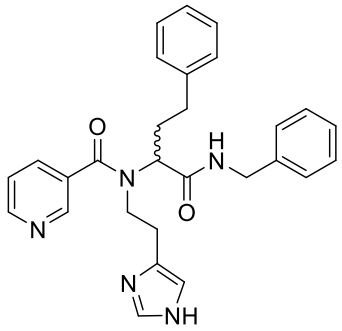

27

General procedure starting from commercially available nicotinic acid (**21**), histamine (**6**) (1 mmol), 3-phenylpropanal (**8**) (1 mmol) and benzyl isocyanide (**10**) (1 mmol) in MeOH (4 mL). Afterwards purification of crude **27** by preparative HPLC using a gradient of acetonitrile + 0.05% formic acid from 10% to 100% afforded the desired product **27** as a white solid in 11% yield.

^{1}H NMR (500 MHz, acetone-d_6) δ 9.44 (s, 1H), 7.64 – 6.47 (m, 16H), 4.50 (m, 3H), 3.57 (m, 2H), 3.2 – 2.8 (m, 2H). , 2.79 – 2.21 (m, 4H); ^{13}C NMR (126 MHz, acetone-d_6) δ 171.78, 170.52, 142.10, 140.04, 137.40, 134.42, 128.73, 128.42 (2C), 128.41, 128.39, 128.36 (2C), 128.16, 128.00, 127.69 (2C), 126.61, 126.34, 125.85 (2C), 114.85, 59.17, 49.99, 42.84, 33.13, 30.65, 26.10; HRMS (ESI) calcd for $C_{28}H_{30}N_5O_2$ [M+H]+: 468.2394, found: 468.2391.

***N*-(2-(1*H*-imidazol-4-yl)ethyl)-*N*-(2-(cyclohexylamino)-2-oxo-1-(thiophen-2-yl)ethyl)benzamide (28)**

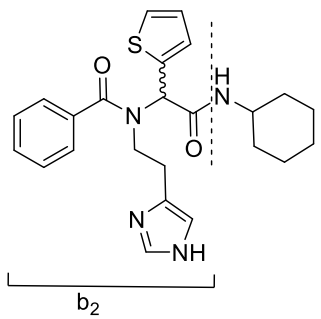

28

General procedure starting from commercially available benzoic acid (**4**) (1 mmol), histamine (**6**) (1 mmol), 2-thiophene-carboxaldehyde (**23**) (1 mmol) and cyclohexyl isocyanide (**24**) (1 mmol) in MeOH (4 mL) afforded the desired product **28** as a pale yellow solid in 26% yield.

^{1}H NMR (500 MHz, acetone-d_6) δ 8.19 (s, 1H), 7.79 (s, 1H), 7.51 (d, J = 5.1 Hz, 2H), 7.46 – 6.77 (m, 7H), 6.71 (s, 1H), 5.90 (s, 1H), 3.68 (m, 3H), 2.93 (s, 1H), 2.59 (s, 1H), 1.88 (m, 2H), 1.69 (m, 2H), 1.57 (m, 1H), 1.27 (m, 5H); ^{13}C NMR (126 MHz, acetone-d_6) δ 171.30, 168.21, 162.19, 138.42, 136.73, 134.47, 133.45, 129.42, 129.15 (2C), 128.27, 127.49 (2C), 126.27, 117.78, 59.03, 48.52, 40.27, 32.39 (2C), 25.41, 24.75 (2C); HRMS (ESI) calcd for $C_{24}H_{29}N_4O_2S$ [M+H]+: 437.2006, found: 437.2000, calcd for b_2 fragment (m/z): 338.0963, found: 338.0949.

***N*-(2-(1*H*-imidazol-4-yl)ethyl)-*N*-(2-(cyclohexylamino)-2-oxo-1-(thiophen-2-yl)ethyl)nicotinamide (29)**

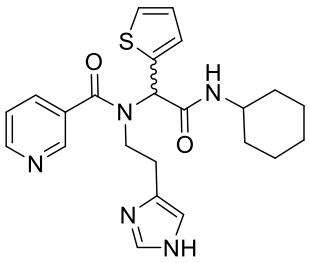

29

General procedure starting from commercially available nicotinic acid (**21**) (1 mmol), histamine (**6**) (1 mmol), 2-thiophene-carboxaldehyde (**23**) (1 mmol) and cyclohexyl isocyanide (**24**) (1 mmol) in MeOH (4 mL) afforded the desired product **29** as a pale yellow solid in 16% yield.

^{1}H NMR (500 MHz, acetone-d_6) δ 8.54 (s, 1H), 8.12 (s, 1H), 7.69 – 6.64 (m, 6H), 5.84 (s, 1H), 3.79 (s, 1H), 3.60 (s, 2H), 2.92 (s, 1H), 2.12 (m, 1H), 1.89 (m, 2H), 1.70 (m, 2H), 1.58 (m, 1H), 1.25 (m, 5H); ^{13}C NMR (126 MHz, acetone-d_6) δ 169.83, 168.36, 150.93, 148.10, 139.23, 135.53, 134.65, 133.51, 129.98, 128.29, 126.85, 124.38, 123.91, 117.95, 59.99, 49.95, 49.57, 33.37 (2C), 26.62, 26.34, 25.78 (2C); HRMS (ESI) calcd for $C_{23}H_{28}N_5O_2S$ [M+H]+: 438.1958, found: 438.1954.

***N*-(2-(1*H*-imidazol-4-yl)ethyl)-*N*-(2-(benzylamino)-2-oxo-1-(thiophen-2-yl)ethyl)nicotinamide (30)**

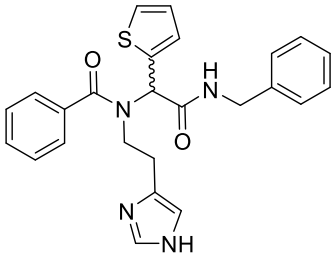

30

General procedure starting from commercially available benzoic acid (**4**) (1 mmol), histamine (**6**) (1 mmol), 2-thiophene-carboxaldehyde (**23**) (1 mmol) and benzyl isocyanide (**10**) (1 mmol) in MeOH (4 mL). Afterwards purification of crude **30** by preparative HPLC using a gradient of acetonitrile + 0.05% formic acid from 10% to 100% afforded the desired product **30** as a pale yellow solid in 26% yield.

^{1}H NMR (500 MHz, acetone-d_6) δ 8.82 (s, 1H), 8.16 (s, 1H), 7.49 – 7.24 (m, 10 H), 7.07 (m, 1H), 6.87 (s, 1H), 6.66 (s, 1H), 5.87 (s, 1H), 4.52 (s, 2H), 3.54 (s, 2H), 2.99 (m, 1H), 2.62 (s, 1H); ^{13}C NMR (126 MHz, acetone-d_6) δ 172.08, 169.90, 163.16, 140.40, 139.12, 137.57, 135.46, 134.95, 130.38, 129.87, 129.07 (2C), 128.91 (2C), 128.51 (2C), 127.61, 127.08 (2C), 126.76, 118.17, 60.35, 50.16, 43.98, 26.16; HRMS (ESI) calcd for $C_{24}H_{24}N_5O_2S$ [*M*+H]$^+$: 445.1693, found: 445.1688.

***N*-(2-(1H-imidazol-4-yl)ethyl)-*N*-(2-(benzylamino)-2-oxo-1-(thiophen-2-yl)ethyl)nicotinamide (31)**

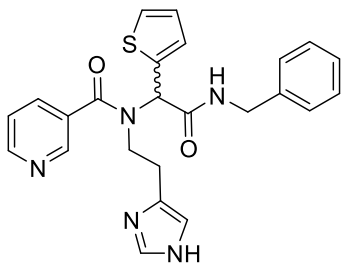

31

General procedure starting from commercially available nicotinic acid (**21**) (1 mmol), histamine (**6**) (1 mmol), 2-thiophene-carboxaldehyde (**23**) (1 mmol) and benzyl isocyanide (**10**) (1 mmol) in MeOH (4 mL). Afterwards purification of crude **31** by preparative HPLC using a gradient of acetonitrile + 0.05% formic acid from 10% to 100% afforded the desired product **31** as a pale yellow solid in 26% yield.

^{1}H NMR (500 MHz, acetone-d_6) δ 9.14 (s, 1H), 8.52 (s, 1H), 8.14 (s, 1H), 7.69 – 7.00 (m, 11H), 6.69 (s, 1H), 5.87 (s, 1H), 4.51 (m, 2H), 3.59 (s, 2H), 2.99 (m, 1H), 2.66 (s, 1H); ^{13}C NMR (126 MHz, acetone-d_6) δ 169.80, 169.40, 162.66, 150.88, 148.05, 140.55, 139.02, 135.50, 134.56, 133.38, 130.28, 129.06 (2C), 128.59 (2C), 128.47, 127.60, 126.63, 123.86, 117.68, 60.60, 50.46, 44.02, 26.27; HRMS (ESI) calcd for $C_{24}H_{24}N_5O_2S$ [*M*+H]$^+$: 446.1645, found: 446.1641.

***N*-(1-(cyclohexylamino)-1-oxo-4-phenylbutan-2-yl)-*N*-(2-morpholinoethyl)benzamide (32)**

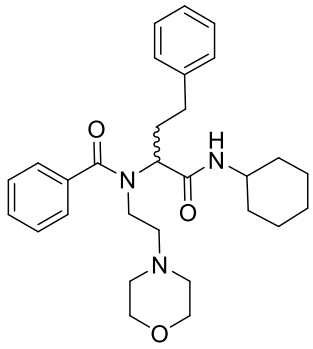

32

General procedure starting from commercially available benzoic acid (**4**) (1 mmol), 4-(2-aminoethyl)morpholine (**22**) (1 mmol), 3-phenylpropanal (**8**) (1 mmol) and cyclohexyl isocyanide (**24**) (1 mmol) in MeOH (4 mL) afforded the desired product **32** as a white solid in 26% yield.

^{1}H NMR (500 MHz, acetone-*d*$_6$) δ 7.63 – 7.36 (m, 5H), 7.34 – 7.06 (m, 6H), 4.68 – 4.25 (m, 1H), 3.79 –3.37 (m, 7H), 2.80 – 2.08 (m, 10H), 1.93 – 1.82 (m, 2H), 1.71 (m, 2H), 1.60 (m, 1H), 1.31 (m, 5H); ^{13}C NMR (126 MHz, acetone-*d*$_6$) δ 173.10, 170.15, 142.56, 138.07, 130.18, 129.26 (4C), 129.22 (2C), 127.81 (2C), 126.79, 67.27 (2C), 59.42, 58.02, 54.34 (2C), 48.89, 45.57, 33.62, 33.50, 33.41 (2C), 26.33, 25.63 (2C); HRMS (ESI) calcd for $C_{29}H_{40}N_3O_3$ [M+H]+: 478.3064, found: 478.3058.

***N*-(1-(cyclohexylamino)-1-oxo-4-phenylbutan-2-yl)-*N*-(2-morpholinoethyl)nicotinamide (33)**

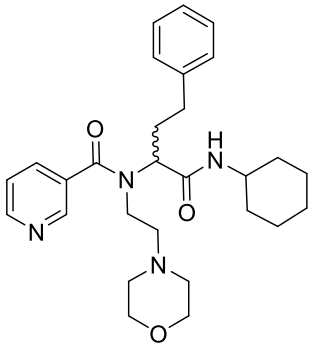

33

General procedure starting from commercially available nicotinic acid (**21**) (1 mmol), 4-(2-aminoethyl)morpholine (**22**) (1 mmol), 3-phenylpropanal (**8**) (1 mmol) and cyclohexyl isocyanide (**24**) (1 mmol) in MeOH (4 mL) afforded the desired product **33** as a white solid in 12% yield.

^{1}H NMR (500 MHz, acetone-*d*$_6$) δ 8.63 (m, 2H), 7.95 – 7.06 (m, 8H), 4.56 (s, 1H), 3.79 – 3.29 (m, 7H), 2.80 – 2.06 (m, 10H), 1.89 (m, 2H), 1.72 (m, 2H), 1.59 (m, 1H), 1.32 (m, 5H); ^{13}C NMR (126 MHz, acetone-*d*$_6$) δ 170.85, 169.85, 151.18, 148.66, 142.35, 135.27, 133.82, 129.26 (2C), 129.25 (2C), 126.82, 124.13, 67.32 (2C), 59.63, 57.87, 54.54 (2C), 49.08, 45.48, 33.57, 33.45 (2C), 33.32, 26.30, 25.65 (2C); HRMS (ESI) calcd for $C_{28}H_{39}N_4O_3$ [*M*+H]$^+$: 479.3017, found: 479.3012.

***N*-(1-(benzylamino)-1-oxo-4-phenylbutan-2-yl)-*N*-(2-morpholinoethyl)benzamide (34)**

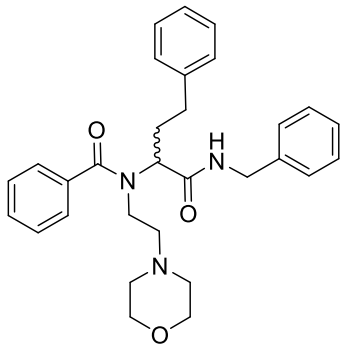

34

General procedure starting from commercially available benzoic acid (**4**) (1 mmol), 4-(2-aminoethyl)morpholine (**22**) (1 mmol), 3-phenylpropanal (**8**) (1 mmol) and benzyl isocyanide (**10**) (1 mmol) in MeOH (4 mL). Afterwards purification of crude **34** by preparative HPLC using a gradient of acetonitrile + 0.05% formic acid from 5% to 100% afforded the desired product **34** as a white solid in 26% yield.

^{1}H NMR (500 MHz, acetone-*d*$_6$) δ 8.41 (s, 1H), 7.61 – 6.95 (m, 15H), 4.81 – 4.51 (m, 1H), 4.49 – 4.21 (m, 2H), 3.86 – 3.19 (m, 6H), 2.88 – 2.24 (m, 7H), 2.05 – 1.88 (m, 3H); ^{13}C NMR (126 MHz, acetone-*d*$_6$) δ 172.07, 171.29, 142.95, 140.76, 137.87, 130.28, 129.26 (4C), 129.19 (4C), 128.37 (2C), 127.90 (2C), 127.78, 126.76, 66.94 (2C), 60.31, 57.23, 53.99 (2C), 46.78, 43.53, 33.64, 31.05; HRMS (ESI) calcd for $C_{30}H_{36}N_3O_3$ [*M*+H]$^+$: 486.2757, found: 486.2746.

***N*-(1-(benzylamino)-1-oxo-4-phenylbutan-2-yl)-*N*-(2-morpholinoethyl)nicotinamide (35)**

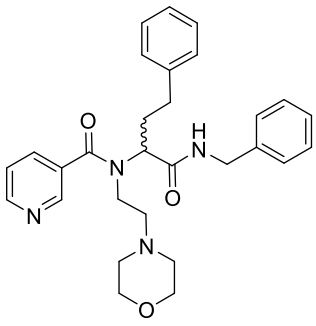

35

General procedure starting from commercially available nicotinic acid (**21**) (1 mmol), 4-(2-aminoethyl)morpholine (**22**) (1 mmol), 3-phenylpropanal (**8**) (1 mmol) and benzyl isocyanide (**10**) (1 mmol) in MeOH (4 mL). Afterwards purification of crude **35** by preparative HPLC using a gradient of acetonitrile + 0.05% formic acid from 15% to 100% afforded the desired product **35** as a white solid in 4% yield.

^{1}H NMR (500 MHz, acetone-d_6) δ 8.62 (s, 2H), 8.33 (s, 1H), 7.80 (s, 1H), 7.28 (m, 11H), 4.87 – 4.48 (m, 1H), 4.47 – 4.20 (m, 2H), 3.91 – 3.18 (m, 6H), 2.73 (m, 6H), 2.49 – 2.15 (m, 3H), 2.03 – 1.87 (s, 1H); ^{13}C NMR (126 MHz, acetone-d_6) δ 170.94, 170.02, 151.30, 148.75, 142.76, 140.67, 135.27, 133.64, 129.29 (4C), 129.23 (2C), 128.40 (2C), 127.84, 126.81, 124.10, 66.92 (2C), 60.42, 57.30, 54.13 (2C), 46.76, 43.57, 33.60, 31.06; HRMS (ESI) calcd for $C_{29}H_{35}N_4O_3$ [*M*+H]$^+$: 487.2704, found:487.2699.

***N*-(2-(cyclohexylamino)-2-oxo-1-(thiophen-2-yl)ethyl)-*N*-(2-morpholinoethyl)benzamide (36)**

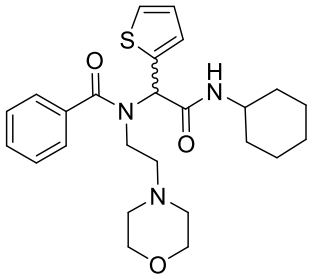

36

General procedure starting from commercially available benzoic acid (**4**) (1 mmol), 4-(2-aminoethyl)morpholine (**22**) (1 mmol), 2-thiophene-carboxaldehyde (**23**) (1 mmol) and cyclohexyl isocyanide (**24**) (1 mmol) in MeOH (4 mL) afforded the desired product **36** as a white solid in 26% yield.

^{1}H NMR (500 MHz, acetone-d_6) δ 7.50 (d, *J* = 5.2 Hz, 1H), 7.45 (m, 5H), 7.21 (s, 2H), 7.07 – 7.00 (m, 1H), 6.02 (s, 1H), 3.75 (m, 1H), 3.52 – 3.25 (m, 6H), 2.39 (s, 1H), 2.25 – 2.07 (m, 2H), 1.96 (m, 3H), 1.88 (m, 2H), 1.69 (m, 2H), 1.57 (m, 1H), 1.36 – 1.16 (m, 5H); ^{13}C NMR (126 MHz, acetone-d_6) δ 172.30, 168.40, 139.62, 137.94, 130.21, 129.37, 129.30 (2C), 127.86, 127.54 (2C), 127.39, 67.31 (2C), 57.95, 54.46 (2C), 49.25, 33.35, 33.32 (2C), 26.28, 25.61, 25.55 (2C); HRMS (ESI) calcd for $C_{29}H_{39}N_3O_3$ [*M*+H]$^+$: 456.2315, found: 456.2310.

***N*-(2-(benzylamino)-2-oxo-1-(thiophen-2-yl)ethyl)-*N*-(2-morpholinoethyl)nicotinamide (37)**

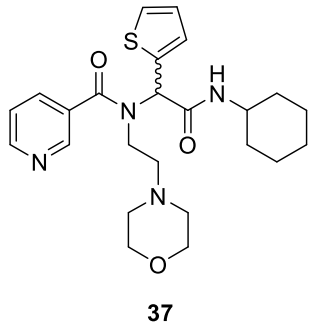

37

General procedure starting from commercially available nicotinic acid (**21**) (1 mmol), 4-(2-aminoethyl)morpholine (**22**) (1 mmol), 2-thiophene-carboxaldehyde (**23**) (1 mmol) and cyclohexyl isocyanide (**24**) (1 mmol) in MeOH (4 mL) afforded the desired product **37** as a yellow solid in 43% yield.

^{1}H NMR (500 MHz, acetone-d_6) δ 8.52 (dd, J = 4.9, 1.6 Hz, 2H), 7.83 (s, 1H), 7.56 – 7.40 (m, 2H), 7.33 – 7.11 (m, 2H), 7.09 – 6.95 (m, 1H), 5.85 (s, 1H), 3.75 (s, 1H), 3.61 – 3.36 (m, 6H), 2.37 (s , 1H), 2.18 – 2.06 (m, 3H), 2.06 – 1.95 (m, 2H), 1.91 – 1.83 (m, 2H), 1.74 – 1.64 (m, 2H), 1.57 (m, 1H), 1.40 – 1.11 (m, 5H); ^{13}C NMR (126 MHz, acetone-d_6) δ170.17, 168.12, 151.27, 148.42, 139.13, 135.09, 133.75, 129.69, 128.11, 127.53, 124.25, 67.27 (2C), 57.88, 54.49 (2C), 49.30, 33.29, 33.27 (2C), 26.25, 25.58, 25.53 (2C); HRMS (ESI) calcd for $C_{24}H_{33}N_4O_3S$ [*M*+H]$^+$: 457.2268, found: 457.2260.

***N*-(2-(benzylamino)-2-oxo-1-(thiophen-2-yl)ethyl)-*N*-(2-morpholinoethyl)benzamide (38)**

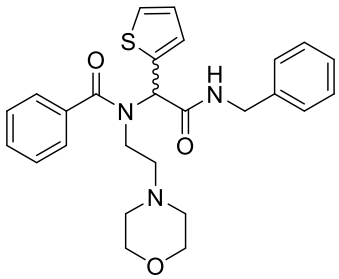

38

General procedure starting from commercially available benzoic acid (**4**) (1 mmol), 4-(2-aminoethyl)morpholine (**22**) (1 mmol), 2-thiophene-carboxaldehyde (**23**) (1 mmol) and benzyl isocyanide (**10**) (1 mmol) in MeOH (4 mL) afforded the desired product **38** as a brown solid in 21% yield. ^{1}H NMR (500 MHz, acetone-d_6) δ 8.18 (s, 1H), 7.48 (d, J = 4.8 Hz, 1H), 7.46 – 7.39 (m, 7H), 7.34 (t, J = 7.6 Hz, 2H), 7.26 (m, 2H), 7.02 (m, 1H), 5.94 (s, 1H), 4.58 (m, 1H), 4.46 (m, 1H), 3.60 (m, 2H), 3.36 (s, 4H), 2.53 (s, 1H), 2.17– 1.96 (m, 5H); ^{13}C NMR (126 MHz, acetone-d_6) δ 172.08, 169.38, 140.33, 139.32, 137.65, 130.34 (2C), 129.41, 129.29 (2C), 129.19 (2C), 128.40, 127.89, 127.81, 127.64 (2C), 127.02, 67.13 (2C), 60.53, 57.57, 54.29 (2C), 45.85, 43.74; HRMS (ESI) calcd for $C_{26}H_{30}N_3O_3S$ [M+H]$^+$: 464.2002, found: 464.1998.

***N*-(2-(benzylamino)-2-oxo-1-(thiophen-2-yl)ethyl)-*N*-(2-morpholinoethyl)nicotinamide (39)**

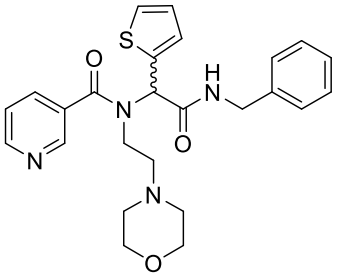

39

General procedure starting from commercially available nicotinic acid (**21**) (1 mmol), 4-(2-aminoethyl)morpholine (**22**) (1 mmol), 2-thiophene-carboxaldehyde (**23**) (1 mmol) and benzyl isocyanide (**10**) (1 mmol) in MeOH (4 mL) afforded the desired product **39** as a yellow solid in 20% yield. ^{1}H NMR (500 MHz, acetone-d_6) δ 8.69 – 8.57 (m, 2H), 8.06 (s, 1H), 7.82 (d, J = 6.9 Hz, 1H), 7.55 – 7.47 (m, 1H), 7.44 (dd, J = 7.4, 5.0 Hz, 1H), 7.33 (s, 4H), 7.29 – 7.18 (m, 2H), 7.04 (dd, J = 5.2, 3.5 Hz, 1H), 5.89 (s, 1H), 4.58 – 4.40 (m, 2H), 3.61 (s, 2H), 3.41 (s, 4H), 2.52 (s, 1H), 2.27 – 2.05 (m, 5H); ^{13}C NMR (126 MHz, acetone-d_6) δ 170.09, 169.13, 151.39, 148.54, 140.16, 138.90, 135.16, 133.46, 129.80, 129.21 (2C), 128.41 (2C), 128.21, 127.85, 127.24, 124.21, 67.03 (2C), 60.05, 57.62, 54.31 (2C), 46.08, 43.69; HRMS (ESI) calcd for $C_{25}H_{29}N_4O_3S$ [M+H]$^+$: 465.1955, found: 465.1951.

Synthesis of 1-(benzylamino)-1-oxo-4-phenylbutan-2-yl benzoate (40) via Passerini reaction

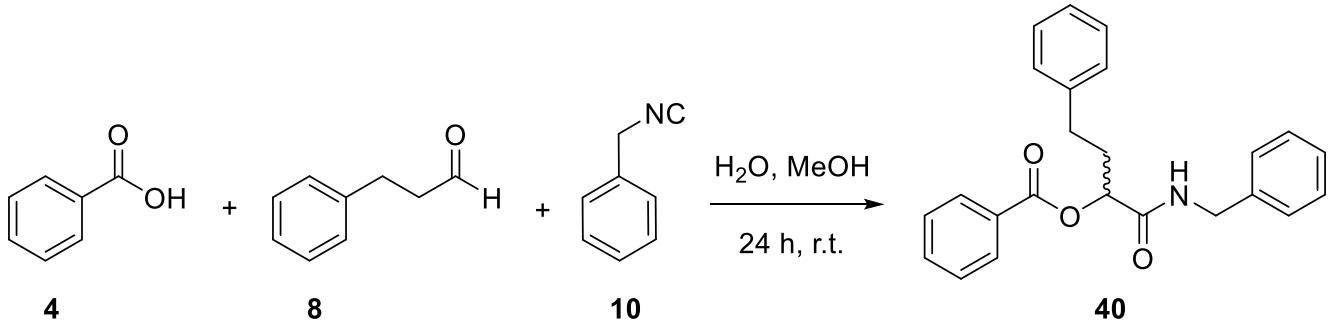

4 **8** **10** **40**

To a 10-mL round-bottomed flask charged with H_2O (4 mL) and MeOH (0.5 mL), the aldehyde **8** (1 mmol, 1 equiv), carboxylic acid **4** (1 mmol, 1 equiv) and isocyanide **10** (1 mmol, 1 equiv) were added. The reaction mixture was stirred at room temperature for 24 h. The precipitating solid was filtered, was washed with ether (2 × 20 mL) and was dried. The desired product **40** was obtained as a white solid in 54% yield.

^{1}H NMR (500 MHz, acetone-d_6) 8.10 – 8.04 (m, 2H), 7.95 (d, J = 30.3 Hz, 1H), 7.68 – 7.61 (m, 1H), 7.55 – 7.48 (m, 2H), 7.32 – 7.15 (m, 10H), 5.34 (t, J = 6.2 Hz, 1H), 4.53 – 4.37 (m, 2H), 2.84 (dd, J = 9.0, 6.8 Hz, 2H), 2.39 – 2.24 (m, 2H); ^{13}C NMR (126 MHz, acetone-d_6) δ 170.28, 166.25, 142.09, 140.34, 134.18, 130.79, 130.58 (2C), 130.41, 129.38 (2C), 129.28 (4C), 129.13 (2C), 128.19 (2C), 127.69, 126.83, 74.93, 43.19, 34.75, 32.09; HRMS (ESI) calcd for $C_{24}H_{24}NO_3$ [*M*+H]$^+$: 374.1751, found: 374.1723.

Synthesis of 4-phenethyl-4,5,6,7-tetrahydro-3*H*-imidazo[4,5-c]pyridine (56) via Pictet–Spengler reaction

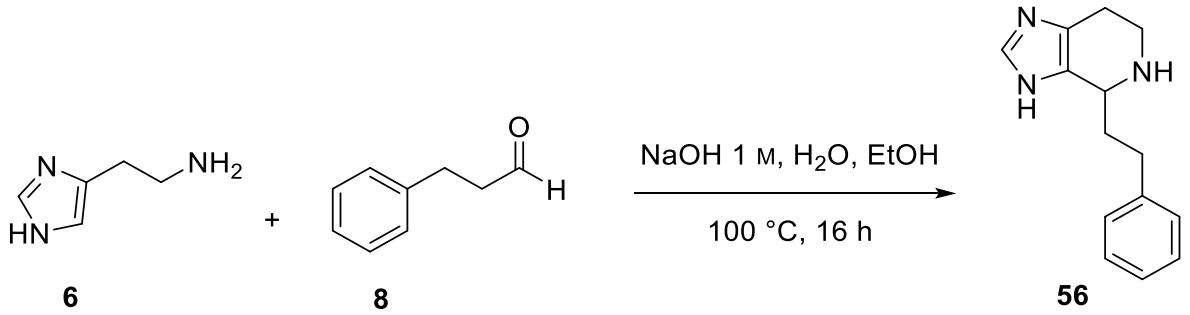

6 **8** **56**

To a 50-mL round-bottomed flask charged with histamine **8** (50 mg, 0.44 mmol) solution in H_2O (2 mL) and sodium hydroxide 1 M (0.4 mL), 3-phenylpropanal **6** (59 mg, 0.44 mmol) in EtOH (4 mL) was added. The reaction mixture was stirred at 100 °C for 16 h and was allowed to cool to room temperature. Solvent was removed under vacuum and the crude material was purified by preparative HPLC using a gradient of acetonitrile + 0.05 % formic acid from 10% to 100% to afford the desired product **56** as a beige solid in 10% yield.

^{1}H NMR (500 MHz, methanol-d_4) 7.70 (s, 1H), 7.32–7.27 (m, 4H), 7.20 (m, 1H), 4.48 (m, 1H), 3.68 (m, 1H), 3.43 (m, 1H), 3.03 (m, 2H), 2.89 (t, J = 8.5 Hz, 2H), 2.45 (m, 1H), 2.11 (m, 1H); ^{13}C NMR (126 MHz, methanol-d_4) δ 142.05, 137.29, 131.23, 129.82 (2C), 129.54 (2C), 127.55, 124.68, 55.49, 42.45, 35.63, 32.56, 20.53; HRMS (ESI) calcd for $C_{14}H_{18}NO_3$ [*M*+H]$^+$: 228.1501, found: 228.1482.

Modeling and docking

The X-ray crystal structures of the DnaN in complex with griselimycin (PDB code: 5AGV[6]) and previously discovered synthetic inhibitors (PDB code: 3D1G[7], 4K3S[8], 3QSB[9], and 4MJQ[10]) were used for our modeling studies. Before docking simulations, ligands and protein were prepared using Molecular Operating Environment (MOE) version 2018.01, Chemical Computing Group Inc., 1010 Sherbrooke St. West, Suite 910, Montreal, Quebec, H3A 2R7, Canada. Molecular Builder panel in MOE software was used to build the 3D structures for all designed Ugi-4CR and Passerini-3CR compounds. After converting all ligands in their 3D structures, the energy of compounds was minimized up to 0.1 Gradient using MOE force field Amber10:EHT, and the database was generated. This database was docked into griselimycin binding site using the Alpha Triangle placement method with an induced fit for refinement, alpha HB and affinity as score, and 30 placement poses for each ligand. The binding site in the protein was extended to 4.5 Å around griselimycin atoms. Subsequently, docking poses were sorted according to the binding score (S) field in the mdb window, and each complex was analyzed for the interactions. The compounds showing the highest scored poses and well accommodated inside the binding site of DnaN were selected.

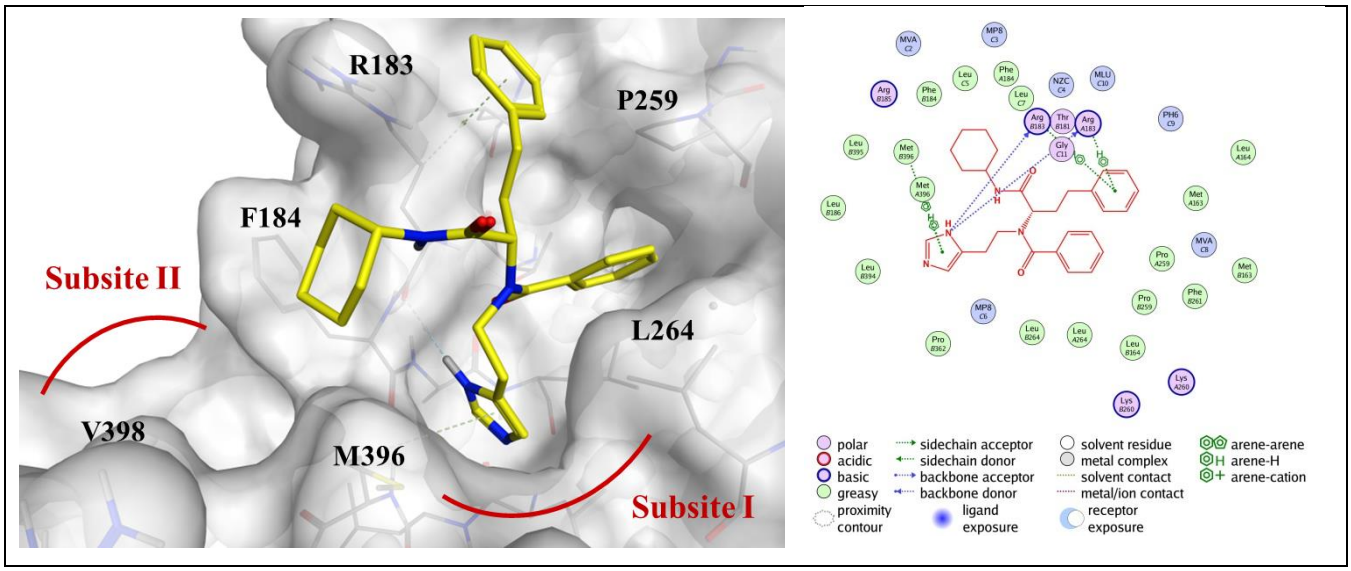

Figure S49 (A) Docking pose of **25** (yellow) in the subsite I of the DNA polymerases binding site of DnaN: protein surface (gray); (B) 2D ligand interactions of **25**.

X-ray crystal structure determination

Compounds **26**, **28** and **35** were dissolved in acetone-d_6 at room temperature. Crystals were obtained by slow evaporation of solvent. Single crystal X-ray diffraction data were collected at 142 K on a Bruker AXS X8APEX CCD diffractometer operating with graphite-monochromatized Mo Kα radiation. Frames of 0.5° oscillation were exposed. Deriving reflections were in the θ range of 2–29° with a completeness of ~ 99%. Structure solution and full least-squares refinement with anisotropic thermal parameters of all non-hydrogen atoms were performed using SHELX.[11]

Crystallographic data of the compounds:

26: Monoclinic, $P2_1/c$, a = 11.529(4), b = 22.224(8), c = 9.804(4) Å, β = 97.671(9)°.

28: Monoclinic, $P2_1/c$, a = 19.2697(7), b = 12.0455(4), c = 9.7293(3) Å, β = 100.201(2)°.

35: Triclinic, P-1, a = 9.7414(5), b = 11.4916(6), c = 23.1073(14) Å, α = 98.386(3), β = 101.510(3), γ = 90.175(3)°.

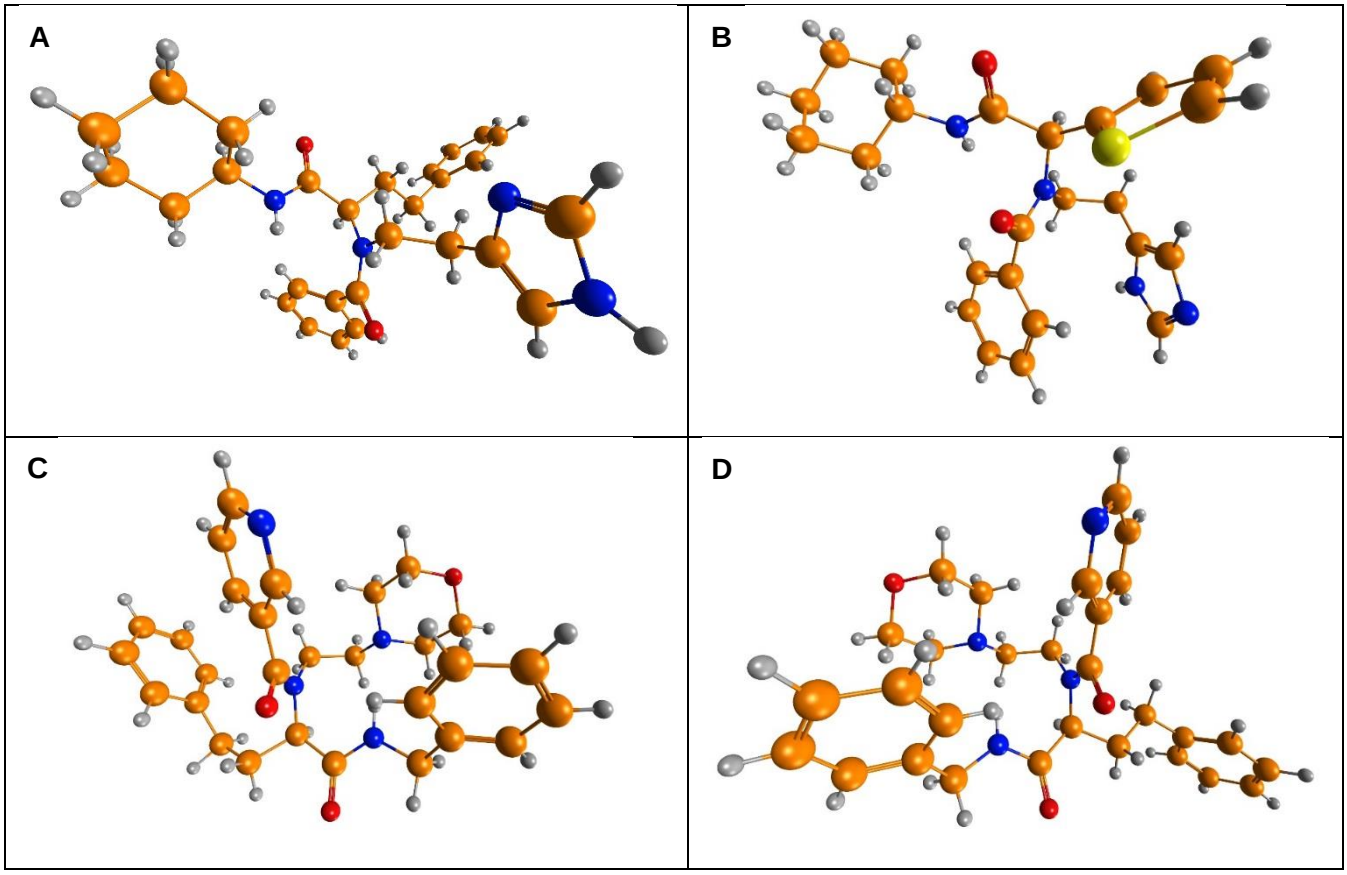

Figure S50. Crystal structures of compounds **26** as *R*-enantiomer (A), **28** as *S*-enantiomer (B), **35** as *R*-enantiomer (C), and **35** as *S*-enantiomer (D).

STD NMR study for 19 and RU7 with *M. tuberculosis* sliding clamp DnaN

Preparation of ligand samples:

- 12.5 µL of **19** (10 mM) stock solution in DMSO-d_6 was added to 14.74 µL of phosphate buffer (50 mM, NaCl 150 mM, pH = 7) in H_2O and 222.76 µL of phosphate buffer in D_2O. The mixture was transferred to a 4 mm NMR tube (final concentration of **19** = 500 µM; DMSO = 5%).
- 2.5 µL of **RU7** (10 mM) stock solution in DMSO-d_6 was added to 12.17 µL of phosphate buffer in H_2O, 10 µL of DMSO-d_6, and 225.33 µL of phosphate buffer in D_2O. The mixture was transferred to a 4 mm NMR tube (final concentration of **RU7** = 100 µM; DMSO = 5%).

Preparation of ligand and DnaN samples:

- 14.74 µL of *M.tb.* DnaN (84.8 µM) in phosphate buffer in H_2O was added to 12.5 µL of **19** (10 mM) stock solution in DMSO-d_6 and 222.76 µL of phosphate buffer in D_2O. The mixture was transferred to a 4 mm NMR tube (final concentration of DnaN = 5 µM; **19** = 500 µM; DMSO = 5%).
- 12.17 µL of *M.tb.* DnaN (102.64 µM) in phosphate buffer in H_2O was added to 2.5 µL of **RU 7** (10 mM) stock solution in DMSO-d_6, 10 µL of DMSO-d_6, and 225.33 µL of phosphate buffer in D_2O. The mixture was transferred to a 4 mm NMR tube (final concentration of DnaN = 5 µM; **RU7** = 100 µM; DMSO = 5%).

Preparation of 19 and RU7 mixture for the STD-NMR competitive experiment:

2.5 µL of **19** (50 mM) and 2.5 µL of **RU7** (10 mM) stock solutions in DMSO-d_6 were added to 12.17 µL of phosphate buffer in H_2O, 7.5 µL of DMSO-d_6, and 225.33 µL of phosphate buffer in D_2O. The mixture was transferred to a 4 mm NMR tube (final concentration of **19** = 500 µM; **RU7** = 100 µM; DMSO = 5%).

Preparation of 19, RU7, DnaN mixture for the STD-NMR competitive experiment:

12.17 µL of *M.tb.* DnaN (102.64 µM) in phosphate buffer in H_2O was added to 2.5 µL of **19** (50 mM) and 2.5 µL of **RU7** (10 mM) stock solutions in DMSO-d_6, 7.5 µL of DMSO-d_6, and 225.33 µL of phosphate buffer in D_2O. The mixture was transferred to a 4 mm NMR tube (final concentration of DnaN = 5 µM; **19** = 500 µM; **RU7** = 100 µM; DMSO = 5%).

^{1}H-STD-NMR binding experiments

All ^{1}H-STD-NMR experiments were performed at 25 °C on a Bruker UltraShield Plus 500 MHz spectrometer. The on-resonance irradiation on DnaN was set to 0 ppm.

First, the ^{1}H-NMR spectra of **19** and **RU7** samples prepared as mentioned above were recorded. Subsequently, on- and off-resonance ^{1}H-NMR spectra were recorded with 1024 scans. ^{1}H-STD-NMR spectra were obtained by subtracting the on-resonance spectrum from the corresponding off-resonance spectrum. ^{1}H-STD-NMR analysis revealed that ligand **19** bind to DnaN with good to moderate interaction as indicated by the intensity of the peaks in the STD NMR (Figure S51).[12]

^{1}H-STD-NMR competition experiments

First, the ^{1}H-NMR spectrum of **19** and **RU7** mixture prepared as mentioned above was recorded. Subsequently, on- and off-resonance ^{1}H-NMR spectra were recorded with 1024 scans. ^{1}H-STD-NMR spectra were obtained by subtracting the on-resonance spectrum from the corresponding off-resonance spectrum. ^{1}H-STD NMR spectrum showed the appearance of **RU7** peaks and disappearance (or reduced intensity) of **19** peaks indicating that they bind to the same binding site (Figure S53).

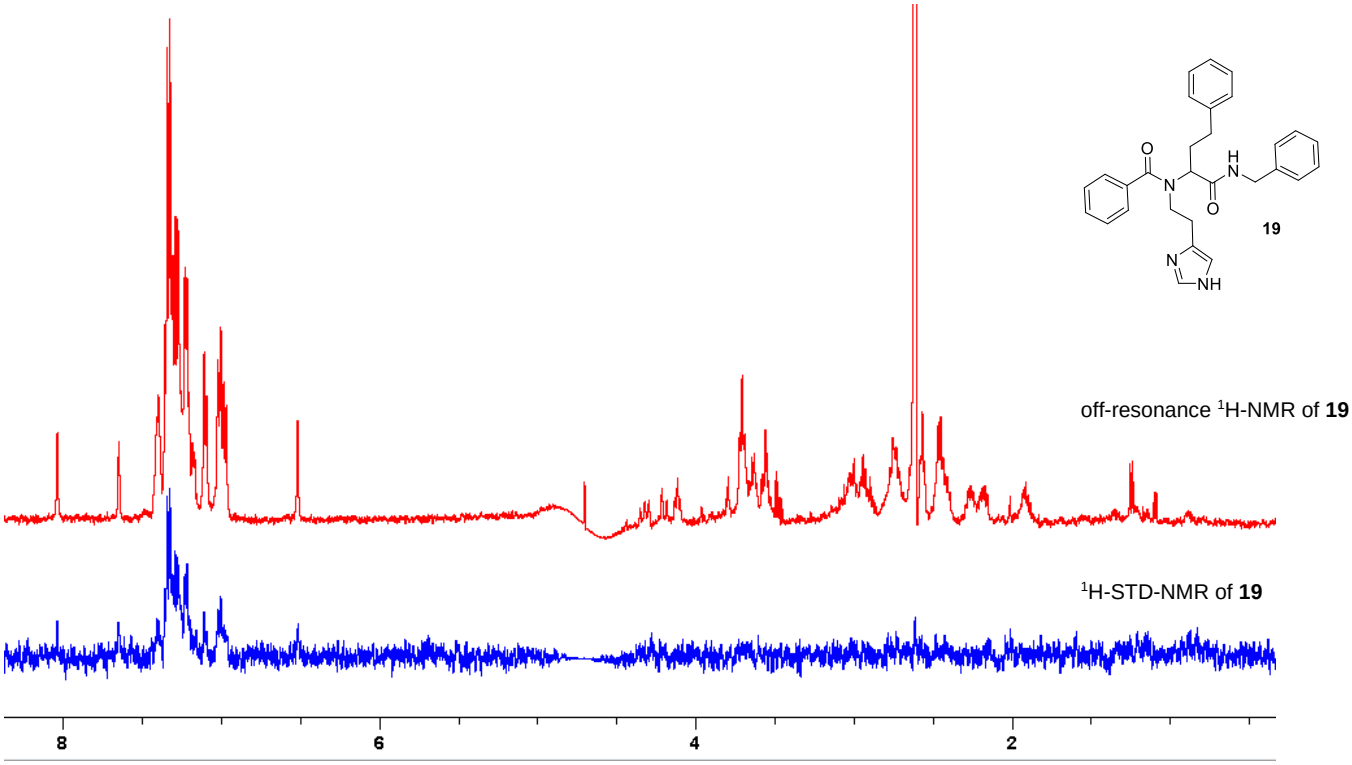

Figure S51. Off-resonance, and STD-NMR spectra for ligand **19**.

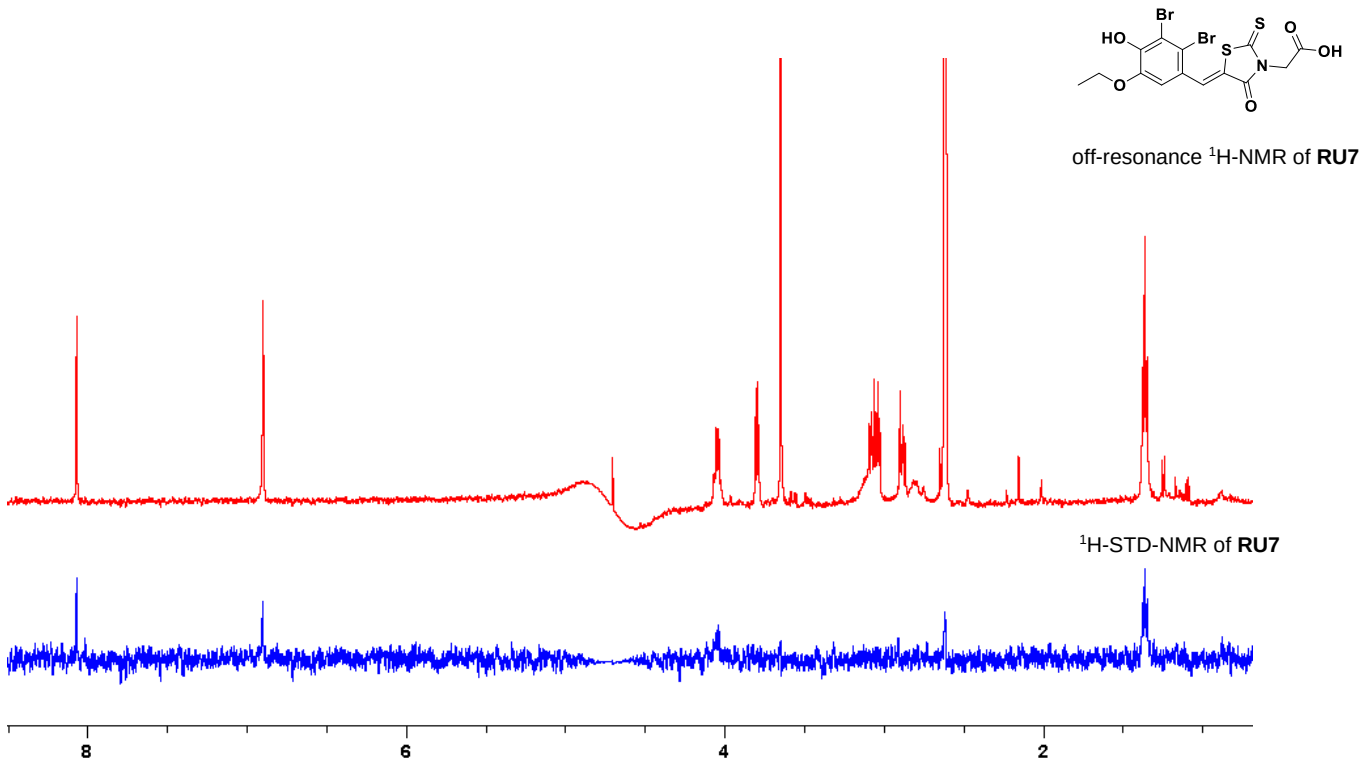

Figure S52. Off-resonance, and STD-NMR spectra for ligand **RU7**

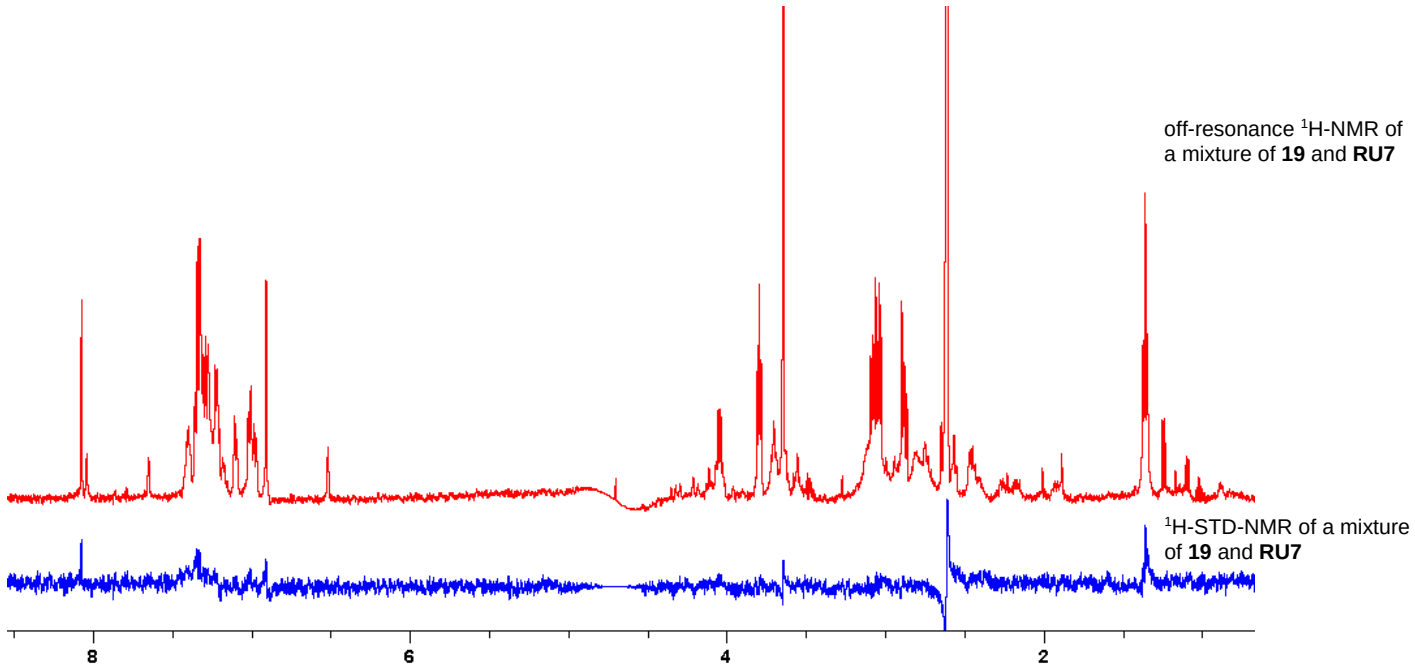

Figure S53. Off-resonance, and STD-NMR spectra for **19** and **RU7** mixture.

Protein expression and purification

The *dnaN* genes were cloned and heterologously expressed in *E. coli* BL21 (DE3) as fusion proteins consisting of full length DnaN with *N*-terminal Strep-tag II and TEV-protease recognition site from expression constructs based on a modified pCOLADuet-1. The cells were grown in ZYM-5052 auto-inducing medium[13] at 20 °C for 20–24 h. The cell pellets were resuspended in Tris-HCl (pH 7.5, 20 mM)/NaCl (150 mM) and lysed by sonication. The proteins were isolated from the supernatant after centrifugation using a self-packed 10 mL column with Strep-Tactin Superflow High Capacity (IBA) and eluted from the column with a single step of 5 mM d-desthiobiotin. The affinity tag was cleaved off with TEV protease (1:50 mg/mg) at 4 °C overnight. Gel filtration was carried out as final polishing step with a HiPrep Superdex 200 16/60 GL column (GE Healthcare) in Tris-HCl (pH 7.5, 20 mM)/NaCl 150 mM. Chromatographic steps were carried out on an Äkta Purifier system (GE Healthcare). The samples were analyzed by SDS-PAGE (12%), and protein concentrations were determined from the absorbances at 280 nm with the extinction coefficients as calculated by Protparam.[14]

Stability study of *M. smegmatis* DnaN using thermal shift assay (TSA)

Prior to protein templated reaction we monitored the stability of *Mycobacterium smegmatis* DnaN under the conditions of the Ugi reaction using thermal shift assay (TSA), showing no significant change in melting temperature (T_m) of the protein (60 °C) up to 48 h, making it compatible for KTGS.

Method

The concentration of the SYPRO orange 5000x dye (Sigma-Aldrich) and *M. smegmatis* DnaN giving the ideal signal was investigated by using different concentrations of DnaN (0.2, 0.1, 0.05, and 0.025 mg/mL) at various dye concentrations (10X, 5X and 2.5X). The experiments were performed in a 96-well PCR plate (Thermoscientific). The final volume per well was 25 µL including 20 µL of 20 mM Tris HCl, pH 7.5, 2.5 µL of the dye, and 2.5 µL DnaN. The plate was centrifuged and the melting temperature (T_m) of the protein was measured using a Real-time PCR (Step one plus, Applied biosystem). The conditions of the experiment were adjusted using the software (Step one 2.3). The starting temperature, the ending temperature and the heating rate were 21 °C, 95 °C and 0.5 °C per min, respectively. The melting curves were analyzed using Protein Thermal Shift 1.3 software. The best protein and dye concentrations were found to be 0.025 mg/mL and 10X, respectively. These concentrations were used to find the most suitable buffers for the stability study over 3 days. The buffers that showed the highest T_m, were selected: 50 mM phosphate pH 7, 10 mM acetate pH 5.5, and pH 6 (Figure S54A). The protein was incubated in the mentioned buffers at different time point in 96-well PCR plates at room temperature. The plates were set up by the same way as described before. The change in the T_m was measured for each plate after every 24 h over 3 days (Figure S54B).

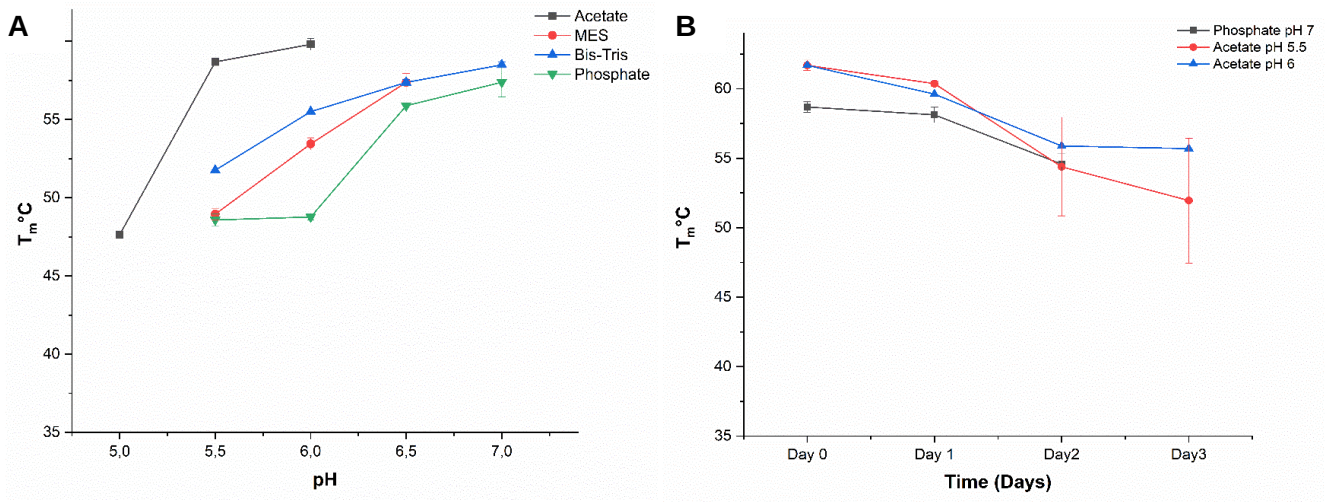

Figure S54. Buffer screening (A), and stability of *M. smegmatis* DnaN over 3 days (B).

***M. smegmatis* DnaN-modification study using ESI-MS**

***M. smegmatis* DnaN in the presence of building blocks.**

M. smegmatis DnaN (50 µL, 0.25 mM in phosphate buffer 0.05 M, pH 7), and the 4 building blocks **4**, **6**, **8**, **10** (0.5 µL each, 50 mM in DMSO) were added to a mixture of DMSO (23 µL) and phosphate buffer (425 µL, 0.05 M, pH 7). The reaction mixture was allowed to rotate on a rotating mixer at room temperature with 10 rpm. After 6 h, HEPES buffer (200 µL, 10 mM HEPES, 150 mM NaCl, pH 7.4) was added to a sample (50 µL) and it was analysed by ESI-MS.

***M. smegmatis* DnaN in the absence of building blocks.**

M. smegmatis DnaN (50 µL, 0.25 mM in phosphate buffer 0.05 M, pH 7) was added to a mixture of DMSO (25 µL) and phosphate buffer (425 µL, 0.05 M, pH 7). The reaction mixture was allowed to rotate on a rotating mixer at room temperature with 10 rpm. After 6 h, HEPES buffer (200 µL, 10 mM HEPES, 150 mM NaCl, pH 7.4) was added to a sample (50 µL) and it was analysed by ESI-MS.

***M. smegmatis* DnaN ESI-MS-measurements**

Protein ESI-MS-measurements were performed by injecting samples (1.5 µL) on a Dionex Ultimate 3000 RSLC system equipped with an Aeris Widepore XB-C8, 150 x 2.1 mm, 3.6 µm dp column (Phenomenex, USA). The gradient was initiated by a 0.5 min isocratic step at 2% ACN + 0.1% FA (B) in 98% H_2O + 0.1% FA (A) at 45 °C, followed by an increase to 75% B in 10 min to end up with a 3 min step at 75% B before re-equilibration with initial conditions. Flow rate was set to 300 µL/min and UV spectra were recorded with a DAD in ranging from 200 to 600 nm. The LC flow was split to 75 µL/min before entering the maXis 4G qToF mass spectrometer (Bruker Daltonics, Bremen, Germany) equipped with the standard Bruker ESI source. The source temperature was set to 180 °C, capillary voltage to 4000 V, dry-gas flow 6.0 L/min and the nebulizer was set to 1.1 bar. All mass spectra were acquired in positive ionization mode ranging from 600–1800 m/z at 2.5 Hz scan rate. Deconvolution for determination of the protein masses was performed with the Maximum Entropy algorithm (Copyright 1991-2004 Spectrum Square Associates, Inc.).

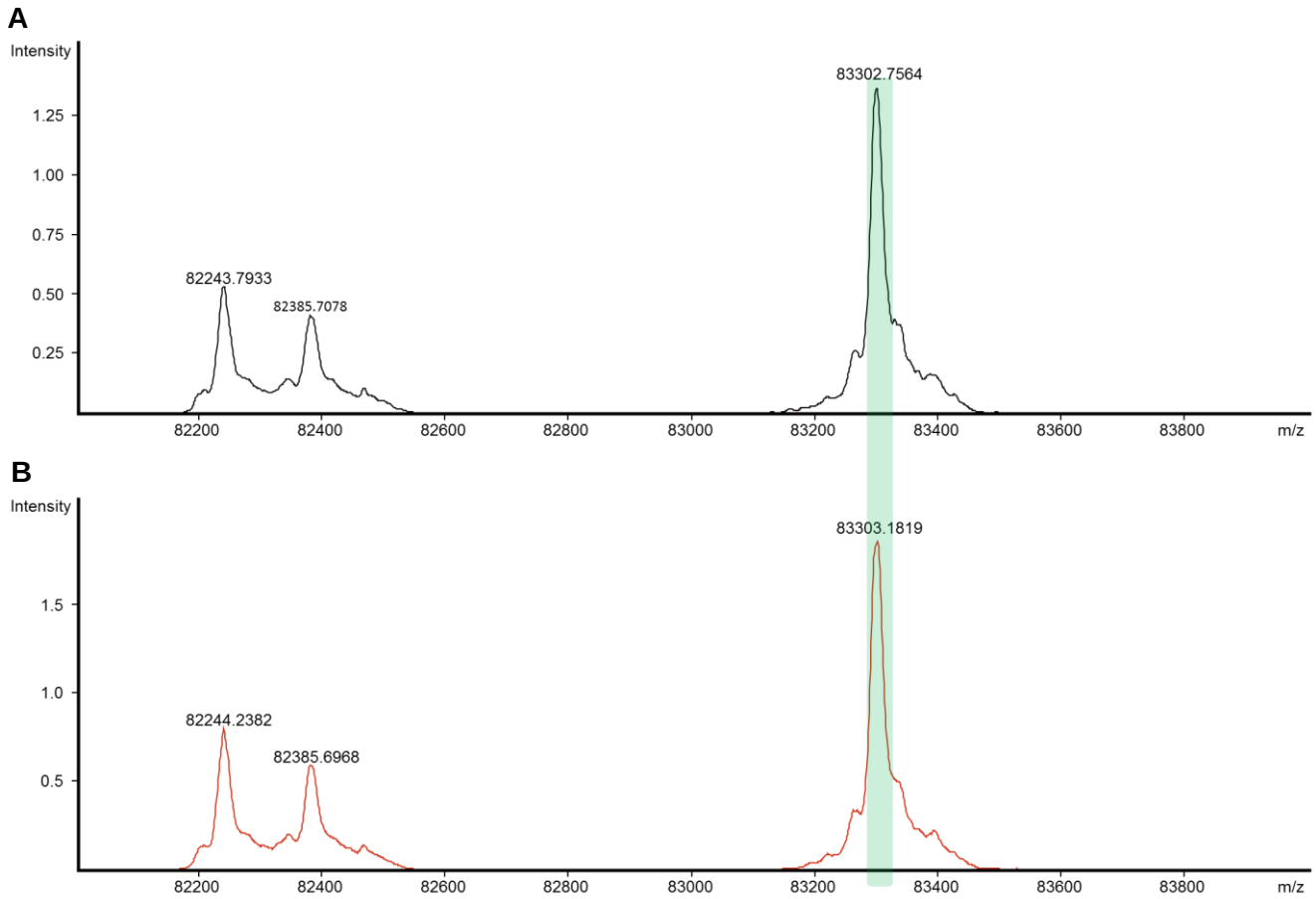

Figure S55. Mass spectra of *M. smegmatis* DnaN (41.65 kDa) without building blocks (A) and in the presence of building blocks (B).

DnaN binding study by surface plasmon resonance (SPR)

The SPR experiments were performed using a Reichert SR7500DC surface plasmon resonance spectrometer (Reichert Technologies, Depew, NY, USA), and medium density carboxymethyl dextran hydrogel CMD500M sensor chips (XanTec Bioanalytics, Düsseldorf, Germany) according to reported protocol. Double distilled (dd) water was used as the running buffer for immobilization.[15] HBS-EP buffer (10 mM HEPES, 150 mM NaCl, 3 mM EDTA, 0.005% v/v tween 20, pH 7.4) containing 5% v/v DMSO was used as the running buffer for binding study. All running buffers were filtered and degassed prior to use. Either *M. tuberculosis* β-sliding clamp (42.44 kDa) or *M. smegmatis* β-sliding clamp (41.65 kDa) was immobilized in one of the two flow cells by standard amine coupling procedure. The other flow cell was left blank to serve as a reference. The system was initially primed with borate buffer 100 mM (pH 9.0), then the carboxymethyldextran matrix was activated by a 1:1 mixture of *N*-ethyl-*N*′-(3-dimethylaminopropyl)carbodiimide hydrochloride (EDC) 100 mM and *N*-hydroxysuccinimide (NHS) 100 mM at a flow rate of 10 µL/min for 7 min. The β-sliding clamp was diluted to a final concentration of 40 µg/mL in 10 mM sodium acetate buffer (pH 4.5) and was injected at a flow rate of 10 µL/min for 7 min. Non-reacted surface was quenched by 1 M ethanolamine hydrochloride (pH 8.5) at a flow rate of 25 µL/min for 3 min. A series of 10 buffer injections was run initially on both reference and active surfaces to equilibrate the system resulting in a stable immobilization level of approximately 2000 µ refractive index unit (µRIU). Binding experiments were performed at 20 °C. Ugi products dissolved in DMSO were diluted with HBS-EP buffer (final concentration of compound: 250 µM; DMSO: 5% v/v) and were injected at a flow rate of 30 µL/min. Griselimycin (GM) at concentration of 50 µM was used as a positive control. Single-cycle kinetics were applied for K_D determination. The association time was set to 60 s, and the dissociation phase was recorded for 120 s. Ethylene glycol 80% in the running buffer was used for regeneration of the surface. Differences in the bulk refractive index due to DMSO were corrected by a calibration curve (nine concentrations: 3–7% v/v DMSO in HBS-EP buffer). Data processing and analysis were performed by Scrubber software (Version 2.0c, 2008, BioLogic Software). Sensorgrams were calculated by sequential subtractions of the corresponding curves obtained from the reference flow cell and the running buffer (blank). SPR responses are expressed in resonance unit (RU). The K_D values were calculated by global fitting of the kinetic curves. (Table S10 and Figure S56).

Table S9. Chemical structures and RU responses of 16 Ugi and 1 Passerini derivatives from the combinatorial library using *M. smegmatis* DnaN.

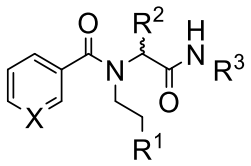

Compound	R^1	R^2	R^3	X	RU at 250 µM
25	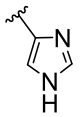	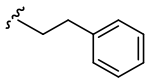	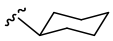	CH	12.1
26				N	0.1
19			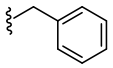	CH	17.8
27				N	1.1
28			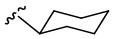	CH	1.4
29				N	0.0
30			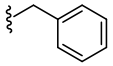	CH	0.4
31				N	1.1
32	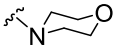	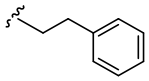	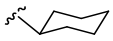	CH	1.8
33				N	0.0
34			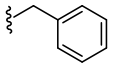	CH	0.0
35				N	0.0
36				CH	0.0
37				N	9.7
38			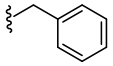	CH	3.9
39				N	0.0
40	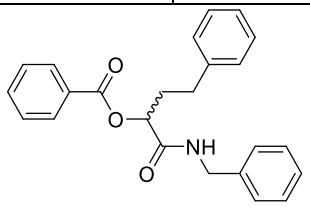				1.8
GM	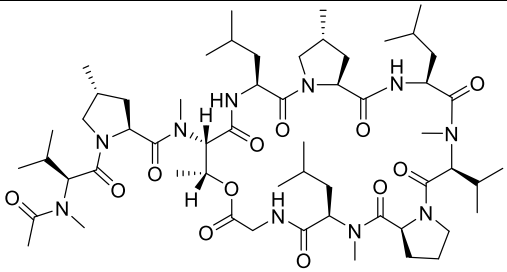				8.0 (at 50 µM)

Table S10. Amplification factors, kinetics, binding affinities, antibacterial activities, and cytotoxicity of the Ugi hit compounds **19**, **25**, and a non-hit **38**.

Compd	AF[a]	R_{max} (RU)[b]	k_{on} ($M^{-1}s^{-1}$)[c]	k_{off} (s^{-1})[d]	K_D (μM)[e] Mtb DnaN	MIC (μM)		
						E. coli TolC[f]	*M. luteus* DSM-1790	*M. smegmatis* mc^2155
19	17	22 ± 1	127 ± 7	0.082 ± 0.002	650 ± 40	128	128	> 128
25	20	35 ± 4	9 ± 1	0.0046 ± 0.0002	510 ± 80	128	128	> 128
38	-	26 ± 1	109 ± 7	0.246 ± 0.006	2300 ± 200	n.d.[g]	> 128	> 128

[a] Amplification factor calculated as $AF = \frac{\text{AUC(DnaN-guided reaction)}}{\text{AUC(blank reaction)}}$, where AUC is the area under the curve from the total ion current (TIC) chromatogram; [b] Maximum analyte binding capacity; [c] k_{on}: association rate constant; [d] k_{off}: dissociation rate constant; [e] K_D: equilibrium dissociation constant; [f] TolC deficient; [g] Not determined.

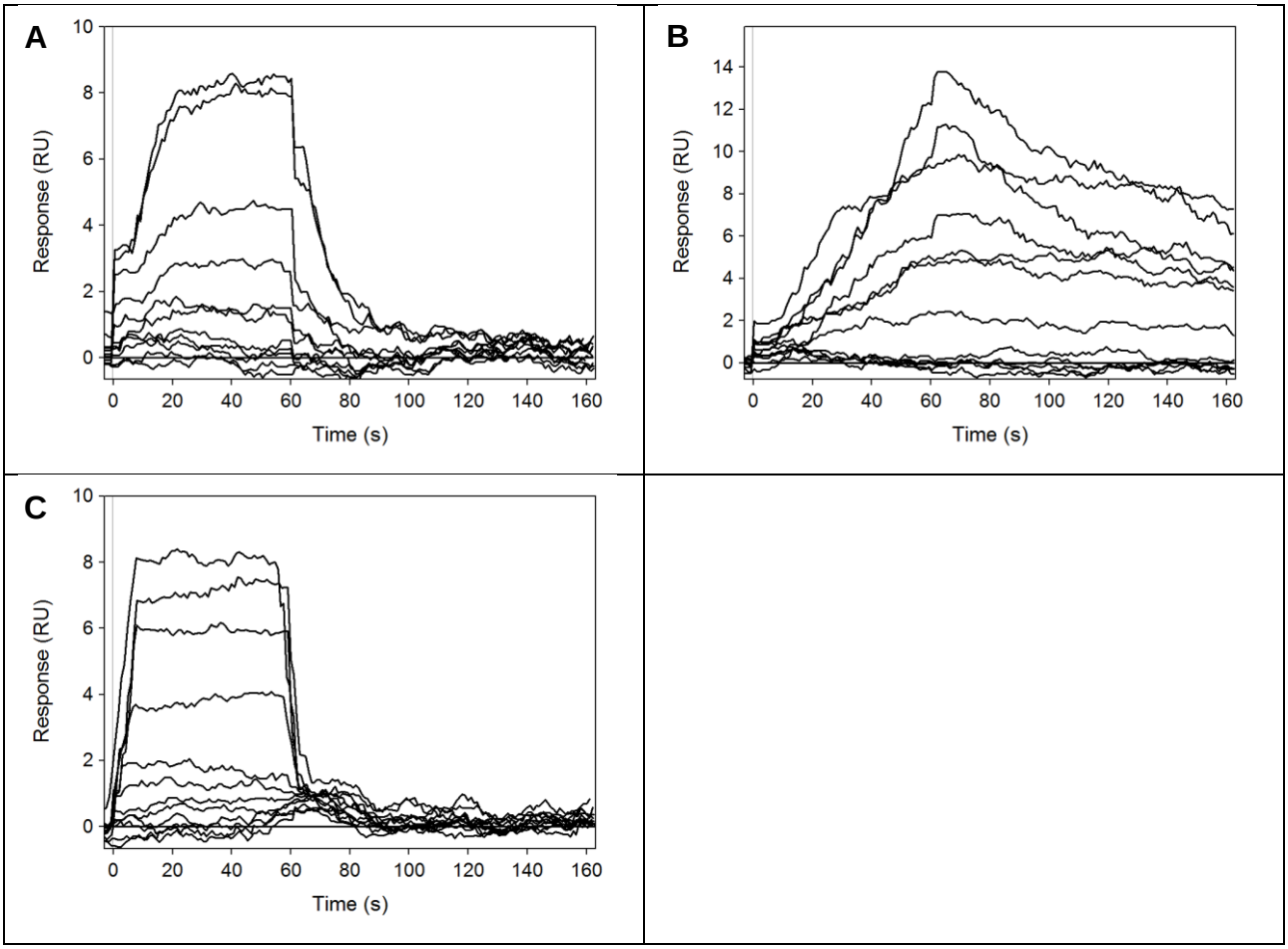

Figure S56. Sensorgrams overlay of compound **19** (A), **25** (B), and **38** (C) at concentrations of 3–2000 μM running over an immobilized *M. tuberculosis* DnaN.

Antimicrobial activity screening

All compounds were prepared as DMSO stocks and minimum inhibitory concentrations were determined as described elsewhere.[6] Bacteria were handled according to standard procedures and were obtained from the German Collection of Microorganisms and Cell Cultures (DSMZ) and the American Type Culture Collection (ATCC) or were part of our internal strain collection. In brief, bacterial cultures were diluted in M7H9 medium (Difco™ Middlebrook 7H9 broth supplemented with BBL™ Middlebrook ADC enrichment and 2 mL/L glycerol; used for *Mycobacterium smegmatis* mc^2155) or Müller-Hinton broth (0.2% beef infusion solids, 1.75% casein hydrolysate, 0.15% starch, pH 7.4; used for *E. coli* and *M. luteus*) to achieve a final inoculum of approximately 10^4 to 10^5 cfu/mL. Compounds were tested as serial dilution in 96-well plates and MIC values were determined after 16–48 h incubation at 30–37°C (Table S10).

LC-HRMS chromatograms and NMR spectra of the synthesized compounds

Compound 2

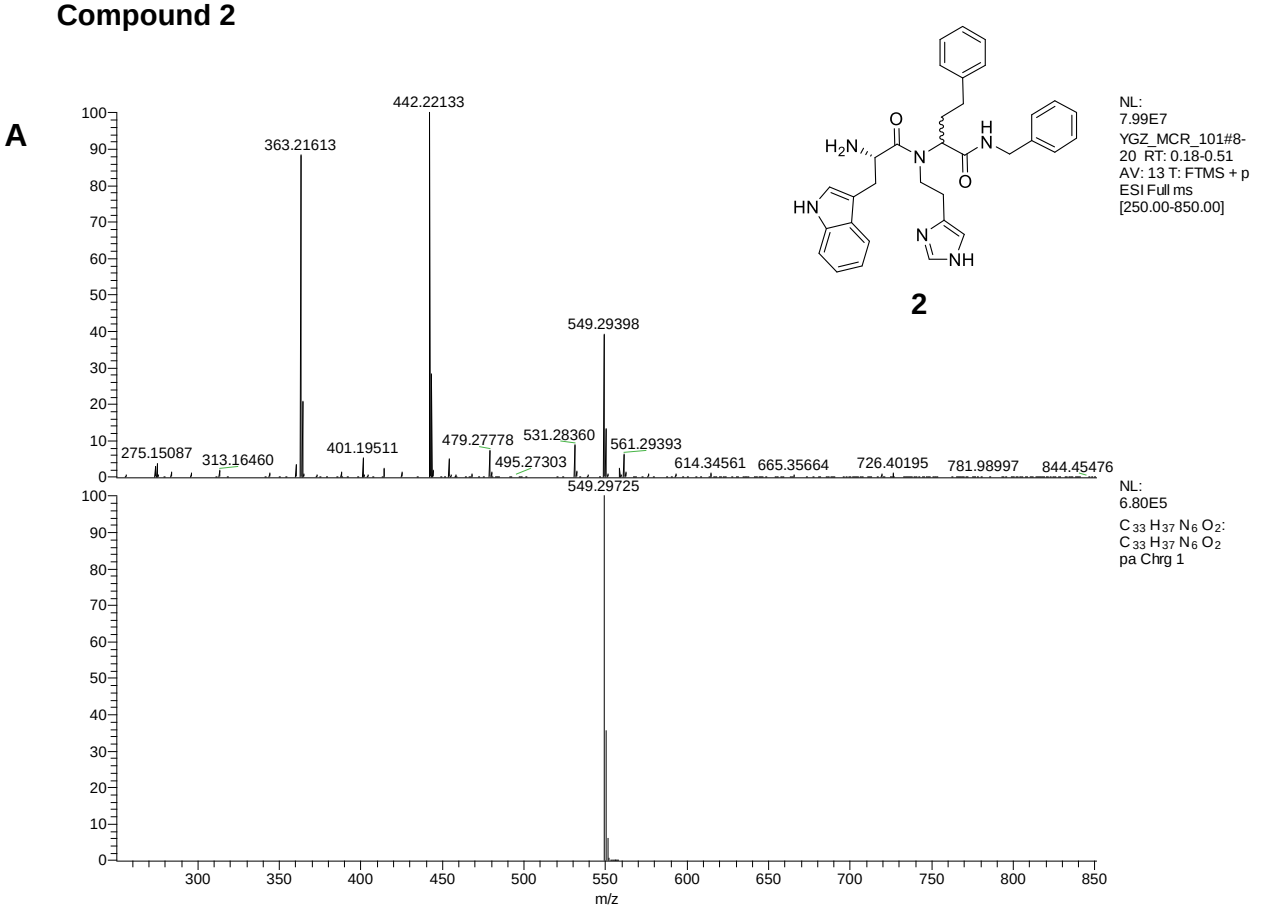

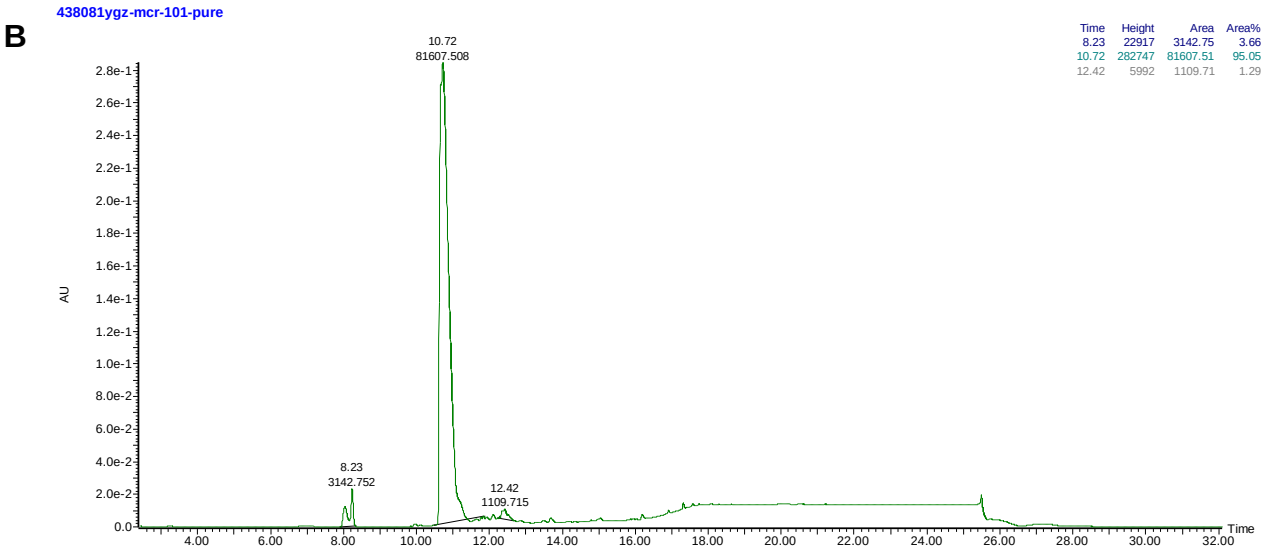

Figure S57: (A) Mass spectrum (HR-MS); (B) UV chromatogram (LC-MS) of compound **2**.

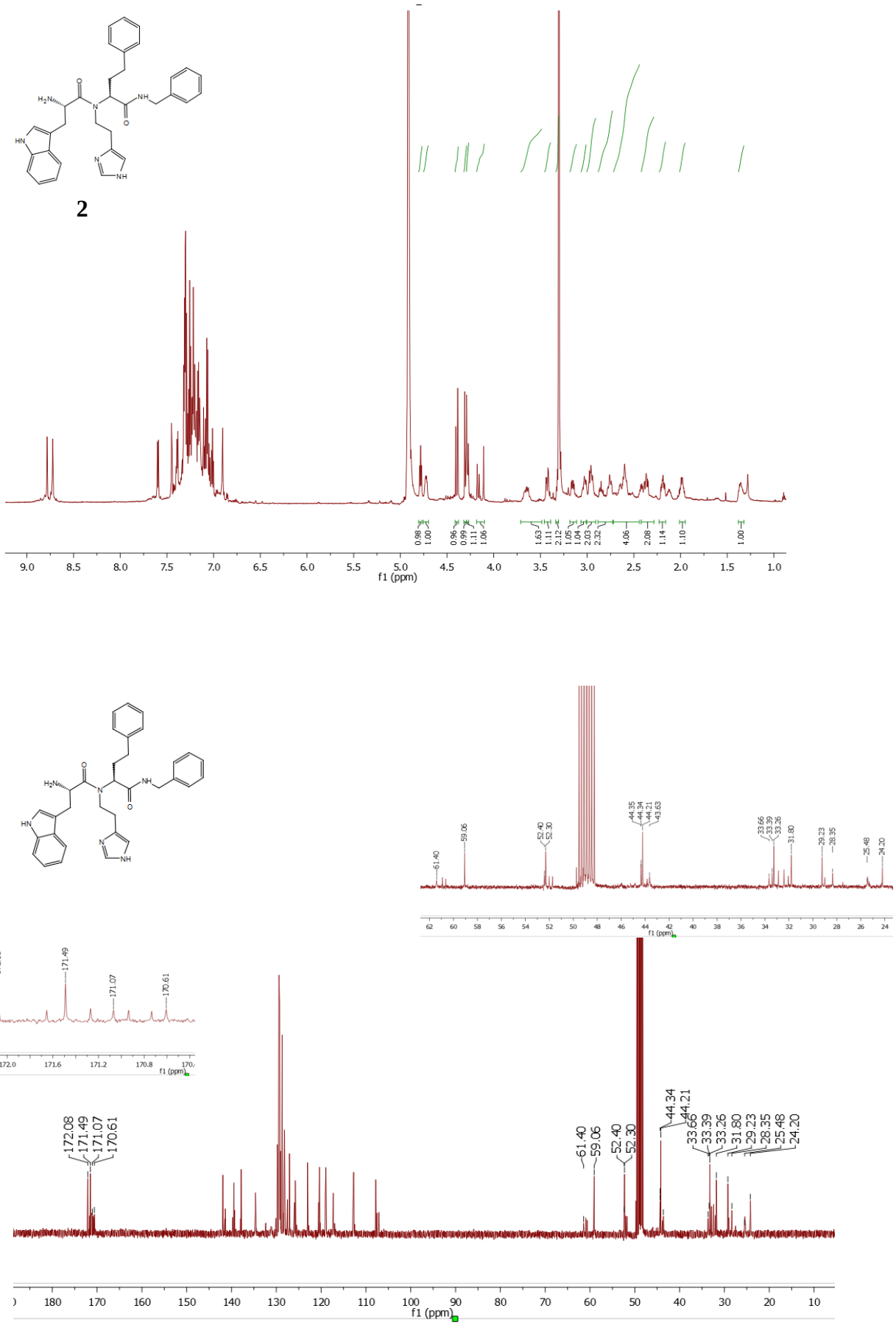

Figure S58: ^{1}H-, ^{13}C-NMR spectra of compound **2** and assignment for the major diastereoisomers.

Compound 11

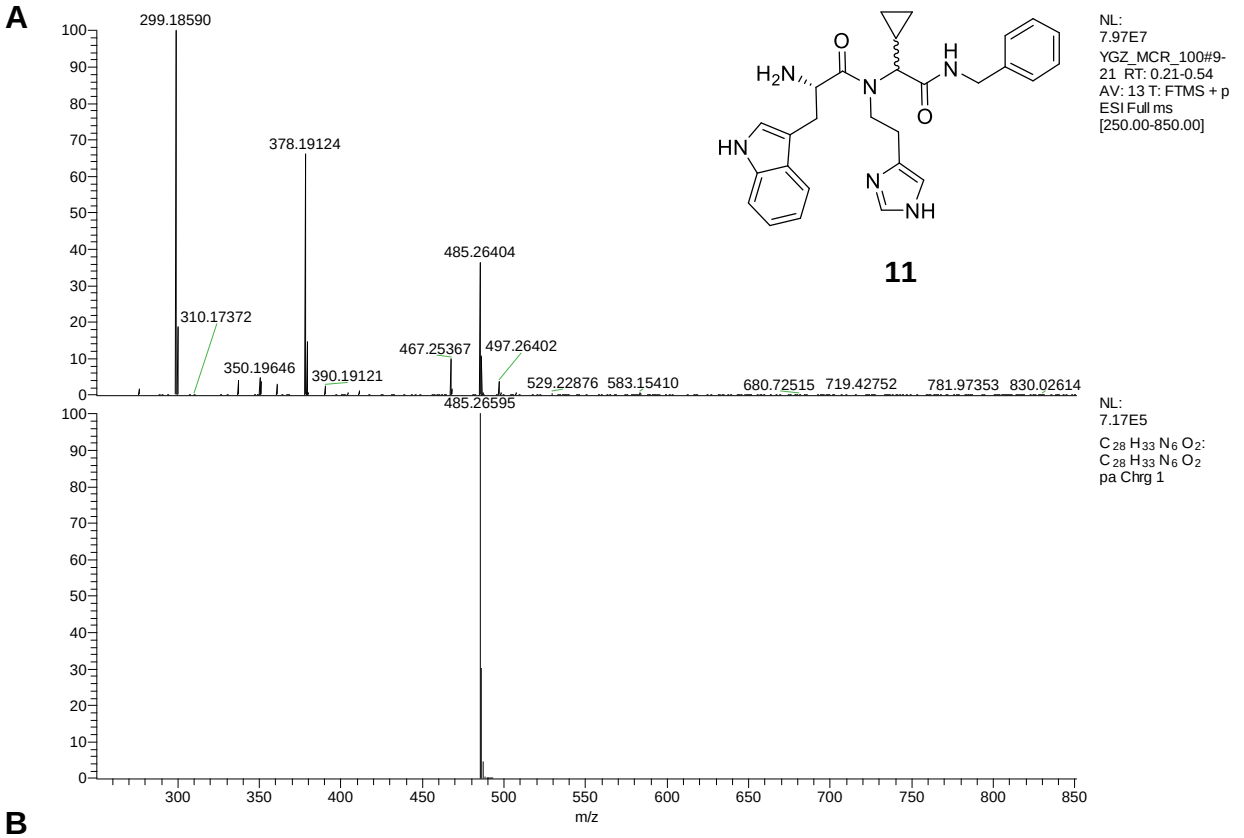

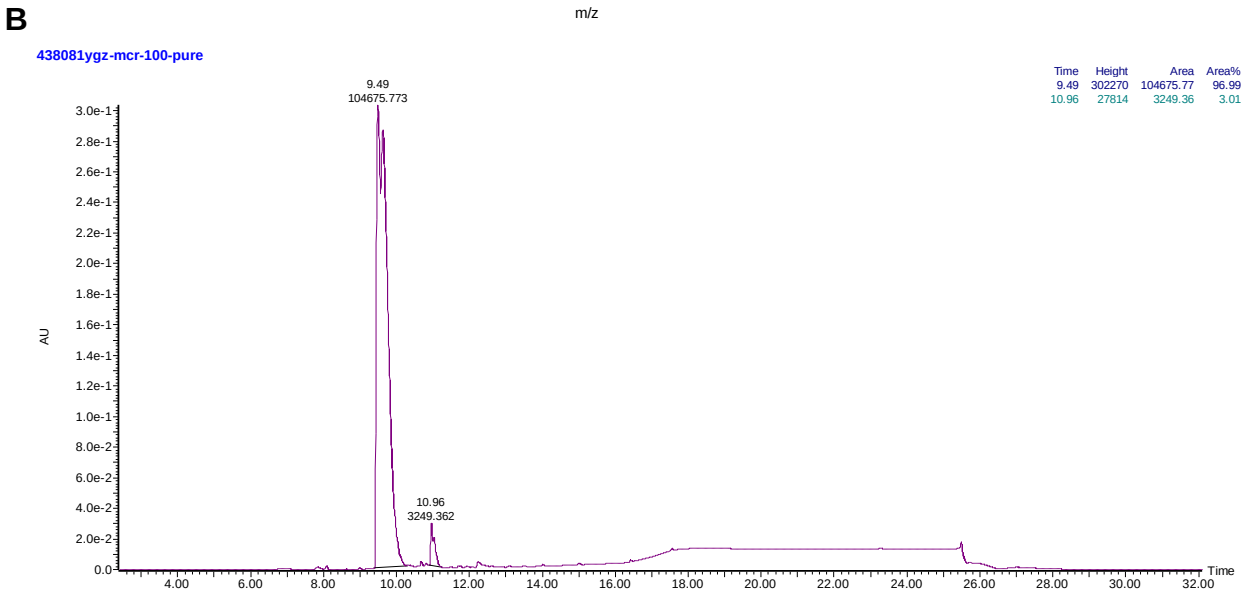

Figure S59: (A) Mass spectrum (HR-MS); (B) UV chromatogram (LC-MS) of compound **11**.

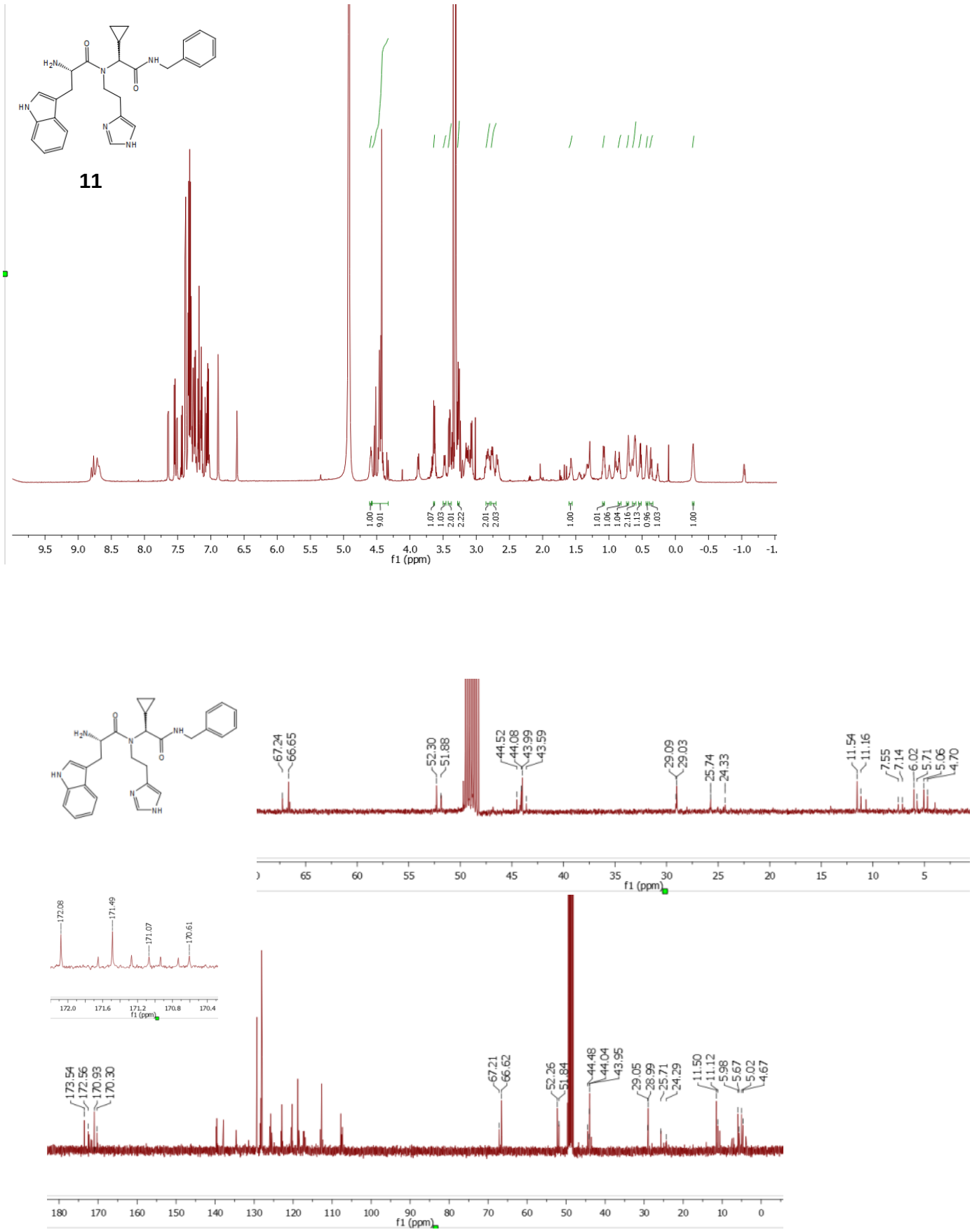

Figure S60: ^{1}H-, ^{13}C-NMR spectra of compound **11** and assignment for the major diastereoisomers.

Compound 13

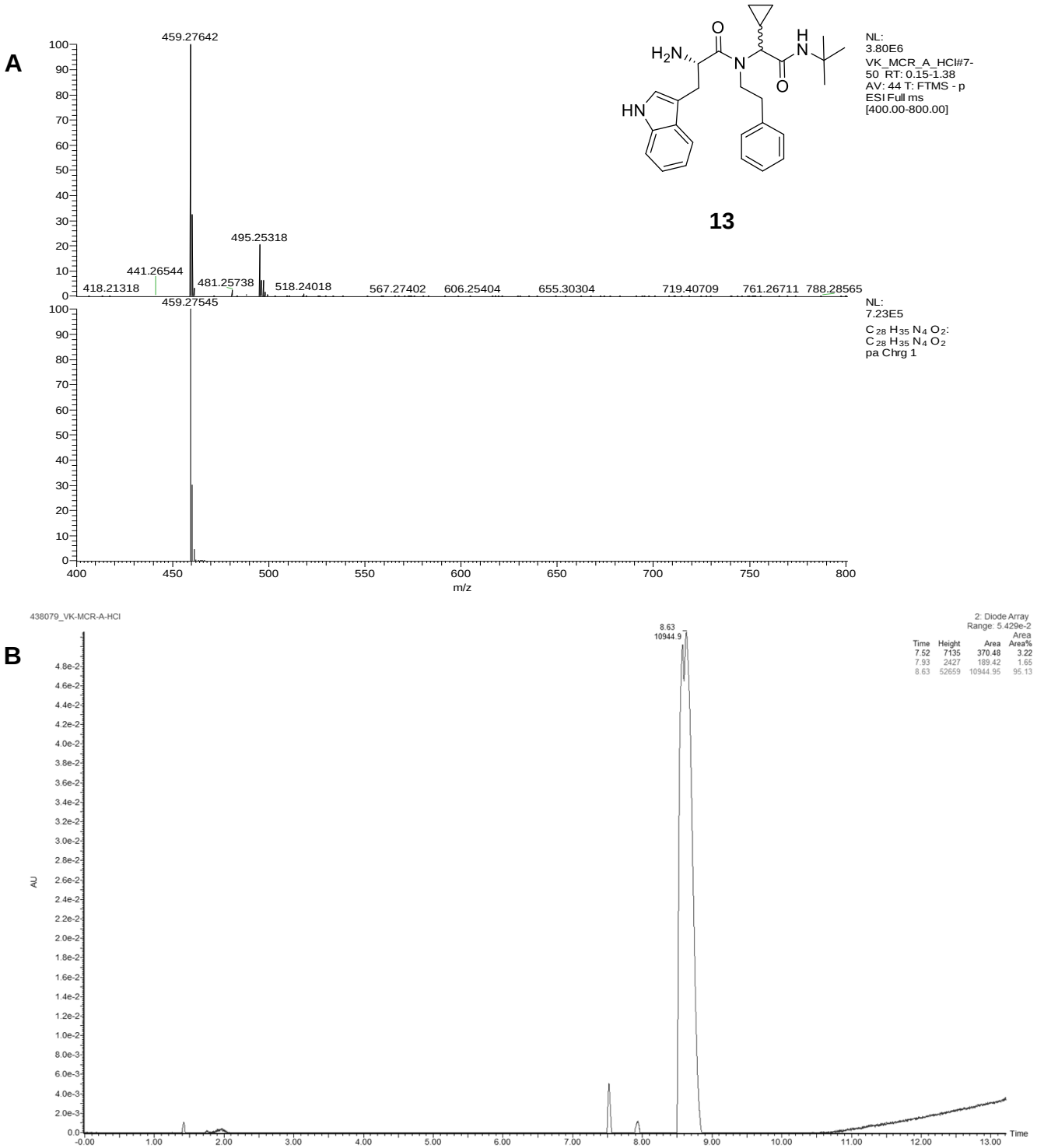

Figure S61: (A) Mass spectrum (HR-MS); (B) UV chromatogram (LC-MS) of compound **13**.

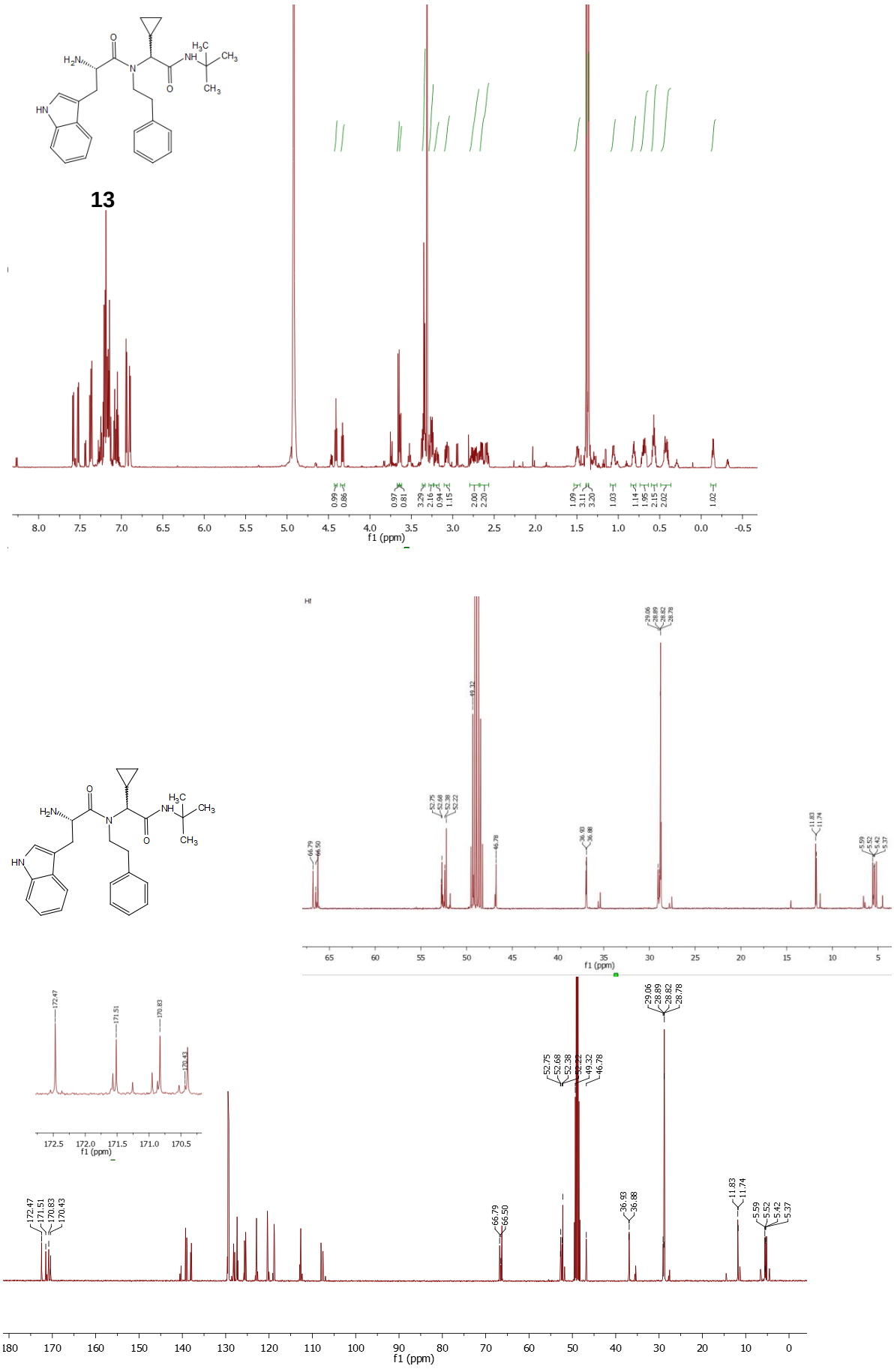

Figure S62: ^{1}H-, ^{13}C-NMR spectra of compound **13** and assignment for the major diastereoisomers.

Compound 14

A

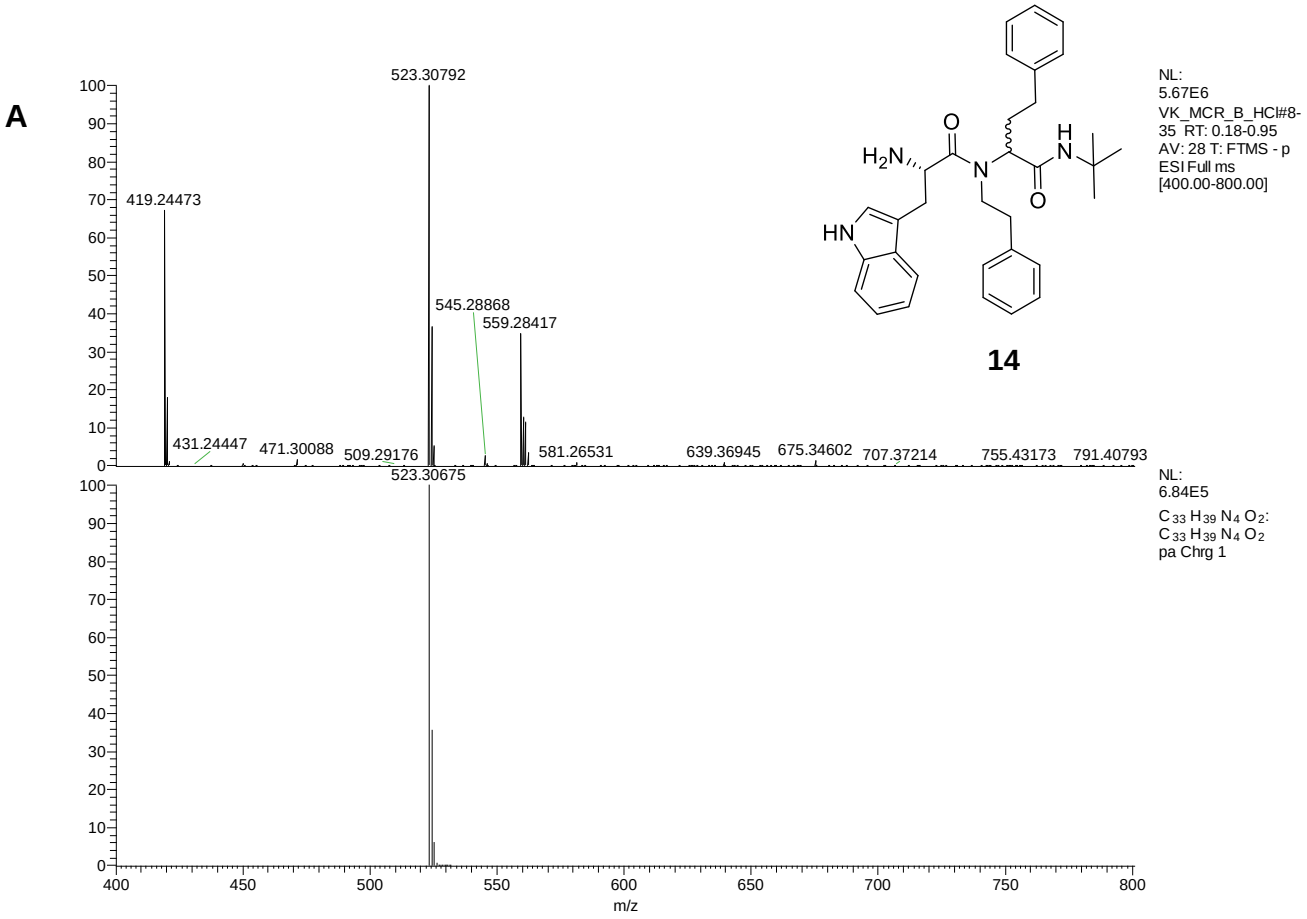

14

B

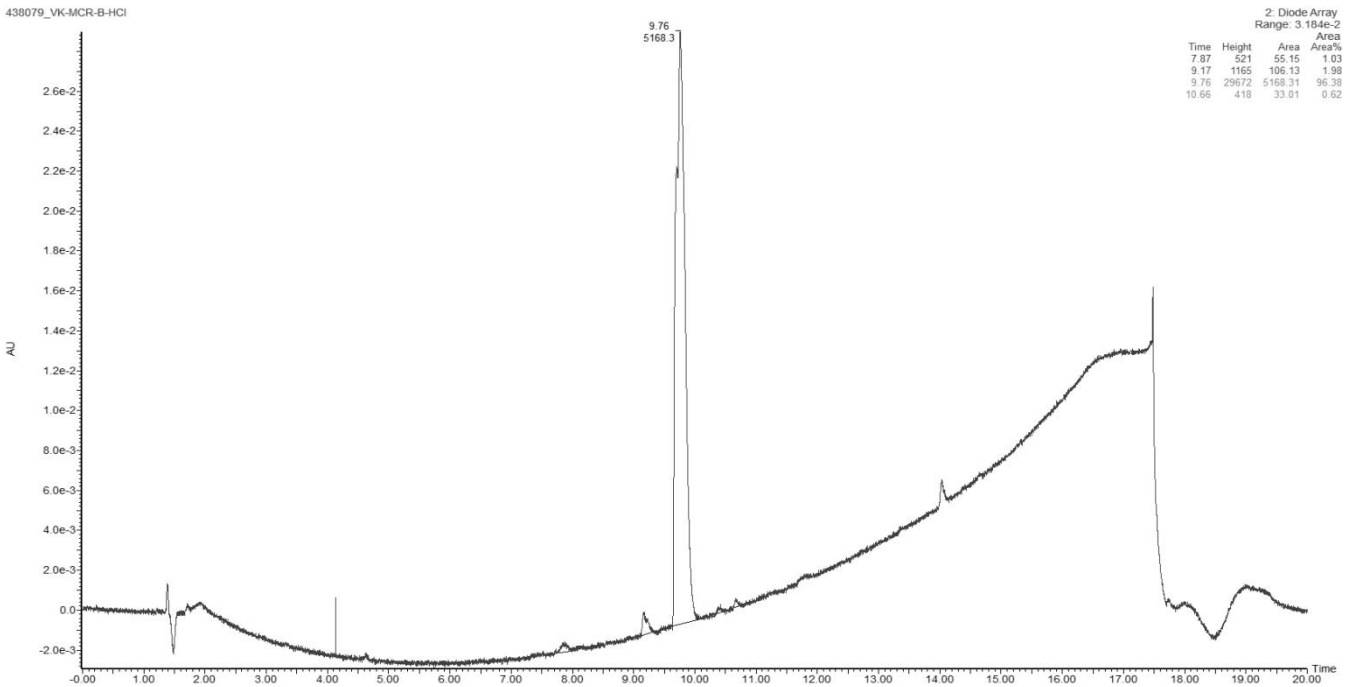

Figure S63: (A) Mass spectrum (HR-MS); (B) UV chromatogram (LC-MS) of compound **14**.

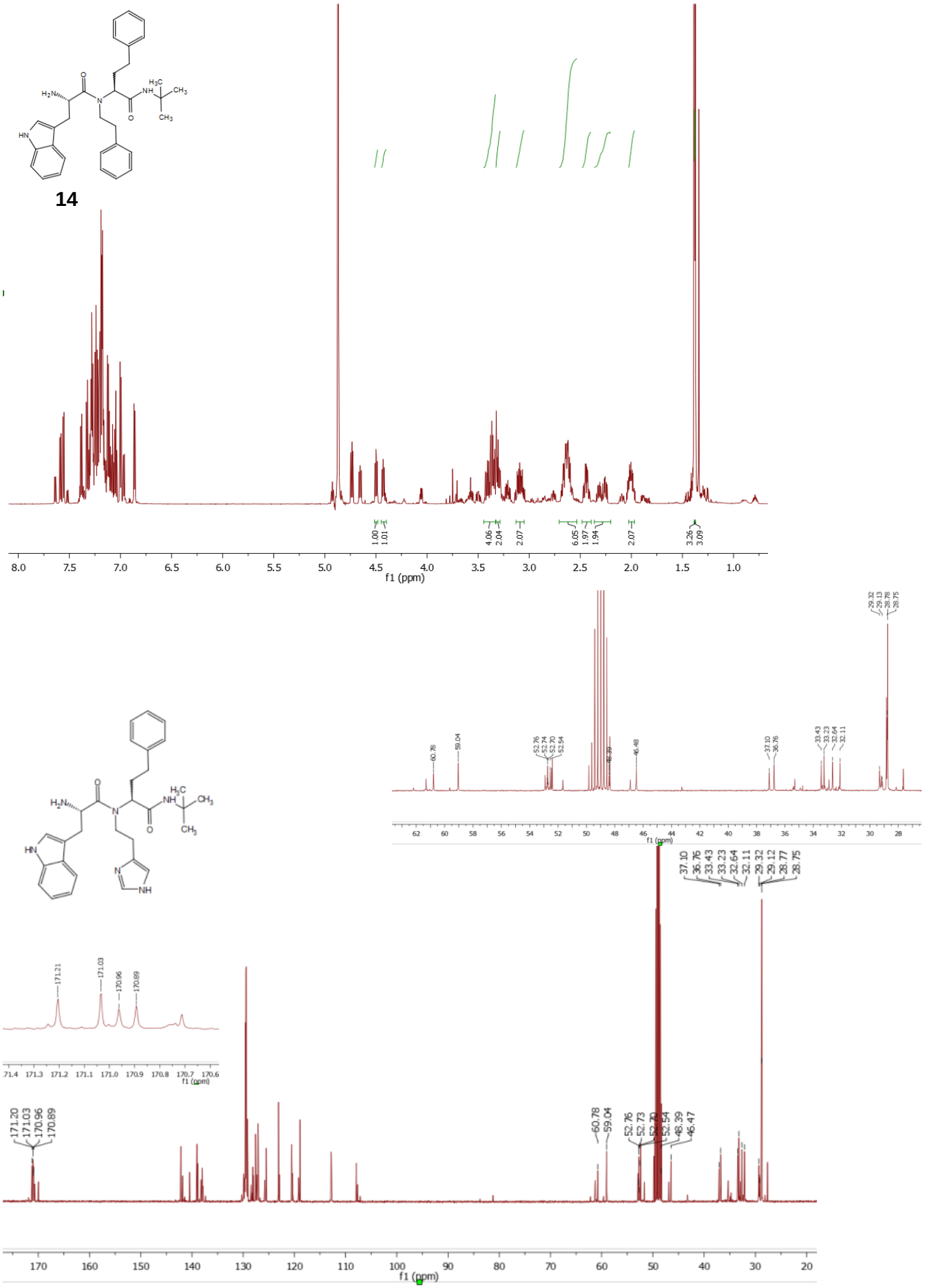

Figure S64: ^{1}H-, ^{13}C-NMR spectra of compound **14** and assignment for the major diastereoisomers

Compound 15

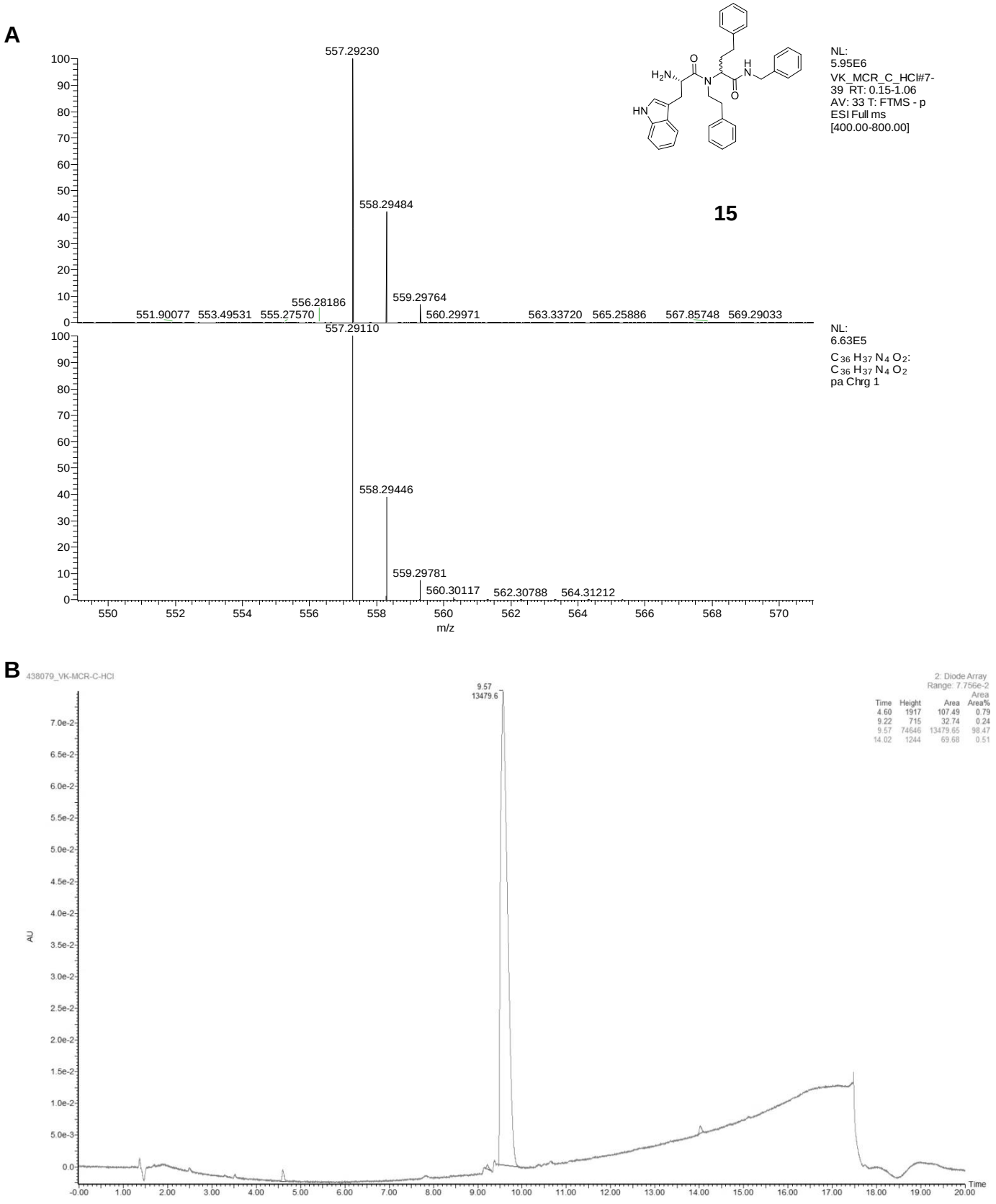

Figure S65: (A) Mass spectrum (HR-MS); (B) UV chromatogram (LC-MS) of compound **15**

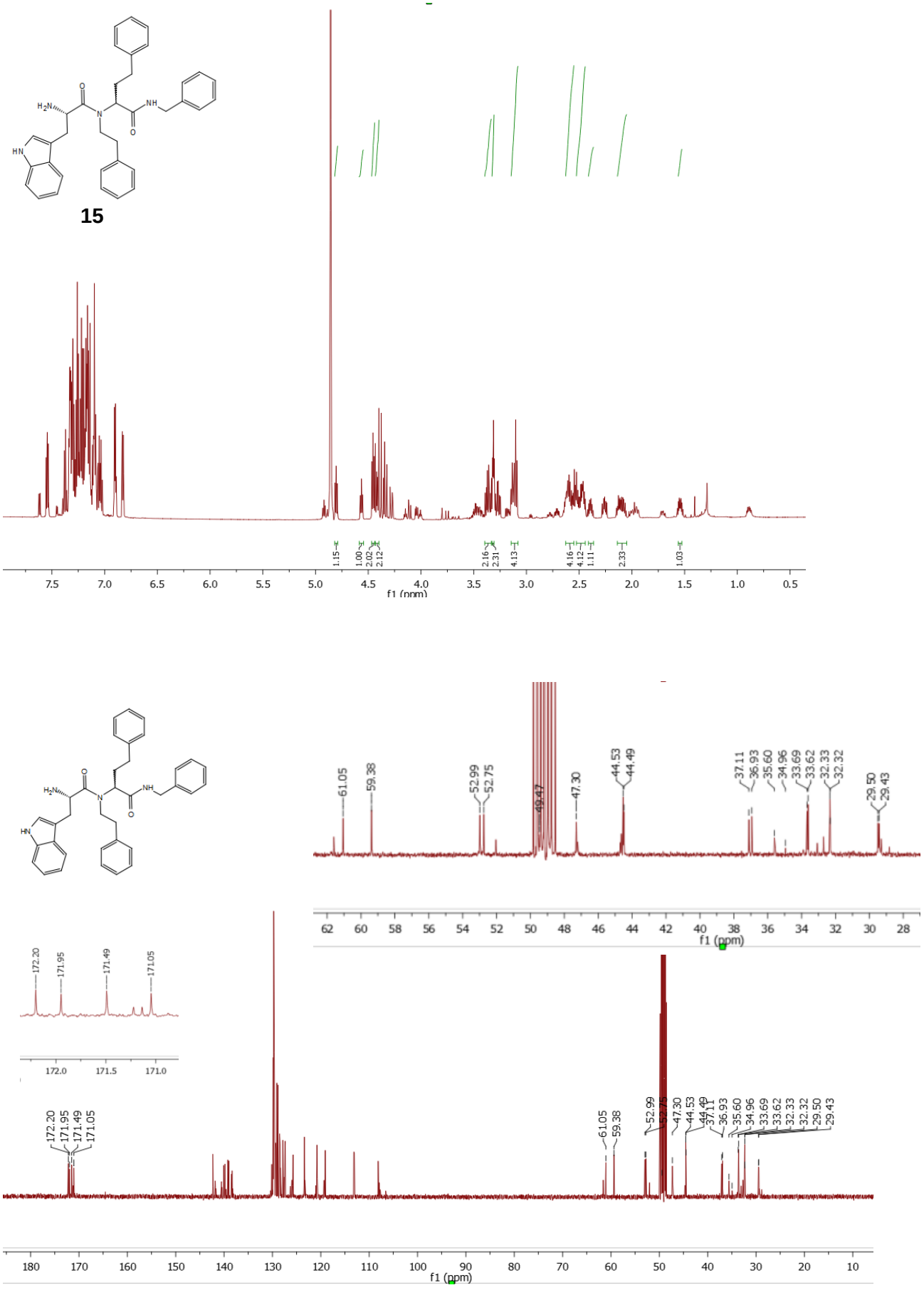

Figure S66: ^{1}H-, ^{13}C-NMR spectra of compound **15** and assignment for the major diastereoisomers.

Compound 16

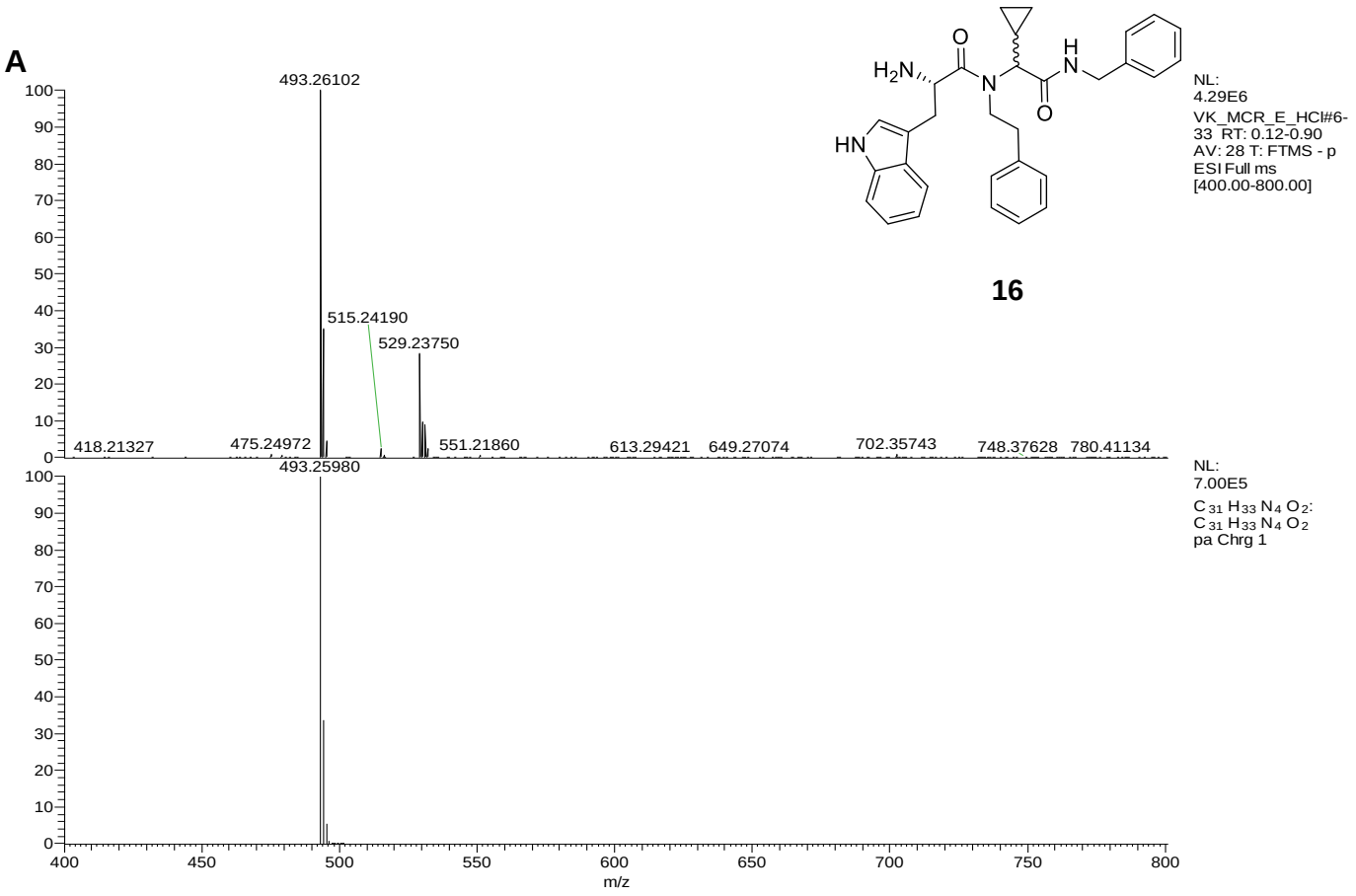

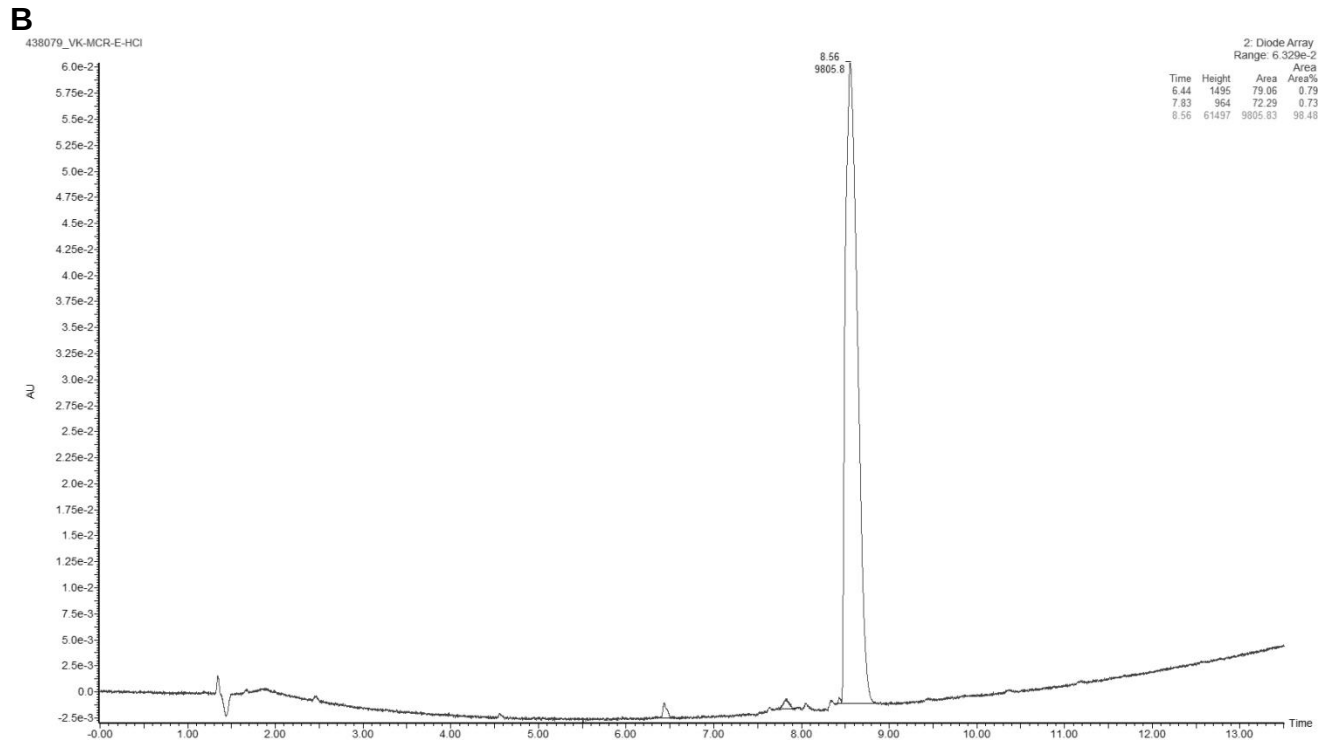

Figure S67: (A) Mass spectrum (HR-MS); (B) UV chromatogram (LC-MS) of compound **16**.

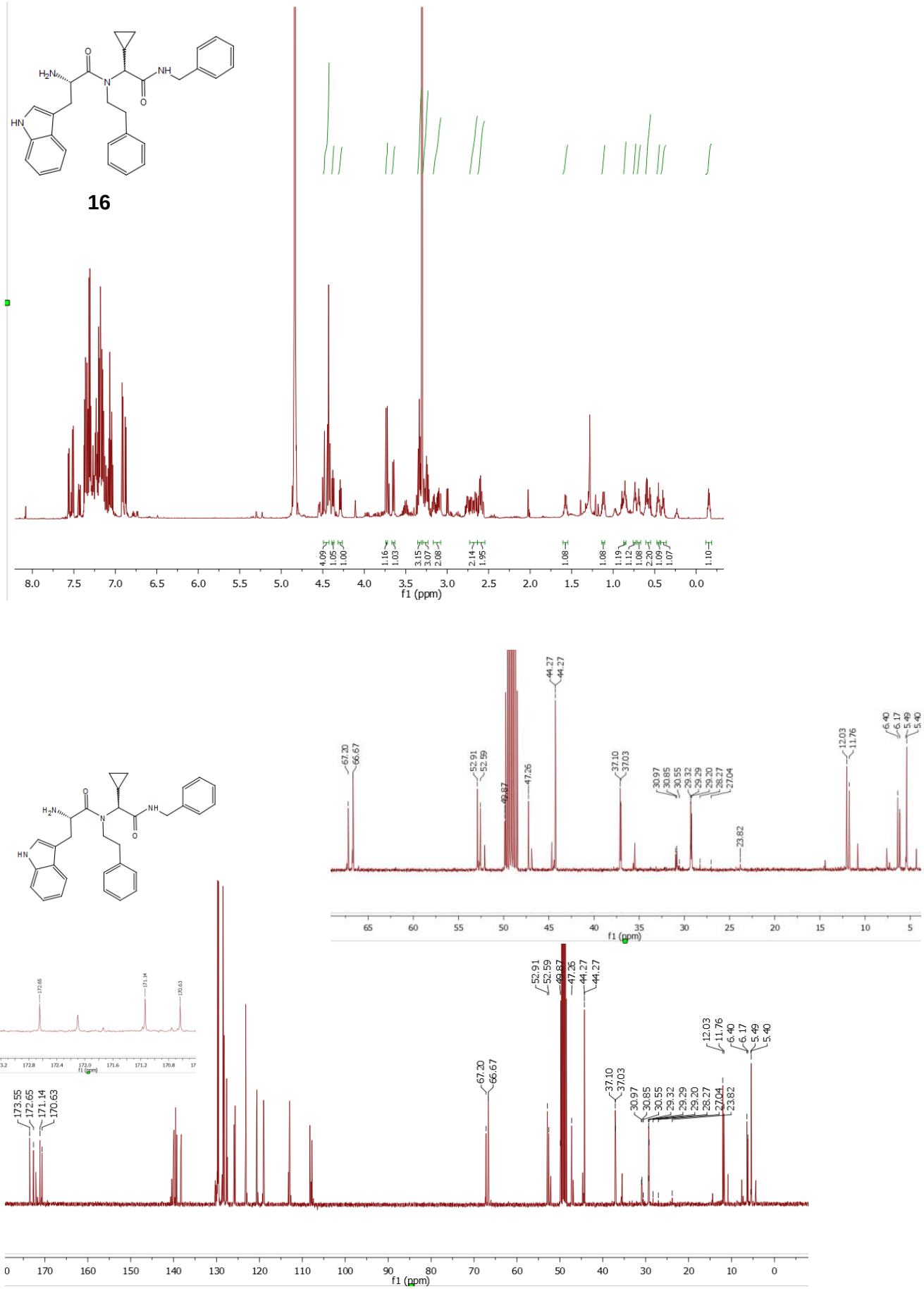

Figure S68: ^{1}H-, ^{13}C-NMR spectra of compound **16** and assignment for the major diastereoisomers.

Compound 17

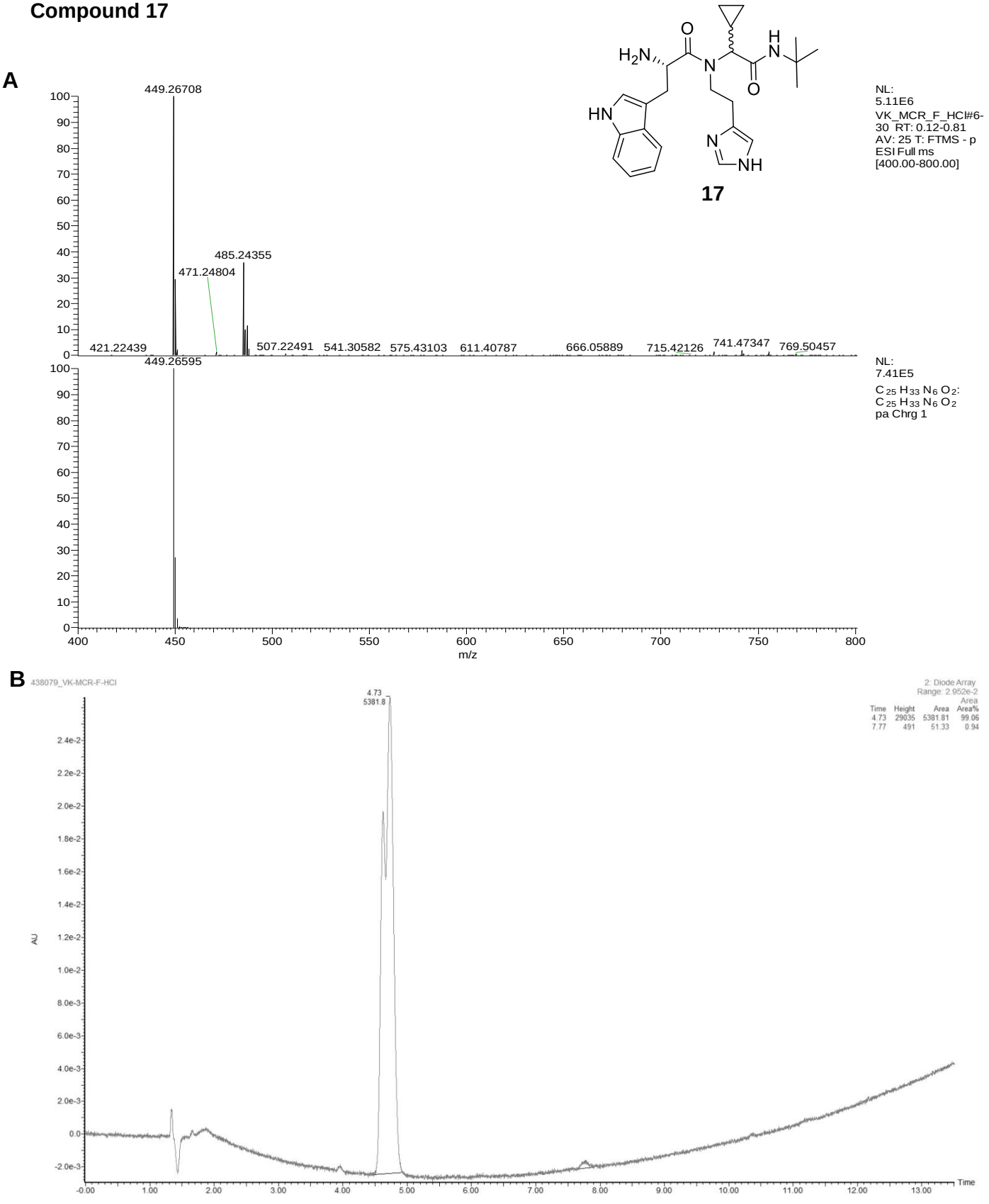

Figure S69: (A) Mass spectrum (HR-MS); (B) UV chromatogram (LC-MS) of compound **17**.

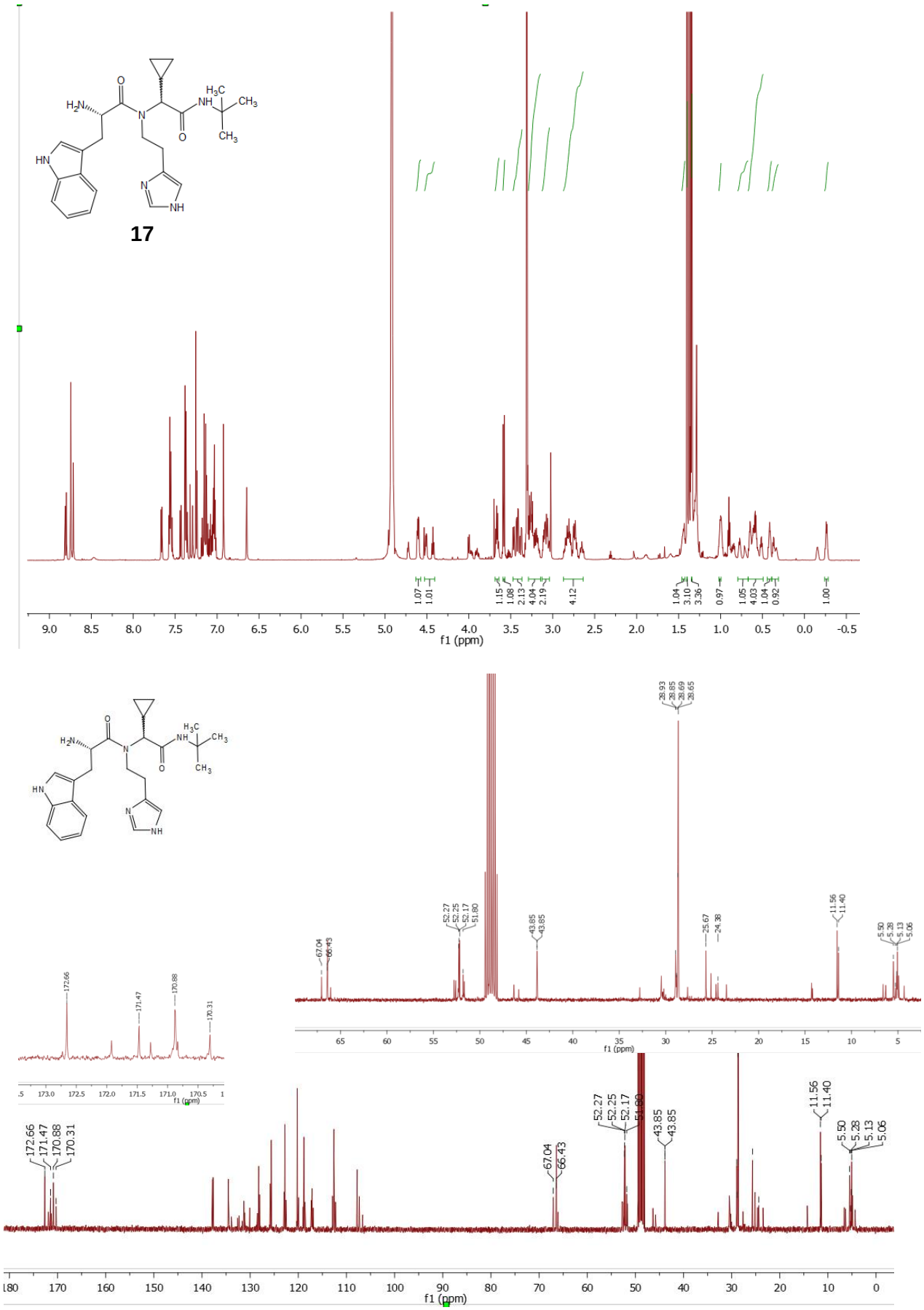

Figure S70: ^{1}H-, ^{13}C-NMR spectra of compound **17** and assignment for the major diastereoisomers.

Compound 18

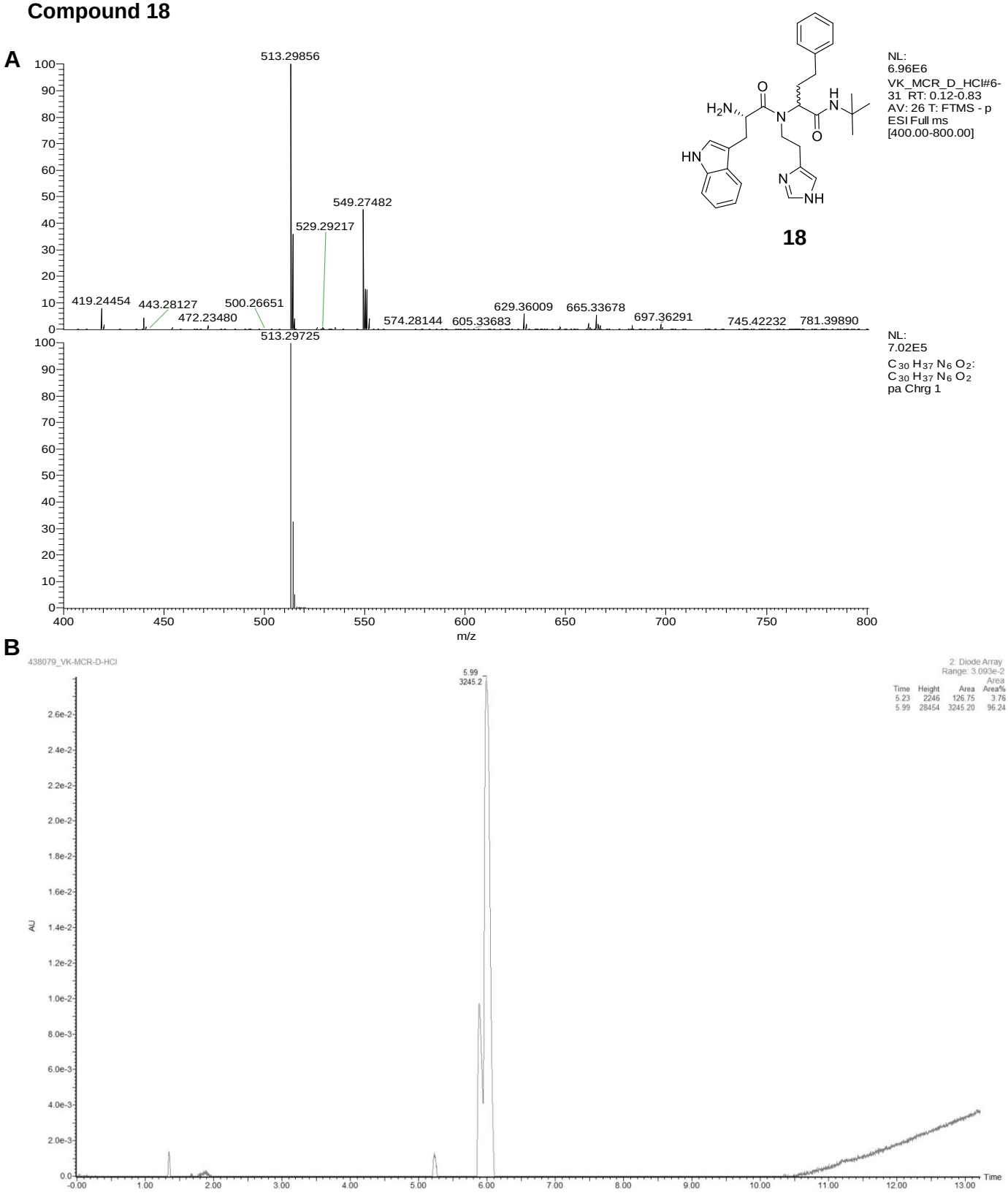

Figure S71: (A) Mass spectrum (HR-MS); (B) UV chromatogram (LC-MS) of compound **18**.

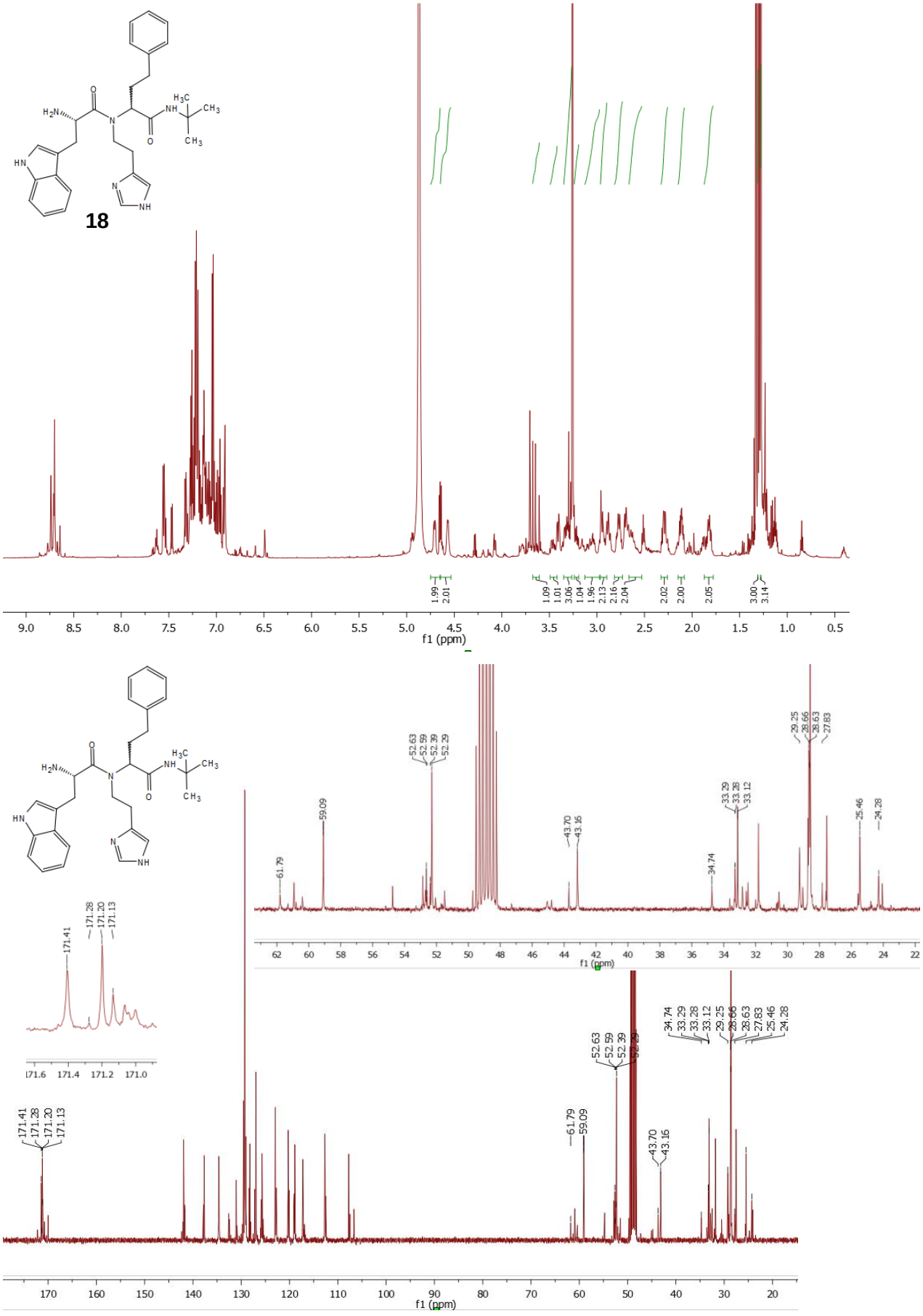

Figure S72: ^{1}H-, ^{13}C-NMR spectra of compound **18** and assignment for the major diastereoisomers.

Compound 19

A

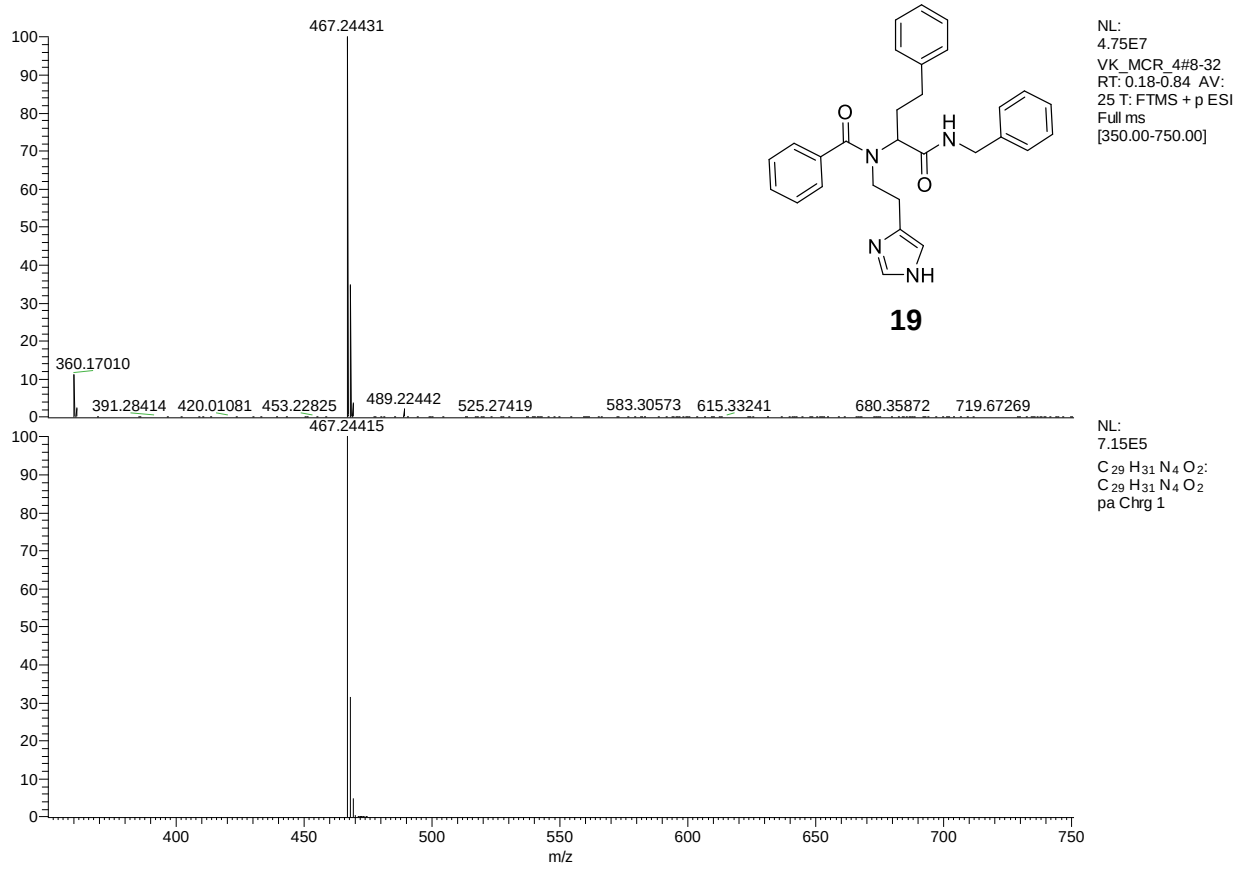

19

B

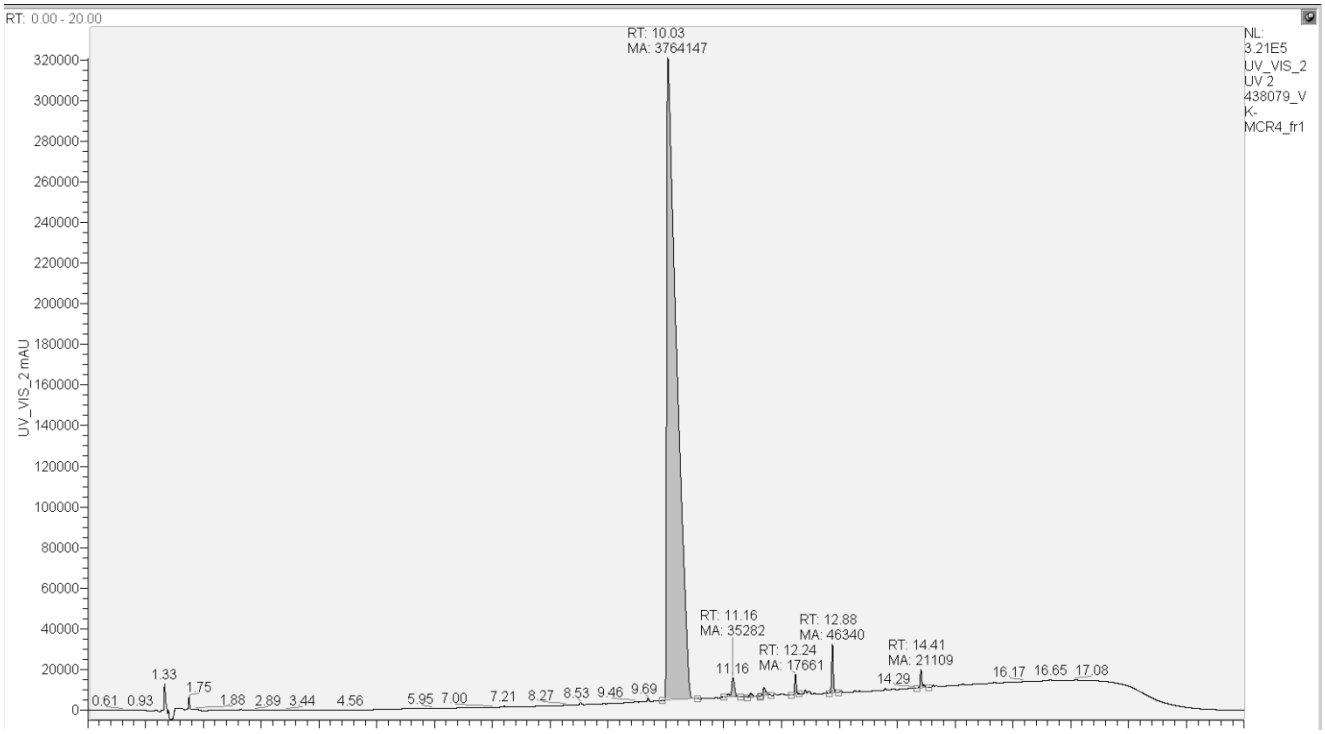

Figure S73: (A) Mass spectrum (HR-MS); (B) UV chromatogram (LC-MS) of compound **19**.

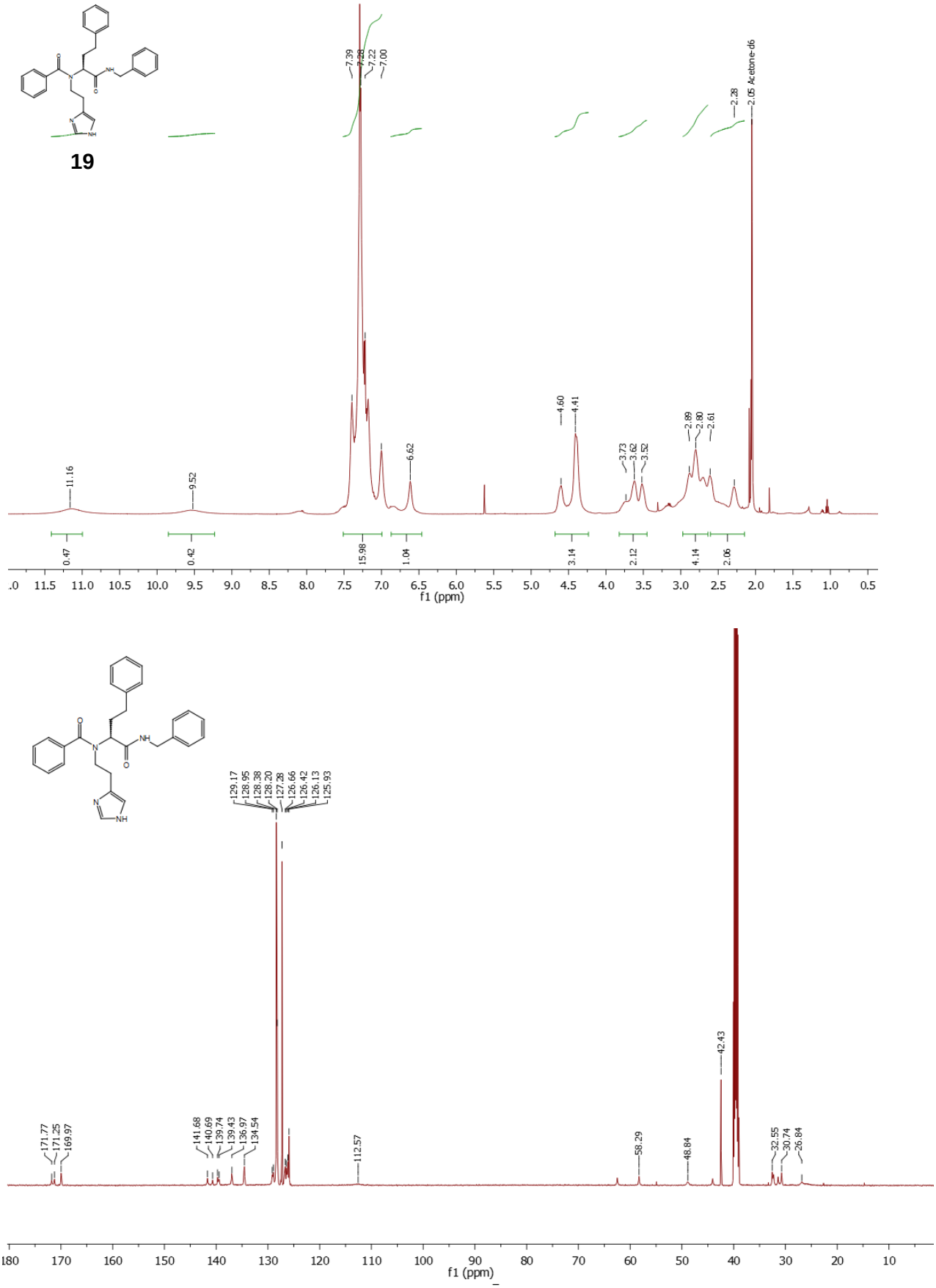

Figure S74: ^{1}H-, ^{13}C-NMR spectra of compound **19.**

Compound 25

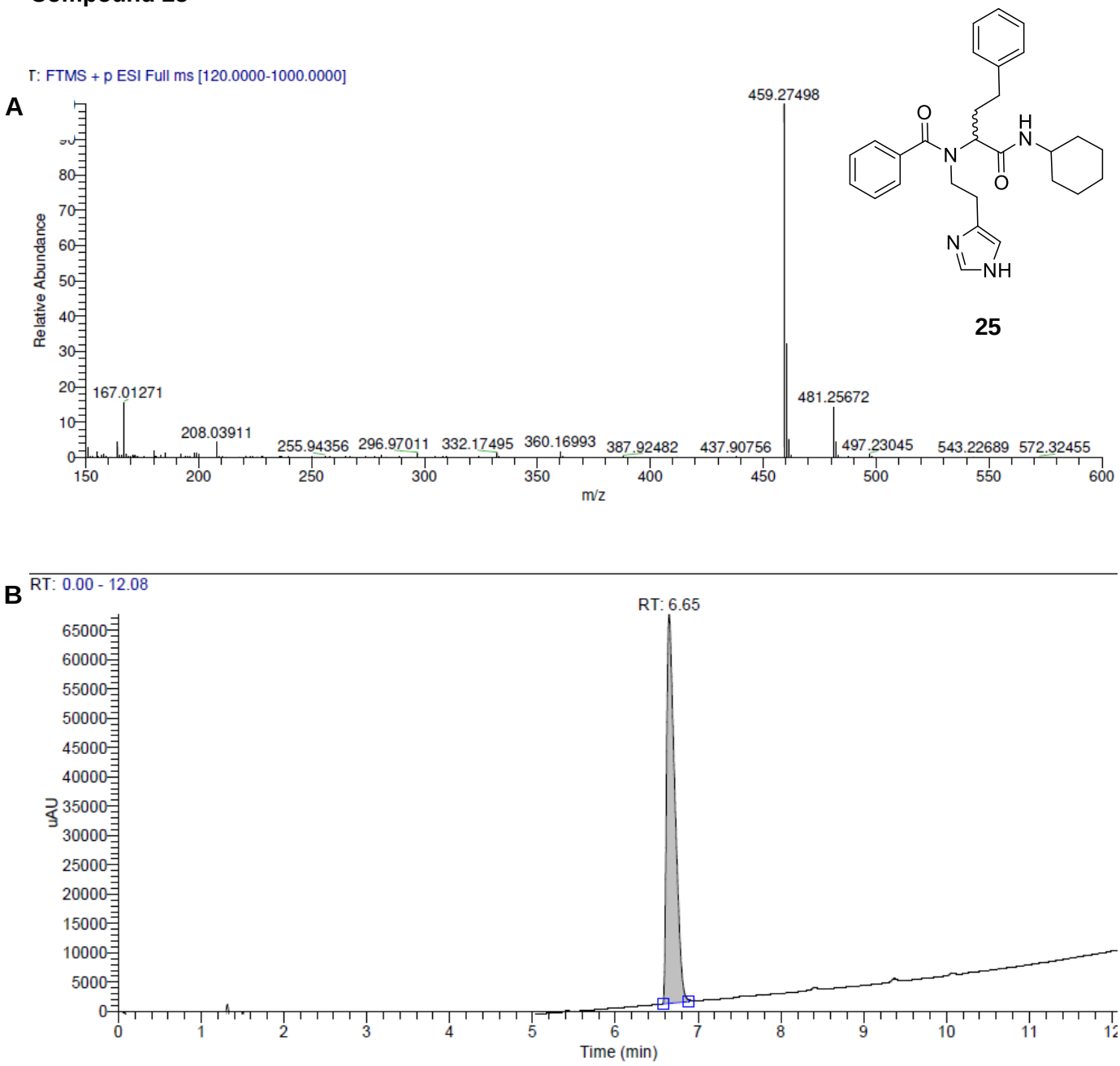

Figure S75: (A) Mass spectrum (HR-MS); (B) UV chromatogram (LC-MS) of compound **25**.

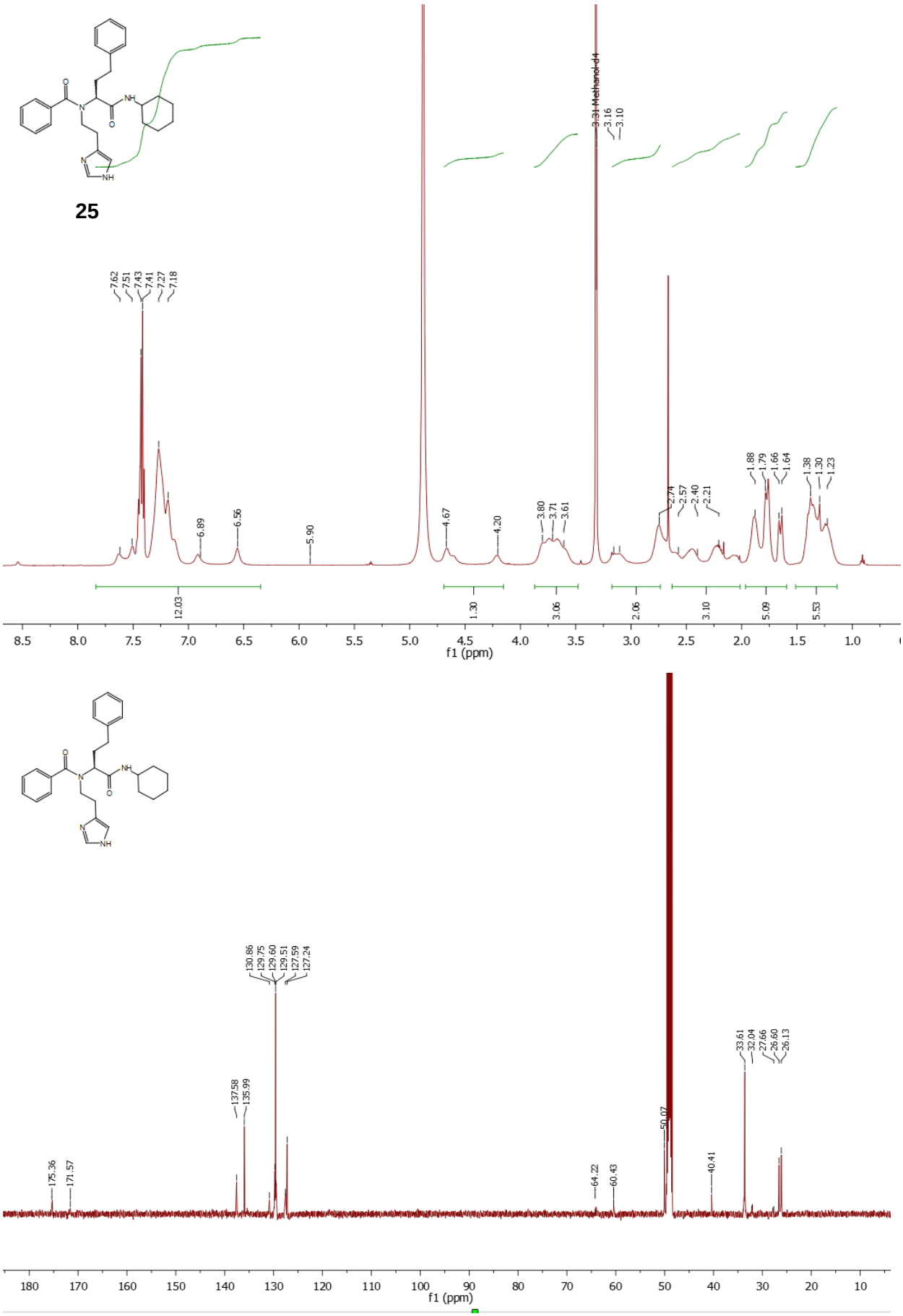

Figure S76: ^{1}H-, ^{13}C-NMR spectra of compound **25**.

Compound 26

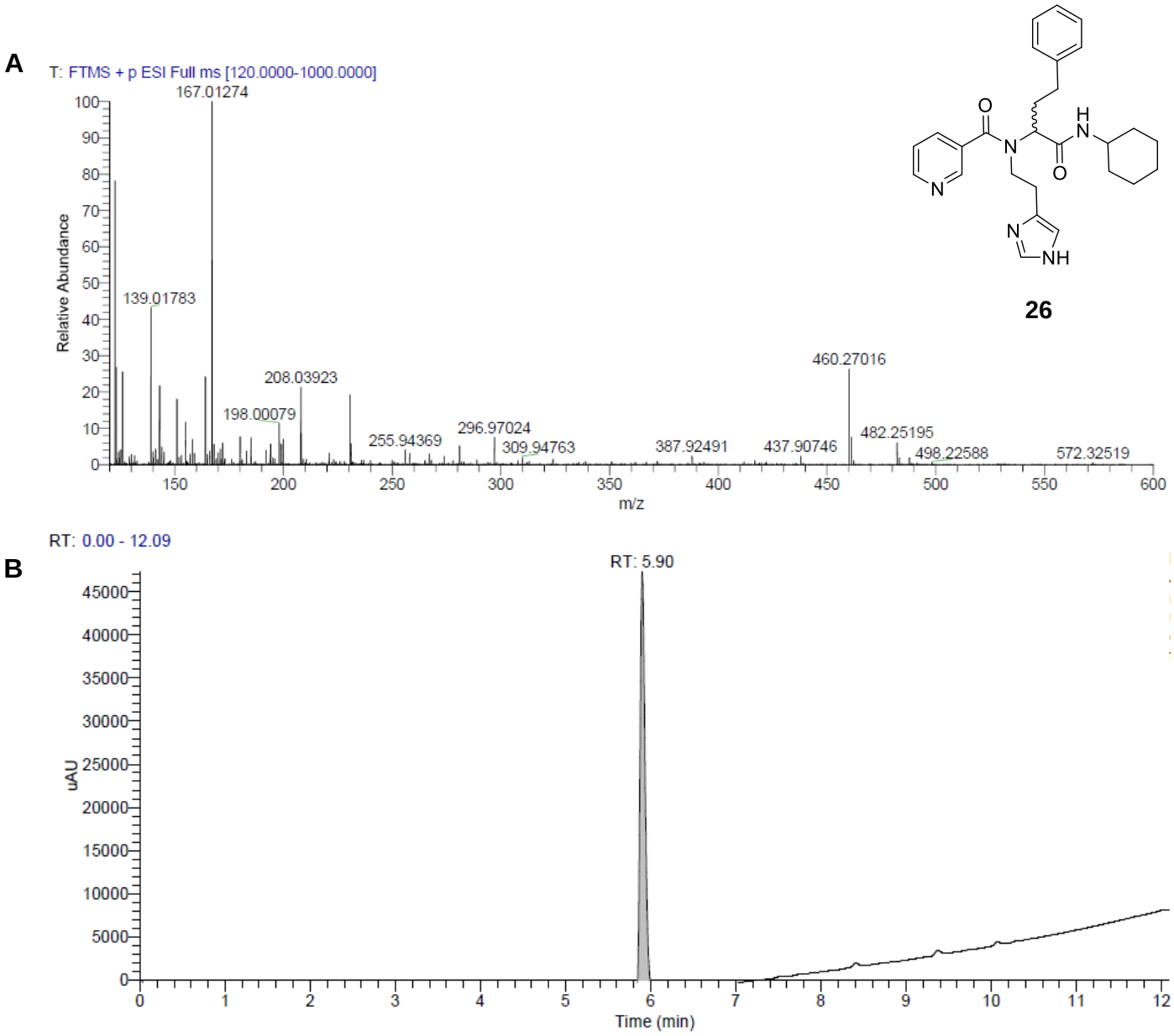

Figure S77: (A) Mass spectrum (HR-MS); (B) UV chromatogram (LC-MS) of compound **26**.

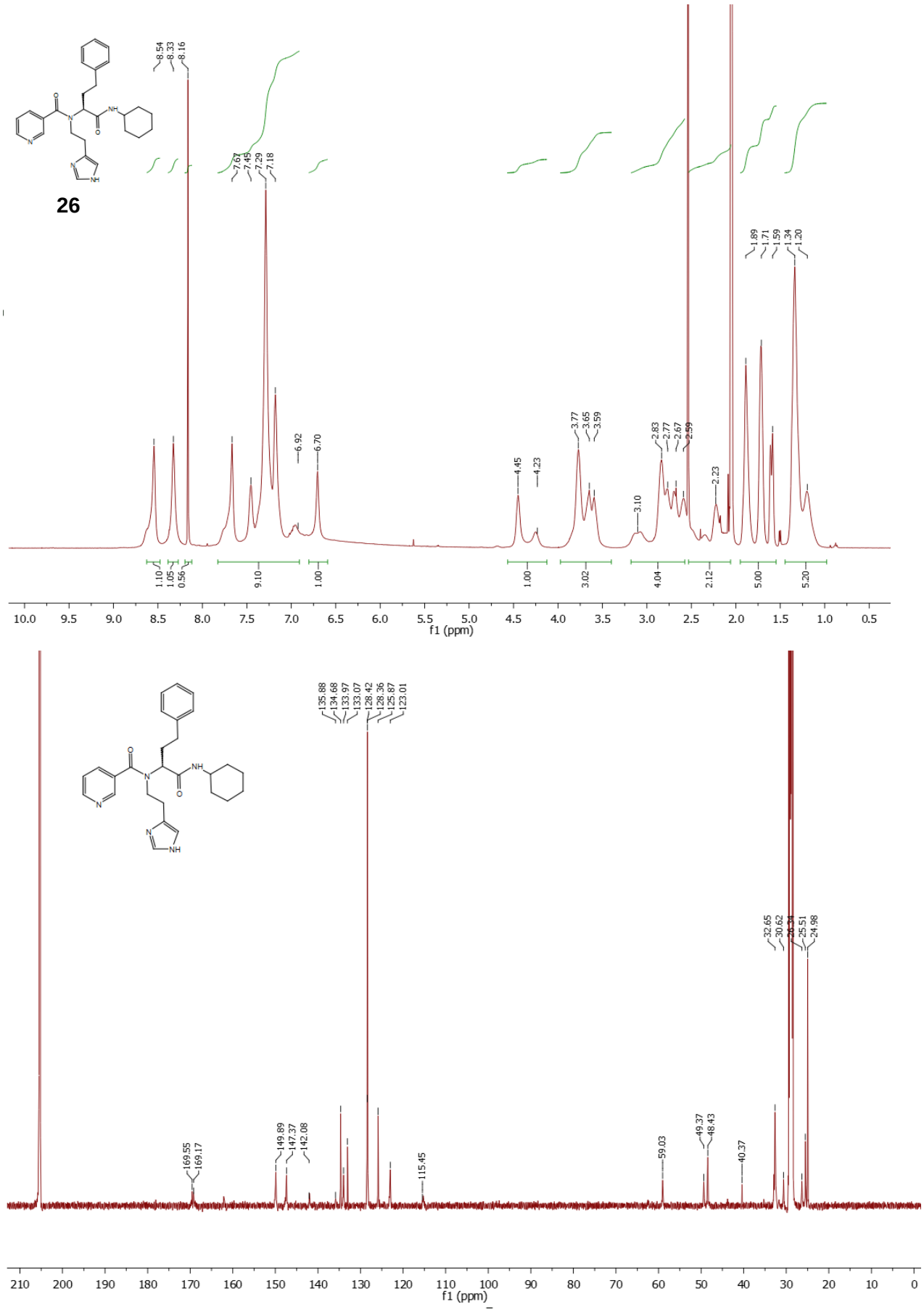

Figure S78: ^{1}H-, ^{13}C-NMR spectra of compound **26.**

Compound 27

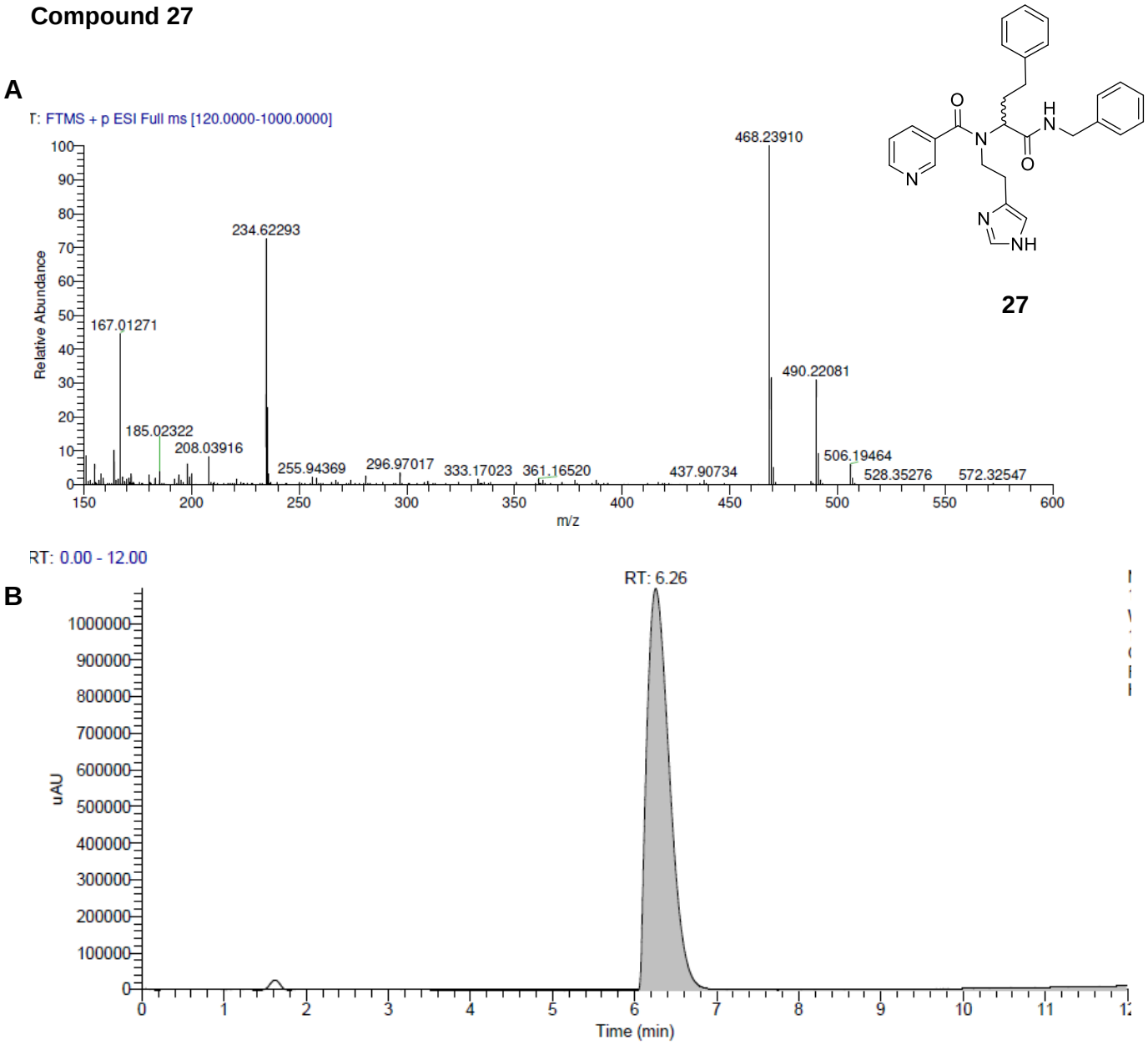

Figure S79: (A) Mass spectrum (HR-MS); (B) UV chromatogram (LC-MS) of compound **27**.

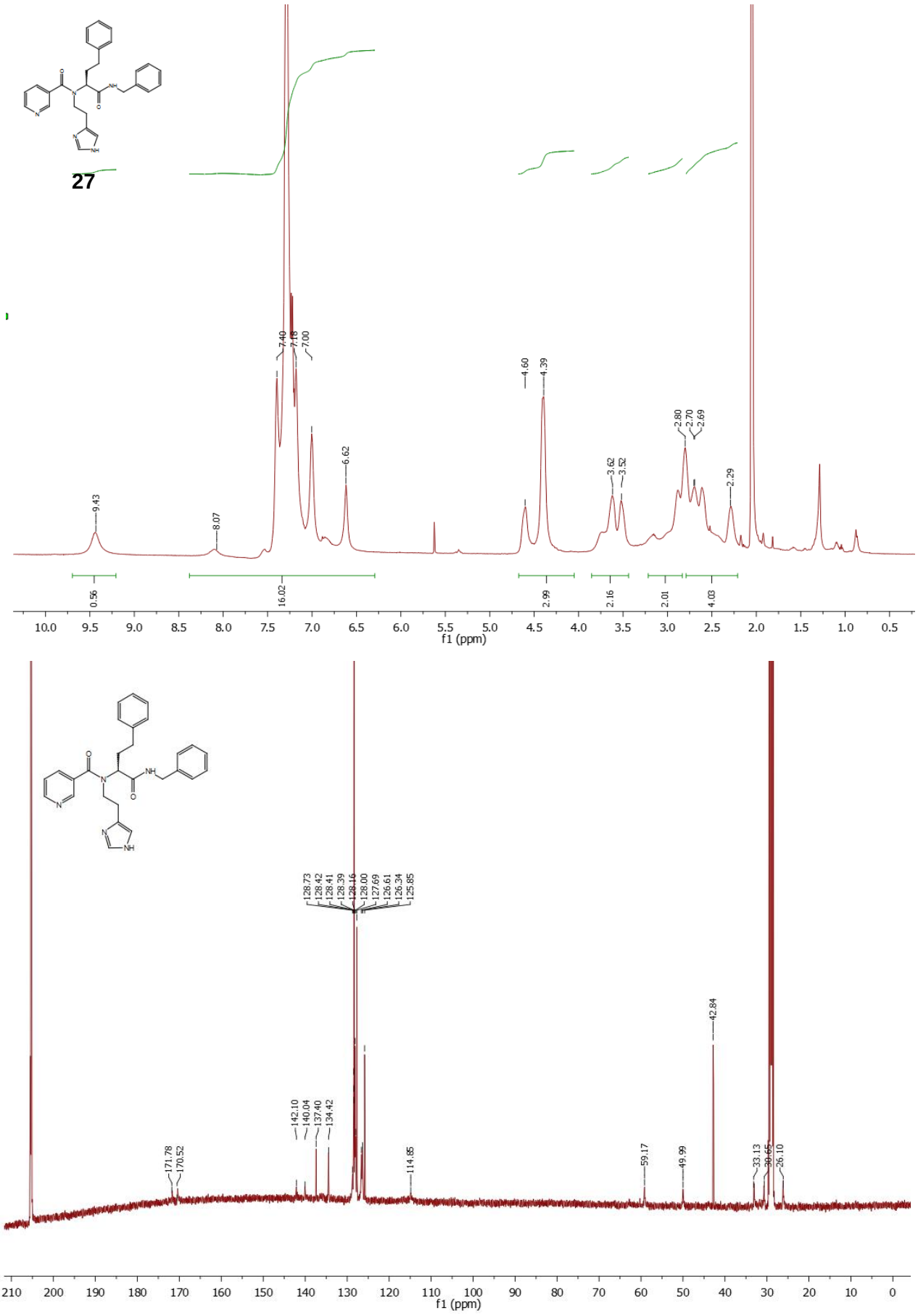

Figure S80: ^{1}H-, ^{13}C-NMR spectra of compound **27**.

Compound 28

A

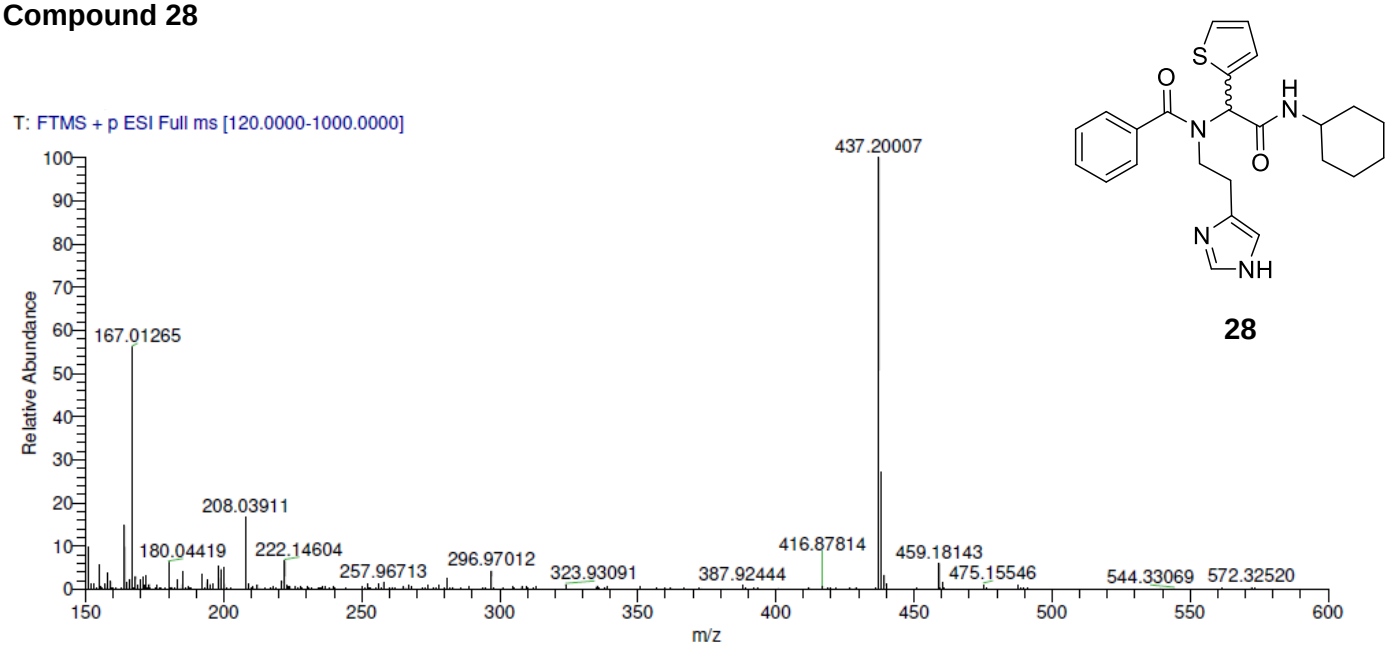

B

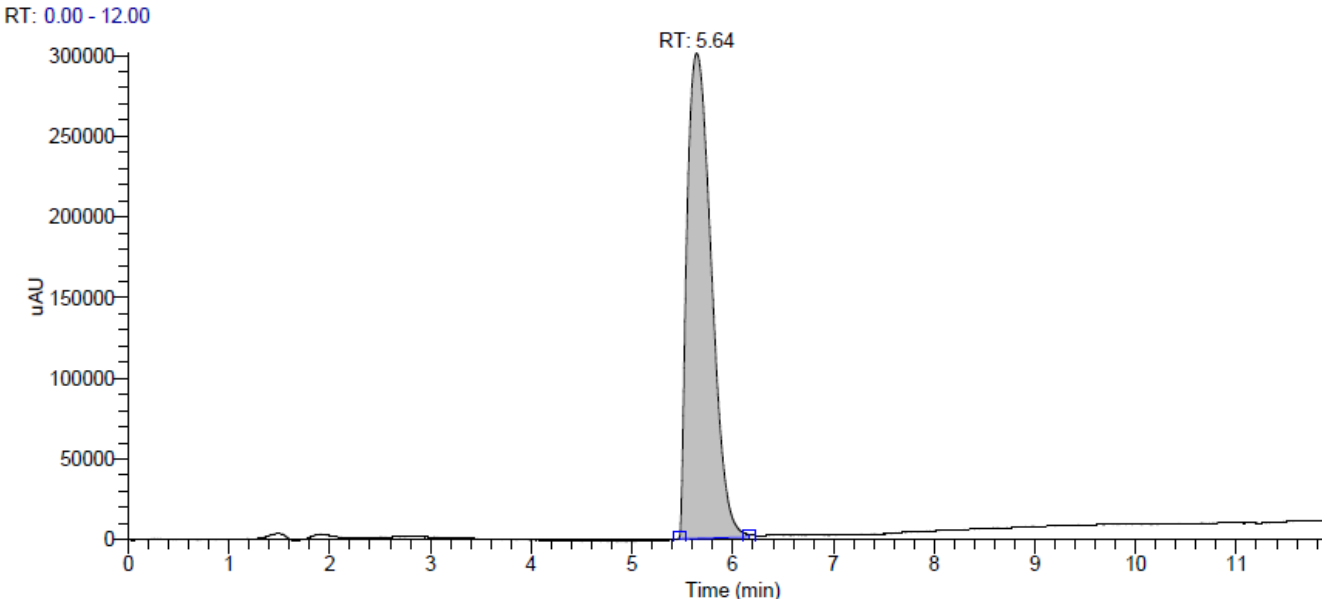

Figure S81: (A) Mass spectrum (HR-MS); (B) UV chromatogram (LC-MS) of compound **28.**

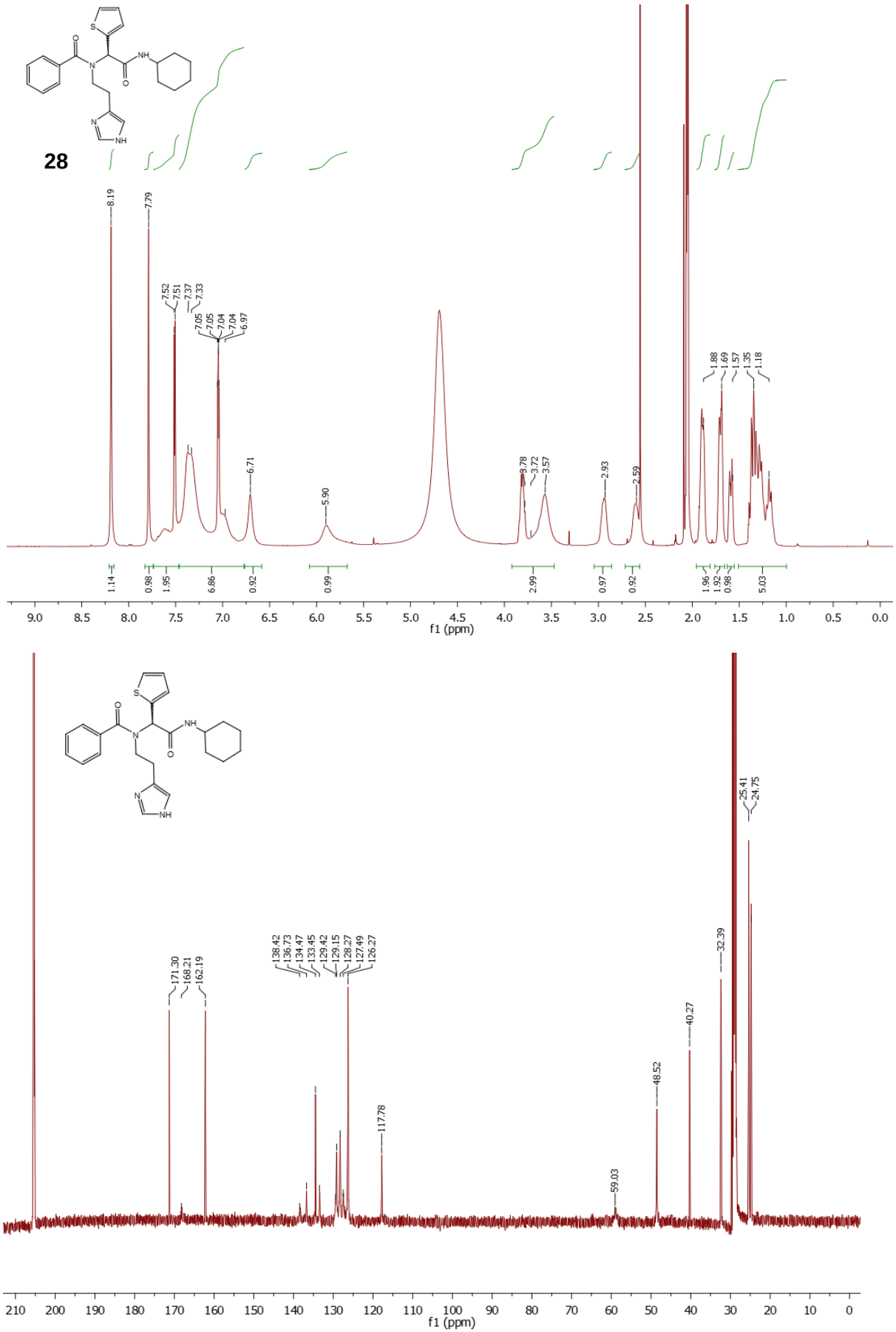

Figure S82: ^{1}H-, ^{13}C-NMR spectra of compound **28**.

Compound 29

A

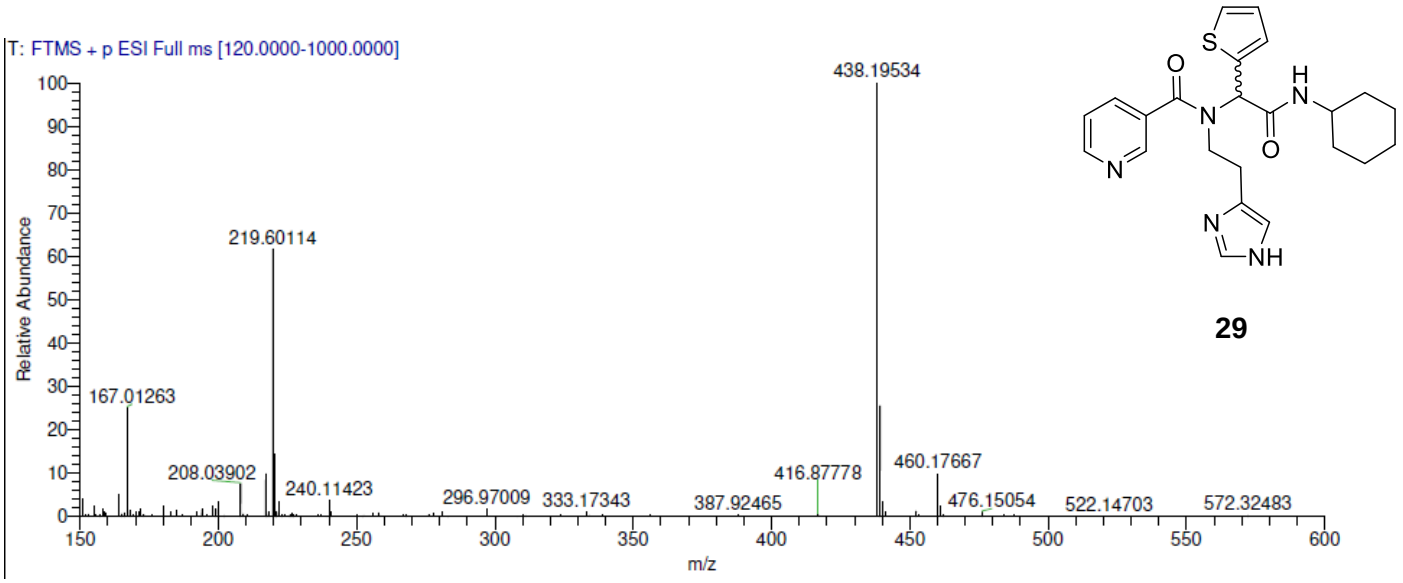

B

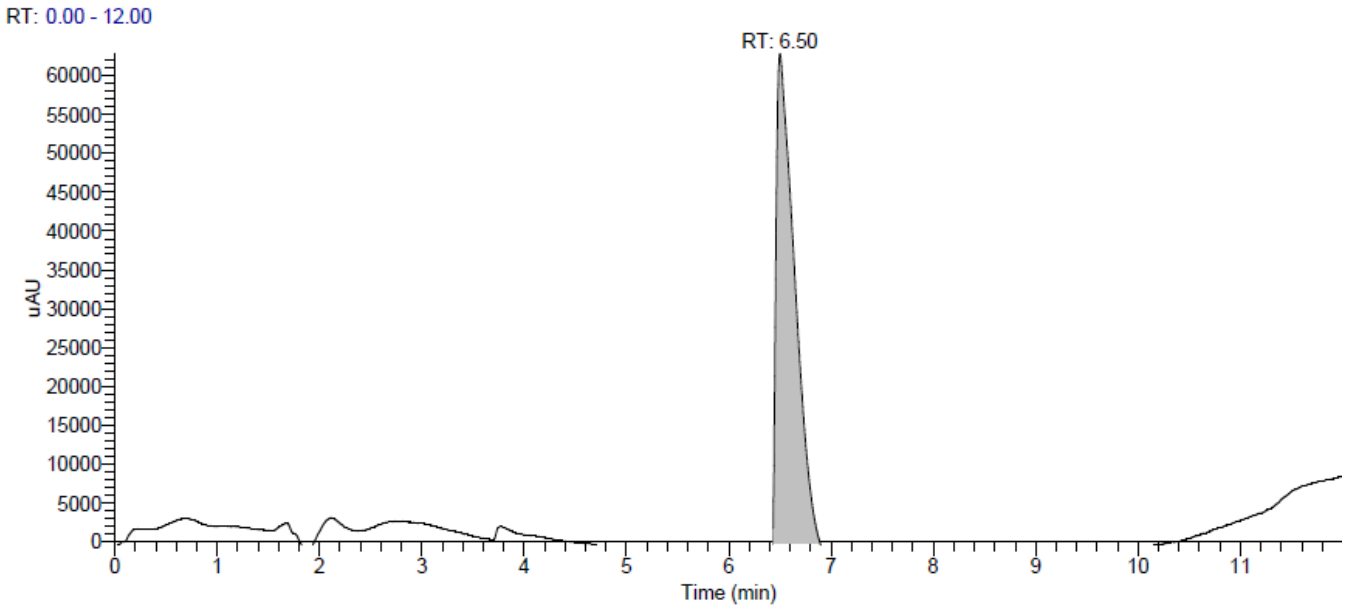

Figure S83: (A) Mass spectrum (HR-MS); (B) UV chromatogram (LC-MS) of compound **29.**

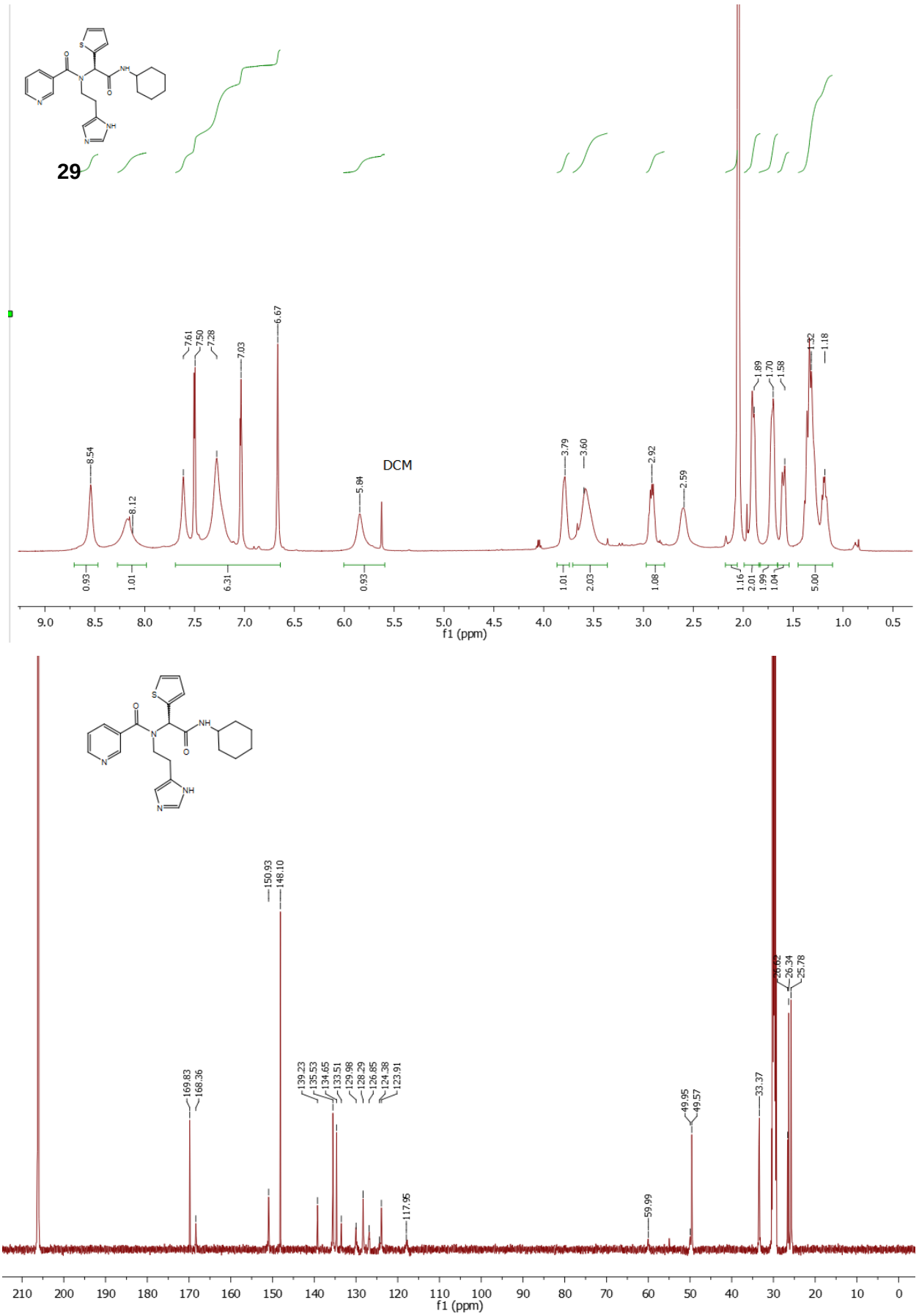

Figure S84: ^{1}H-, ^{13}C-NMR spectra of compound **29**.

Compound 30

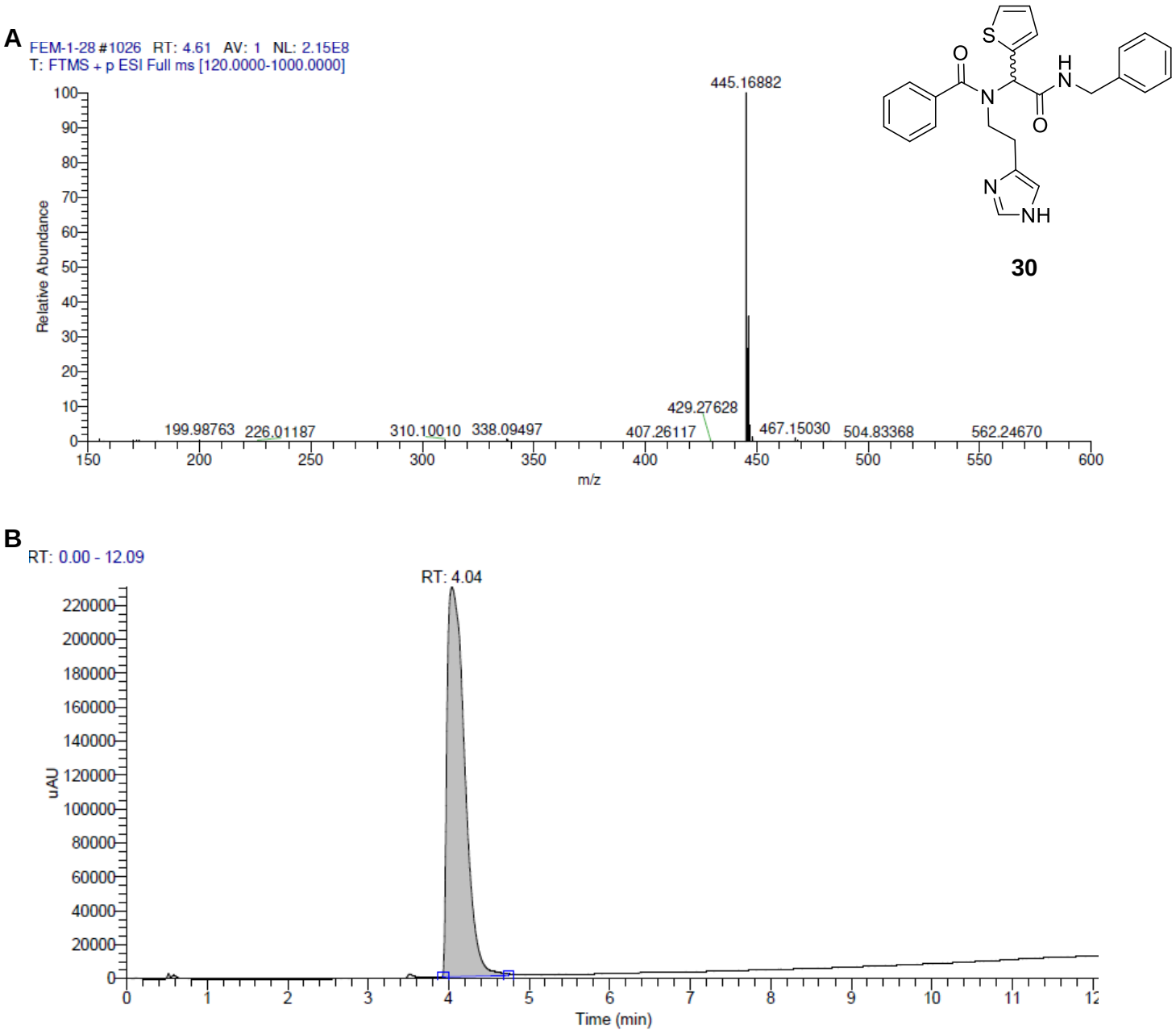

Figure S85: (A) Mass spectrum (HR-MS); (B) UV chromatogram (LC-MS) of compound **30.**

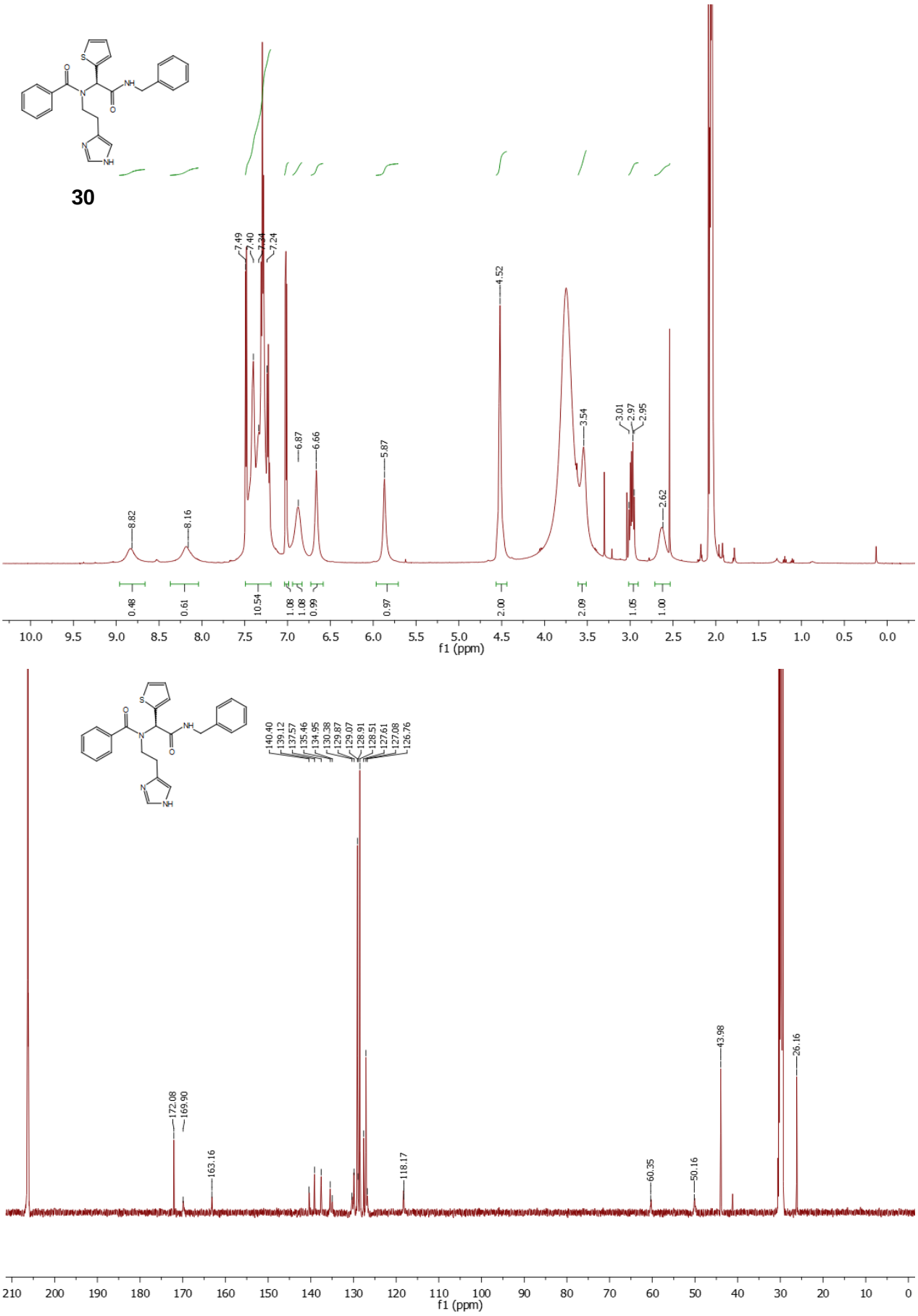

Figure S86: ^{1}H-, ^{13}C-NMR spectra of compound **30**.

Compound 31

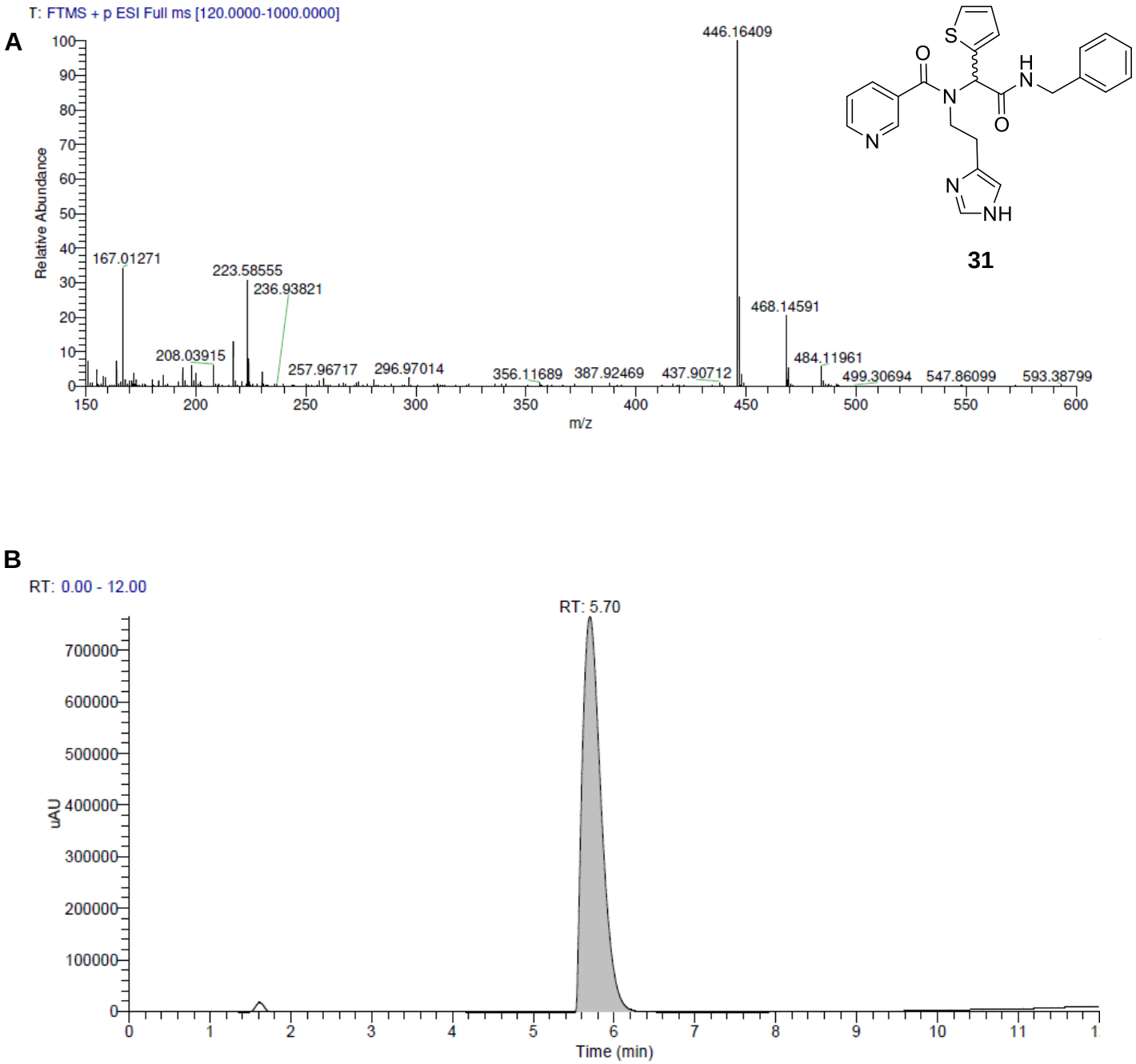

Figure S87: (A) Mass spectrum (HR-MS); (B) UV chromatogram (LC-MS) of compound **31.**

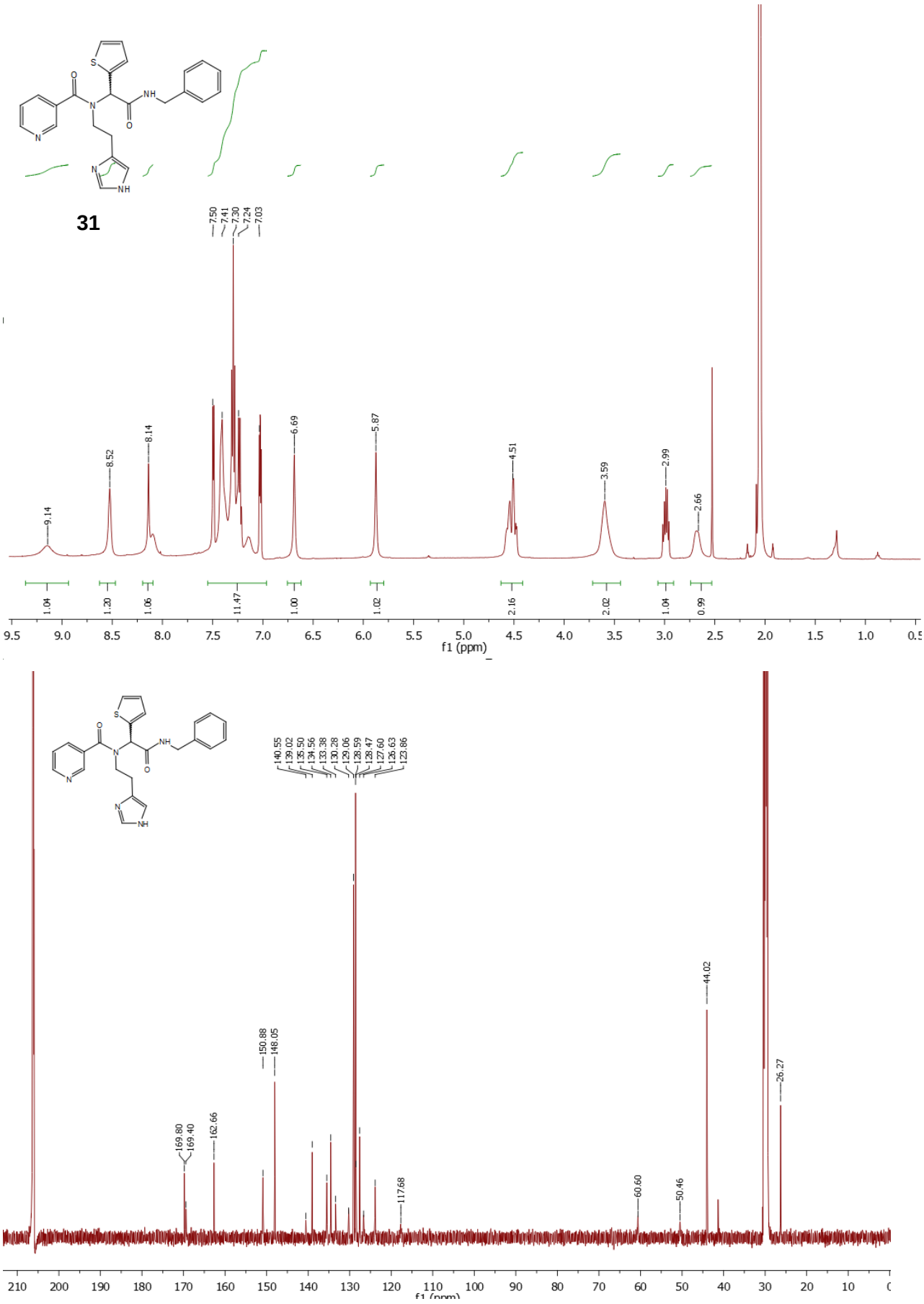

Figure S88: ^{1}H-, ^{13}C-NMR spectra of compound **31**.

Compound 32

A

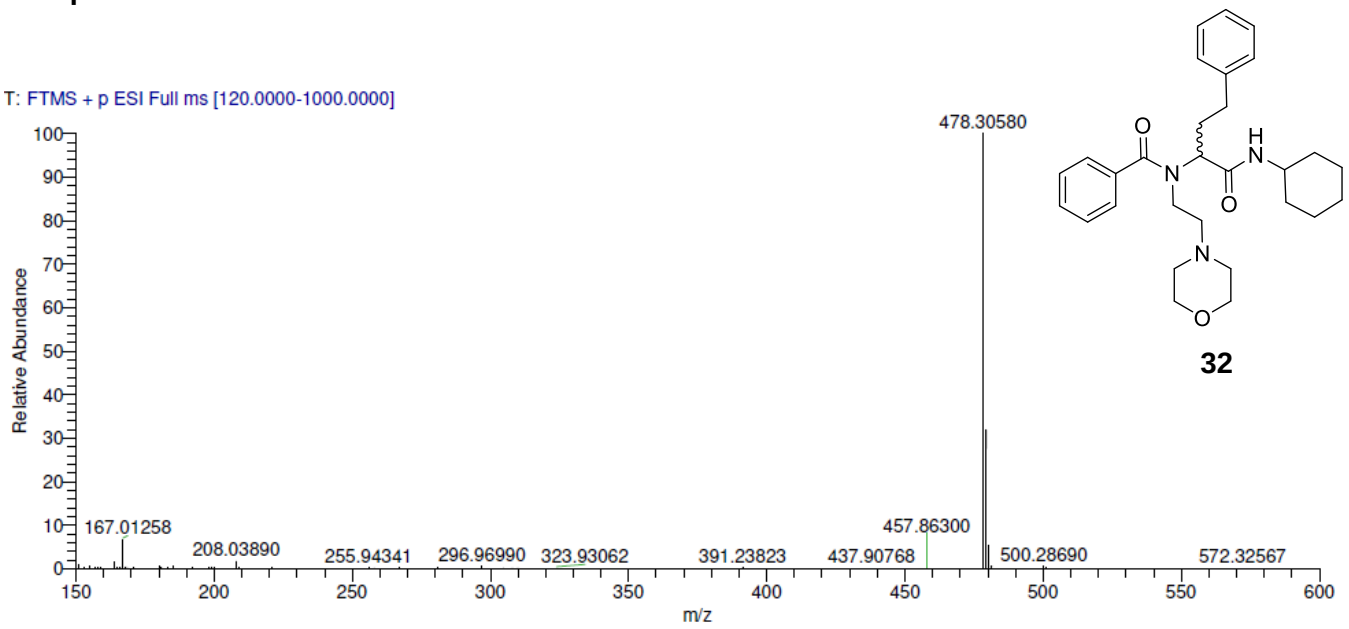

B

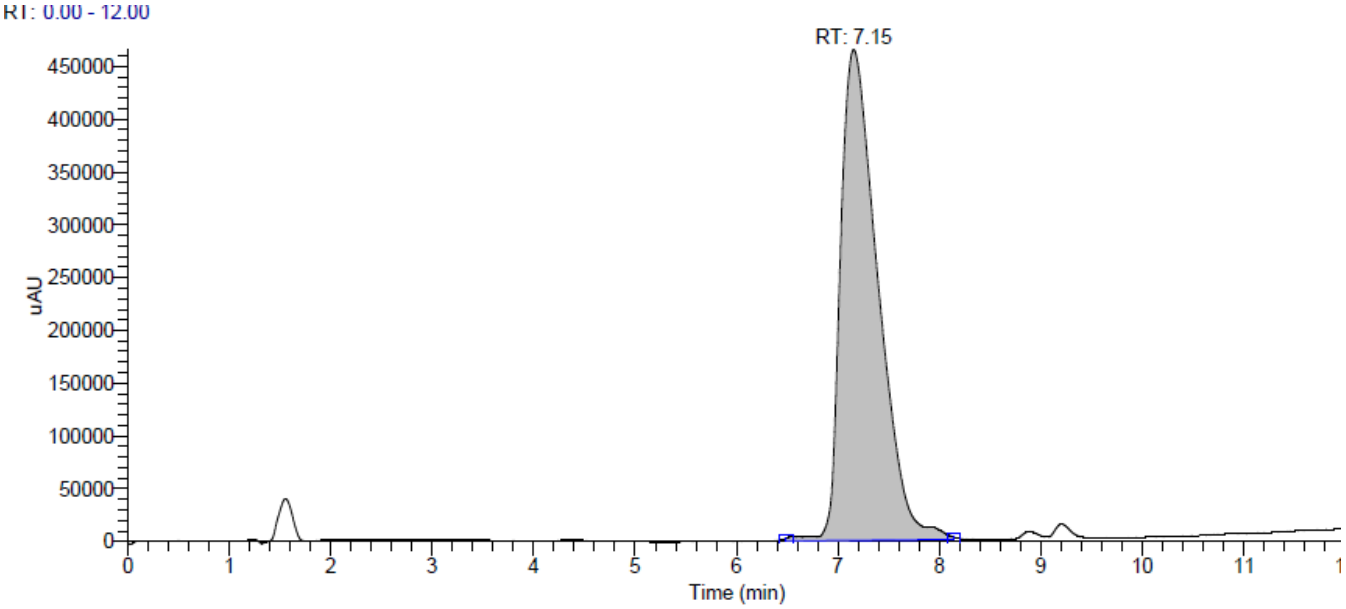

Figure S89: (A) Mass spectrum (HR-MS); (B) UV chromatogram (LC-MS) of compound **32.**

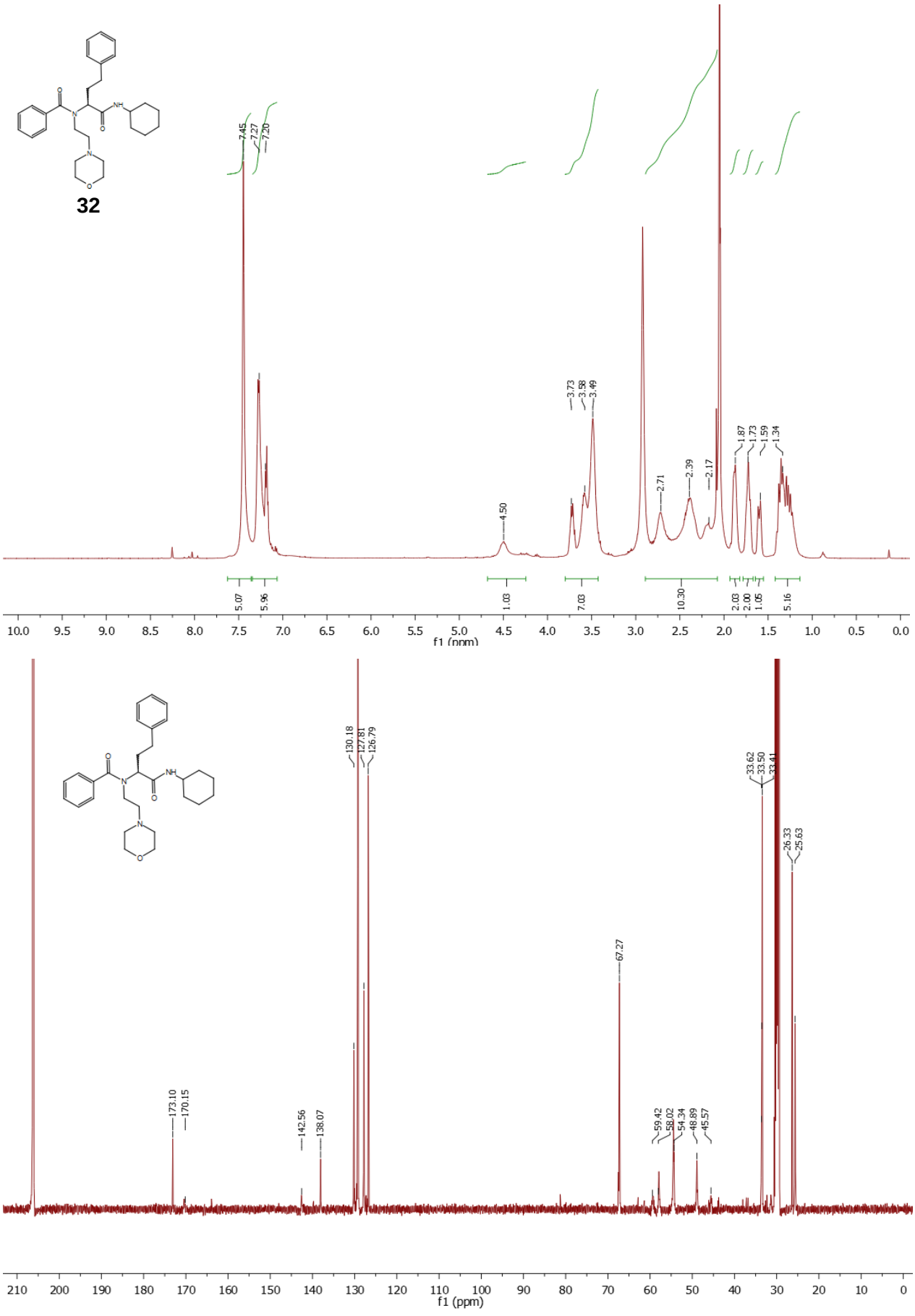

Figure S90: ^{1}H-, ^{13}C-NMR spectra of compound **32**.

Compound 33

A

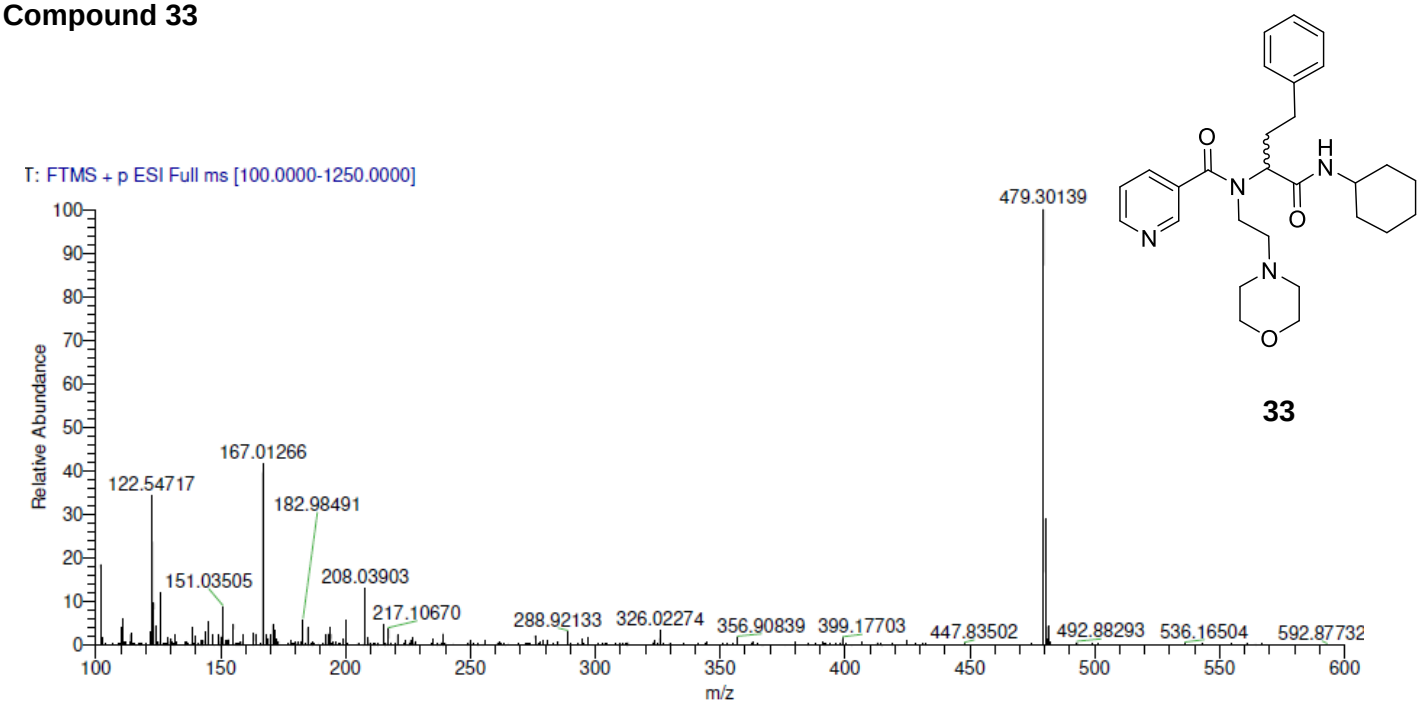

B

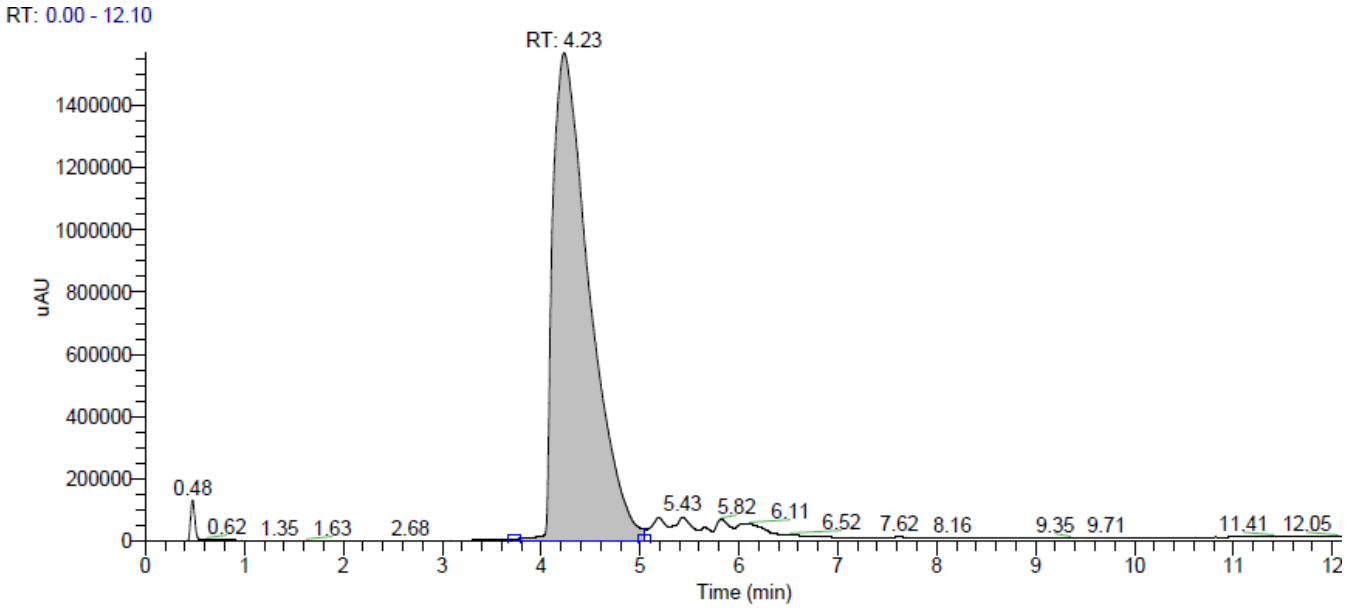

Figure S91: (A) Mass spectrum (HR-MS); (B) UV chromatogram (LC-MS) of compound **33.**

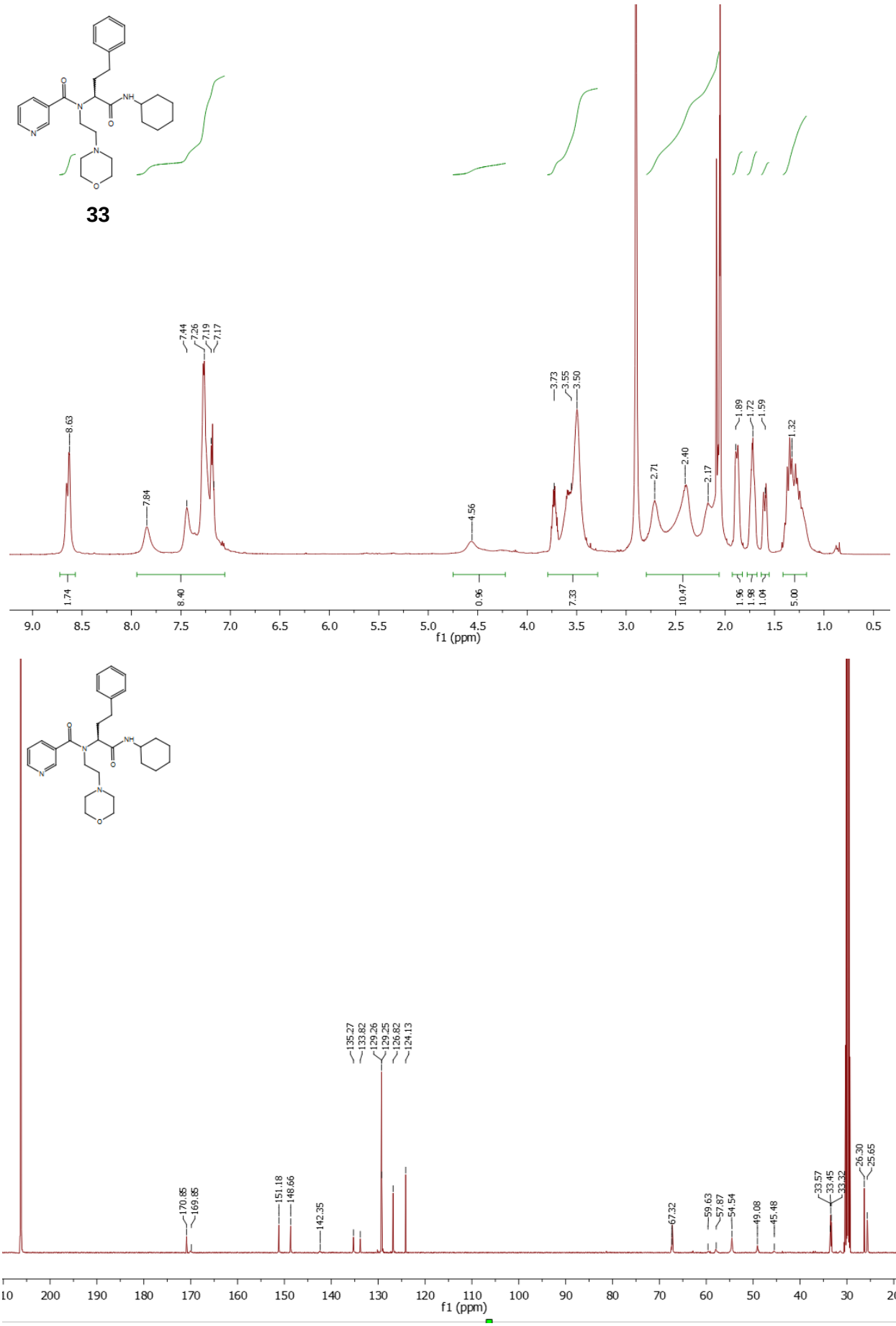

Figure S92: ^{1}H-, ^{13}C-NMR spectra of compound **33.**

Compound 34

A

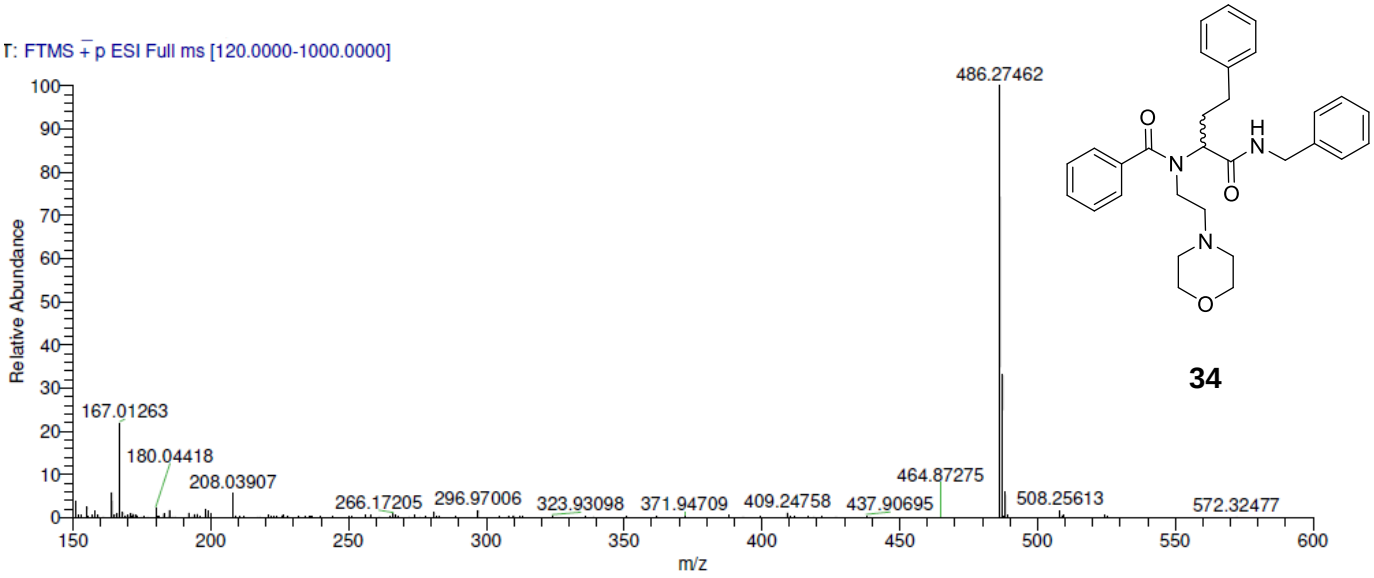

B

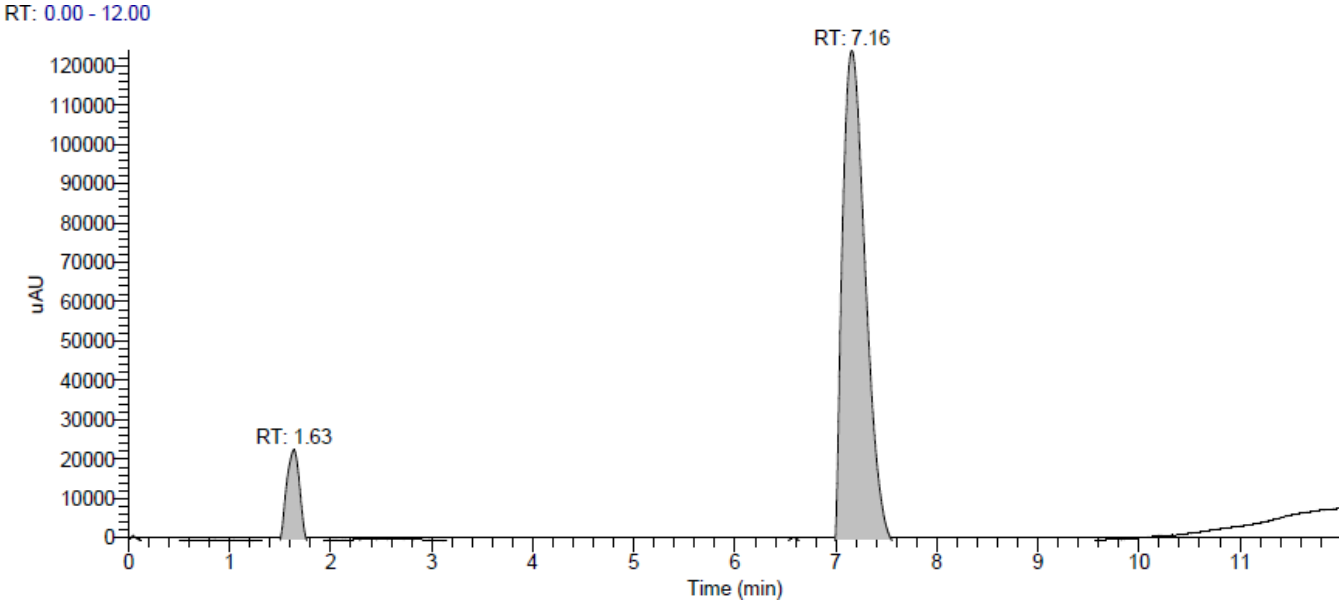

Figure S93: (A) Mass spectrum (HR-MS); (B) UV chromatogram (LC-MS) of compound **34**.

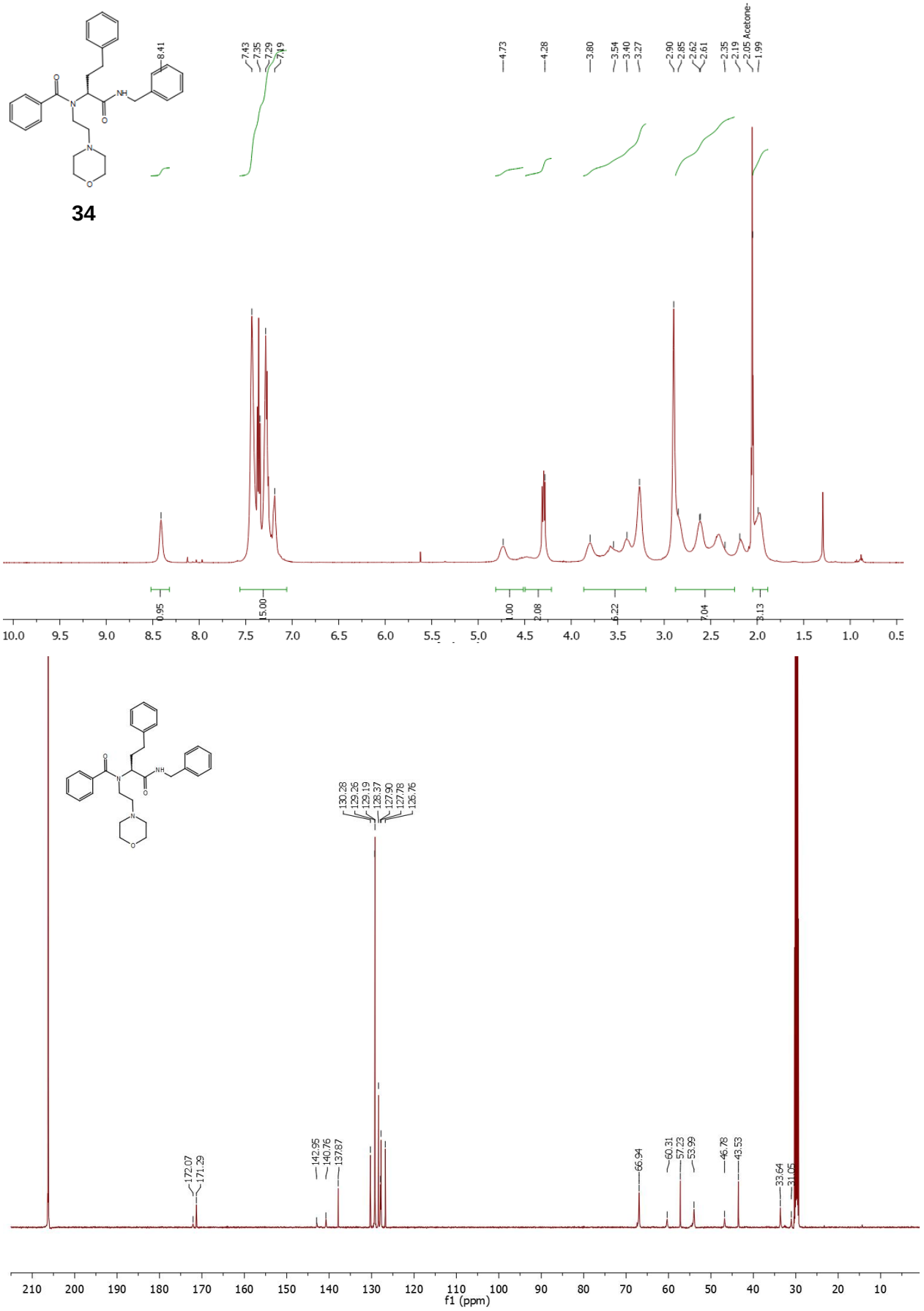

Figure S94: ^{1}H-, ^{13}C-NMR spectra of compound **34**.

Compound 35

A

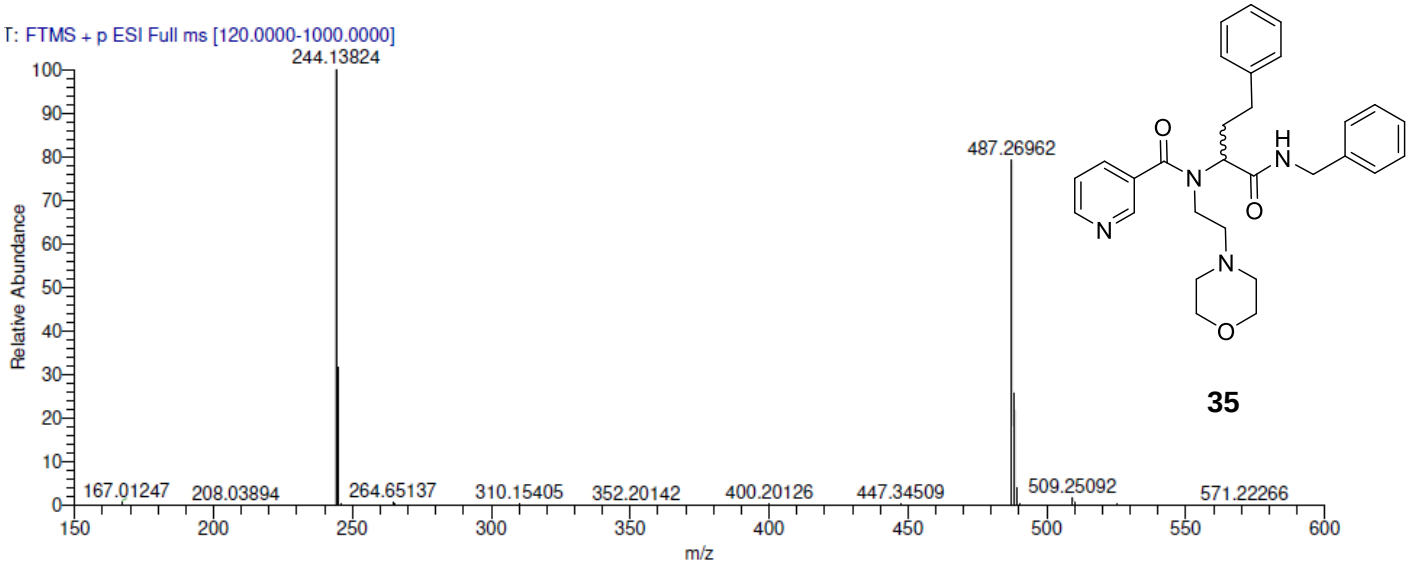

B

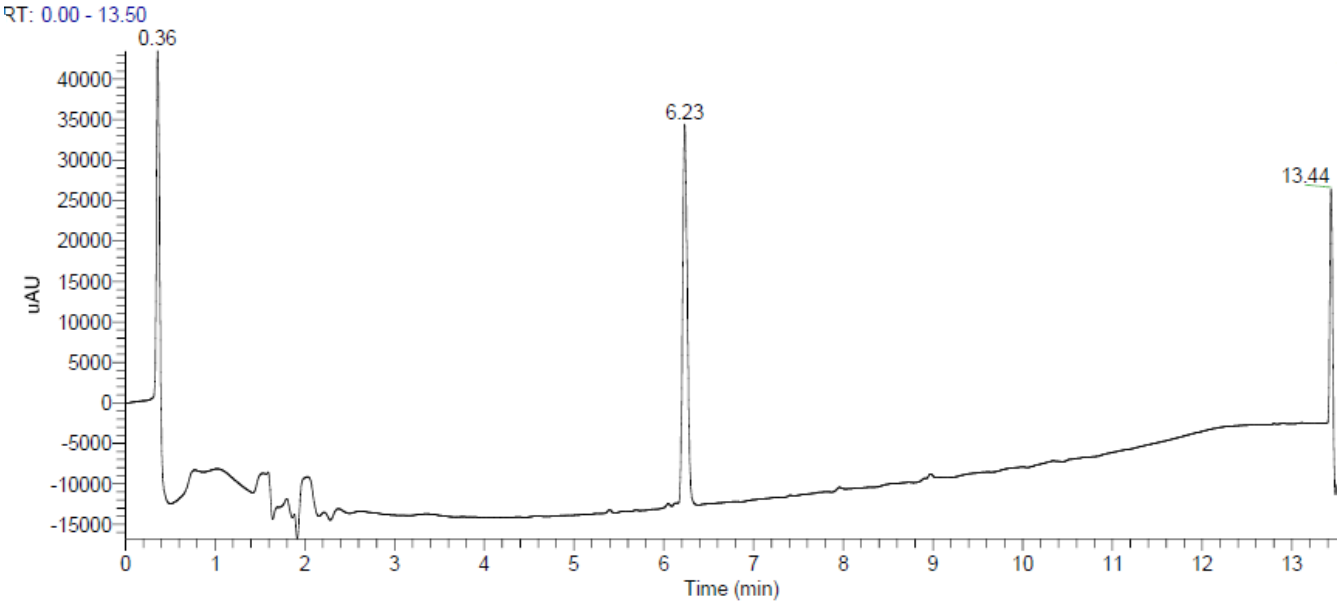

Figure S95: (A) Mass spectrum (HR-MS); (B) UV chromatogram (LC-MS) of compound **35.**

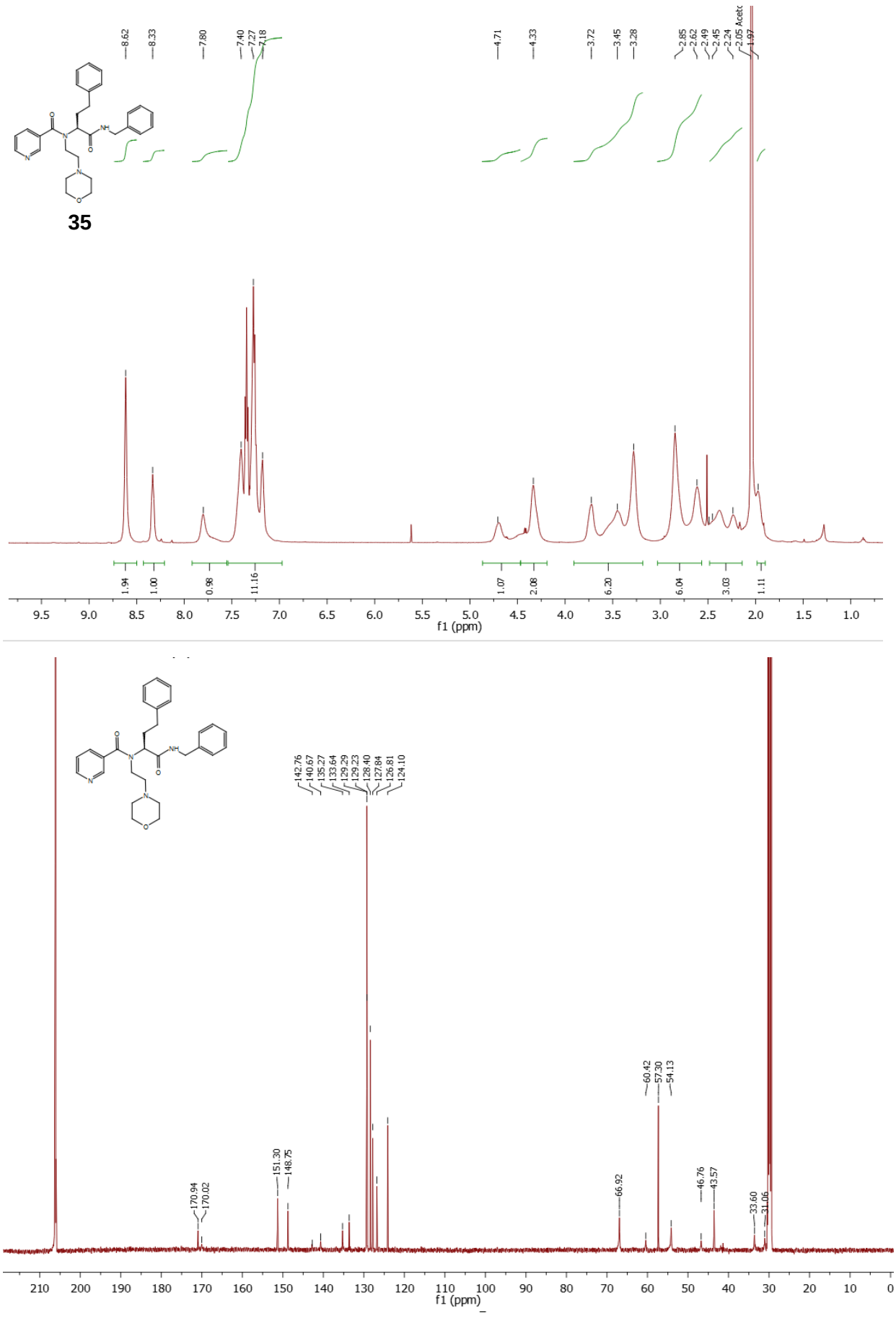

Figure S96: ^{1}H-, ^{13}C-NMR spectra of compound **35**.

Compound 36

A

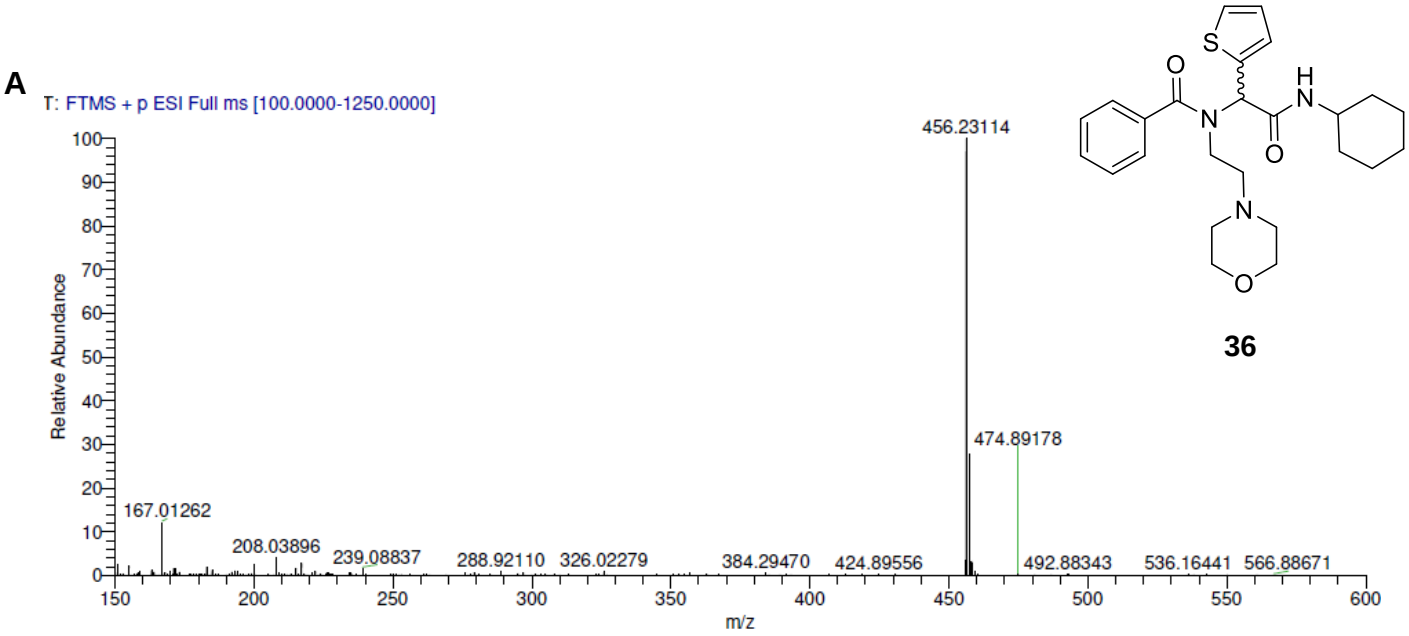

B

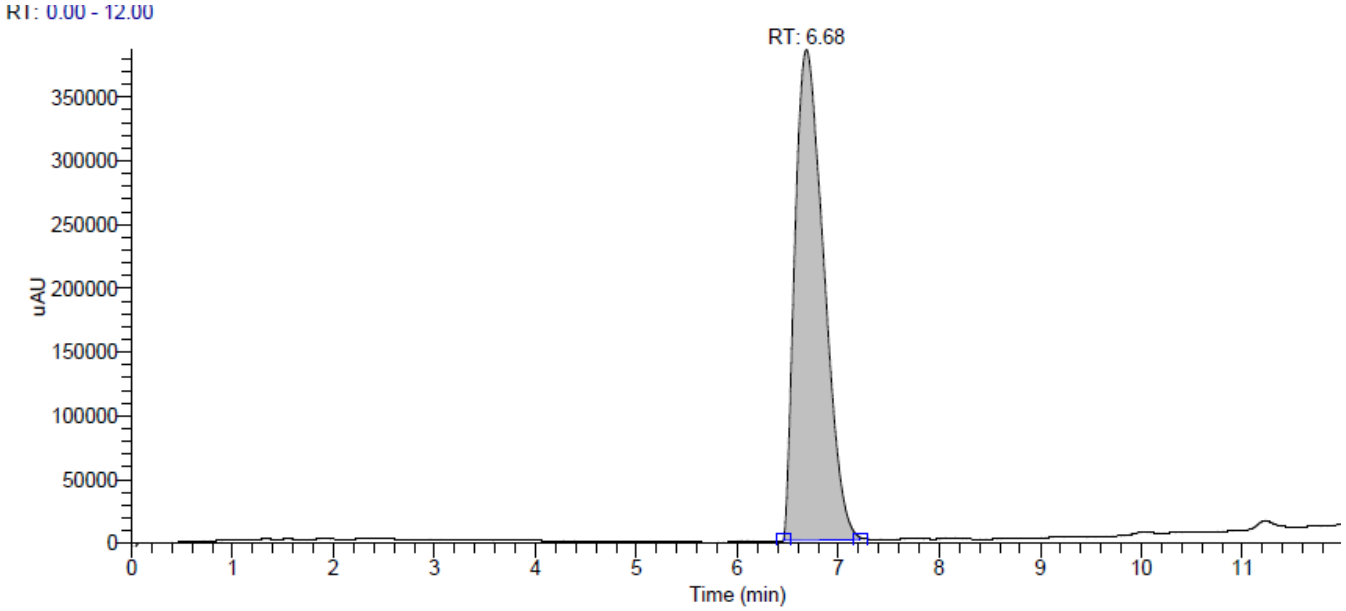

Figure S97: (A) Mass spectrum (HR-MS); (B) UV chromatogram (LC-MS) of compound **36.**

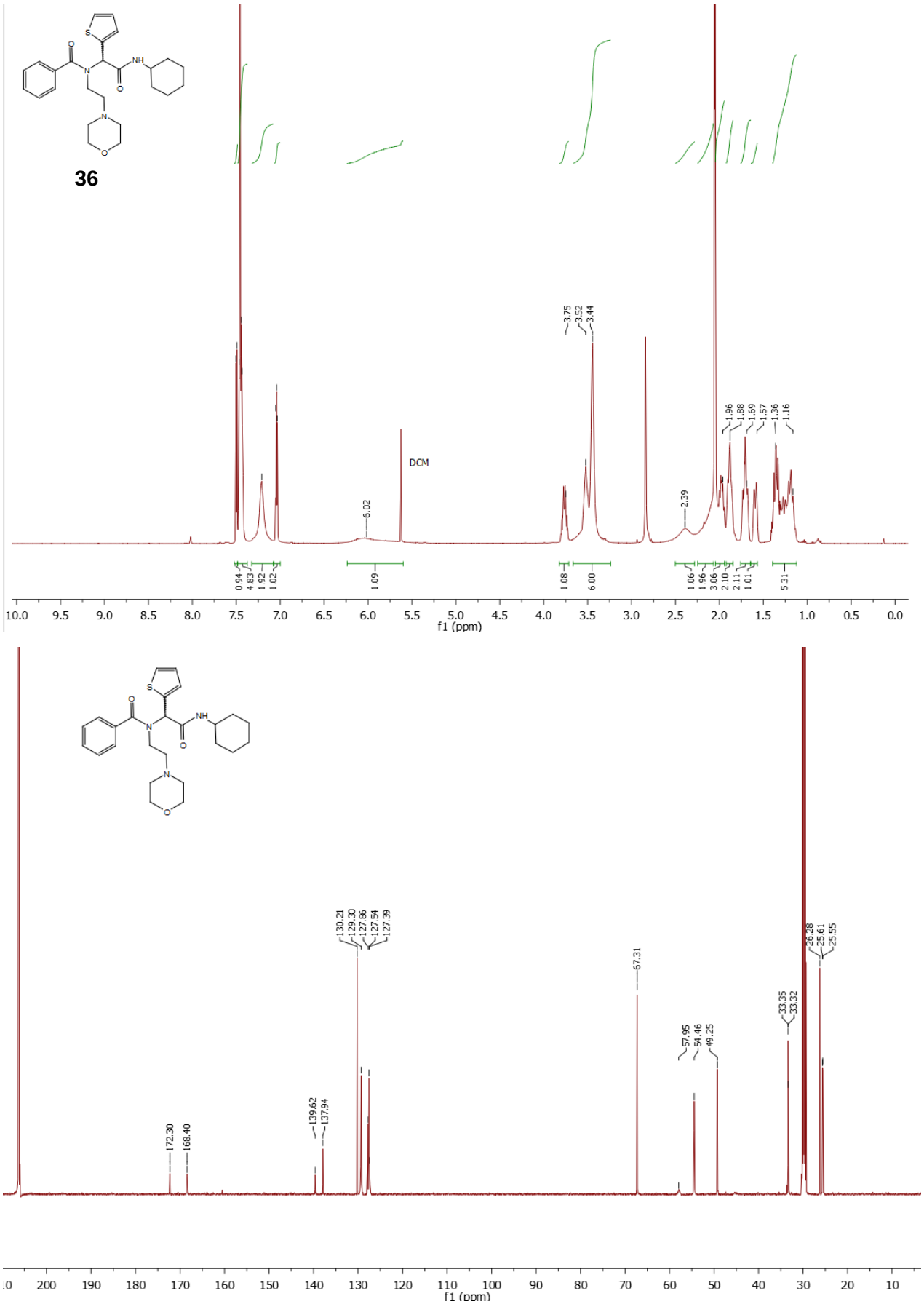

Figure S98: ^{1}H-, ^{13}C-NMR spectra of compound **36**.

Compound 37

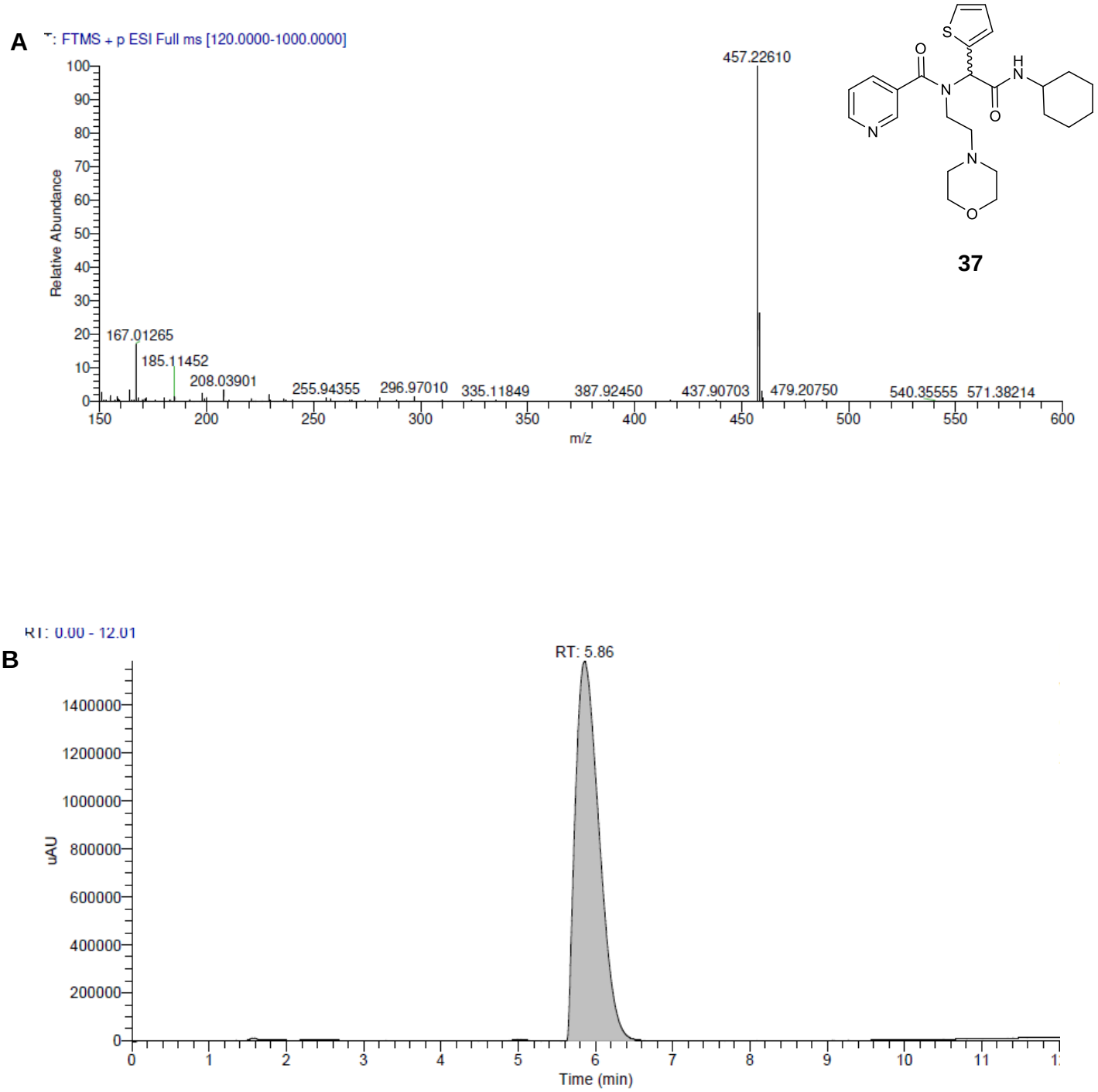

Figure S99: (A) Mass spectrum (HR-MS); (B) UV chromatogram (LC-MS) of compound **37.**

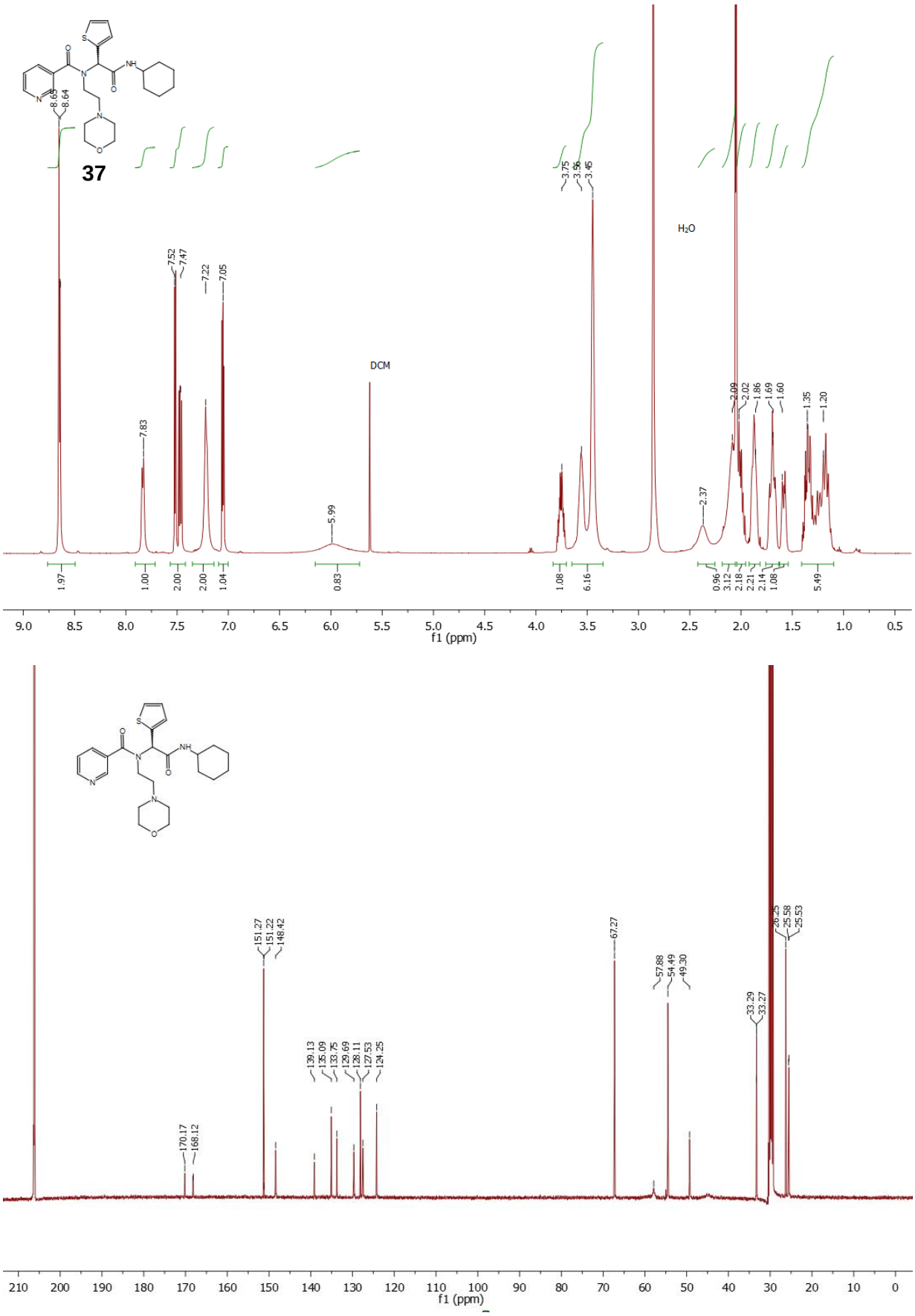

Figure S100: ^{1}H-, ^{13}C-NMR spectra of compound **37**.

Compound 38

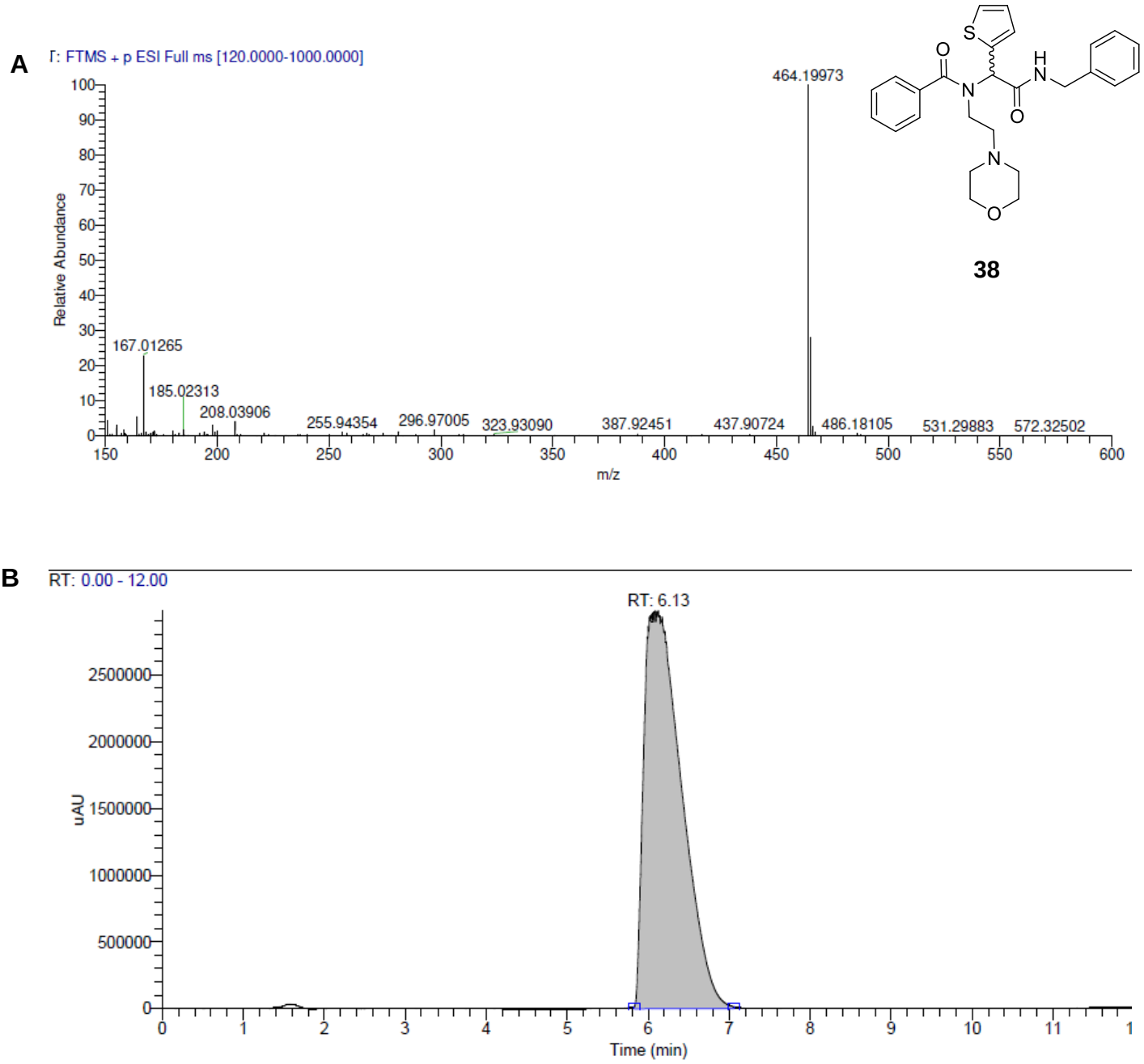

Figure S101: (A) Mass spectrum (HR-MS); (B) UV chromatogram (LC-MS) of compound **38.**

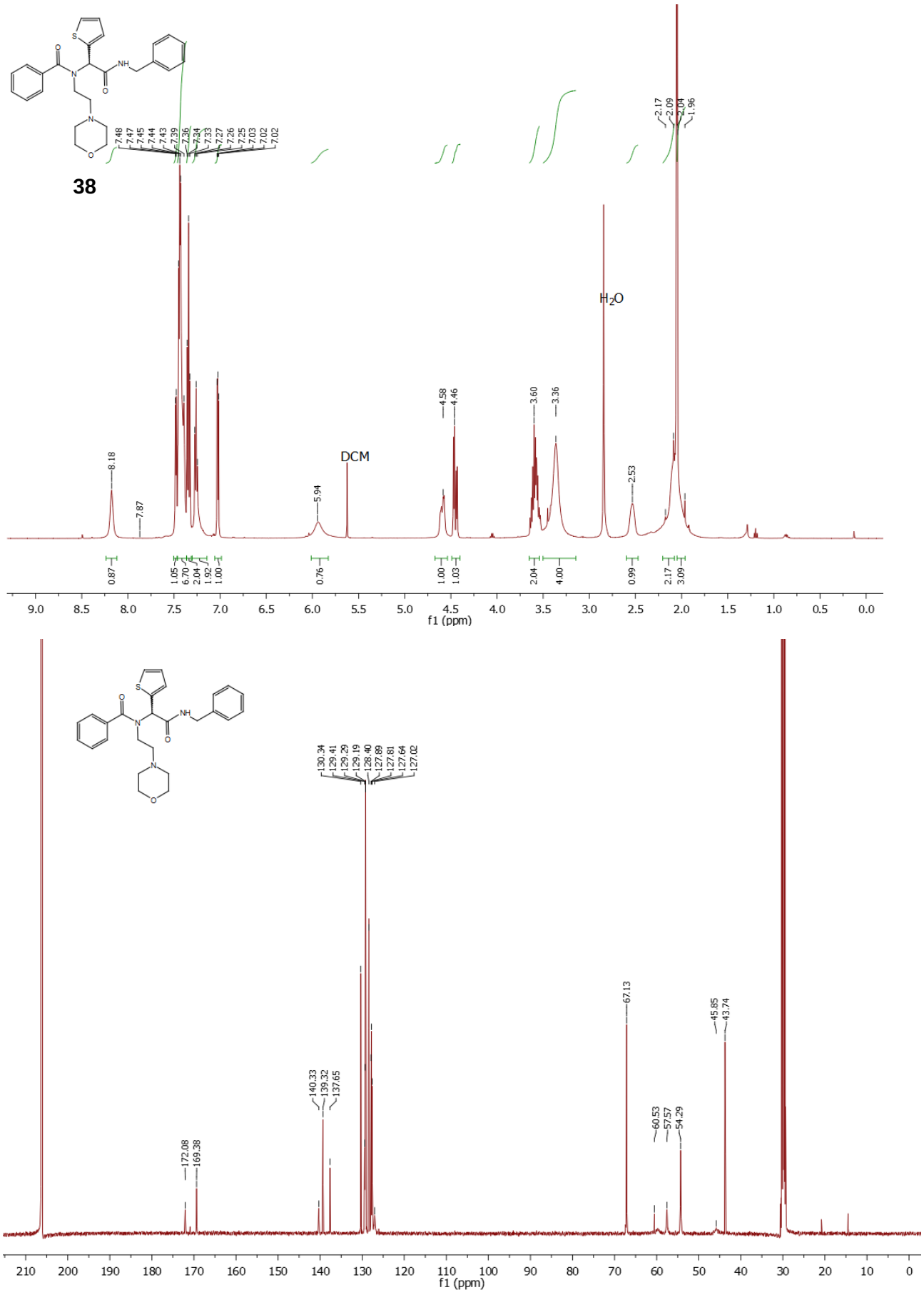

Figure S102: ^{1}H-, ^{13}C-NMR spectra of compound **38**.

Compound 39

A

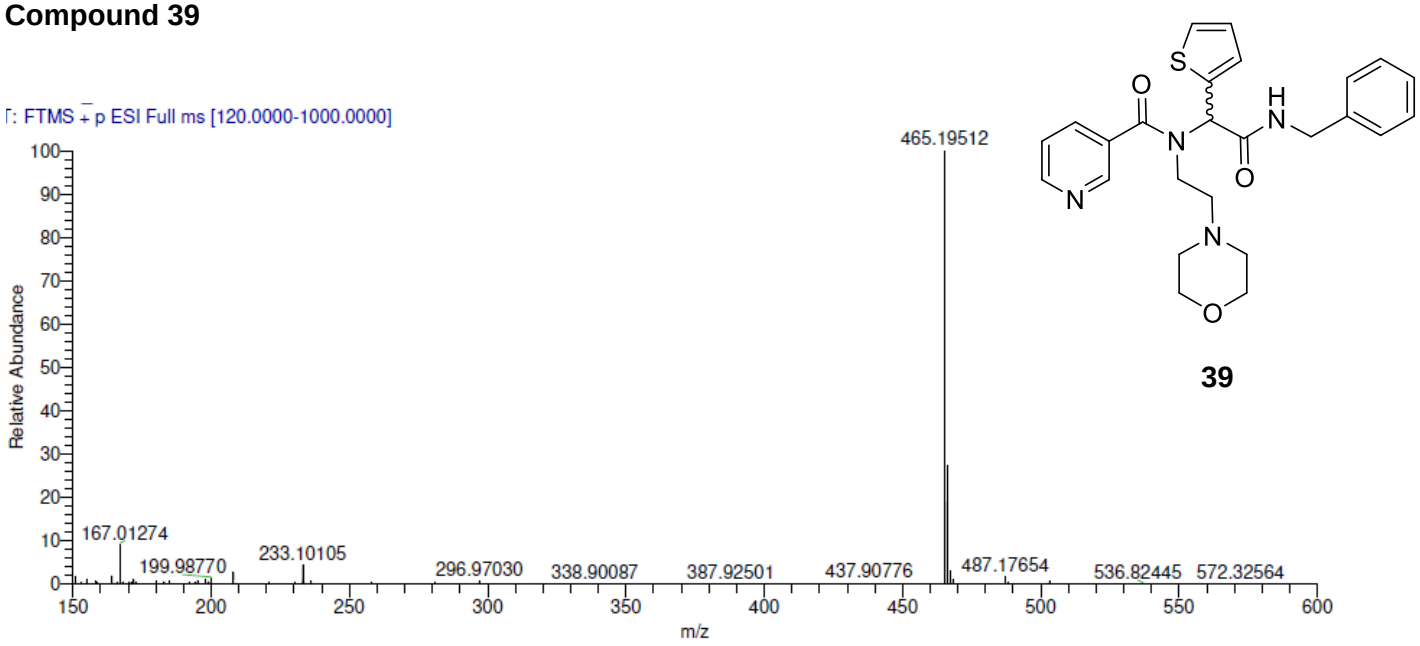

B

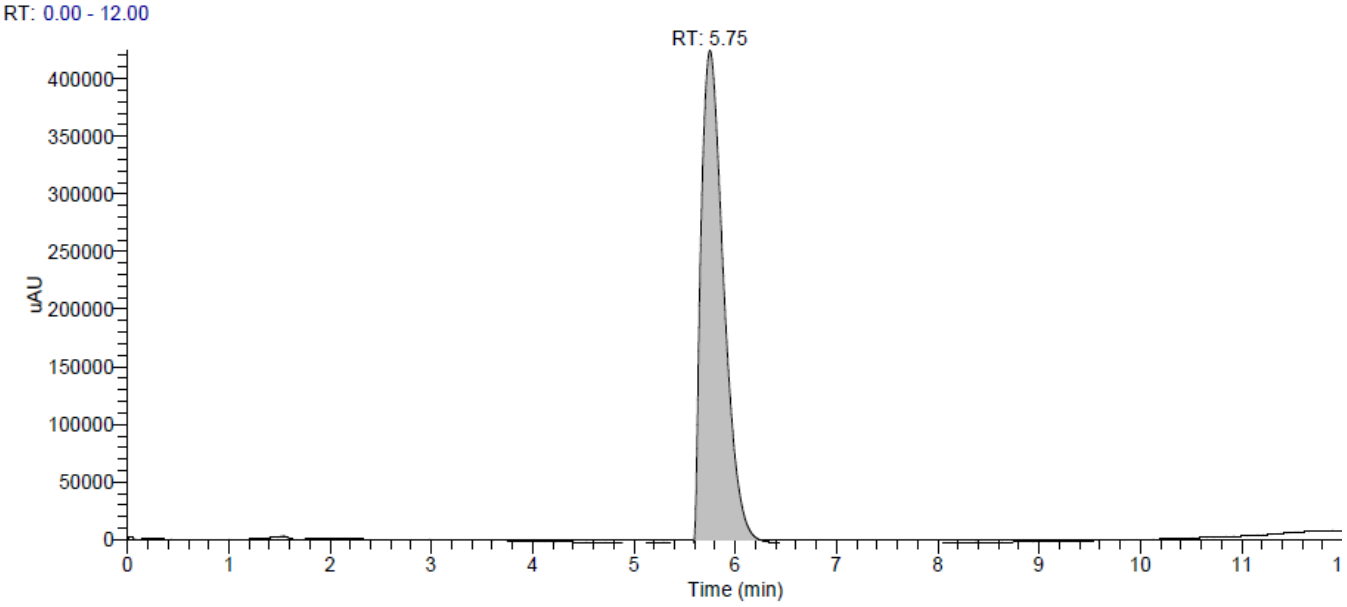

Figure S103: (A) Mass spectrum (HR-MS); (B) UV chromatogram (LC-MS) of compound **39.**

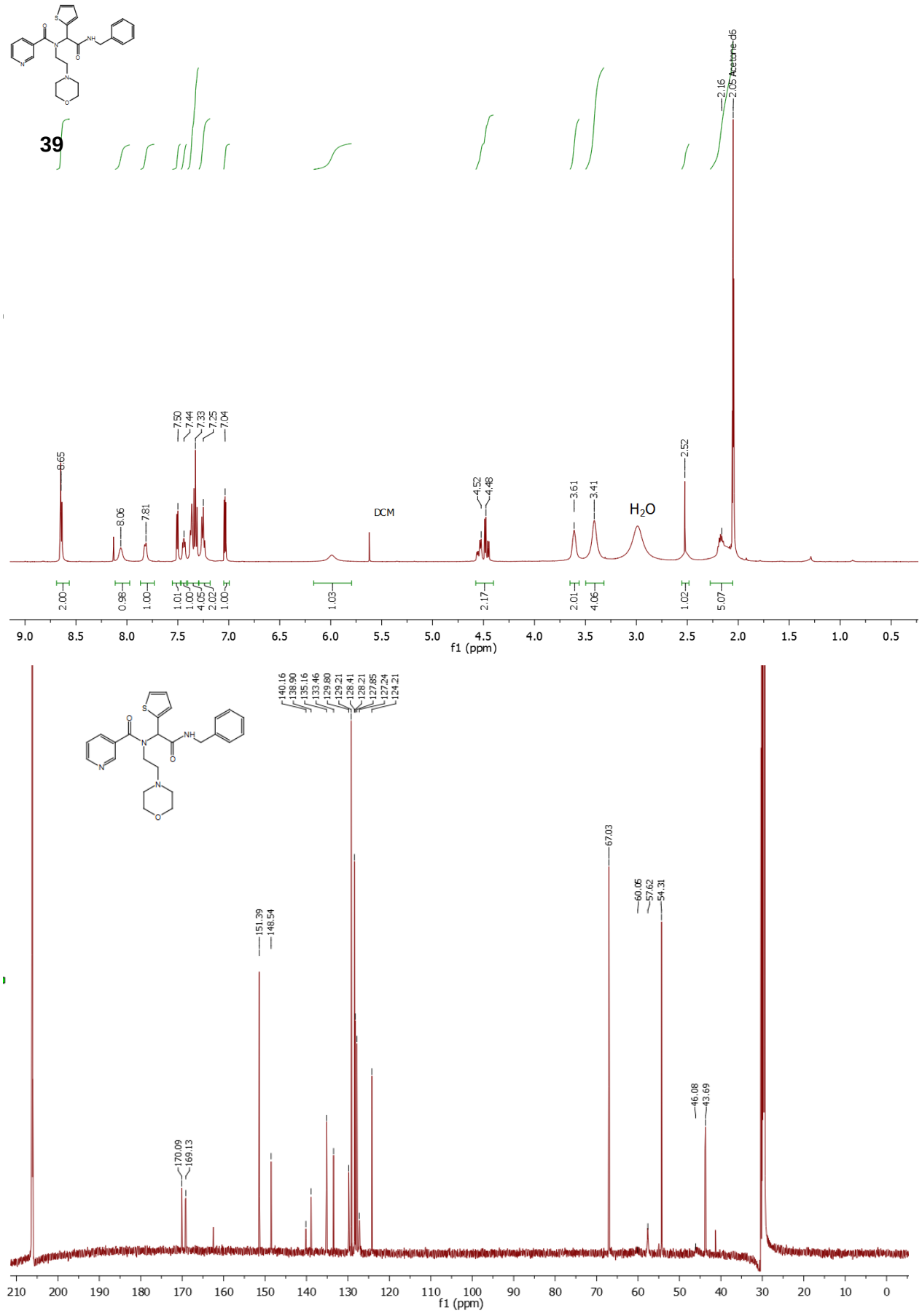

Figure S104: ^{1}H-, ^{13}C-NMR spectra of compound **39**.

Compound 40

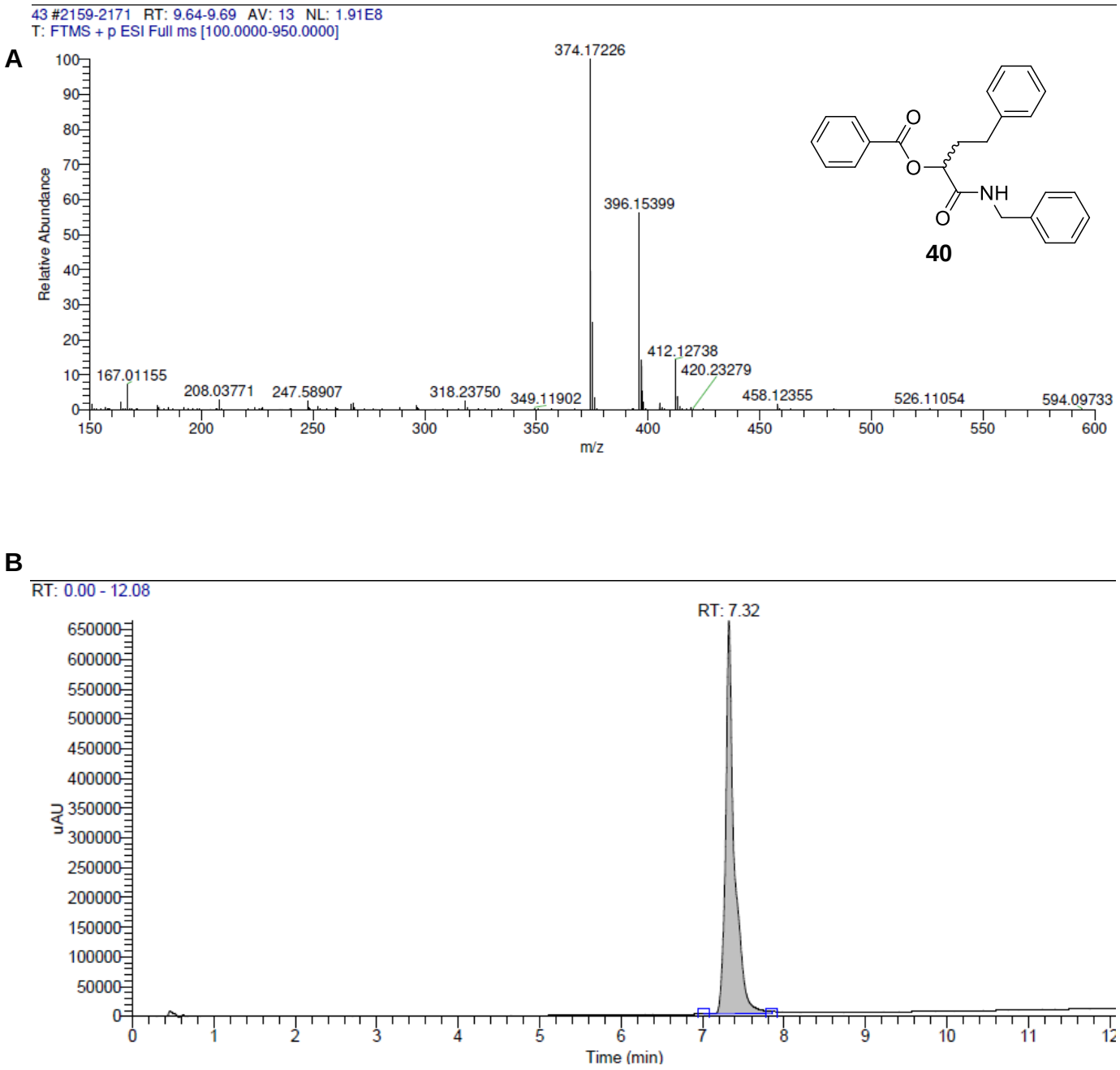

Figure S105: (A) Mass spectrum (HR-MS); (B) UV chromatogram (LC-MS) of compound **40.**

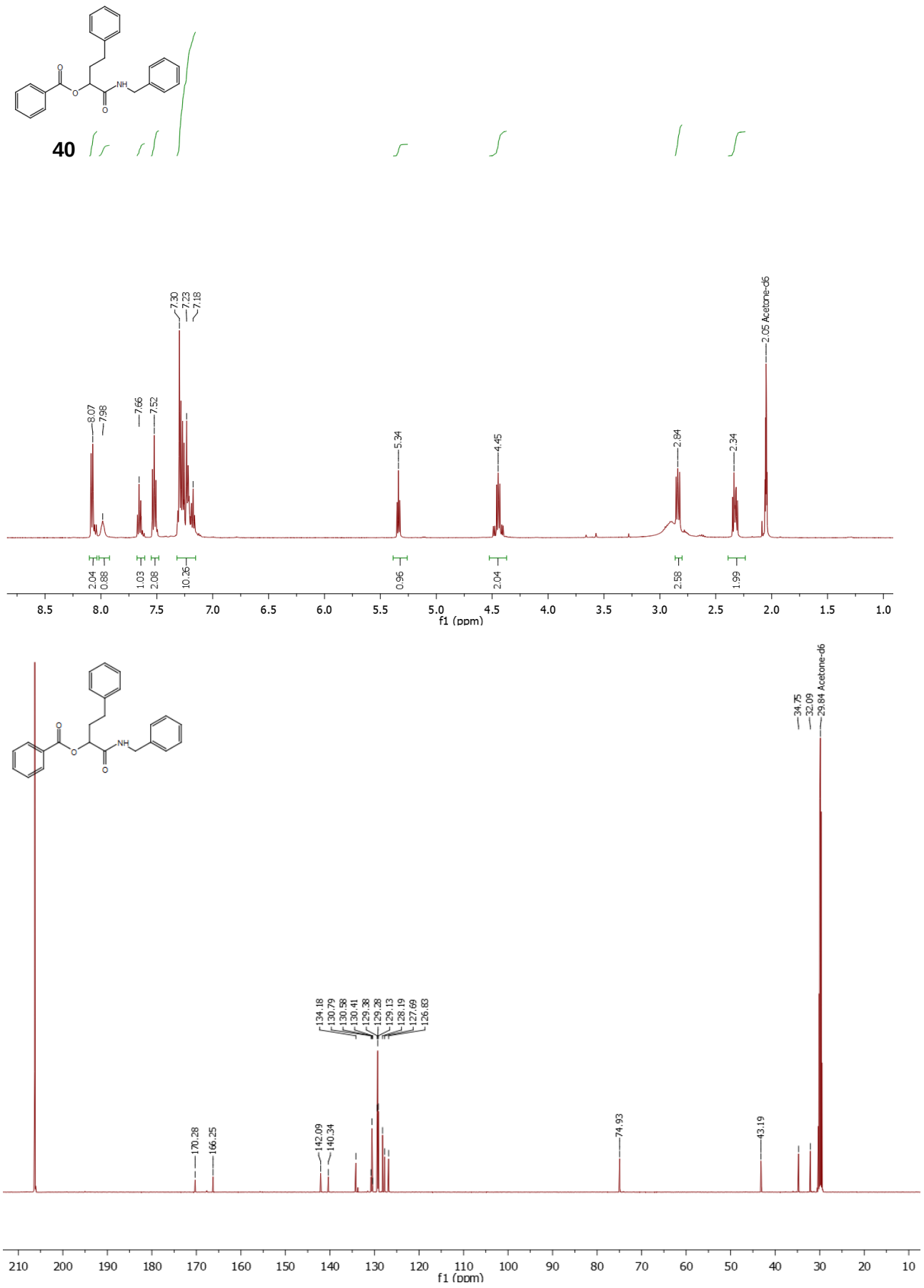

Figure S106: ^{1}H-, ^{13}C-NMR spectra of compound **40**.

Compound 56

A

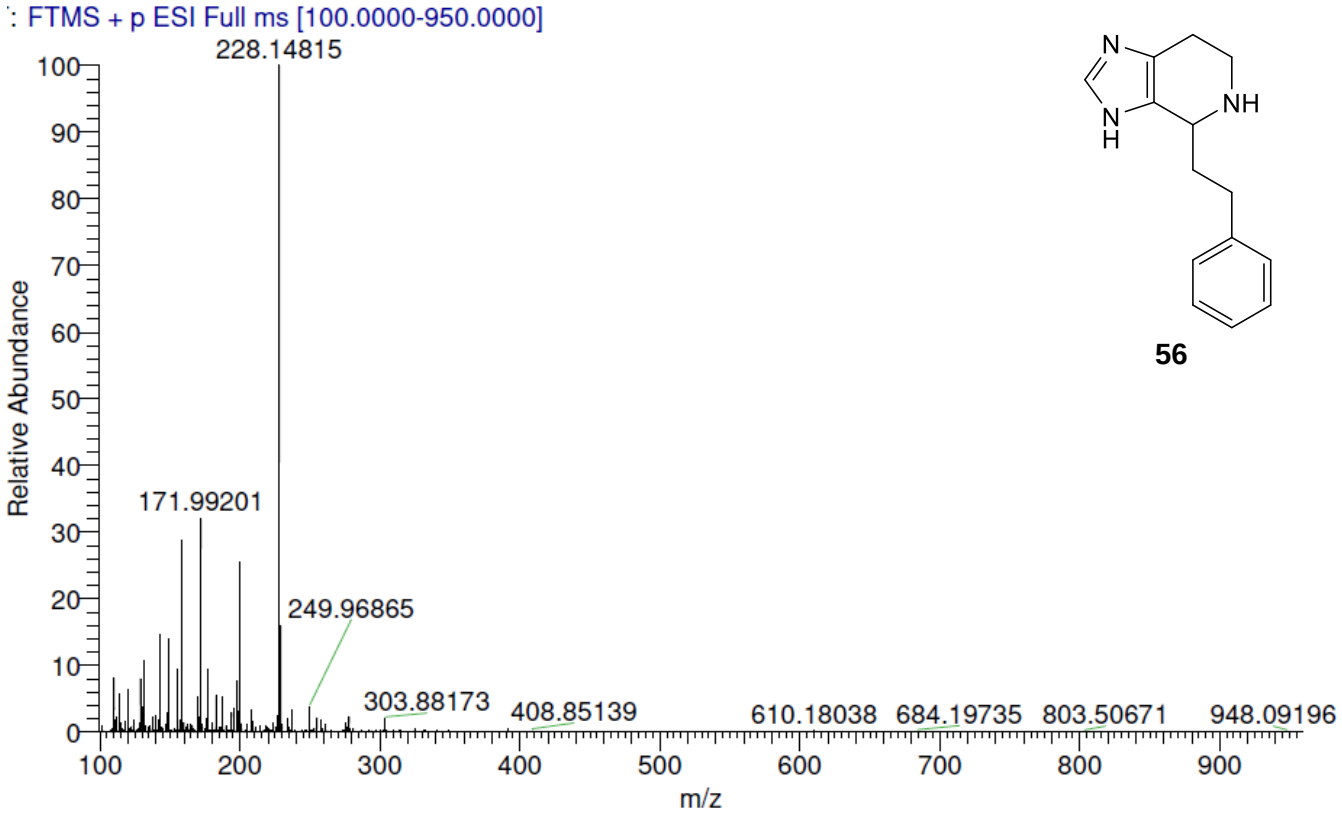

B

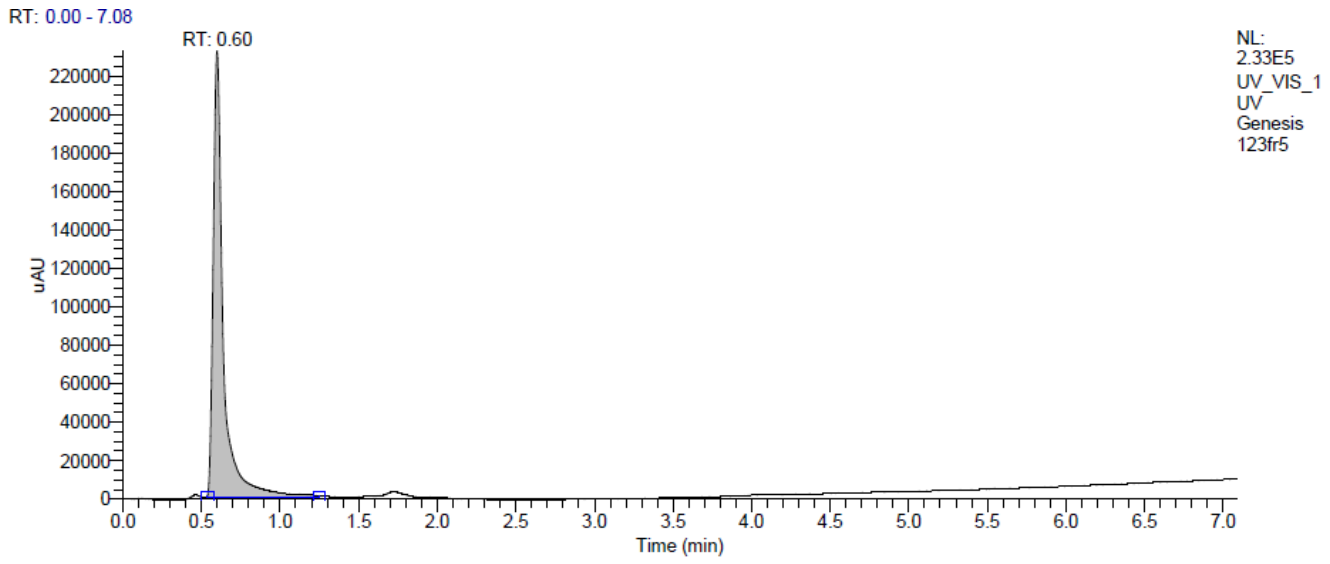

Figure S107: (A) Mass spectrum (HR-MS); (B) UV chromatogram (LC-MS) of compound **56.**

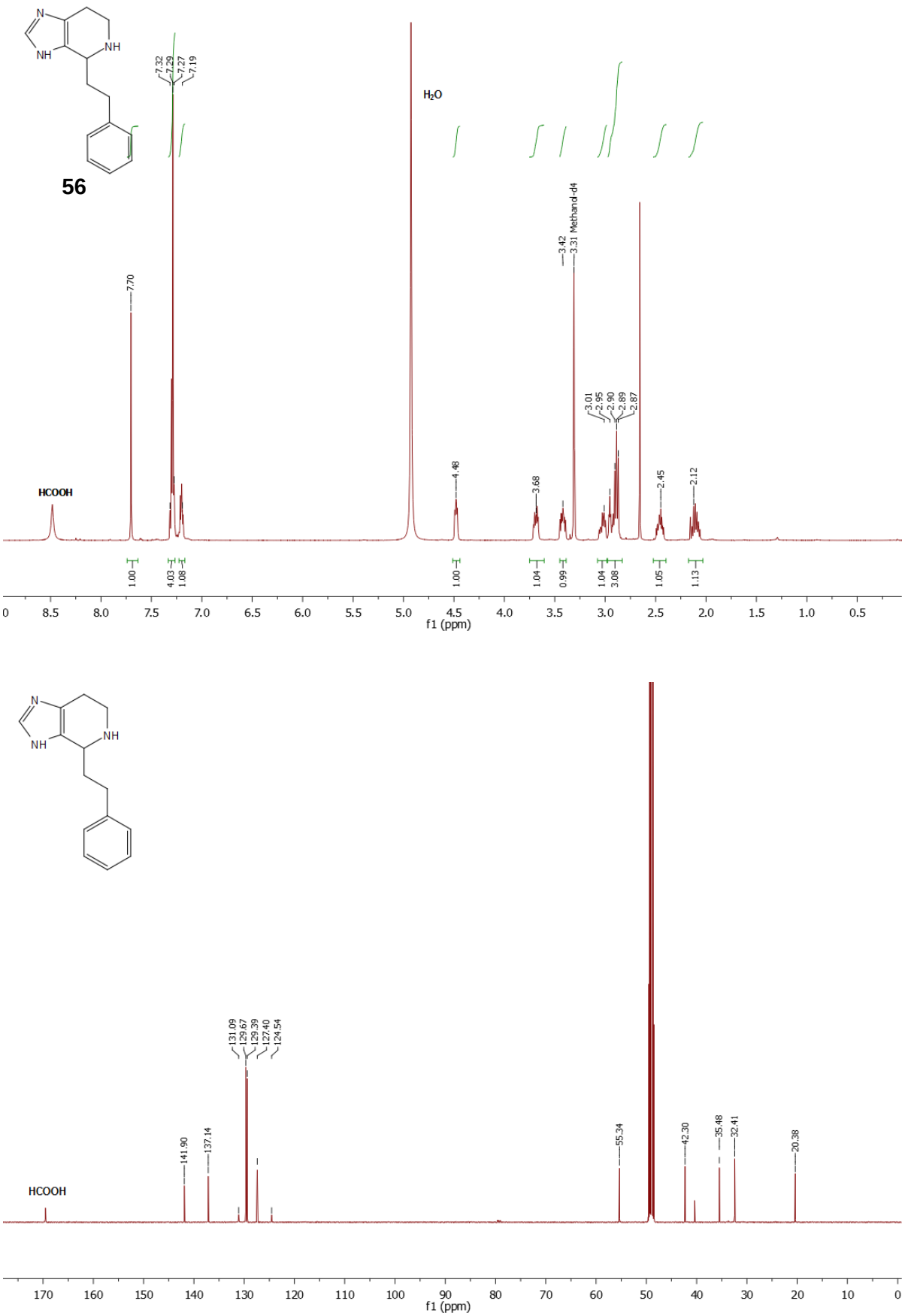

Figure S108: ^{1}H-, ^{13}C-NMR spectra of compound **56**.

References:

[1] P. R. Gerber, K. Müller, *J. Comput.-Aided Mol. Des.* **1995**, *9*, 251.
[2] H. Gohlke, M. Hendlich, G. Klebe, *Perspect. Drug Discovery Des.* **2000**, *20*, 115.
[3] LeadIT version 2.3.2; BioSolveIT GmbH, Sankt Augustin, Germany, **2017**, www.biosolveit.de/LeadIT.
[4] M. K. Larson and J. R. Whitaker, *J. Dairy Sci.* **1970**, *53*, 262.
[5] H. Köster, T. Craan, S. Brass, C. Herhaus, M. Zentgraf, L. Neumann, A. Heine, G. Klebe, *J. Med. Chem.* **2011**, *54*, 7784.
[6] A. Kling, P. Lukat, D. V. Almeida, A. Bauer, E. Fontaine, S. Sordello, N. Zaburannyi, J. Herrmann, S. C. Wenzel, C. König et al., *Science.* **2015**, *348*, 1106.
[7] R. E. Georgescu, O. Yurieva, S.-S. Kim, J. Kuriyan, X.-P. Kong, M. O'Donnell, *Proc. Natl. Acad. Sci. U. S. A.* **2008**, *105*, 11116.
[8] Z. Yin, Y. Wang, L. R. Whittell, S. Jergic, M. Liu, E. Harry, N. E. Dixon, M. J. Kelso, J. L. Beck, A. J. Oakley, *Chem Biol.* **2014**, *21*, 481.
[9] G. Wijffels, W. M. Johnson, A. J. Oakley, K. Turner, V. C. Epa, S. J. Briscoe, M. Polley, A. J. Liepa, A. Hofmann, J. Buchardt et al., *J. Med. Chem.* **2011**, *54*, 4831.
[10] Z. Yin, M. J. Kelso, J. L. Beck, A. J. Oakley, *J. Med. Chem.* **2013**, *56*, 8665.
[11] G. M. Sheldrick, *Acta Crystallogr., Sect. A: Cryst. Phys., Diffr., Theor. Gen. Crystallogr.* **2008**, *64*, 112.
[12] A. Viegas, J. Manso, F. L. Nobrega, E. J. Cabrita, *J. Chem. Educ.* **2011**, *88*, 990.
[13] F. W. Studier, *Protein Expression Purif.* **2005**, *41*, 207.
[14] E. Gasteiger, *Nucleic Acids Res.* **2003**, *31*, 3784.
[15] C. Henn, S. Boettcher, A. Steinbach, R. W. Hartmann, *Anal. Biochem.* **2012**, *428*, 28.

Author Contributions

M.Y.U. and F.M. performed the experiments, synthesized the compounds, wrote the manuscript, and contributed equally to the study. V.R.J. and A.A. contributed to the synthesis and binding study. P.L. expressed and purified the DnaN proteins. J.H. analyzed the antibacterial activity. M.K. contributed to interpretation of the NMR spectra. M.D.W., W.B. and R.M. contributed to the interpretation of the results and revised the manuscript. W.A.M.E. and A.K.H.H. conceived and designed the study and revised the manuscript.